

# **EFFECT OF DIAPHRAGM WALL CONSTRUCTION ON ADJACENT DEEP FOUNDATION**

To the Faculty of  
Geosciences, Geoengineering and Mining  
of the Technische Universität Bergakademie Freiberg

approved

## **THESIS**

to attain the academic degree of

**Doktor-Ingenieur**

**DR.-ING.**

Submitted

by M.Sc. geotechnical engineering, Ahmed Zaki Mohamed

born on the 7<sup>th</sup> of October 1981 in Kalyobia, Egypt

Reviewers: Prof. Dr. -Ing. Herbert Klapperich, Freiberg  
Prof. Dr. rer. nat. Rafeq Azzam, Aachen  
Prof. Dr. Marawan Shahin, Tanta, Egypt

Data of the award: 8<sup>th</sup> February 2017

## ACKNOWLEDGMENT

The research was financially supported by the Egyptian Ministry of Higher Education and the German Academic Exchange Service known as DAAD. This support is gratefully acknowledged.

I wish words could be enough to show my appreciation to my supervisor Prof. Dr.-Ing Herbert Klapperich for supervising me in my research. From the early beginning he discussed with me my topic and he guided me gently in my further steps. He always allowed me to freely express my ideas and let me discuss with him at any time. I had a chance to attend several conferences and to see several construction sites because of his support and encouragement.

The idea of my research was suggested by Prof. Marawan Shahin during our consulting work for a construction project in Cairo. I greatly appreciate his suggestion for such an interesting topic. Many thanks also go to him due to his useful discussion during my work and for reviewing my thesis.

During my work in the geotechnical department at the TU Freiberg Dr.-Ing habil. Tamashkovics was helping me with several kinds of support that I greatly appreciate. He helped me in my numerical analysis and also introduced me to open-source software that can be used later in my further research. In my first week in Freiberg he assisted me in finding accommodation.

I also would like to thank Prof. Dr. Rafiq Azzam for reviewing my thesis and for his scientific discussion with me.

Prof. Mair from the University of Cambridge provided me with PhD dissertation when I asked him for it. This dissertation was very helpful for my work and I highly appreciate his help.

Many thanks go to Frau Brigitte Hegenberg for helping me to improve my thesis presentation by language corrections. I also enjoyed the friendly atmosphere with her small family.

Many thanks go to Prof. Dr.-Ing. habil. Heinz Konietzky as he provided me with FLAC 3D program and I also appreciate his time with me for discussion. I feel very grateful to Dr. Herbst as he helped me in my numerical simulation and mathematical calculations. I also would like to thank my colleague Gunter for his help with Matlab software. Many thanks go to Frau Dorothee Heidrich and Frau Angela Griebisch for their help.

My friends, flat mates and colleagues in Freiberg made my life easy and I was really happy and grateful for such nice atmosphere.

The greatest thanks go to my parents who raised me up and greatly supported me during my educational journey.

## ABSTRACT

The need of using the underground space was limited in the human history, but in the last century and due to the increase of world population, the use of the underground space has become essential. Underground metro stations, deep garages, tunnels and basements, etc... are examples of using the underground space inside the cities. The use of underground space is conducted through deep excavation or tunneling. Several techniques are used to conduct the deep excavation and one of the most popular and well known techniques used for deep excavation is the diaphragm walling technique which is widely used specially inside the cities to safe space because it requires a very small space to conduct a deep reinforced concreted wall under the ground. However, the construction of such walls causes deformation of the surrounding ground and it could also affect the nearby existing structures. In some recorded cases the slurry trench failed and causes a great deformation which effect the nearby structures. However, Minor damages and cracks were observed in buildings near stable slurry trenches, because the soil deformation was high.

The existing structures inside the cities have been constructed on shallow or deep foundations and this research was oriented to study the effect of diaphragm wall installation on the existing adjacent piled foundation. Very limited studies were made to investigate such an effect. At Cambridge university centrifuge model tests were conducted to investigate the effect of slurry reduction on single piles. Field observation was conducted in several projects and showed the settlement and deformation of buildings located on deep foundation during the diaphragm wall trenching. Numerical analysis was conducted using FLAC 3D to simulate the laboratory and the available field works. FLAC 3D is a commercial software and it depend in its analysis on finite difference method. The purpose of the simulation was to verify the used numerical analysis method. The results from the numerical analysis were in a good agreement with the available field data results, and they were also in good agreement with the laboratory test results regarding soil settlement but it was not in such good agreement when they were compared regarding the pile. Generally, from the verification the numerical analysis method is considered to be reliable.

A parametric study was performed using the verified numerical analysis method. The flexible nature of the numerical analysis allows to simulate different cases and to study a variety of parameters. The output of the parametric study was the pile deflection, the bending moment and the shaft friction. The study was divided into three main parts while each part contains

several parameter combinations. The first part studied the effect of the single and double panel(s) on the single pile group that has different piles numbers and formations. The second and third parts studied the effect of multiple panels on connected pile groups and piled raft foundation, respectively. Generally, the studied parameters can be divided into three main groups. The first is related to the trench which includes the panel dimension, the number of panels and the slurry level inside the panel. The effect of slurry pressure reduction at some levels inside the trench was also studied. The second group concerned the soil type and ground water level. The third group is related to the deep foundation which includes pile characteristics, location, and formation within the group. The results from the parametric study showed that the pile behavior was greatly affected by panel length, groundwater level, slurry level inside the trench and steadiness of the slurry pressure. The piles were also affected by the different stages of construction related to the pile location from the constructed panel. The piles within the group act together so they behave different from each other according to their position.

The effect of the pile on the trench stability is presented through a simple analytical approach which is based on the wedge analysis. The analytical approach provided equations that calculate the factor of safety in two and three dimensions. The pile location was governing the equation that calculate the factor of safety because the pile could be fully inside the failure wedge or intersect with the failure surface. A comparative study was conducted to find out the effect of the different pile location and other parameters on the safety factor. Generally, this comparative study showed that the pile located within the failure wedge reduces the factor of safety, while the pile that intersects the failure surface could increase it. The pile row near a trench that contains piles inside the failure wedge and others intersects the failure surface act together to balance the failure wedge. The factor of safety results of some cases from the analytical approach were also compared with those calculated from the numerical analysis. In general, the factor of safety from the numerical analysis was higher than that calculated from the proposed analytical approach.

This research helped to understand the trenching effect on the ground surface and on the nearby piled foundations. It provided charts that could help to predict the soil deformation and earth pressure coefficient which could be used in the design. It showed through the parametric study the precautions that should be taken into consideration during trenching process near piled foundation. This research provided a design method for the slurry trench panel near piled foundation.

## TABLE OF CONTENTS

<b>Acknowledgment</b> .....	<b>ii</b>
<b>Abstract</b> .....	<b>iii</b>
<b>Table of Contents</b> .....	<b>v</b>
<b>List of Figures</b> .....	<b>xi</b>
<b>List of Tables</b> .....	<b>xx</b>
<b>List of Notations</b> .....	<b>xxi</b>
<b>Chapter 1: Introduction</b> .....	<b>1</b>
1.1 Background .....	1
1.2 Aims of the research .....	2
1.3 Research content (thesis layout) .....	3
<b>Chapter 2: Literature review</b> .....	<b>4</b>
2.1 Introduction.....	4
2.2 Deep foundation stress strain mechanism (pile foundation).....	4
2.2.1 Piles under vertical load.....	5
2.2.1.1 End-bearing capacity in cohesion-less soil .....	6
2.2.1.2 Shaft friction capacity in cohesion-less Soil .....	7
2.2.1.3 Pile settlement due to vertical load .....	8
2.2.1.4 Pile group under vertical load .....	10
2.2.2 Pile subjected to direct lateral load .....	10
2.2.2.1 Ultimate lateral capacity .....	11
2.2.2.2 Deflection of piles under lateral load.....	12
2.2.2.3 P-y Curves.....	12
2.2.2.4 Pile group under lateral load .....	13
2.2.3 Pile subjected to passive lateral load .....	14
2.2.3.1 Pile under lateral soil movement (theory).....	14
2.2.3.2 Pile near embankment.....	15
2.2.3.3 Pile in or near slopes .....	17
2.2.3.4 Piles near deep excavations .....	18
2.3 Diaphragm wall installation.....	21
2.3.1 Bentonite slurry and filter cake.....	22
2.3.2 Analytical solution of slurry trench stability .....	23
2.3.2.1 Analytical solution in cohesive soils.....	23

2.3.2.2 Analytical solution in cohesion-less soils .....	25
2.3.2.3 Analytical solution applicable for cohesion and cohesion-less soil.....	27
2.3.3 Soil deformation due to slurry trenching .....	29
2.3.3.1 Soil deformation calculation using analytical solution .....	29
2.3.3.2 Soil deformation calculation using numerical analysis .....	30
2.4 Summary .....	32
<b>Chapter 3: Previous Field Data and Laboratory Works .....</b>	<b>33</b>
3.1 Introduction.....	33
3.2 Diaphragm walls and deep excavations .....	33
3.3 Effect of slurry trenching on ground surface (Green field) .....	36
3.3.1 Case histories .....	37
3.3.2 Field tests (Tested panels).....	40
3.3.3 Laboratory works .....	44
3.4 diaphragm wall installation adjacent to deep foundation .....	48
3.4.1 Case histories .....	48
3.4.1.1 Charter underground station (Hong Kong) .....	48
3.4.1.2 Full scale field test (Amsterdam).....	50
3.4.1.3 Underground basement (Giza, Egypt) .....	50
3.4.1.4 Underground stations (Amsterdam).....	51
3.4.2 Laboratory test .....	52
3.4.2.1 Test description .....	52
3.4.2.2 Test procedure.....	53
3.4.2.3 Test results .....	53
3.4.2.4 General conclusion and comments .....	55
3.5 Data collection and discussion.....	56
3.5.1 Stress change.....	57
3.5.2 Settlement .....	61
3.5.3 Horizontal displacement .....	62
3.6 Summary .....	64
<b>Chapter 4: Numerical analysis and verification .....</b>	<b>65</b>
4.1 Introduction.....	65
4.2 Numerical analysis and theoretical background .....	65
4.2.1 Finite difference sequence .....	66
4.2.2 Equation of motion and constitutive relation.....	67
4.2.3 Constitutive model .....	67

4.2.3.1 Mohr-Coulomb model .....	68
4.2.3.2 Hardening soil model .....	69
4.3 Simulation of full-scale field test and soil model .....	69
4.3.1 Soil properties .....	69
4.3.2 Soil modeling .....	70
4.3.3 Geometry modeling and meshing .....	71
4.3.4 Results and comparison .....	72
4.4 Laboratory work modeling .....	74
4.4.1 Numerical modeling of the experiment .....	74
4.4.1.1 Model Geometry .....	74
4.4.1.2 Soil modeling .....	75
4.4.1.3 Guide wall modeling .....	75
4.4.1.4 Pile modeling .....	75
4.4.1.5 Latex membrane and trench modeling .....	77
4.4.2 Results from the experiment numerical modeling .....	78
4.4.2.1 Surface soil settlement .....	78
4.4.2.2 Pile deflection and bending moment .....	81
4.4.2.3 Pile shear friction and bearing capacity .....	82
4.4.2.4 General discussion of the results .....	85
4.5 Modeling of previous working projects .....	85
4.5.1 Numerical modeling of Charter underground station (Hong Kong) .....	86
4.5.1.1 Diaphragm wall panels near Courts of Justice .....	86
4.5.1.2 Diaphragm wall panels near Swire House .....	90
4.5.2 Numerical modeling of two story basement (Giza) .....	93
4.5.2.1 Diaphragm wall panels and adjacent building characteristics .....	93
4.5.2.2 Soil properties .....	94
4.5.2.3 Numerical modeling .....	94
4.5.2.4 Numerical results and comparison .....	95
4.6 Summary .....	97
<b>Chapter 5: Parametric study .....</b>	<b>99</b>
5.1 Introduction .....	99
5.2 Modeling of studied parameters .....	99
5.2.1 Soil profile and properties .....	99
5.2.2 Guide wall, diaphragm wall panels and slurry .....	100
5.2.3 Piled foundation and offset distance .....	101

5.3 Parametric study plan.....	102
5.3.1 Part I - the effect of single or double trench panels on isolated pile group	102
5.3.1.1 Parameters and model groups of Part I.....	103
5.3.1.2 Combination of the studied parameters .....	103
5.3.1.3 Typical mesh model of Part I.....	108
5.3.2 Part II - multiple panels effect on several connected pile groups.....	108
5.3.2.1 Geometry and model groups of Part II .....	109
5.3.2.2 Parameters combination of Part II .....	110
5.3.2.3 Mesh models of Part II.....	110
5.3.3 Part III - multiple panels effect on piled raft foundation .....	111
5.3.3.1 Geometry of Part III.....	112
5.3.3.2 Parameters combination of Part III.....	113
5.3.3.3 Mesh model of Part III.....	114
5.4 Results and discussion .....	114
5.4.1 Part I- results .....	114
5.4.1.1 Trench dimension (PI-MG1-C1 and C2).....	114
5.4.1.2 Pile group location and the pile position within the group (PI-MG1-C3)	
.....	117
5.4.1.3 Groundwater level (PI-MG1-C4).....	120
5.4.1.4 Slurry level (PI-MG1-C5).....	122
5.4.1.5 Soil properties (PI-MG1-C6) .....	123
5.4.1.6 Slurry pressure reduction at some assumed levels (PI-MG1-C7).....	124
5.4.1.7 Pile length (PI-MG1-C8) .....	125
5.4.1.8 Pile diameter (PI-MG1-C9) .....	126
5.4.1.9 Effect of slurry level and slurry pressure reduction on piles with	
different formation within model groups (MG 1, 2, 3 and 4).....	127
5.4.1.10 Double panel (MG 5-C1 and 2) .....	132
5.4.2 Part II- results.....	135
5.4.2.1 Effect of panel construction stages .....	135
5.4.2.2 The behavior of pile according to its location within the foundation	136
5.4.2.3 Effect of groundwater table, slurry level and slurry pressure reduction	
.....	138
5.4.2.4 Effect of panel length.....	140
5.4.2.5 Effect of pile group formation .....	141
5.4.3 Part III- results .....	142



5.4.3.1	Panels construction stages effect on piles at different locations.....	142
5.4.3.2	Comparison between different piles within the piled raft foundation	143
5.4.3.3	Effect of different groundwater tables and slurry levels.....	145
5.4.3.4	Panel length effect on the pile.....	145
5.4.3.5	Effect of the number of piles within the raft.....	146
5.4.3.6	Connected pile group in comparison with the pile raft foundation ...	147
5.4.4	General overview of the parametric study results.....	148
5.5	effect of trenching on the pile shaft friction coefficient .....	149
5.6	Summary .....	153
<b>Chapter 6:</b>	<b>Analytical approach .....</b>	<b>155</b>
6.1	Introduction.....	155
6.2	Trenching near a single pile (Situation I) .....	155
6.2.1	Case 1: pile above the failure surface .....	155
6.2.1.1	Two-dimensional approach of Case 1.....	156
6.2.1.2	Three-dimensional approach of Case 1.....	158
6.2.2	Case 2: pile intersects the failure surface.....	161
6.2.2.1	Two-dimensional approach of Case 2.....	161
6.2.2.2	Three-dimensional approach of Case 2.....	162
6.3	Trenching near group(s) of piles (Situation II) .....	163
6.4	Comparative study .....	164
6.4.1	Comparison regarding two-dimensional analysis approach .....	164
6.4.2	Comparison regarding three-dimensional analysis approach .....	166
6.4.3	Comparison regarding the effect of several piles .....	168
6.5	Comparison between factor of safety from the proposed approach and numerical analysis.....	169
6.5.1	Factor of safety calculation in FLAC 3D.....	170
6.5.2	Numerical modeling for factor of safety calculation .....	170
6.6	Summary .....	173
<b>Chapter 7:</b>	<b>Conclusions and recommendations .....</b>	<b>175</b>
7.1	Soil deformation due to trenching.....	175
7.2	Effect of trenching on the earth pressure coefficient .....	176
7.3	Numerical modeling of The trenching process near piled foundation.....	176
7.4	Parametric study.....	176
7.4.1	Deflection of the pile .....	177
7.4.2	Bending moment of the pile.....	177

7.4.3 Pile shaft friction.....	178
7.5 Effect of pile on trench stability.....	178
7.6 Recommendation for further work.....	179
<b>References.....</b>	<b>180</b>
<b>APPENDIX A: Typical code used for modeling with FLAC3D.....</b>	<b>A-1</b>
<b>APPENDIX B: Parametric study Figures.....</b>	<b>B-1</b>
B.1 Results of Part I model groups.....	B-1
B.2 Results of Part II model groups.....	B-11
B.3 Results of Part III model groups.....	B-14

## LIST OF FIGURES

<i>Number</i>	<i>Page</i>
Fig. 2-1: Pressure distribution and soil disturbance for single pile (after Tomlinson and Woodward, 2008) .....	5
Fig. 2-2: Axially loaded pile .....	5
Fig. 2-3: Pile behavior under load (a) Load settlement curve for compressive load to failure in pile (b) Load transfer from head of pile to shaft at points A, B and D (after Tomlinson and Woodward, 2007) .....	6
Fig. 2-4: Relation of cavity expansion limit pressure and end-bearing capacity (after Randolph et al., 1994) .....	7
Fig. 2-5: measured profiles of shaft friction (Lehane et al., 1993) .....	8
Fig. 2-6: Relationship of settlement and settlement/ load (after Chin, 1970) .....	9
Fig. 2-7: Distribution of unit stress before and after lateral load (after Reese & van Impe, 2001) .....	10
Fig. 2-8: Variation of soil resistance along laterally loaded piles (Fleming et al., 2009) ..	10
Fig. 2-9: Hansen's method for calculating ultimate lateral resistance of short piles (a) soil reactions (b) shearing force diagram (c) bending moment diagram (Hansen, 1961) .....	11
Fig. 2-10: p-y curves for laterally loaded piles (a) typical p-y Curve (b) shape of curves at various depths x below soil surface (c) family of P-y curves for proposed criteria (after Reese et al. 1974) .....	12
Fig. 2-11: Pile group under lateral load (after Fleming et al., 2009) .....	13
Fig. 2-12: The modified soil resistance for a p-y curve for a single pile in case of pile group interaction (Reese and van Impe, 2001) .....	13
Fig. 2-13: Piles in soil undergoing lateral movement .....	15
Fig. 2-14: Soil displacement mechanism and loading (after Stewart et al., 1994) .....	16
Fig. 2-15: Pile subjected to lateral soil displacement (Jeong et al. 2003) .....	17
Fig. 2-16: Forces on stabilized piles .....	17
Fig. 2-17: Development of maximum (a) head deflection and (b) bending moment of the pile during and after excavation (after Leung et al., 2006) .....	19
Fig. 2-18: A suggested curve to determine the interaction level for friction pile (Korff, 2013) .....	21
Fig. 2-19: (a) Stress diagram in zone of soil impregnated with slurry (after Elson, 1968) ..	23

Fig. 2-20 Slurry trench stability: (a) Section through trench. (b) Force polygon for purely cohesive soil ( $\phi = 0$ ). (c) Force triangle for purely cohesion-less soils ( $c=0$ ). (d) stability of trench in sand with natural water level (after Xanthakos, 1994)...	24
Fig. 2-21: (a) The change of width for typical gage points for tested panels (after DiBiagio and Myrvoll, 1972) (b) Arching effect of trenches in clay (after Xanthakos, 1994).....	24
Fig. 2-22: Assumed failure condition in trench, and stability analysis (after Aas, 1976)	25
Fig. 2-23: sliding wedge shape (a) (after Prater, 1973) (b) (Piaskowski, 1965) (c) (after Walz and Prager, 1978).....	26
Fig. 2-24: Analytical approach (a) (after Xanthakos, 1994) (b) (Fox 2004).....	28
Fig. 2-25: 3D analysis for frictional/cohesive soils (a) (after Li et al. 2013) (b) (after Han et al. 2013).....	28
Fig. 3-1: Diaphragm wall construction in Vijzelgracht station (Korff, 2013).....	34
Fig. 3-2: East Slurry wall (Meyerowitz, 2006).....	34
Fig. 3-3: Diaphragm walls in Berlin.....	35
Fig. 3-4: Diaphragm wall Failure in Cologne and current situation.....	36
Fig. 3-5: Effect of slurry trenching on building (Cowland and Thorley, 1985).....	38
Fig. 3-6: Instrumentation plane for tested panel (after Stround and Sweeney, 1977).....	42
Fig. 3-7: lateral pressure distribution with depth (Ng et al, 1999).....	43
Fig. 3-8: Failure surface detection (Tsai et al., 2000).....	44
Fig. 3-9: Section of the tank showing the Framework (Elson, 1968).....	45
Fig. 3-10: normalized Settlement due to diaphragm wall installation with (a) normalized distance (b) normalized height to trench length (after Powrie and Kantartzi, 1996).....	47
Fig. 3-11: Charter Station and adjacent building (after Davies and Henkel, 1982).....	49
Fig. 3-12: Diaphragm wall near Swire House (after Davies and Henkel, 1982).....	49
Fig. 3-13: Instrumentation layout of the test (Wit de and Lengkeek, 2002).....	50
Fig. 3-14: Buildings horizontal displacement measuring method (Korff, 2013).....	51
Fig. 3-15: Test preparation and sequence (Choy, 2004).....	53
Fig. 3-16: Soil and trench pressure with time during testing (3.0m width diaphragm wall) (Choy, 2004).....	54
Fig. 3-17: Change in soil stress during slurry reduction (6.0m width diaphragm wall) (Choy, 2004).....	54
Fig. 3-18: Soil deformation after test (Choy, 2004).....	54

Fig. 3-19: Failure surface recorded on both sides of the 6m trench CKC16 (Choy, 2004)	55
Fig. 3-20: Normalized horizontal stress with depth	57
Fig. 3-21: Normalized settlement to normalized distance from the trench due to the diaphragm walls installation	61
Fig. 3-22: Settlement to distance from the trench due to the diaphragm walls installation	62
Fig. 3-23: Horizontal displacement with normalized depth	63
Fig. 4-1: Basic cycle of explicit calculation method (Itasca, 2013)	66
Fig. 4-2: mass subjected to time-varying force (Itasca, 2013)	66
Fig. 4-3: Mohr-Coulomb yield surface in principal stress space. (Itasca, 2013)	68
Fig. 4-4: Mohr-Coulomb failure criterion (Itasca, 2013)	68
Fig. 4-5: Relation between mobilized friction angle and plastic shear strain for different soil layers	71
Fig. 4-6: Mesh geometry of the tested panel	72
Fig. 4-7: Trench modeling	72
Fig. 4-8: Soil horizontal displacement	73
Fig. 4-9: Soil settlement	74
Fig. 4-10: General geometry, construction stages and typical mesh used for simulation.	75
Fig. 4-11: Fully bonded reinforcement mechanical representation (Itasca, 2013)	76
Fig. 4-12: Behavior of pile in normal direction ( $u_n$ is the relative normal displacement between pile and host medium) (Itasca, 2013)	76
Fig. 4-13: Shell element used in simulating the latex membrane	78
Fig. 4-14: Typical effect of pile installation on soil settlement	78
Fig. 4-15: Soil settlement due to slurry reduction for 6 m length single panel	79
Fig. 4-16: Soil settlement due to slurry reduction for 3.0 m length multiple panels	80
Fig. 4-17: Pile bending moment and deflection due to slurry reduction (CKC15)	81
Fig. 4-18: Pile bending moment and deflection due to slurry reduction (CKC16)	82
Fig. 4-19: Pile shaft friction during slurry reduction	83
Fig. 4-20: Reduction of pile end bearing at different slurry levels	84
Fig. 4-21: Diaphragm wall construction stages near Courts of Justice (Davies and Henkel, 1982)	86
Fig. 4-22: Trench modeling	87
Fig. 4-23: Trench mesh modeling	88
Fig. 4-24: Settlement at different stages	88

Fig. 4-25: Horizontal displacement from different stages and locations .....	89
Fig. 4-26: Piles deflection and bending moment .....	90
Fig. 4-27: Mesh geometry and pile caps .....	91
Fig. 4-28: Horizontal soil displacement.....	92
Fig. 4-29: Piles row deflection and bending moment.....	92
Fig. 4-30: Construction site plane and section of the studied building.....	93
Fig. 4-31: The construction stages of the panels adjacent to the studied building .....	94
Fig. 4-32: Plastic shear strain and mobilized friction angle.....	95
Fig. 4-33: Model Geometry .....	95
Fig. 4-34: Soil settlement.....	96
Fig. 4-35: Piles deflection and bending moment .....	97
Figure 5-1: Relation between plastic shear strain and mobilized friction angle.....	100
Figure 5-2: Model groups and parametric study parameters .....	105
Figure 5-3: Parameters combinations of Part I .....	107
Figure 5-4: Parameters combination of Part I.....	108
Figure 5-5: Planes of model group 1.....	109
Figure 5-6: Plane of model group 2 .....	110
Figure 5-7: Parameters combination of Part II .....	111
Figure 5-8: Typical mesh geometry of Part II model groups.....	111
Figure 5-9: Planes of Part III model .....	113
Figure 5-10: Parameters combination of Part III .....	113
Figure 5-11: Typical mesh geometry of Part III model groups .....	114
Figure 5-12: Pile deflection and bending moment for parameter combination (PI-MG1-C1) at pile offset distance (x) = 2.0 m .....	115
Figure 5-13: Pile shaft friction for parameter combination (PI-MG1-C1) .....	115
Figure 5-14: Pile deflection and bending moment for parameter combination (PI-MG1-C2) at pile offset distance (x) = 2.0 m .....	116
Figure 5-15: Pile shaft friction for parameter combination (PI-MG1-C2) .....	116
Figure 5-16: Piles deflection and bending moment for parameter combination (PI-MG1-C3) at x = 3.5 m (in the same pile group) .....	118
Figure 5-17: Pile shaft friction for parameter combination (PI-MG1-C3) at x = 3.5 m..	119
Figure 5-18: Pile deflection and bending moment at different offsite distances for parameter combination (PI-MG1-C3) for Panel length (L = 6.0 m) and Pile (P1) .....	119
Figure 5-19: Pile shaft friction for parameter combination (PI-MG1-C3) .....	120

Figure 5-20: Pile deflection and bending moment at different groundwater levels for parameter combination (PI-MG1-C4).....	121
Figure 5-21: Pile shaft friction at different groundwater levels for parameter combination (PI-MG1-C4).....	121
Figure 5-22: Pile deflection and bending moment at different slurry levels for parameter combination (PI-MG1-C5) for panel length = 6.0 m.....	122
Figure 5-23: Pile shaft friction at different slurry levels for parameter combination (PI-MG1-C5).....	122
Figure 5-24: Pile deflection and bending moment at different groundwater levels for parameter combination (PI-MG1-C6) at slurry level (SL = 1.0 m).....	123
Figure 5-25: Pile shaft friction at different slurry levels for parameter combination (PI-MG1-C6).....	124
Figure 5-26: Pile deflection and bending moment at different slurry pressure reduction levels for parameter combination (PI-MG1-C7) at $x = 2.0$ m and SL = 0.5 m .....	125
Figure 5-27: Pile shaft friction at different slurry pressure reduction levels for parameter combination (PI-MG1-C7) at SL = 0.5 m.....	125
Figure 5-28: Pile deflection and bending moment at different values of pile impeded length for parameter combination (PI-MG1-C8) and trench depth (H=30m) .....	126
Figure 5-29: Pile shaft friction at different values of pile impeded length for parameter combination (PI-MG1-C8).....	126
Figure 5-30: Pile deflection and bending moment at different pile diameter values (PI-MG1-C9) and at trench depth (H=30 m) .....	127
Figure 5-31: Pile shaft friction at different pile diameter values (PI-MG1-C9).....	127
Figure 5-32: Pile deflection and bending moment of piles within model group (MG2) at slurry level (SL=0.5m).....	128
Figure 5-33: Pile shaft friction of piles within model group (MG2) at slurry level (SL = 0.5 m) .....	128
Figure 5-34: Pile deflection and bending moment within model group (MG3) at slurry level (SL = 0.5 m).....	129
Figure 5-35: Pile shaft friction at different of piles within model group (MG3) at slurry level (SL = 0.5 m) .....	129
Figure 5-36: Pile deflection and bending moment of piles within model group (MG4) at slurry level (SL=0.5m).....	130

Figure 5-37: Shaft friction of piles within model group (MG4) at slurry level (SL = 0.5 m)	130
Figure 5-38: Pile deflection and bending moment at different formations	131
Figure 5-39: Shaft friction of piles at different formations	131
Figure 5-40: Deflection and bending moment of piles near double or single panel at slurry level	133
Figure 5-41: Shaft friction of piles near double or single panel	133
Figure 5-42: Deflection and bending moment of piles near double or single panel at slurry level (SL = 0.5 m) and at slurry reduction position (SP = 13.0 to 14.0 m)	134
Figure 5-43: Pile shaft friction at slurry reduction position (SP = 13.0 to 14.0 m)	134
Figure 5-44: Pile deflection and bending moment for first pile within pile group (G <sub>1-5</sub> )	135
Figure 5-45: Pile deflection and bending moment for the first row of pile groups parallel to the trench (Row <sub>L1</sub> )	136
Figure 5-46: Pile shaft friction for the first and third pile groups rows parallel to the trench	136
Figure 5-47: Pile deflection and bending moment for the first row of pile groups perpendicular to the trench (Row <sub>p5</sub> )	137
Figure 5-48: Pile shaft friction at slurry reduction position (SP = 13.0 to 14.0 m)	138
Figure 5-49: Pile deflection and bending moment for different groundwater levels at G1-5	138
Figure 5-50: Pile shaft friction for different groundwater levels	139
Figure 5-51: Pile deflection and bending moment at different slurry pressure reduction positions (SP) and at slurry levels for pile group G <sub>1-5</sub>	140
Figure 5-52: Pile shaft friction at different slurry pressure reduction positions (SP) and at slurry levels	140
Figure 5-53: Pile deflection and bending moment at different panel lengths	141
Figure 5-54: Pile deflection and bending moment for pile models MG1 and MG2 for the first row (R <sub>L1</sub> )	141
Figure 5-55: Pile deflection and bending moment at different panels construction stages for pile P <sub>1-11</sub>	142
Figure 5-56: Pile shaft friction at different panels construction stages	143
Figure 5-57: Pile deflection and bending moment for piles within the first row parallel to the trench (R <sub>L1</sub> )	144
Figure 5-58: Pile shaft friction at different panels construction stages	144



Figure 5-59: Pile deflection and bending moment of pile P1-11 for different groundwater levels .....	145
Figure 5-60: Pile deflection and bending moment for different panel lengths .....	146
Figure 5-61: Pile deflection and bending moment for some piles within the first row parallel to the trench ( $R_{L1}$ ) in model group MG1 and corresponding piles in MG2...146	
Figure 5-62: Pile deflection and bending moment for some piles in Part II compared to corresponding piles in Part III at slurry level ( $SL = 0.5$ m).....	147
Figure 5-63: Pile shaft friction for some piles in Part II and corresponding piles in Part III .....	148
Figure 5-64: Correction of reduction factor related to distance from the trench.....	153
Figure 6-1: Pile above the failure surface (two-dimensional approach).....	156
Figure 6-2: Pile above the failure surface (three-dimensional approach).....	159
Figure 6-3: Pile intersects the failure surface (two-dimensional approach) .....	161
Figure 6-4: Pile intersects the failure surface (three-dimensional approach) .....	163
Figure 6-5: Several piles intersect the failure surface (three-dimensional approach) .....	164
Figure 6-6: Effect of different friction angles on factor of safety (two-dimensional approach).....	165
Figure 6-7: Effect of different slurry densities on factor of safety (two-dimensional approach).....	165
Figure 6-8: Effect of different water levels on factor of safety (two-dimensional approach) .....	166
Figure 6-9: Effect of pile location on factor of safety (two-dimensional approach) .....	166
Figure 6-10: Difference between two and three dimensional analytical approaches .....	167
Figure 6-11: Effect of panel length at different pile locations on safety factor.....	167
Figure 6-12: Effect of failure surface inclination angle on safety factor .....	168
Figure 6-13: Effect of slurry level on safety factor.....	168
Figure 6-14: The cases used for comparison .....	169
Figure 6-15: Comparison between the different cases.....	169
Figure 6-16: Typical numerical modeling mesh for factor of safety calculation .....	170
Figure B-1: Pile deflection and bending moment for parameter combination (PI-MG1-C1) for pile offset distance ( $x$ ) = 3.5 m.....	B-1
Figure B-2: Pile deflection and bending moment for parameter combination (PI-MG1-C2) for pile offset distance ( $x$ ) = 3.5 m.....	B-1
Figure B-3: Piles deflection and bending moment for parameter combination (PI-MG1-C3) .....	B-2

Figure B-4: Piles shaft friction for parameter combination (PI-MG1-C3).....	B-3
Figure B-5: Pile deflection and bending moment for parameter combination (PI-MG1-C3) for panel length (L=3.0m).....	B-3
Figure B-6: Pile deflection and bending moment for parameter combination (PI-MG1-C5) for panel length (L=3.0m).....	B-3
Figure B-7: Pile deflection and bending moment for parameter combination (PI-MG1-C6) for slurry level of 0.5m .....	B-4
Figure B-8: Pile deflection and bending moment for parameter combination (PI-MG1-C7) for pile offset distance (x) = 3.5 m.....	B-4
Figure B-9: Pile shaft friction at different slurry pressure reduction levels for parameter combination (PI-MG1-C7) at SL = 0.5 m.....	B-4
Figure B-10: Pile deflection and bending moment for at different values of pile impeded length for parameter combination (PI-MG1-C8) at trench depth 20m .....	B-5
Figure B-11: Pile deflection and bending moment for at different values of piles diameter (PI-MG1-C8) at trench depth 20m.....	B-5
Figure B-12: Pile deflection and bending moment at different values of pile impeded length for parameter combination (PI-MG2-C1) at slurry level (SL = 1.5 m) .....	B-5
Figure B-13: Pile deflection and bending moment for different piles within the model group (PI-MG3-C1) at slurry level (SL = 1.5 m).....	B-6
Figure B-14: Pile deflection and bending moment for different piles within the model group (PI-MG4-C1) at slurry level (SL = 1.5 m).....	B-6
Figure B-15: Pile deflection and bending moment for different pile formations at slurry level.....	B-6
Figure B-16: Pile deflection and bending moment of piles within model group (MG2) at slurry reduction position (SP = 13.0 to 14.0 m).....	B-7
Figure B-17: Pile shaft friction at different values of piles within model group (MG2) at slurry reduction position (SP = 13.0 to 14.0 m) and slurry level.....	B-7
Figure B-18: Pile deflection and bending moment of piles within model group (MG3) at slurry reduction position (SP = 13.0 to 14.0 m) and slurry level (SL = 1.0m) .....	B-8
Figure B-19: Pile shaft friction at different values of piles within model group (MG3) at slurry reduction position (SP = 13.0 to 14.0 m).....	B-8
Figure B-20: Pile deflection and bending moment of piles within model group (MG4) at slurry reduction position (SP = 13.0 to 14.0 m).....	B-9

Figure B-21: Pile shaft friction at different values of piles within model group (MG4) at slurry reduction position (SP = 13.0 to 14.0 m).....	B-9
Figure B-22: Pile deflection and bending moment at different formations and slurry reduction position (SP = 13.0 to 14.0 m).....	B-10
Figure B-23: Pile shaft friction at different formations and slurry reduction position ..	B-10
Figure B-24: Pile deflection and bending moment near double panel or single panel with different lengths (SL =1.5).....	B-11
Figure B-25: Pile deflection and bending moment near double panel or single panel with different lengths (SP= 13.0 to 14.0m) and (SL =1.0) .....	B-11
Figure B-26: Pile deflection and bending moment for first pile in different pile groups .....	B-12
Figure B-27: Pile deflection and bending moment for Row <sub>L3</sub> .....	B-12
Figure B-28: Pile deflection and bending moment for Row <sub>p9</sub> .....	B-13
Figure B-29: Pile deflection and bending moment for different groundwater levels for G <sub>6-1</sub> .....	B-13
Figure B-30: Pile deflection and bending moment at different slurry pressure reduction positions and slurry levels G <sub>6-1</sub> .....	B-13
Figure B-31: Pile deflection and bending moment for different pile group models formation at Row <sub>L4</sub> .....	B-14
Figure B-32: Pile deflection and bending moment at different panels construction stages for pile P15-11 .....	B-14
Figure B-33: Pile deflection and bending moment for different piles within the middle row perpendicular to the trench (Row <sub>p11</sub> ) .....	B-14
Figure B-34: Pile deflection and bending moment for different groundwater levels for pile P <sub>15-21</sub> .....	B-15
Figure B-35: Pile deflection and bending moment for different model groups and piles in the middle row perpendicular to the trench (Row <sub>p11</sub> ) .....	B-15
Figure B-36: Pile deflection and bending moment for some piles in Part II compared to corresponding piles in Part III at slurry level (SL =1.5 m).....	B-15

## LIST OF TABLES

<i>Number</i>	<i>Page</i>
Table 2-1: different slurry trenching analytical methods.....	28
Table 3-1: Effect of wall installation on K-value (Symons and Carder, 1993).....	38
Table 3-2: Ground displacement from primary activities (Korff, 2013).....	51
Table 3-3: Summary of successful centrifuge tests (Choy, 2004).....	52
Table 3-4: Summary of diaphragm wall installation field results.....	58
Table 4-1: Field test soil properties .....	69
Table 4-2: Laboratory test pile properties.....	77
Table 4-3: Interface friction angles of the different pile segments.....	77
Table 4-4: Soil properties at the basement location.....	94
Table 5-1: Soil properties used in the parametric study .....	100
Table 5-2: Piles properties used in the parametric study .....	102
Table 5-3: Percentage of change in pile deflection between MG1 and MG2.....	147
Table 5-4: Percentage of change in pile behavior due to all studied parameters.....	148
Table 5-5: Shaft friction coefficient reduction factor due to trenching ( $k_r$ ).....	150
Table 6-1: Different studied cases for trench stability.....	171

## LIST OF NOTATIONS

$A_b$	cross section area of the pile base
$A_s$	the surface area of the pile
$B$	trench width (Panel thickness)
$c'$	drained shear strength
$D$	pile diameter
$E$	deformation modulus (young's modulus)
$E_i$	initial tangent modulus
$E_{oed}$	oedometer stiffness modulus
$E_{oed}$	oedometer stiffness modulus
$E_{50}^{ref}$	secant stiffness in standard drained triaxial test
$E_{oed}^{ref}$	tangent stiffness for primary oedometer loading
$E_{ur}^{ref}$	unloading-reloading reference deformation modulus
$f_b$	pile end bearing force
$f_{bh}$	pile horizontal force acting on the trench wall
$F_{hp}$	pile passive earth pressure force
$F_{pr}$	pile resisting force for the sliding wedge
$f_s$	pile shear force
$FS$	factor of safety
$F_s$	minimum factor of safety (corresponding to $\theta_{cr}$ )
$G$	soil shear modulus
$H$	trench depth
$H_{cr}$	critical high
$H_{max}$	maximum trench depth
$H_p$	pile length inside
$H_s$	depth of slurry
$H_w$	water depth
$i_o$	stagnation gradient
$K$	soil bulk modulus
$K_a$	active earth pressure
$K_n$	normal stiffness
$K_o$	at rest earth pressure
$K_p$	passive earth pressure

$K_s$	shear stiffness
$L$	trench length
$N$	reaction normal to the sliding surface
$N_c$	pile bearing capacity factor
$P$	applied load in pile
$P_a$	active earth pressure
$P_f$	slurry pressure
$P_h$	horizontal pressure
$P_s$	slurry pressure
$P_u$	pile limiting pressure
$P_w$	water pressure
$q$	surcharge load
$q_b$	pile base resistance (end-bearing pressure)
$Q_b$	pile bearing capacity
$q_{bL}$	limit base resistance
$q_c$	cone penetration test resistance
$q_r$	surcharge transfer to the side of the panel
$Q_s$	pile friction capacity
$q_s$	surcharge load
$Q_{tot}$	total pile capacity
$s$	soil settlement
$S$	shear force acting along the base of sliding surface
$s_p$	pile settlement
$s_{pb}$	pile settlement due to its tip load
$s_{pe}$	pile elastic shortening
$s_{pf}$	Pile settlement due to load transfer through friction
$S_s$	the side of the panel shear resistance
$s_u$	undrained shear strength
$T$	trench thickness
$W$	weight of the wedge
$x$	distance of pile from the trench
$x_t$	distance of ground surface settlement from the trench
$Z_w$	water depth from the surface
$\delta$	interface friction angle
$\delta_h$	horizontal displacement

$\delta_v$	vertical displacement
$\epsilon_f$	strain needed to mobilize the limit friction angle
$\epsilon_p$	plastic strain
$\phi$	effective friction angle
$\phi_n$	interface normal friction angle
$\phi_s$	interface shear friction angle
$\gamma$	unit weight of soil
$\gamma'$	effective unit weight of soil
$\gamma'_f$	effective unit weight of the fluid on the trench
$\gamma_{bs}$	buoyant unit weight of the slurry-saturated soil
$\gamma_f$	unit weight of the fluid on the trench
$\gamma_{ss}$	total unit weight of the soil when it saturated with the slurry
$\theta$	angle of bottom failure plane from horizontal
$\theta_{cr}$	critical angle of bottom failure plane from horizontal (corresponding to $F_s$ )
$\rho$	mass density
$\sigma'_v$	effective stress
$\sigma'_h$	effective horizontal stress
$\sigma_{ij}$	stress tensor components
$\sigma_n$	normal stress
$\sigma'_n$	effective normal stress
$\sigma'_{rc}$	radial effective stress after consolidation
$\sigma'_{ri}$	initial radial effective stress
$\sigma_{v0}$	overburden pressure
$\sigma'_{v0}$	effective overburden pressure
$\tau_s$	shear strength
$\psi$	dilation angle





# CHAPTER 1: INTRODUCTION

## 1.1 BACKGROUND

Deep excavations are required for several purposes inside cities and they can be achieved by several techniques. For several decades, the diaphragm walls (slurry walls) have been widely used as a technique for conducting such deep excavations, especially inside the cities. However, the installation of diaphragm walls in the crowded cities could be a challenge because it causes deformation for the surrounding ground which may have an effect on the nearby existing buildings. The deep foundation type is commonly used as a foundation system for such buildings inside the cities specially under the high-rise buildings. For this reason, the construction of the diaphragm wall near the deep foundations might not be avoided. The need to study the effect of the diaphragm wall installation on the existing deep foundation and the effect of existing deep foundation on the stability of the slurry trench are considered an important research topic. However, there are very limited studies regarding this issue and many questions are still need to be understood and this research was conducted to be a step for answering such questions.

The stability of the slurry trench is not always an indication of the low soil deformation around the trench because such deformation depends on several factors including soil properties, dimension of the slurry trench, groundwater table and slurry level, etc...., some of these factors cause a higher effect than others. A high deformation could happen as an example due to factors that are not included in the design such as low slurry level, rising in groundwater table or discontinuity of slurry pressure. In some cases, the deformation due to slurry trench could be higher than that due to deep excavation.

The ground deformation during the trenching process is divided into vertical and horizontal movement. The vertical movement is the settlement around the trench and it decreases with the distance far from the trench until it is considered to be negligible at a distance equal to double the trench depth. The horizontal movement is a soil displacement towards the trench and the shape of it is mainly depending on the soil profile. This ground deformation is transferred to the existing piled foundations which were mainly designed to sustain vertical loading with an appropriate factor of safety. Such a vertical load is assumed to be balanced with the end bearing and skin friction forces generated by the piles which also should be designed for a specified settlement. Accordingly, this ground deformation would affect the existing piles. The horizontal movement of the soil creates a passive load on the pile. This passive load causes a bending moment on the pile which probably was not designed for such a moment. In addition,

the trenching process reduces the coefficient of earth pressure, which in turn affects the pile skin friction capacity. In this case, the existing pile that was designed with a critical safety factor could suffer damage or total dysfunction. However, if this pile as in normal cases is within a connected group of piles or piled raft its load could be carried by the other piles that are at far distance from the trench.

The ground deformation due to trenching is normally measured in the field. It can be predicted using numerical analysis which is considered as an acceptable tool in simulation of the different geotechnical engineering problems. However, only the three-dimensional analysis will provide reliable results because the trench panel excavated inside the soil considered a three-dimensional problem. In the same line, the calculation of the trench stability using two-dimensional analysis provide low values of factor of safety compared to the three-dimensional analysis.

## 1.2 AIMS OF THE RESEARCH

Several researchers studied the trenching process and its effect on ground surface. However, the previous research work regarding the effect of such process on piles was limited and it did not draw a full picture of such problem. The main objective of this research is to study the effect of the trenching process near piled foundations. In order to understand such a problem, a three-dimensional numerical analysis was conducted using commercial software FLAC3D which uses finite difference analysis. This numerical analysis method was calibrated with the field and laboratory data. It was used to form a parametric study that provides a better understanding of the problem. The stability of the panel that is trenched near a piled foundation was presented through several equations that calculate the factor of safety.

The main research program objectives were as follows:

- Collection of the available field data and laboratory testing results related to trenching process.
- Verification of a numerical modeling method that can be used to simulate the slurry trenching process near piled foundation using previous data from the field and the laboratory works.
- Creation of a numerical parametric study that shows the effect of slurry trenching process on nearby piled foundation.
- Study of several parameters combinations that represent realistic cases from the normal field works.
- Discussion of the stability of the slurry trench panel that located near existing pile(s) by using the wedge analysis method.

- Derivation of equations that calculate the factor of safety of diaphragm wall panels that are trenched near the pile.

### 1.3 RESEARCH CONTENT (THESIS LAYOUT)

This research contains 7 chapters and 2 appendices. Chapter 2 discusses the literature review that includes two main parts. The first part provides a general overview of the deep foundations stress-strain mechanism. It discusses the pile or pile group that is subjected to either vertical or lateral load. The different types of passive lateral load and their effect on the pile are also discussed. The second part presents the diaphragm wall installation process. It shows the different methods of calculating the trench stability and ground deformation during the trenching process.

Chapter 3 presents the available data from the field and the laboratory works related to the diaphragm wall installation process. These data include the soil settlement, the horizontal displacement and the change of lateral earth pressure. The maximum and minimum values of ground deformation and earth pressure coefficient collected from different projects are presented.

Chapter 4 describes the numerical analysis method that can be used to simulate the interaction between the slurry trench and the existing piled foundation. Verify such method by modeling field and laboratory works that are available from the literature.

Chapter 5 creates a numerical parametric study related to the effect of the trenching process on nearby piles. It explains the effect of each parameter separately or combined with other parameters. It provides a reduction factor for the pile skin friction coefficient based on the parametric study results.

Chapter 6 studies the stability of single panel that is trenched near a piled foundation. It provides an analytical approach that can be used to solve such a problem.

Chapter 7 summarizes the main conclusions and discusses what can be recommended for future work.

Appendix A shows the code used for modeling with FLAC 3D.

Appendix B presents some of the parametric study results.

## CHAPTER 2: LITERATURE REVIEW

### 2.1 INTRODUCTION

The installation of the diaphragm walls causes deformation and change in stresses in the surrounding soil. The nearby existing piled foundation could be affected by such a construction process. Since there is only a very limited information about the direct effect of slurry trenching on piled foundations, this chapter discusses in general the behavior of the existing pile under normal condition and then goes through the effect of different other construction activities on the behavior of nearby piles such as embankment construction, slope and deep excavations. The slurry trench stability and deformation attract the attention of many researchers who tried to understand the stress mechanism around the trench. Understanding of such a mechanism will possibly help to find out the effect of slurry trench on piles.

The mechanism of the stress and strain in the piled foundation for bored and driven piles is discussed in section 2.2 which includes the pile capacity and the effect of passive loading on the pile behavior. Section 2.3 focuses on diaphragm wall installation including bentonite slurry, trench stability and deformation prediction methods. The last section 2.4 provides a summary of the chapter.

### 2.2 DEEP FOUNDATION STRESS STRAIN MECHANISM (PILE FOUNDATION)

Deep foundations are very common structural elements used for engineering projects for different purposes. The design of deep foundation until now depends on empirical methods. The installation method greatly affects the design of pile (Tomlinson and Woodward, 2008). On the other hand Fleming et al. (2009) showed that not only soil conditions are the important factor for design of deep foundation, but also the structure condition such as the allowable settlement or tilt also playing a big role. In contrast, Poulos (1989) showed that the geotechnical characterization of the site is considered to be more effective than the analysis method. The philosophy of the pile behavior is not so clear but generally, the pressure distribution and soil disturbance of a single pile are considered to be the same for all types of piles as shown in Figure 2-1 (Tomlinson and Woodward, 2008).

Generally, the pile is subjected to vertical loads such as the buildings load but it could be also subjected to lateral loads. There are two types of lateral load that could be considered. The first one is the direct load which is considered to be an application of external force on the pile and causes the pile to move horizontally and the soil in this case will act passively against the

applied force. The second type is the passive loading which occurred due to the soil movement (Fleming et al., 2009). The different types of loads are to be described in the following sections.

### 2.2.1 PILES UNDER VERTICAL LOAD

During the last decades, the pile bearing capacity calculations are discussed by several researchers. The commonly higher values of factor of safety presented in different code manuals indicate the complication of understanding the pile stress strain mechanism and bearing capacity. Randolph (2003) emphasizes that it is quite impossible to determine the pile axial capacity with an accuracy lower than  $\pm 30\%$  for many soil types and pile tests are the most reliable technique. Generally, the pile carries the load by friction and end bearing. The bearing capacity of the pile is affected mainly by soil characteristics, pile diameter and type. The calculation of the pile ultimate total axial capacity ( $Q_{tot}$ ) is equal to the summation of the pile friction capacity ( $Q_s$ ) and end bearing (base) capacity ( $Q_b$ ) as shown in Figure 2-2.

$$Q_{tot} = Q_b + Q_s = A_b q_b + A_s \tau_s \quad 2.1$$

where:

$A_b$  is the cross section area of the pile base

$q_b$  is the end-bearing pressure

$A_s$  is the surface area of pile shaft

$\tau_s$  is the shear strength of the soil along the pile shaft

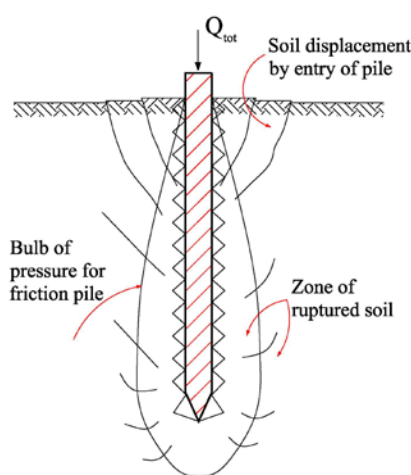


Fig. 2-1: Pressure distribution and soil disturbance for single pile (after Tomlinson and Woodward, 2008)

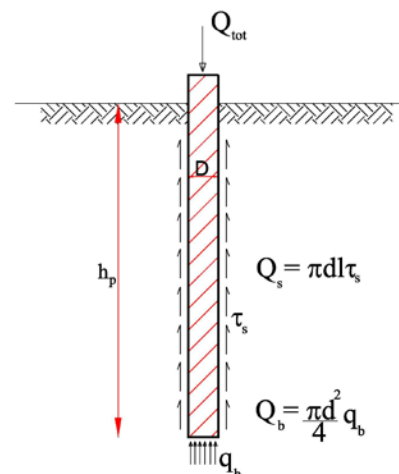


Fig. 2-2: Axially loaded pile (after Fleming et al., 2009)

Tomlinson and Woodward (2007) studied the pile behavior under vertical load as presented in Figure 2-3. The pile that is subjected to load behaves initially elastically until point “A” and by increasing of the load, yielding observed at the pile-soil interface, while slippage happened when the load reaches point “B”. In this case, the shaft friction should be fully mobilized. Point “C” appeared when the load is reversed. They also showed that the friction mobilization

required a settlement of 0.3 % to 1 % of pile diameter, while mobilization of end bearing required settlement of 10 % to 20 % of pile diameter. A large settlement is expected for an additional small amount of load after the full mobilization of the bearing resistance as indicated by point “D”, which also indicates the ultimate limit state. Point E on the curve represents the load that may cause damage or distortion to the structural framework. On the other hand, (Fleming et al. 2009) showed that the mobilization of the pile friction required a displacement of the pile ranges between 0.5 to 2 % of the pile diameter while the pile end bearing mobilization required displacement ranges between 5 to 10 % of the pile diameter. There is quite a difference between the range of displacement that is required for friction and bearing mobilization according to both researchers. In general, the settlement should not exceed 10% according to BS 8004 and the pile concrete capacity should also be taken into consideration. This chapter focused only on the pile capacity on cohesion-less soils.

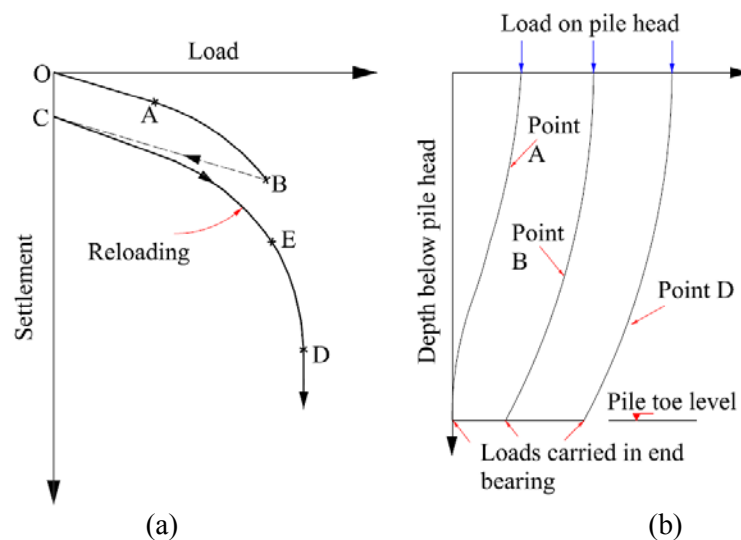


Fig. 2-3: Pile behavior under load (a) Load settlement curve for compressive load to failure in pile (b) Load transfer from head of pile to shaft at points A, B and D (after Tomlinson and Woodward, 2007)

### 2.2.1.1 End-bearing capacity in cohesion-less soil

The calculation of pile end-bearing was discussed by several researchers. Poulos & Davis (1980) showed that the pile critical depth is related to the diameter of the pile. (Randolph et al. 1994) discussed the factors that affect the axial capacity of driven pile in sand. They tried to solve some of the pile design uncertainties (high quality field data, parametric study). They showed that there are two main methods that can determine the driven piles capacity in sand. The first method is based on the friction angle, stiffness and density while the second one relies on results of in situ tests which mainly depend on CPT and SPT. These methods were widely discussed by the American Petroleum Institute (2002).

The end bearing ( $q_b$ ) can be calculated according to Meyerhof (1976) using the following equation

$$q_b = N_q \sigma'_v \quad 2.2$$

where:  $N_q$  is the bearing capacity factor range from 8 to 12 for loose sand and more than 40 for very dense sand (API, 2002). It varies with the friction angle  $\phi'$ .  $\sigma'_v$  is the effective vertical stress.

The end bearing resistance increases with depth but it become constant at certain depth (Randolph, 2003). Similarly, Kulhawy (1984) showed that the increase in length of the driven pile in sand not necessarily increases the pile end bearing capacity. The relation between the end-bearing pressure and the effective stress shows a nonlinear increase with depth in reducing rate (Fleming et al. 2009). There are two factors, which describe this gradual decrease.

1. There is inverse proportionality between secant friction angle and mean stress at failure (Bolton, 1986)
2. The ratio of shear stiffness to strength (rigidity index) is inversely proportional to the shear strength

Randolph et al. (1994) showed that under the pile tip an assumed rigid cone of soil with angle  $\alpha$  can be estimated from the angle of friction. There is a soil zone outside this region and it is subjected to isotropic stress which is equal to the limit pressure  $P_{lim}$  that is shown in Figure 2-4. The following equation shows the estimation of end-bearing from limit pressure.

$$q_b = p_{lim} (1 + \tan \phi' \tan \alpha) \quad 2.3$$

The value of limit pressure for cohesionless soil was discussed and evaluated by Yu and Houlsby (1991) and Carter et al. (1986) in their closed form solution. Both solutions have used Mohr-Coulomb elastic perfectly plastic model. They depended on several parameters such as effective stress  $p'_o$ , friction angle  $\phi'$ , dilation angle  $\psi$ , Poisson's ratio  $\nu$  and shear modulus  $G$ .

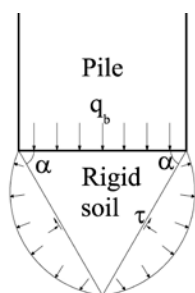


Fig. 2-4: Relation of cavity expansion limit pressure and end-bearing capacity (after Randolph et al., 1994)

### 2.2.1.2 Shaft friction capacity in cohesion-less Soil

The shaft friction (side resistance)  $\tau_s$  depends on the normal effective stress  $\sigma'_n$  and the friction angle between the pile and the soil, the normal effective stress  $\sigma'_n$  is directly proportional with

the vertical effective stress  $\sigma'_v$  with a ratio of  $k$ . The shaft friction can be calculated according to Meyerhof (1976) from the following equation

$$\tau_s = \sigma'_n \tan \delta = k \sigma'_v \tan \delta \quad 2.4$$

The angle of friction between soil and pile  $\delta$  was studied by Kishida and Uesugi (1987). They have studied the surface roughness effect and discussed a relation between the interface friction angle  $\delta$  and the soil friction angle  $\phi$ . Such a relation could be presented according to soil properties and material of the pile surface, a range of 0.75 to 1 was suggested for  $\delta / \phi$ .

The effective stress ratio  $k$  depends on three main factors, the in-situ coefficient of earth pressure, the pile installation method and the sand initial density (Fleming et al., 2009). In sandy soils, the pile shaft capacity during pile driving increases with depth until it reaches a certain depth and then it could be limited or even decreased (Vesic 1969; Vesic 1977). A research group in Imperial College, UK (Lehane et al., 1993) studied the pile shaft friction in sand with pile depth using instrumented pile tests in centrifuge. Figure 2-5 shows the local shear stress (shaft friction) with the instrumented depth, which is characterized by three clusters according to distance from pile tip along the shaft ( $h$ ) normalized by 0.1 m pile diameter ( $h/d$ ). The cone resistance ( $q_c$ ) results factorized by 100 are also plotted for comparison purposes. The factorized cone resistance values ( $q_c/100$ ) are closer to that shown by the shaft friction measured near to the pile tip.

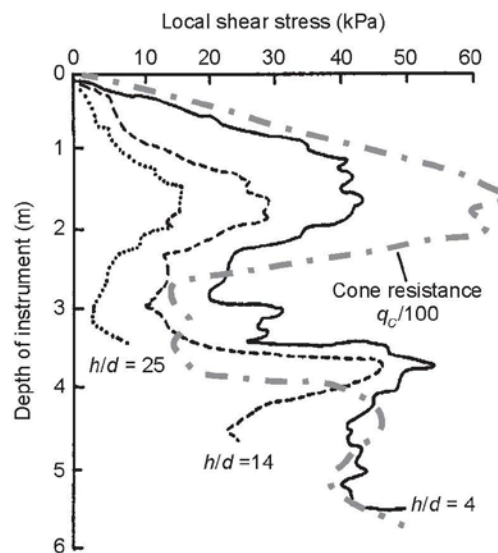


Fig. 2-5: measured profiles of shaft friction (Lehane et al., 1993)

### 2.2.1.3 Pile settlement due to vertical load

The calculation of pile settlement is based on the empirical correlation while the best way to determine the pile settlement is through the pile load test. The typical shape of the pile settlement curve is shown in Figure 2-6a. Chin (1970) provided a method of estimating the pile ultimate load by plotting the pile settlement due to friction and end bearing and settlement to



pile load  $s/P$  as shown in Figure 2-6b. The first part “A” should represent the settlement due to shaft friction, while part “B” represents the settlement due to end bearing. However, Fleming (1992) found that this could not be strictly true due to the nature of the hyperbolic function of the shaft and base performance and it could lead to over prediction of the ultimate load as well. For this reason he developed a simple hyperbolic function that could be used to analyze pile settlement and took into consideration the elastic shortening of the pile. According to Fleming (1992), the settlement of a single pile can be divided into three main parts.

$$S_{pt} = S_{pc} + S_{pb} + S_{pf} \quad 2.5$$

where:

$S_{pt}$  is the total pile settlement

$S_{pc}$  is the elastic compression of the pile shaft (pile elastic shortening)

$S_{pb}$  is the settlement of the pile tip due to load

$S_{pf}$  is the settlement of the pile due to load transfer through friction to the pile shaft.

The first part of the equation could be ignored if the pile is purely rigid. In most cases, the pile is not considered to be purely rigid and the pile elastic shortening calculation is considered to be complex. A simplification was made by Fleming (1992) by considering the shortening in three stages. He provided a calculation method for the other settlement values based on the hyperbolic function.

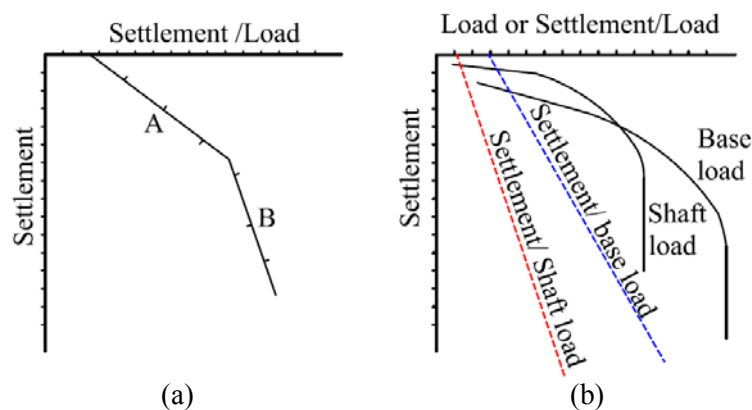


Fig. 2-6: Relationship of settlement and settlement/ load (after Chin, 1970)

An approximate solution was developed by Fleming et al. (2009) in order to understand the way of the load transfer from the pile to the soil under working conditions. The solution was based on studying the response of pile in elastic soil which provides an expression for pile stiffness in a closed form. The manner of load transfer was divided into pile shaft and base. The pile shaft calculation considered the pile surrounded by concentric cylinders of soil, with shear stress of each cylinder. They developed equations that could be used instead of the design charts like that collected and developed by Poulos and Davis (1980).

### 2.2.1.4 Pile group under vertical load

It was accepted by many researchers such as Tomlinson and Woodward (2008) and Fleming et al. (2009), that in most cases the single pile without a group supporting capacity is higher than that in a group. A group effect factor should be taken into consideration for the design of piles in group. Design charts were developed by Poulos and Davis (1980) to show the effect of group on the pile. The design charts include the spacing, number and size of piles, etc...

### 2.2.2 PILE SUBJECTED TO DIRECT LATERAL LOAD

The soil response for direct lateral load on piles was summarized by Reese and van Impe (2001) and they showed that the reaction modulus that could be used for lateral piled load design is defined by the depth below ground surface  $z$  and pile deflection  $y$ . The unit stress distribution before and after lateral load on pile is described in Figure 2-7.

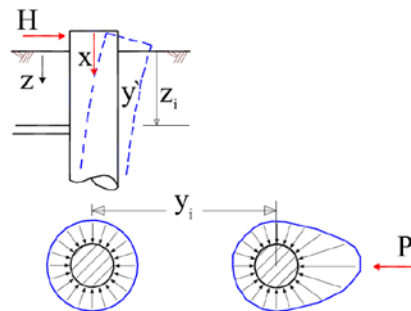


Fig. 2-7: Distribution of unit stress before and after lateral load (after Reese & van Impe, 2001)

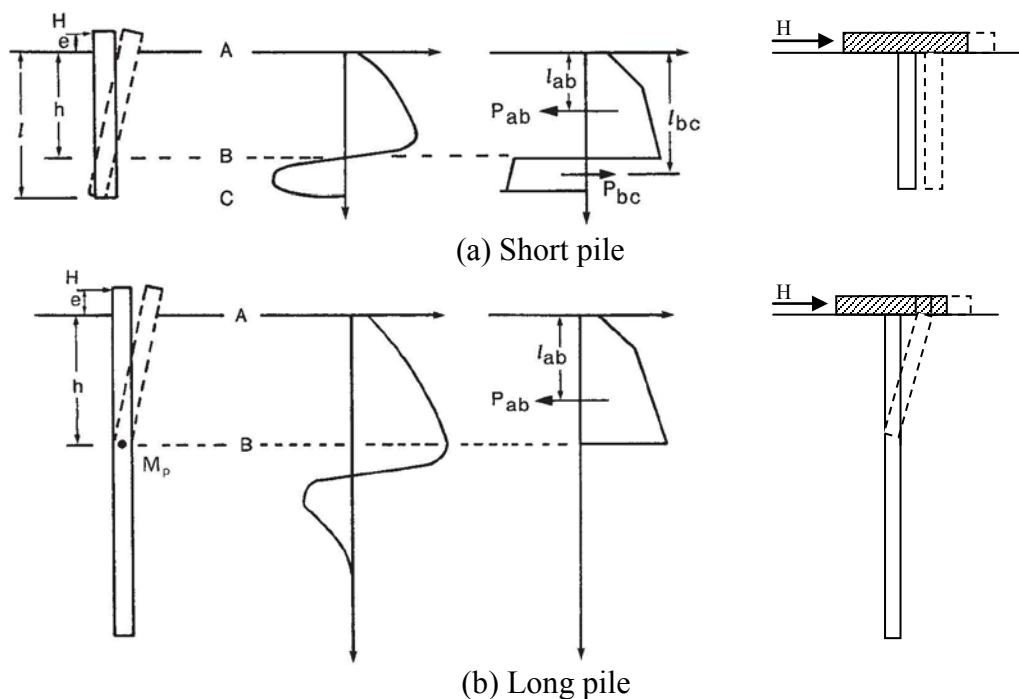


Fig. 2-8: Variation of soil resistance along laterally loaded piles (Fleming et al., 2009)

There are two modes of pile collapse and they are classified into short and long piles. The pile that rotates as a rigid body is called short pile, and that which rotates in upper part above a

plastic point is called long pile (Fleming et al., 2009). Figure 2-8 shows the variation of soil resistance according to the classification of short and long piles for unrestrained piles and restrained piles. The mechanism of failure affects the bending moment shape and calculation type. In order to know the pile behavior whether it act as short or long pile the stiffness factors are determined which depend on the “EI” values.

The plastic moment for a short pile is calculated as  $P_{bc}(l_{bc}-h)$ , where  $h$  is the depth of hinge point and  $P$  is the relevant equivalent force. The maximum horizontal force can be calculated from the force and equilibrium moment equations. The plastic moment for long piles is equal to that at axis B, while the pressure acting below it can be ignored. The maximum horizontal force can be calculated by the equilibrium moment equation.

### 2.2.2.1 Ultimate lateral capacity

The calculation of the pile ultimate resistance depends on the soil type (cohesive or cohesionless soil) and the pile mode of failure (short or long). Hansen (1961) developed a method that can be used to determine the ultimate lateral capacity ( $H_u$ ) of short rigid piles. The main idea was depending on calculating the moment about the point of rotation “x”. Horizontal elements were used to divide the passive resistance diagram as shown in Figure 2-9.

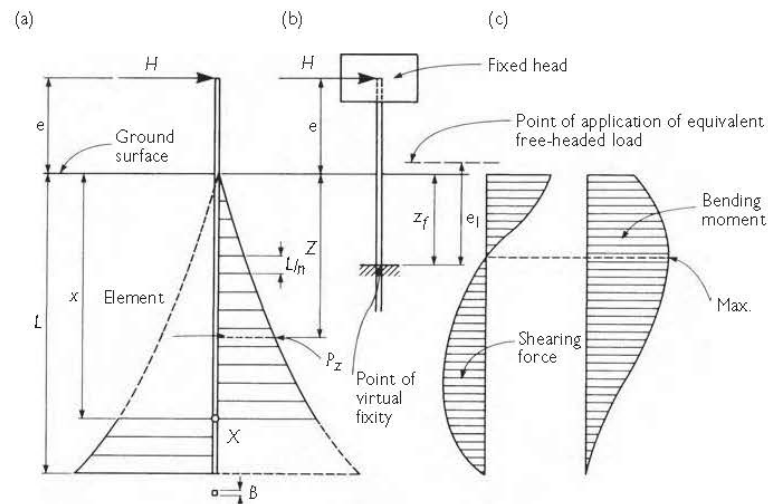


Fig. 2-9: Hansen’s method for calculating ultimate lateral resistance of short piles (a) soil reactions (b) shearing force diagram (c) bending moment diagram (Hansen, 1961)

The unit passive resistance can then be calculated for each element, which also depends on the passive pressure friction and cohesion coefficients. By calculating the moment at point “x” which is equal to zero, the value of ultimate pile horizontal resistance  $H_u$  can be calculated from Equation 2.6

$$H_u(e + x) = \sum_0^x p_z \frac{L}{n} B(x - z) + \sum_x^{x+L} p_z \frac{L}{n} + B(z - x) \quad 2.6$$

The maximum moment can then be calculated at the point of zero shear and it should not exceed the ultimate moment of resistance  $M_u$ . Fleming et al. (2009) finalized design charts that can be used to determine the soil resistance for short and long piles in cohesion-less soils.

### 2.2.2.2 Deflection of piles under lateral load

Matlock and Reese (1960) suggested a subgrade reaction approach that used the coefficient of subgrade reaction ( $k$ ) in order to calculate the pile lateral deflection and also calculate the pile shear force and bending moment. Another approach was studied by Randolph (1981) based on finite element and boundary element modeling and is known as the elastic continuum approach. The pile deflection under lateral load is at its upper part and it may extend to about 10 times its diameter (Fleming et al., 2009). The tolerable limits of pile lateral deflection can be defined by simple methods. One of these methods is described by (Tomlinson, Woodward 2008). They assumed that the pile at an arbitrary depth is fixed. According to Figure 2-9, the deflection that of free head and fixed head piles can be calculated from Equations 2.7 and 2.8, respectively.

$$y = \frac{H(e + z_f)^3}{3EI} \quad 2.7$$

$$y = \frac{H(e + z_f)^3}{12EI} \quad 2.8$$

where:  $H$  is the horizontal working load,  $z_f$  is the assumed depth from ground surface to the virtual fixation point,  $E$  is the elastic modulus of the material forming the pile and  $I$  is the pile moment of inertia.

### 2.2.2.3 P-y Curves

The relation between the pile deflections ( $y$ ) at any depth due to soil resistance ( $p$ ) is known as the P-y curve that is not affected by the pile shape and stiffness. It was first obtained by Rees et al., (1974) for sand. Figure 2-10 shows the typical P-y curves.

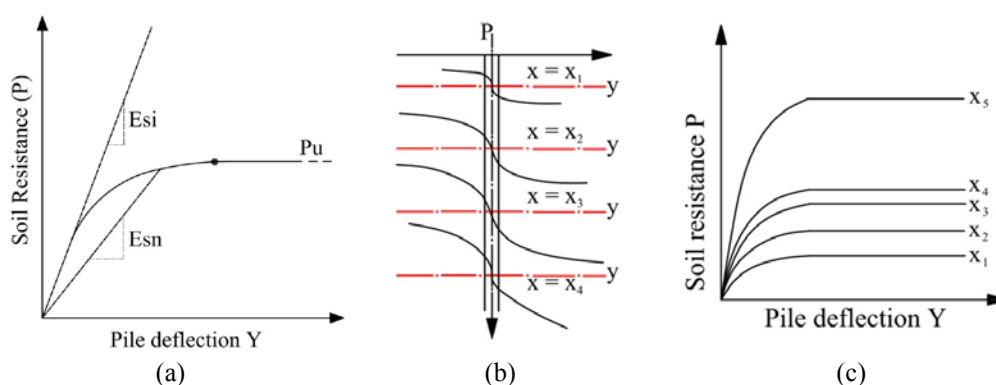


Fig. 2-10: p-y curves for laterally loaded piles (a) typical p-y Curve (b) shape of curves at various depths  $x$  below soil surface (c) family of P-y curves for proposed criteria (after Reese et al. 1974)

### 2.2.2.4 Pile group under lateral load

In general, the laterally loaded pile group forms a block failure as shown in Figure 2.11a, where the load is parallel to the individual blocks (Fleming et al., 2009). They found out that the shear stress  $\tau_s$  shown in Figure 2-11b on the sides of the soil block could be calculated as

$$\tau_s = K \sigma' \nu \tan \phi' \quad 2.9$$

Where  $K$  lies between  $K_o$  and  $K_p$ . In this case, the spacing  $s$  should be

$$s/D < K p^2 / 2K \tan \phi' \quad 2.10$$

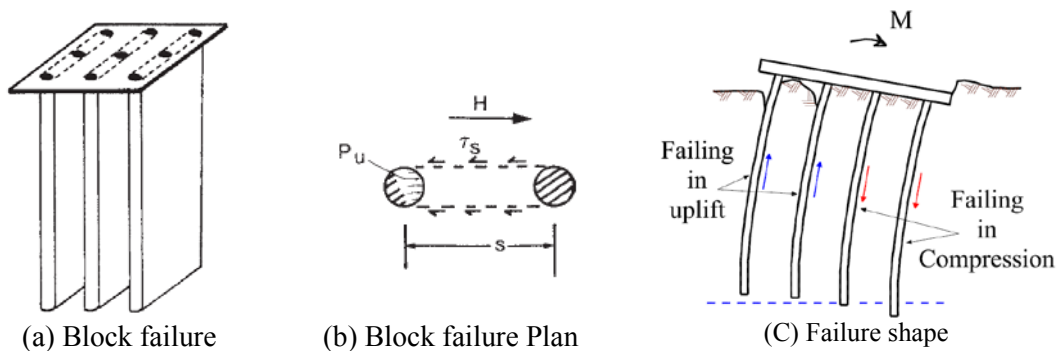


Fig. 2-11: Pile group under lateral load (after Fleming et al., 2009)

The expected failure in the pile group is presented in Figure 2-11c. The group could be subjected to rotation and translation. The compression load of the piles in the back will increase while the front piles compression load will decrease due to the uplift. The capacity of pile will then be calculated based on the original axial load and that one from the lateral loading.

The modification on the p-y curve that was made by Reese and van Impe (2001) included the pile group reduction effect on the individual piles within the group. Such modification is presented in Figure 2-12. It could allow computing the loading of each pile in the group and hence the deflection and bending moment.

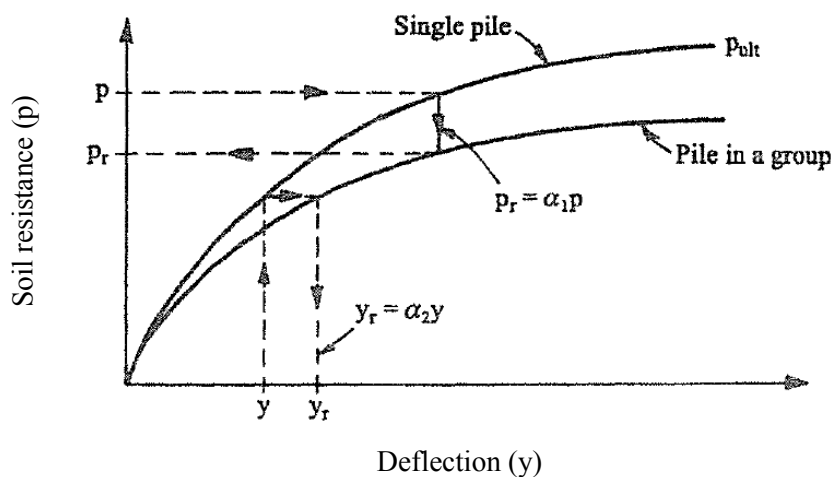


Fig. 2-12: The modified soil resistance for a p-y curve for a single pile in case of pile group interaction (Reese and van Impe, 2001)

### 2.2.3 PILE SUBJECTED TO PASSIVE LATERAL LOAD

The pile could be subjected to passive soil movement due to several reasons, for example the embankments near existing piles, tunneling, piles surrounded by soil subjected to later spread after earth quick, piles near slopes or different types of excavations including slurry trenching.

#### 2.2.3.1 Pile under lateral soil movement (theory)

The pile response under soil lateral movement in general was studied by many researchers. Poulos & Davis (1980) developed an approach based on the elastic interaction between moving soil and pile. They assumed the pile to be a vertical strip divided into elements as shown in Figure 2-13a. The soil was assumed an isotropic elastic material. The soil Young's modulus and resisting force were allowed to vary along the pile. A displacement was imposed between the pile and the adjacent soil to solve the problem. A thin strip equation of flexure was written in finite difference form in order to obtain the pile displacement. The displacement equation could be written as

$$[D]\{\rho\} = \frac{DL^4}{E_p I_p} \{p\} \quad 2.11$$

where:

$\{\rho\}$  Pile-displacement vector

$[D]$  the matrix of the finite difference coefficient

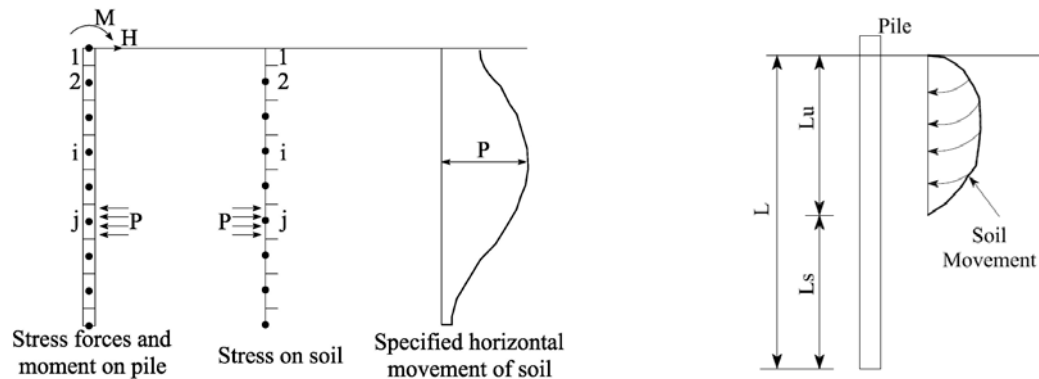
$\{p\}$  horizontal pressure vector

They used this method to develop several charts to examine the pile behavior under different factors including pile diameter, soil movement distribution, boundary conditions, etc...

The lateral response of vertical pile to lateral soil movement was theoretically analyzed by Chen and Poulos (1996). A specified free-field soil movement profile and simplified boundary-element were used to compute the pile response. The finite element was used for simulating the pile group effect. They provided design charts for the pile maximum bending moment and head deflection. Their solution was based on simulating the pile subjected to lateral soil movement as shown in Figure 2-13b, where  $L_u$  is the pile length in the unstable soil layer and  $L_s$  is its length in the stable one. The soil movement was assumed to be only lateral. The pile was modeled as a simple elastic beam while the soil was modeled as an elastic continuum. The horizontal pile soil interaction process and pile stiffness are used to determine the lateral displacement of the pile and the soil elements. The pile flexibility was taken into consideration.

Vertical passive piles subjected to passive loading were elastically analyzed by Xu, Poulos (2001). The boundary pile soil element was used to model the soil and pile interaction. They provide a realistic estimation of the pile behavior under different soil movements.

A series of laboratory tests were conducted by Pan et al. (2002) to study the horizontal soil movement on piles. In their study they focused on the ultimate soil pressure acting along the pile length, in order to understand the interaction between piles and moving soil. They found that in most cases the ultimate soil pressure was inversely proportional to pile spacing.



a: (after Poulos and Davis 1980)

b: (after Chen and Poulos 1996)

Fig. 2-13: Piles in soil undergoing lateral movement

Ghee (2010) took into consideration the vertical load over the pile during subjecting it to lateral soil movement. In his study, he focused on experimental simulation with several parameters such as axial load, the ratio of moving to stable soil layer, soil properties and pile diameter. The group effect of the piles was taken into consideration. Qin and Guo (2013) also discussed the results of Ghee (2010) and they came to the conclusion that the piles arranged in a row of two piles had the same results as those of single pile when subjected to lateral soil movement. The group factor was directly proportional to the pile spacing within the group. The maximum bending moment and shear are in a linear relation for both single pile and piles in a group. Hirari (2016) introduced an analytical approach based on the three-dimensional soil displacement. He found out that the 3-D method did not show a greater difference than Poulos & Davis (1980) 1-D method. Bauer (2016) derived a calculation method for later pressure on piles based on results from numerical parametric study. He defined the main factors that influence the lateral pressure on piles as pile roughness, shape and size in addition to the undrained shear strength of the soil and the strain rate of soil moving around the pile.

### 2.2.3.2 Pile near embankment

Many researchers studied the effect of embankment on nearby piles. Cole (1980) recorded the rotation of a bridge piled foundation in Scotland due to lateral soil pressure below ground surface. Such a pressure was due to the embankment fill near the bridge abutment.

Stewart et al. (1994) performed a series of centrifuge model tests in order to predict a method that can estimate the bending moment and deflection for a pile adjacent to an embankment. The piles were located on a soft clay layer underlying dense sand layer and the embankment was constructed later. They developed design charts for different surcharge loads and pile rigidity.

The method was based on a simple soil deformation mechanism. An approximate soil-pile displacement was assumed. They used a simple triangle displacement mechanism to drive the soil displacement as shown in Figure 14. The lateral displacement  $y_s$  at any depth is related to the average mobilized shear stress  $\tau_{mob}$ . It was calculated based on approximating the lower boundary plasticity solution for the collapse of an infinitely wide strip footing. Active and passive zones of stress were assumed one under the footing and one at the free surface. The pile existence shows the difference in Mohr's circles in the two zones and hence the load carried by the pile can then be estimated. As shown in Figure 2-14, the pile cap was represented by a moment  $M_{head}$  at the top preventing the rotation by allowing deflection. The load  $P_m$  on the pile was chosen to be applied at the location where the soil is displaced more than the pile deflection. Below this zone, the pile is considered to be unloaded and then fixed at the location where the pile did not show any deflection. In this case the pile is equivalent to a cantilever. The relative soil-pile displacement is used to determine the pressure acting on the pile as following.

$$P_m = 5.33G_r(y_s - y_p)/D \quad 2.12$$

where  $y_s$  is soil displacement  
 $y_p$  is pile deflection

$G_r$  is reduced shear modulus in the zone around the pile

Two centrifuge model tests were carried out by Springman et al. (1995) in order to investigate the response of piled full high bridge abutments to the construction sand embankment. They found out that the empirical correlation suggested by Stewart et al. (1994) underestimated the bending moment values of pile groups connected into elevated caps, and adjacent to embankments constructed on deep soft layers.

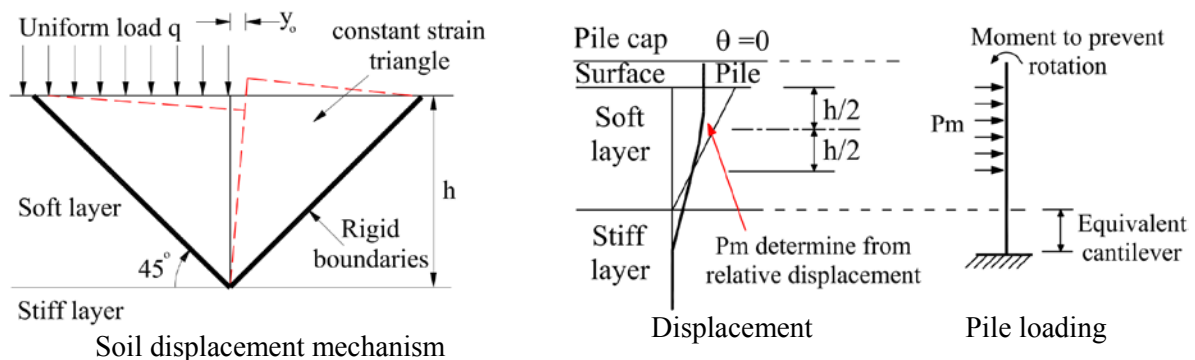


Fig. 2-14: Soil displacement mechanism and loading (after Stewart et al., 1994)

The finite element analysis was used by Goh et al. (1997) to study the embankment effect on the existing single pile. They compared the results from full-scale tests and the centrifuge model tests with their numerical results. They made a parametric study. The results were used to develop an empirical design equation, which can be used to quickly estimate the pile bending moment for the case of piled foundations near sloped embankment base.



### 2.2.3.3 Pile in or near slopes

It is highly expected for piles that support slopes or located near slopes to carry lateral loading. Ito and Matsui (1975) discussed the lateral force on stabilizing piles due to plastic soil deformation. He showed that the distance between the piles in a row affects the value of lateral force acting on the pile. The lateral force is directly proportional to friction angle or cohesion. Poulos (1976) made a theoretical analysis to study the behavior of laterally loaded piles in cohesive soil near to a slope or cut. The elastic theory was used until the soil was allowed to yield. He found that the slope affects pile if it is at a distance less than four diameters from the top of the slope. The effect of slope on piles is influenced by the pile stiffness. Poulos (1995) studied the effect of piles on the slope. He showed that the pile could be used to stabilize the soil slope; however, it could fail due to different slope failure modes. Jeong et al. (2003) simplified a numerical approach in order to analyze the pile subjected to lateral soil movement in a slope. Their study was made with uncoupled pile/slope analysis, where the method was intermediate between continuum analysis (coupled analysis) and the pressure based Bishop's method (uncoupled analysis). In the uncoupled analysis method, they assumed that the failure surface divides the soil into a sliding soil (passive portion) which is supported by a row of piles that transfer the load to the underlying layer (active portion). They first determine the pressure-displacement curves and then they can be used as an input for the beam resting on nonlinear soil spring supports which represent the pile as shown in Figure 2-15. The stabilization of the slope and pile is shown in Figure 2-16, where Bishop method was implemented to determine the critical sliding surface. The pile shear force and bending moment at the location of intersection were used to determine its resisting moment ( $M_{cr}$ ). They found out that the three-dimensional finite element analysis provides a less conservative safety factor than the uncoupled analysis. They recommended that the pile top should be restrained to achieve stabilization for the soil.

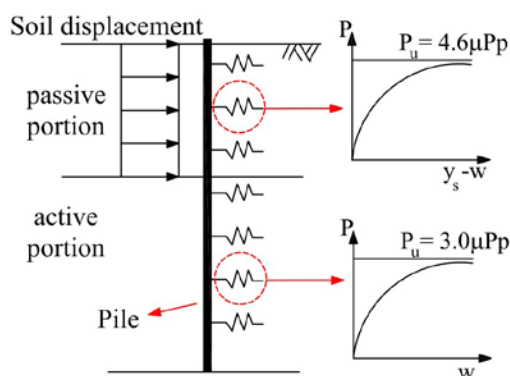


Fig. 2-15: Pile subjected to lateral soil displacement (Jeong et al. 2003)

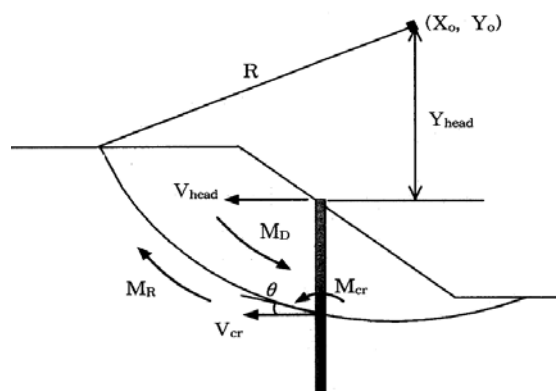


Fig. 2-16: Forces on stabilized piles (Jeong et al. 2003)

Ellis et al. (2010) developed a design method for the pile used to stabilize the slope. Their approach used two and three dimensional finite difference analysis to optimize the gap between the piles. Georgiadis (2012) used the 3D finite element analysis in order to develop the P-y curve for piles near a slope.

#### **2.2.3.4 Piles near deep excavations**

The effect of excavation activities on piles was studied by Finno et al. (1991). Their work was about a case study of 15m deep temporary sheet pile wall implemented very close to piled foundations. The movement of the pile caps was twice larger than expected; however, the results from the finite element method showed that the piles sustained the additional bending moment due to excavation.

Poulos and Chen (1997) used finite element and boundary element methods to study the effect of braced-excavation on single pile. The method was based on the prediction of the soil movement due to excavation and without existing of the pile from the finite element. The Boundary element program was then used to analyze the pile after adding the soil movement from the previous step. Prediction of the pile deflection and bending moment is then possible. They then implement design charts that have variable values of soil properties, excavation depth, pile properties and pile head condition. The pile head condition was the most influencing factor. Their charts were applicable only for braced-excavation. The same approach was used in parallel by Poulos and Chen (1996) to provide charts for the unsupported excavation. The charts from both studies were limitedly verified in field. Hence, Leung et al. (2000) performed series of centrifuge model tests to study the direct influence of conducting un-strutted deep excavation near a single pile foundation in dry dense sand. Their study included the case of a stable and unstable retaining wall. The pile bending moment and deflection near a stable wall were highly influenced by its location from the wall and restriction of its head. The pile tested near the unstable wall and in the failure zone showed a significant moment and deflection, while the piles outside such zone were relatively low in bending moment and deflection values. Leung et al. (2003) used the same procedure of the centrifuge model tests for a group of 2, 4 and 6 piles in a different arrangement. The two piles group arranged in row parallel to the wall showed no difference in comparison with single pile while that perpendicular showed a slight difference regarding pile deflection and bending moment. The more the number of piles the less the values of bending moment and deflection of the pile due to the excavation. The piles near to the wall within the group are effected more than those rear piles, which work as a fixation to the front piles. The effect of excavation on the single pile behavior in clayey soil was discussed by Leung et al. (2006) using centrifuge model tests. The pile deflection and bending moment were observed during the excavation until failure. They

found out that the bending moment of the pile increases with progressing excavation and it was reduced again when the excavation ended and bending moment may be reduced even before completing the excavation for the walls that experienced failure. The trend of pile deflection was always increases with time as shown in Figure 2-17. Ong et al. (2006) performed the same study of Leung et al. (2006) for the stable wall but they showed an increase of bending moment with time contradicting with the results of the unstable wall. The centrifuge model tests simulating excavation near pile groups of different configurations and sizes in soft clayey soil were discussed by Ong et al. (2009). The excavation was carried out in intervals to simulate the strutting. As discussed before, they confirm that a pile in group is influenced less than single pile considering the same distance from the wall. Each pile within the group experiences different bending moment and deflection values.

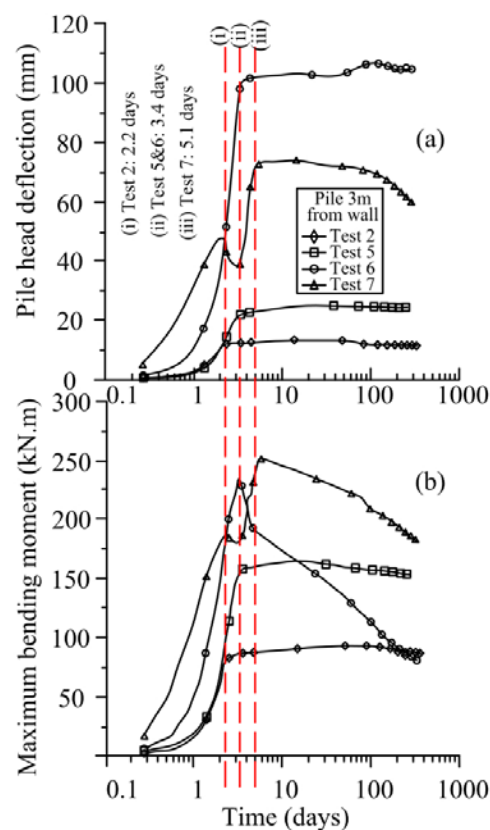


Fig. 2-17: Development of maximum (a) head deflection and (b) bending moment of the pile during and after excavation (after Leung et al., 2006)

The results of a full scale 16m deep strutted deep excavation implemented near existing instrumented pile in mixed soil layers were discussed and analyzed by Goh et al. (2003). A 0.8m diaphragm wall was used to support the excavation. The pile was located 3m from the diaphragm wall and it was monitored using an in-pile inclinometer. The pile was 45m deep and the recorded maximum movement was 28 mm at the upper third (12 m from the top). The soil movement was noticeably higher than the pile movement. A simple numerical simulation for the problem was conducted. The pile was simulated as a beam element, while nonlinear

horizontal springs were used to simulate the soil-pile interaction. The results from the numerical analysis and field data was in a good agreement.

Zhang et al. (2011) developed a new analysis based on the beam on an elastic foundation method in order to predict the free-field soil movements during deep excavation. They used the new method and applied it for an excavation near a single pile. Their results were slightly less than those calculated by Poulos and Chen (1997). They also pointed out that the axial force is also effecting the lateral response of pile at some cases.

Korff (2013) studied the effect of deep excavation on piled buildings through the construction of the north south metro line in Amsterdam. The case histories of her work will be described in the next chapter. It is worth herein to show an overview of her model describing the soil-pile interaction. The intention of her model is to find out the change of skin friction due to the difference in movement values between soil and pile during excavation activities. An interaction level ( $z_i/L_p$ ) was defined and located where the pile and soil displacement are equal. The determination of the interaction level is based on dimension less factors. The main concept of calculating the interaction level can be derived from the following equation

$$\frac{Z_i}{L_p} = \frac{P_2 - P_1}{\Delta S} \quad 2.13$$

where  $P_1$  is the pile displacement from the initial load,  $P_2$  is that due to load and soil displacement and  $\Delta S$  is the soil settlement. The value of  $P_2$  could be calculated based on the following equation.

$$W = \int_0^{L_p} \tau \cdot \pi \cdot D dz + Q_b \quad 2.14$$

where  $W$  is the actual load above pile and  $D$  is the pile diameter and  $Q_b$  is the bearing capacity of the pile. The shaft friction  $\tau$  is a function of pile settlement  $P_2$  and can be calculated from

$$\tau = \tanh\left(\frac{S_z - P_2}{Dz}\right) \cdot \tau_{max} \quad 2.15$$

where  $Dz$  is the relative displacement at which  $\tau_{max}$  (the maximum friction) is reached.

A chart was suggested to be used for the determination of the interaction level ( $z/L_p$ ) based on the analytical solution. The upper part of the curve is applicable for excavation while the lower part is applicable for tunneling as shown in Figure 2-18.

Liyanapathirana and Nishanthan (2016) used the finite element method to study the effect of excavation on adjacent single pile. They verified their numerical simulation by the centrifuge test results conducted by Ong et al. (2006). They performed a parametric study and provided design charts for the case of a single pile near excavation.

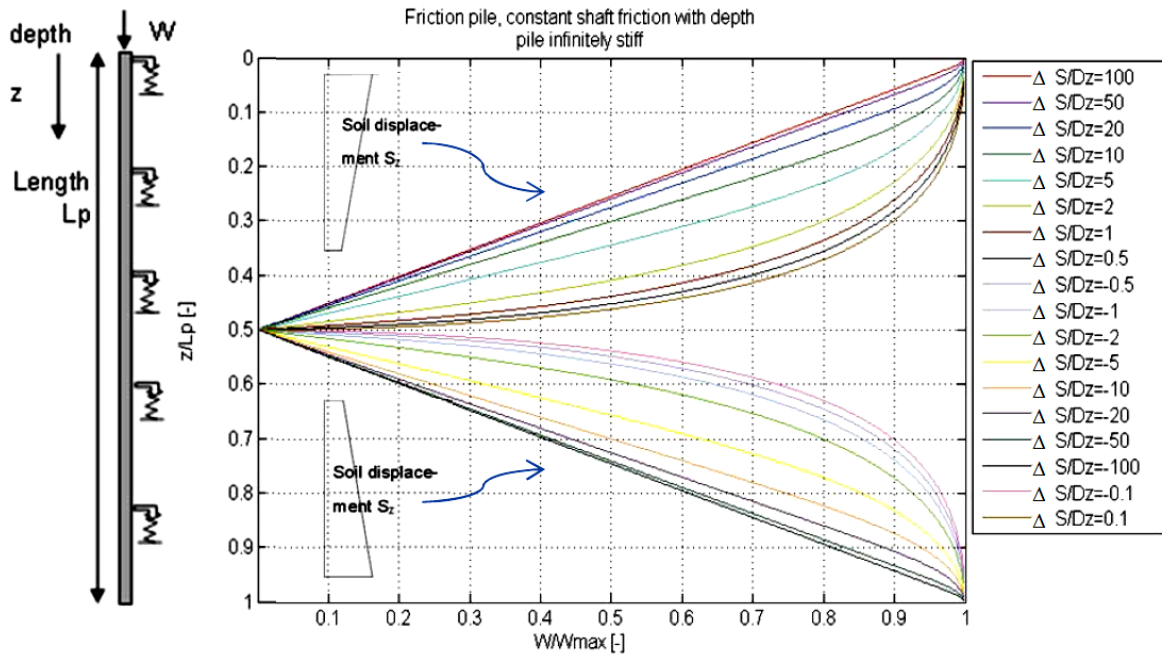


Fig. 2-18: A suggested curve to determine the interaction level for friction pile (Korff, 2013)

### 2.3 DIAPHRAGM WALL INSTALLATION

In the last decades the increasing number of population inside cities encouraged the engineers to use the underground space to solve cities problems. Deep excavation and tunnels are the common methods used for the underground projects. The deep excavation can be supported by several techniques such as sheet piles, retaining walls, secant or tangent pile walls, diaphragm walls ...etc. Soil characteristics, adjacent buildings, site layout, available space ...etc. control the choice of the deep excavation supporting technique.

The diaphragm walls techniques are widely used in supporting deep excavation in the cities as they can be used when space is limited and also as a water barrier. It is also known as slurry walls as the slurry (bentonite) is used for supporting the trench and it was first constructed in the middle of the last century (i.e. about 60 years ago). The execution and design of the diaphragm wall is referred to three phases, the first is related to the excavation of the trench with protection of slurry. The second is the excavation of the pit after the completion of concreting and in this case the wall acts as a ground support. The last stage is the interaction of the wall with the other structure components in case it is a permanent wall. In the three phases there is an effect on the surrounding environment, which causes settlement near the wall and may cause damage for the surrounding structures. This section describes the analysis of the diaphragm wall during trenching and its effect on the ground surface. The case studies and laboratory works discussing the trenching process on adjacent piled structures are to be discussed in details in the next chapter.

### 2.3.1 BENTONITE SLURRY AND FILTER CAKE

There are several functions of bentonite slurries in diaphragm walls such as

- a) Forming hydrostatic pressure that supports the excavation
- b) Suspend detritus
- c) Remain in the trench and don't penetrate to the soil
- d) Easy to be pumped
- e) Easy to be displaced by concrete
- f) Enable recycling

However, these functions are contradicting each other, as the first three required a dense slurry while the others required it to be fluid (Hutchinson et al., 1974). They carried out experiments in cooperation with Cementation Research Ltd in order to enhance the slurry properties. They found out that adding a small amount of fine sand could change the sealing mechanism and decrease dramatically the initial fluid loss. They recommended a lower density of slurry of about  $10.34 \text{ kN/m}^3$  and bentonite concentration above 4 %. On the other hand, and in order to facilitate the placement of concrete they recommended that the slurry density should not exceed  $13 \text{ kN/m}^3$ . Weiss and Winter (1985) showed in their description of DIN 4127 that the bentonite density ranges between  $10.1$  and  $13 \text{ kN/m}^3$ .

The hydrostatic pressure of the slurry which is affected by the formation of the filter cake was discussed by Elson (1968). The stress diagram with and without filter cake is shown in Figure 2-19(a). The diagrams ACD and ABC are representing the stress with and without filter cake, respectively. Generally, the nonexistence of filter cake causes the slurry pressure to be less than theoretical; however, by calculating  $C_a$  from the figure in both cases, the slurry penetration in the soil could increase slightly the apparent shear strength of it, where  $\tau_f$  is the slurry shear strength.

The bentonite concentration increase in slurry affects the slurry wall by improving the stability of the trench in case of the filter cake was not formed. It allows larger particles to suspend on slurry, which helps in filter cake formation in coarse soils. It increases the unit weight of the slurry as more particles suspended on it (Filz et al., 2004). They studied the formation of filter cake for the sandy soil. The particle size of the sand affects the formation of the filter cake as it is considered to be pure bentonite or with silt and fine sand according to the  $D_{15}$  size of the sand, Figure 2-19(b). If the sand is too coarse the slurry is expected to penetrate into the soil as shown in Figure 2-19(c). The distance  $L$  can be calculated based on the slurry and water level and unit weight and the dimensionless stagnation gradient. The bentonite penetration of the sand did not affect significantly its properties as it depends mainly on the voids size, the difference between the slurry and the water levels and the bentonite concentration in the slurry.

On the other hand, Filz et al., (2004) also confirmed that without the formation of filter cake there could be a high possibility of slurry pressure reduction. The local stability without filter cake formation can be calculated from equation 2.16.

$$F_{local} = \frac{i_0 \gamma_w \tan \phi}{\gamma_{bs}} \quad 2.16$$

where  $i_0$  is the stagnation gradient,  $\phi$  is the friction angle of the soil and  $\gamma_{bs}$  is the buoyant unit weight of the slurry-saturated soil and equals  $\gamma_{ss} - \gamma_s$ . where,  $\gamma_{ss}$  is the total unit weight of the soil when it is saturated with the slurry and  $\gamma_s$  is the soil unit weight.

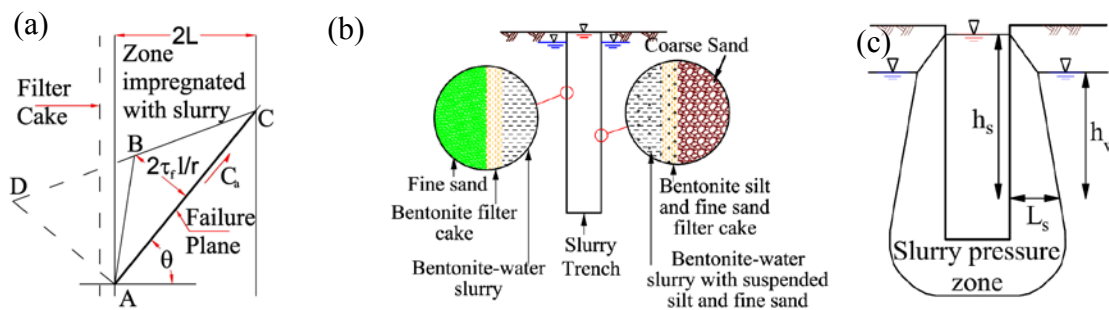


Fig. 2-19: (a) Stress diagram in zone of soil impregnated with slurry (after Elson, 1968)  
 (b) Formation of bentonite filter cakes (c) Slurry penetration into soil (after Filz et al. 2004)

### 2.3.2 ANALYTICAL SOLUTION OF SLURRY TRENCH STABILITY

The type of soil (cohesive or cohesion-less) is affecting the analysis method. The following two sections describe the analysis methods in clay and sandy soils followed by a section describing the analysis methods applicable for both types.

#### 2.3.2.1 Analytical solution in cohesive soils

The stability of slurry trench for cohesive and cohesion-less soils was studied by Nash and Jones (1963). The general idea is to analyze the failure surface as shown in Figure 2-20a. This failure plane is inclined with a value of  $\theta$  from the horizontal and the wedge of failure should be balanced with the slurry pressure  $P_s$ .

The stability calculation for cohesive soils is based on knowing the value of  $H_{cr}$ , which indicates the critical height. The value of  $\theta_{cr}$  in the failure plane can be determined according to the friction angle and used equal to  $45^\circ$  in case of  $\phi = 0^\circ$ .  $P_s$  is the slurry full hydrostatic force. The following simple equation is used to calculate the critical depth:

$$H_{cr} = \frac{4c - 2q}{\gamma - \gamma_s} \quad 2.17$$

where  $q$  is the surcharge that act on surface and  $\gamma_s$  is the unit weight of the slurry and  $c$  is the undrained cohesion.

The trenching process is generally quick and the water content did not change; accordingly, the undrained condition is then considered. The friction angle is then equal to zero and the cohesion “ $c$ ” can be replaced with the undrained shear strength (Xanthakos, 1994).

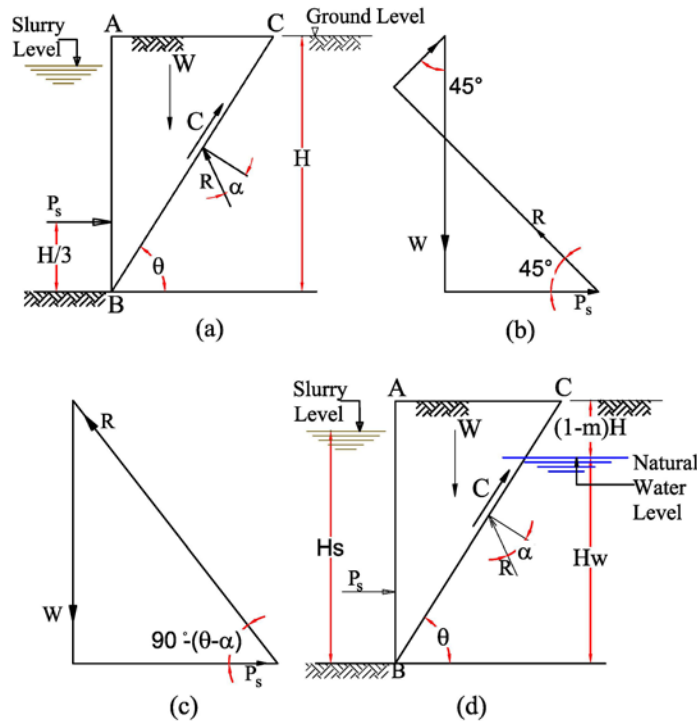


Fig. 2-20 Slurry trench stability: (a) Section through trench. (b) Force polygon for purely cohesive soil ( $\phi = 0$ ). (c) Force triangle for purely cohesion-less soils ( $c=0$ ). (d) stability of trench in sand with natural water level (after Xanthakos, 1994)

Nash and Jones (1963) did not take into consideration the arching effect discussed by Terzaghi (1943), which considered that a shear resistance appears between the parts of soil that are subjected and not subjected to yielding. The trench panel is considered to be a three-dimensional problem and the arching effect should be considered. The field studies conducted by DiBiagio and Myrvoll (1972) showed that the displacement is more in the center of the trench than at its ends as shown in Figure 21(a). The possible shape of arching action of the trench panel was discussed by Xanthakos (1994) and is shown in Figure 2-21 (b). The ends of the panel carry the load of the soil, which tends to creep in the center of the panel. A semi-empirical method was suggested by Aas (1976) and Karlsrud (1983) based on the data provided by DiBiagio and Myrvoll (1972). The failure zone was divided into two parts, upper and lower part. The upper part tends to move vertically and the lower part tends to move into the trench side as shown in Figure 2-22. The undrained shear anisotropic nature was considered. These methods provide a higher safety factor than that obtained from Nash method.

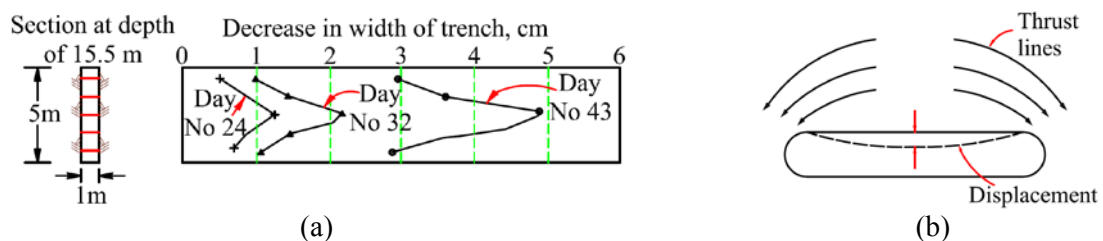


Fig. 2-21: (a) The change of width for typical gage points for tested panels (after DiBiagio and Myrvoll, 1972) (b) Arching effect of trenches in clay (after Xanthakos, 1994)



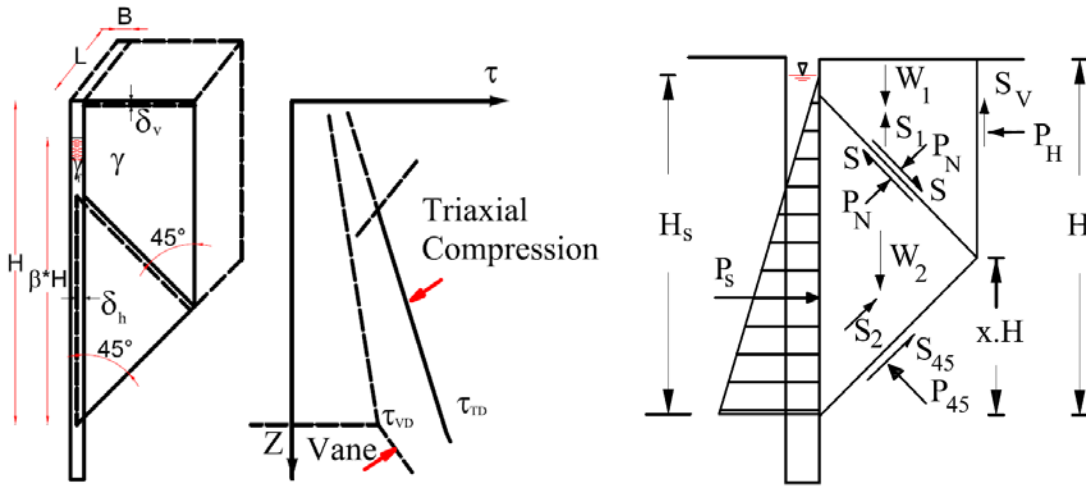


Fig. 2-22: Assumed failure condition in trench, and stability analysis (after Aas, 1976)

The factor of safety can be calculated according to Figure 2-22 from the following equation.

$$F = \frac{\tau_{VD}}{d(\gamma_s - \beta^2\gamma_s)} \left( 2 \frac{\tau_{VD}}{\tau_{TD}} + 0.6 + 0.86 \frac{d}{L} \right) \quad 2.18$$

where:  $\tau_{VD}$  is the van shear strength at depth “d”,  $\tau_{TD}$  is the triaxial compression strength and  $\gamma_s$  is the slurry density.

Tamano et al. (1996) discussed the stability of slurry trenches based on the displacement and water pressure results of a trench tested panel in soft clay. They indicate the lateral earth pressure based on the pressure difference between the horizontal stress and slurry pressure. The positive value of lateral earth pressure means that the soil moves toward the trench creating active or semi-active condition. Accordingly, the earth pressure decreases and balances with the slurry pressure. They found out that this balance indicates that the slurry trench method is acceptable for normally consolidated soft clay. The stability of the slurry trench in cohesive soils using 2-D and 3D methods was recently discussed by Han et al. (2015). In their approach, they used a rotational mechanism. They found that safety factor values obtained from 3-D method is from 1.1 to 1.2 greater than those obtained by the 2-D method. However, the two methods indicate the same results if the trench length to depth is greater than 10.

### 2.3.2.2 Analytical solution in cohesion-less soils

Nash and Jones (1963) predicted a method to calculate the trench stability of cohesion-less soils as was presented in Figure 2-20a and c. They assumed that the factor of safety is not affected by depth and can be calculated from the following equation:

$$F = \frac{2\sqrt{\gamma\gamma_f}\tan\phi}{\gamma - \gamma_f} \quad 2.19$$

The effective friction angle, soil and slurry unit weight are used instead in case of groundwater table as shown in the following equation:

$$F = \frac{2 \sqrt{\gamma' \gamma'_f \tan \phi'}}{\gamma' - \gamma'_f} \quad 2.20$$

Based on slurry trench failure case history, Morgenstern and Amir-Tahmasseb (1965) provided an improvement on the calculation by adding the resistance due to sliding to the wedge edges. They recommended that the increase of slurry density due to suspended particles should be taken into consideration. Prater (1973) suggested also adding additional shear strength during sliding for the sliding rigid soil block as shown in Figure 2-23a.

Piaskowski and Kowalewski (1965) suggested a parabolic cylinder ABC - A'B'C' as a sliding wedge (Figure 2.23b). The failure is assumed to take place in the plan A'B'C' which inclined with angle  $\theta$  from the horizontal.

Walz and Prager (1978) applied the silo theory to a plane surface as shown in Figure 2.23c. A prism was made in failure surface with thickness  $dz$  and was integrated to define the stability. This method is applicable to cohesion and cohesion-less soils.

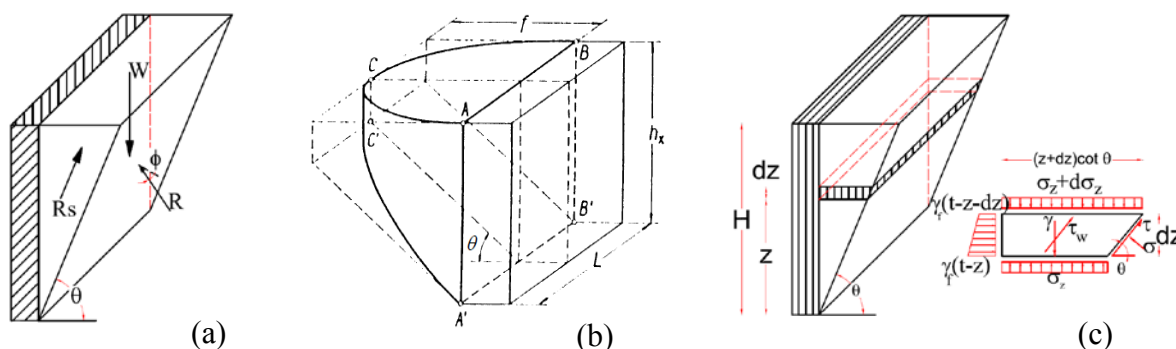


Fig. 2-23: sliding wedge shape (a) (after Prater, 1973) (b) (Piaskowski, 1965) (c) (after Walz and Prager, 1978)

Hajnal et al. (1984) developed an analytical method based on experimental results. They took into consideration the arching effect that was recorded from the experiment. The ratio between the actual slurry pressure and the plastic state horizontal stress is characterizing the stability at any place. The plastic failure state on a place within the trench side is defined if  $K_a = \frac{P_f - P_w}{\sigma_z}$ .

Tsai and Chang (1996) assumed a horizontal compression arch confining the horizontal movement due to earth pressure, where the end of the silo is supported by a half silo and the soil within it moves vertically equivalent to a vertical movement of extension arch. The results of this method lied between Morgenstern and Amir-Tahmasseb (1965) and Walz and Prager (1978) methods after conducting a comparison between factors of safety values from the three methods. This method was later verified by a full scale test conducted by Tsai et al. (2000).

### 2.3.2.3 Analytical solution applicable for cohesion and cohesion-less soil

The cylindrical surface method used for slurry trenching analysis was discussed by Xanthakos (1994). This method depends on considering the slip surface as a circle, which passes through the tip of the trench at point B as shown in Figure 2-24. The factor of safety can then be calculated as the ratio between the resisting moments to the acting moments around the center of rotation O. The resisting moment is consisting of the shear resistance along BC by friction ( $R_f$ ) or cohesion ( $R_c$ ), the slurry pressure  $P_f$  and the cylinder ABC shear resistance. The weight of the wedge and the concentrated load P if exist is causing the overturning moment.

Fox (2004) used the force equilibrium analysis of Coulomb-type to predict the critical angle of failure plane and the safety factor of the slurry-supported trench. He assumed a surface failure plan and the wedge moving as a rigid block. An example failure shape for the method is presented in Figure 2-24b. His methodology is simple and it provides three and two dimensional stability calculations for drained and undrained analysis. It can also be applied for different trench depths, lengths, slurry depths and groundwater table elevation, etc.... However, this methodology cannot predict the settlement and ground movement and cannot be applied for layered soil. The results from the approach showed that the trench length is highly affecting the factor of safety. A comparison was made between the results from the 3D solution approach and field results from Tsai et al. (2000), and they were in a good agreement. This method did not take into consideration the curved failure surface. The importance of the 3D analysis was clarified by Fox (2006). Accordingly, many researchers have recently focused on the 3D analytical solutions. Li et al. (2013) performed an analytical solution based on the horizontal slice method, polygon prism surfaces were forming the failure surface and the three dimensional effect was achieved by including the shear forces acting on the side plan. The analysis considered similar layered soils. The bases of limit equilibrium were used to balance the forces in the vertical direction of each slide and the horizontal direction for the whole sliding mass as shown in Figure 2-25a. The method was compared with the field data of Tsai et al. (2000) and the method of Filz et al. (2004) and Fox (2006). A good agreement was noticed. Han et al. (2013) performed a 3D and 2D analysis to study the stability of slurry trench for frictional /cohesive soil based on limit analysis and rotational mechanism. The 3D rotational mechanism is shown in Figure 2-25 (b). The factor of safety obtained from this method was higher than that obtained from (Fox 2004).

The end effect on toe failure was discussed by Zhang et al. (2016). They used the limit equilibrium stability analysis with a 3D rotational body mechanism that contain central cylinder and two end caps. Figure 2-25c shows “p” the slip surface with spherical coordinates

while its center is at unknown point  $(x_c, y_c, z_c)$ . The following differential equation could then be used to determine the three dimensional slip surface while  $\tan(\phi_m) = \tan(\phi) / FS$ .

$$\frac{d\rho}{d\beta} = -\tan(\phi_m) \sin \sqrt{\rho^2 + \left(\frac{d\rho}{d\alpha}\right)^2} \quad 2.21$$

They showed that the 3D end effects method is more applicable for narrow trenches where the depth of the trench to its length is high.

A summary of the different trench methods is presented in Table 2-1.

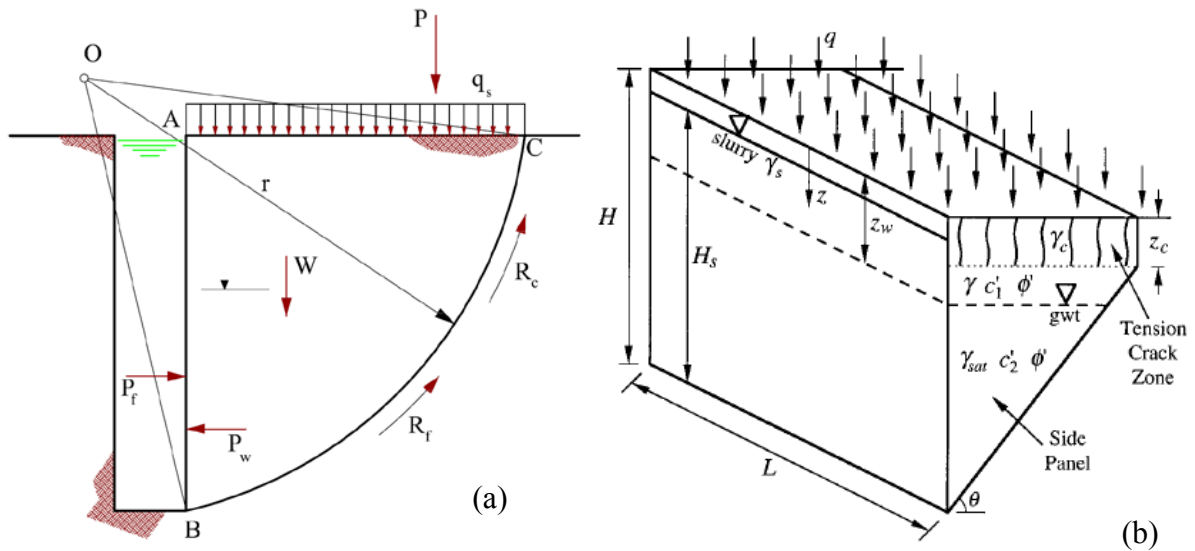


Fig. 2-24: Analytical approach (a) (after Xanthakos, 1994) (b) (Fox 2004)

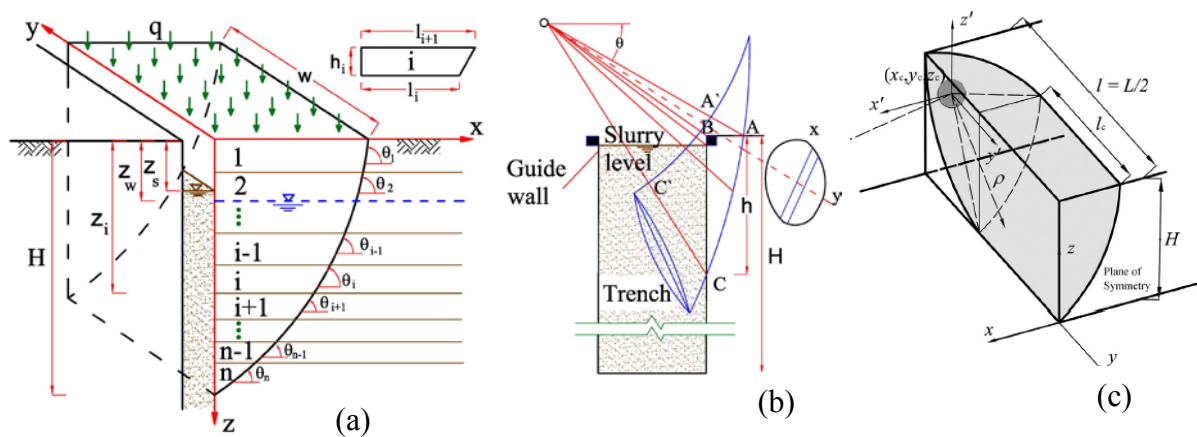


Fig. 2-25: 3D analysis for frictional/cohesive soils (a) (after Li et al. 2013) (b) (after Han et al. 2013) (c) (Zhang et al. 2016)

Table 2-1: Different slurry trenching analytical methods

Literature	Soil type	Method of Calculation /Comment
(Nash, Jones 1963)	Cohesion-less /Cohesive	Two dimensional wedge limit analysis
(Piaskowski, Kowalewski 1965)	Cohesion-less	Three dimensional wedge limit analysis
(Morgenstern and Amir-Tahmasseeb 1965)	Cohesion-less	Two dimensional wedge limit analysis /edge resistance effect
(Elson 1968)	Cohesion-less	Two dimensional wedge limit analysis /filter cake effect

Literature	Soil type	Method of Calculation /Comment
(Prater 1973)	Cohesion-less /Cohesive	Two dimensional wedge limit analysis / edge resistance effect
(Aas 1976)	Cohesive	Two dimensional semi-empirical method / arching effect
(Walz, Prager 1978)	Cohesion-less /Cohesive	Two dimensional/ integration of slice in failure wedge to include side effect
(Karlsruud 1983)	Cohesive	Two dimensional wedge limit analysis / arching effect
(Hajnal et al. 1984)	Cohesion-less	
(Xanthakos 1994)	Cohesion-less /Cohesive	Two dimensional / rotational mechanism
(Tamano et al. 1996)	Cohesive	Difference between soil horizontal stress and slurry pressure
(Tsai, Chang 1996)	Cohesion-less	Failure wedge assumed as a half silo
(Filz et al., 2004)	Cohesion-less	Two dimensional wedge limit analysis /filter cake effect
(Fox 2004)	Cohesion-less /Cohesive	Two and three dimensional wedge analysis
(Han et al. 2013)	Cohesion-less /Cohesive	Three dimensional / rotational mechanism
(Li et al. 2013)	Cohesion-less /Cohesive	
(Han et al. 2015)	Cohesion-less /Cohesive	
(Zhang et al. 2016)	Cohesion-less /Cohesive	

### 2.3.3 SOIL DEFORMATION DUE TO SLURRY TRENCHING

The soil deformation and settlement due to slurry trenching were studied using either mathematical approaches or numerical simulations. The following two sections describe each method.

#### 2.3.3.1 Soil deformation calculation using analytical solution

The lateral displacement of the earth can be calculated from Equation 2.22 which is based on Timoshenko, Goodier (1951) for deep circular cut (Xanthakos, 1994).

$$\delta_h = 0.75(k_o\gamma' - \gamma_f')2L/E_i \quad 2.22$$

Where L is the length of the panel,  $E_i$  is the initial tangent modulus of the clay and  $k_o$  is the at rest earth pressure.

Lei et al. (2001) used the method of complex variables with a simplified conformal transformation function to transfer the exterior of rectangular section into the interior of the circle. In order to obtain an approximate elastic solution capable of calculating the stress distribution and deformation around a rectangle opening such as trench. Uniaxial stress was used. The verification of their method was made using the finite element model. A two-dimensional elastic solution was made by Ng and Lei (2003) as an improvement to the previous method in order to solve the biaxial stress problems. The solution is found to be affected by both soil properties and geometric properties. They provided calculation charts that could help to find empirically the soil deformation and stress during trenching.

Lei et al. (2014) approximately predicted the ground surface settlement due to the diaphragm wall construction along the centerline. The solution was based on applying the total earth

pressure on the trench side walls and base. The soil was assumed to be homogeneous, isotropic and elastic. The settlement was calculated by applying the method of superposition with respect to maximum horizontal total earth pressure changes; soil undrained Young's modulus and trench length. This method was verified with finite element and field data.

### **2.3.3.2 Soil deformation calculation using numerical analysis**

In the last few decades the numerical solutions were widely used in engineering problems. Many researchers studied the diaphragm wall trenching using numerical analysis such as finite element or finite difference analysis.

Gunn and Clayton (1992) discussed the change in stress during diaphragm wall installation and its effect on deformation. They showed that the limit equilibrium analysis did not take into consideration the change in stress and its effect on design. Accordingly, Gunn et al. (1993) used two dimensional finite element mesh to simulate a full trenching process in order to estimate the lateral stress reduction. The soil was modeled using the Mohr-Coulomb model while the slurry was simulated with an equivalent hydrostatic pressure. Their intention was to find out the effect of wall installation on the final wall bending moment after excavation. The cantilever wall was not noticeably effected, while the propped wall was affected. The installation effect is low if the water level is high and vice versa.

De Moor (1994) used the 2D finite element analysis to model the panels during excavation and has found its effect on the lateral stress. The soil was over-consolidated stiff clay and was modelled using the linear elastic perfectly plastic model and the Mohr-Coulomb failure criterion. The slurry was simulated with hydrostatic pressure, while the concreting simulation was made by removing the slurry pressure and adding a linear elastic model element. His approach allowed for calculating the lateral stress distribution and including the adjacent panels' construction effects. The results were verified correctly with field data.

Ng et al. (1995) discussed an approach to solve the trenching process in three dimensions by simulating 2D finite element analyses of the excavated panel using two separated models. These models were divided into a vertical section and a horizontal plane. The  $k_0$  was allowed to change according to the different stages of trenching and concreting. The horizontal analysis was mainly for studying the arching effect while the vertical analysis simulates the construction of the infinite panel. The soil was modeled with the Mohr-Coulomb yield criterion as linear elastic perfectly plastic. The horizontal plane analysis was conducted first and it was made in three stages. Firstly, replacement the soil element by air element, then application of pressure that simulated the slurry pressure and finally replace again the air element with linear elastic concrete element. These stages were repeated for each panel. The results of the horizontal analysis showed that the horizontal stresses at the edges of the panel are much

greater than on center after concreting. However, the displacement at the center was more than that at the edges. The vertical analysis results showed a high concentration of shear stresses at the toe while the lateral stress decreased with depth above the toe and increased with depth below the toe.

Instead of reducing the value of  $k_0$  or to simulate the slurry and concrete by using pressure as was done by (Gunn et al. 1993). The two analysis methods were linked by using the horizontal analysis as a boundary in the vertical analysis. This linking showed that the lateral earth pressure is inversely proportional with the panel length as well as the wet concrete pressure. It was assumed to be correct due to the general good agreement that was found between the analysis and field data regarding the values of  $K_0$  and ground deformation.

A full three-dimensional finite difference analysis was performed using FLAC 3D by Ng and Yan (1998). The soil was stiff clay and modeled using linear elastic perfectly plastic model, while the nonlinear soil stiffness was modeled empirically. The model was made using two planes of symmetry. Quadrilateral elements subdivided into four constant stress triangular sub-elements were used to form the mesh. The stresses acting on the quadrilateral elements are the average of that act on the sub-elements. The excavation was made by setting the zones at the trench location to null elements and apply hydrostatic pressure on the walls surfaces. The concrete was simulated by placing redefine the null element with the linear elastic element and remove the hydrostatic pressure. The comparison between the numerical analysis and some results of centrifuge model tests was in a good contrast. The results showed that the horizontal stress was reduced but the ground deformation was very low.

Gourvenec, Powrie (1999) used the 3D finite element analysis to study the effect of diaphragm wall installation on ground surface. The soil was modeled using a linear elastic plastic model with Mohr-Coulomb failure criterion with an associated flow rule. Unlike Ng and Yan (1998) they simulate multi-panels. They showed that the panel length has a high effect on deformation and stresses. On the other hand, the end effects simulated in 3-D restrict the displacement.

With the progress in the numerical analysis software the simulation of the slurry trenching considered to be more accepted and reliable in the last decade. The new soil models are currently used for such a simulation with more reliable outputs. The anisotropic visco-hypoplastic clay model was used by Grandas-Tavera and Triantafyllidis (2012) to study the corner of a slurry trench. A sophisticated problem of diaphragm wall installation near surrounding buildings was studied and discussed by Comodromos et al. (2013). The effect of a diaphragm wall installation process was modeled by Mohamed (2014) using finite element and finite difference analysis methods with two different soil models. The results from both

methods and models were compared with field data showing that the finite difference method with the strain hardening softening soil model was the most accurate one.

## 2.4 SUMMARY

Understanding the behavior of pile is still a complex issue and its design is based on many empirical assumptions. The pile could be subjected to different types of loads under different conditions which could change its stress-strain mechanism. Several researchers studied the slurry trenching process. The stability and deformation was their main concern. There was a quit agreement that the slurry trench is a three dimensional problem, and the two dimensional solution will be very conservative.

The main points from the literature review could be drawn as follows:

- The behavior of pile subjected to (passive load) lateral soil movement is different when it is subjected to direct lateral load.
- The bending moment and shape of pile deflection is greatly affected by the type of passive load and location of soil movement along the pile.
- The pile head condition and the pile location within a pile group is governing its behavior due to lateral loads.
- The slurry trench is a three-dimensional problem.
- The deformation of the slurry trench will definitely affect the pile with some magnitude according to the dimension of the diaphragm wall (trench length in particular), soil type, slurry level, ground water level.

The passive load on the pile was discussed for several reasons. However, the diaphragm wall effect on piled foundations was not studied as a passive load on the pile. Accordingly, there are main points could be addressed

- What kind of passive load could be added to the pile during a nearby diaphragm installation?
- How the pile could affect the stability of nearby slurry trench stability
- Did the consistency of the slurry pressure due to existence of weak soil layer could affect the nearby piled foundation?
- What would be the effect of the diaphragm wall installation on single pile group, connected pile group and piled raft foundation?

This research is focusing in answering the addressed questions. The results of the field data and laboratory works regarding diaphragm wall installation and its effect in the nearby structures are addressed in the next chapter.



## **CHAPTER 3: PREVIOUS FIELD DATA AND LABORATORY WORKS**

### **3.1 INTRODUCTION**

The previous chapter showed the great effort that was made to understand stability and deformation of slurry trenches. It was accepted that the stability and deformation of trenches are affected by several factors including trench dimension, soil type and slurry level. However, no limit of deformation was provided, the deformation is considered accepted if the slurry is stable. Indeed, the stability of the slurry trench could mean that the trench will not be subjected to failure, but it didn't indicate how much deformation could happen or the effect of such a deformation on the surrounding buildings. The deformation prediction discussed in the previous chapter was based on many assumptions and is applicable to some soils or cases.

A question was raised from the previous chapter of how important is the soil deformation and stress changes during diaphragm wall installation. To answer this question, this chapter provided a collection of data regarding case histories and laboratory tests for diaphragm walls trenching processes from all over the world. The collected data include soil settlement, horizontal displacement and change in stresses (change in  $K_0$  value). The case histories and laboratory work regarding the effect of such trenching process on the piled foundation are discussed in detail in this chapter.

### **3.2 DIAPHRAGM WALLS AND DEEP EXCAVATIONS**

The deep excavations could be performed by conducting slopes with an appropriate factor of safety. However, inside the cities it is almost impossible to form deep excavations with slopes, as in this case a huge area is required to reach the excavation level. Such an area is not available inside the cities. The diaphragm wall technique allows for a vertical cut and hence decrease the space around the pit to a minimum. The use of diaphragm walls for the excavation of the Vijzelgracht station in Amsterdam was very effective to reduce the construction area. The construction of the diaphragm wall panels was a few meters from the buildings as shown in Figure 3-1. The diaphragm walls are widely used around the world for the deep excavations and they could be part of the permanent structure system. The diaphragm wall is still existing and can be seen after the collapse of the World Trade Center in New York as shown in Figure 3-2. It was part of the basement structure of the collapsed building. It can be used as a part of the new building.

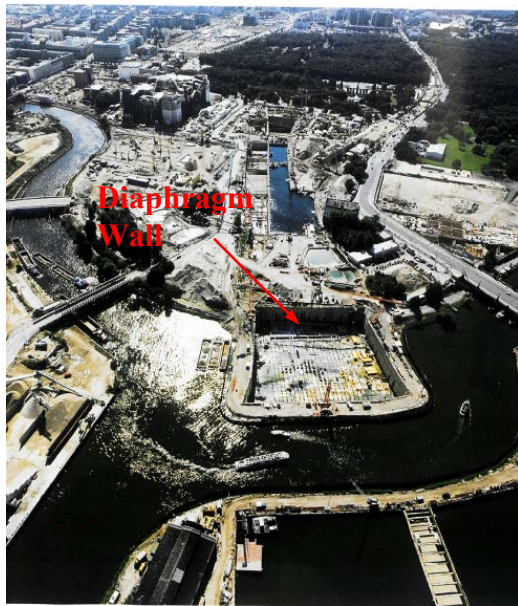


Fig. 3-1: Diaphragm wall construction in Vijzelgracht station (Korff, 2013)

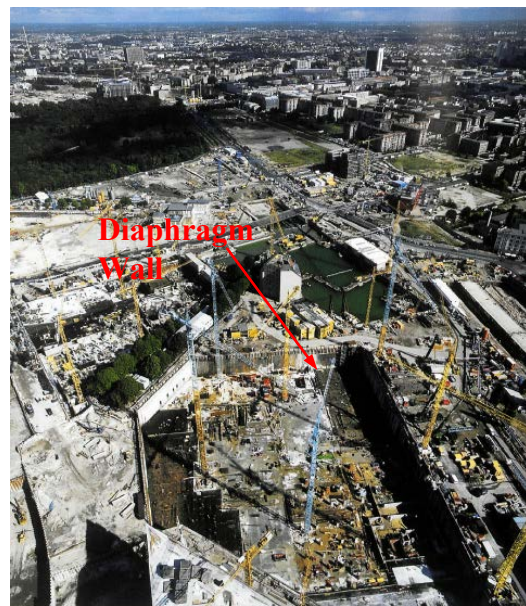


Fig. 3-2: East Slurry wall (Meyerowitz, 2006)

After the unification of Germany, there was a need for new planning and construction for the new political capital, Berlin. The diaphragm wall was a very useful element in several construction projects in Berlin during this time. The diaphragm walls can be obviously seen very clear in the aerial photos collected for Berlin construction projects between 1994 and 2001 by (Reuter 2001a, 2001b). The construction of the underground connection of the Lehrter train station (Bahnhof) in a district in Berlin called Der Spreebogen is shown in Figure 3-3a. The diaphragm wall was also used for Debis basement stories construction for the Potsdamer Platz as shown in Figure 3-3 b.



(a) Lehrter Bahnhof (Reuter, 2001a)



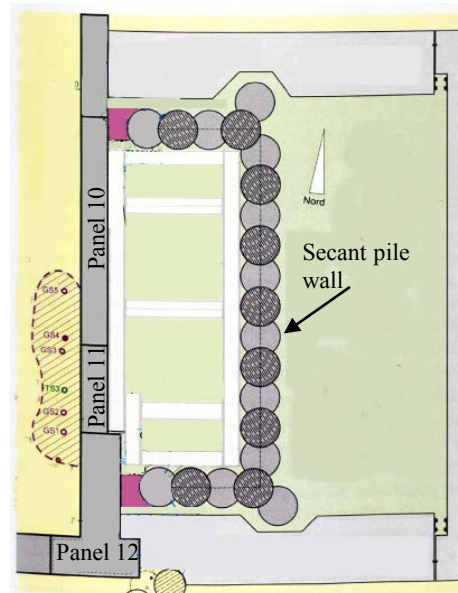
(b) Atrium tower (Reuter, 2001b)

Fig. 3-3: Diaphragm walls in Berlin

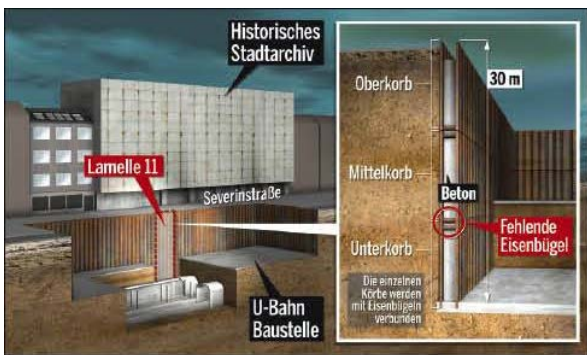
It is obvious that the diaphragm walls were widely used in very complex engineering projects; however, their failure during excavation or trenching could cause a catastrophe. Normally, diaphragm walls constructed in urban areas and their failure could probably affect the nearby structures. In some cases, the failure causes minor damage in form of cracks or tilting like that documented by (Korff, 2013) for a historical house that suffered cracks during excavation for a metro station in Amsterdam. Another case of minor damage happened in the Courts of Justice in Hong Kong during the installation of the diaphragm wall (Davies and Henkel, 1982). The collapse of diaphragm walls could also cause total damage of the nearby buildings, which may lead to the loss of human lives. In Cologne (Köln) 2009 a failure happened during deep excavating which caused the death of two people, total collapse of the nearby historical city archive and some other buildings. The reasons of such a collapse are not clear and still under investigation. However, many researchers have described the problem, such as (Sieler et al. 2012; Katzenbach et al. 2012; Moormann et al. 2014; Sieler et al. 2015; Schwarze et al. 2016). The failure of the historical city archive is shown in Figure 3-4a. The failure of the panel did not happen after finishing the excavation. It happened during stepped dewatering. The water was inside the excavation area with the valuable books from the historical archive. A number of technical challenges were facing the engineers to solve such problems. Freezing was implemented to stabilize the defect area behind the diaphragm wall, while the secant pile wall was used for separating the inspection area as shown in Figure 3-4b. Before dewatering, steel cages were placed in front and back of the diaphragm wall for reinforcement as shown in Figure 3-4c. Dipl. Ing. Steffen Hein (DEKRA Company) provided a photo for the recent situation (Figure 3-4d) during the discussion held on February 2016 in Freiberg.



(a) Failure of the historical archive (Moormann et al. 2014)



(b) Secant pile wall and freezing (Moormann et al. 2014)



(c) Reinforced steel cages in front and back of the diaphragm wall



(d) Recent current situation of the defected area (Photo taken by Dipl. Ing. S. Hein – December, 2015)

Fig. 3-4: Diaphragm wall Failure in Cologne and current situation

### 3.3 EFFECT OF SLURRY TRENCHING ON GROUND SURFACE (GREEN FIELD)

The deformations due to deep excavations have taken a lot of attention. However, the influence of the diaphragm wall trenching on the ground surface should be taken into consideration especially when a thick soft soil is located (Poh and Wong, 1998). The deformation of the ground surface and stress change due to slurry trenches from field observation and laboratory tests are discussed in this section. The soil deformations include settlement and horizontal displacement. This section is divided into three main parts.

- Case histories
- Field tests (Tested panels)
- Laboratory testing

### 3.3.1 CASE HISTORIES

There are several recorded case histories from real construction projects, where the diaphragm wall installation effect on the ground surface was monitored and discussed. Generally, the measurements include settlement and horizontal displacement for the area around the construction. The stress change was rarely monitored as well as trench width.

Morgenstern and Amir-Tahmassebi (1965) studied the failure of some panels of trench excavation due to flood of the River Rhône at Pierre-Bénite, France. The panels were 0.6m in width, length range between 9 and 20m and its depth was ranging between 8 and 28 m. Neither settlement nor horizontal displacements were recorded, only the failure of the panel was described whether exterior or interior. The authors concluded that the ground water level is highly affecting the stability of the trench, and the rise of the water table due to the flood was the reason of failure. The suspension of cuttings with the slurry increases its density; however, the stability of excavation is almost not affected by the slurry strength.

The use of slurry trench in a two tunnel sections project in soft clay in Oslo was discussed by Karlsrud (1983). The first section was a two-storey tunnel at Studentertunden (S.L.) with a wall depth of 21m, while the second section was one-storey tunnel at Jernbanetorget (J.B.T.) with a wall depth of 15m. The settlement, horizontal displacement and earth pressure were monitored for both stations even during the diaphragm wall trenching. The surrounding buildings settlement was monitored as well. The clay of the J.B.T. was much softer than the of S.L. Accordingly, the slurry density used in the J.B.T. was  $13 \text{ kN/m}^3$  while that used for the S.L. was almost equal to the water density. The soil deformation of both sections due to slurry trenching was low; however, it was several times higher due to the main excavation process. The decrease of horizontal earth pressure due to main excavation was not so high compared to that of diaphragm wall trenching.

The effect of secant pile wall construction on the ground deformation and soil stress was discussed by Tedd et al. (1984) as part of the cut and cover tunnel project in London. Soil deformation and lateral earth pressure were measured.

Cowland and Thorley (1985) presented a study for a seven case histories in Hong Kong for the slurry wall trenches. The study includes the effect on the nearby building as well. The soil was almost the same for all the projects, a fill layer was at the top 6m overlying a marine deposits layer. Alluvium layer was in the middle while the lower two layers were composed of completely and highly decomposed granite. The depths of the trenches were between 20 and 50 m with variable lengths and thicknesses. They presented the surface ground settlement from all the sites as a function of the trench depth. The settlement of the buildings near the slurry

trenches area was also presented. The tilt of the buildings was calculated based on the ratio of the foundation/ trench depth ratio and was obtained from:

$$\alpha_{\text{tilt}} = 0.6 + d/H \quad 3.1$$

where d is the foundation depth and H is the slurry trench depth. The buildings settlements and corresponding tilt are presented in Figure 3.5 (a) and (b), respectively.

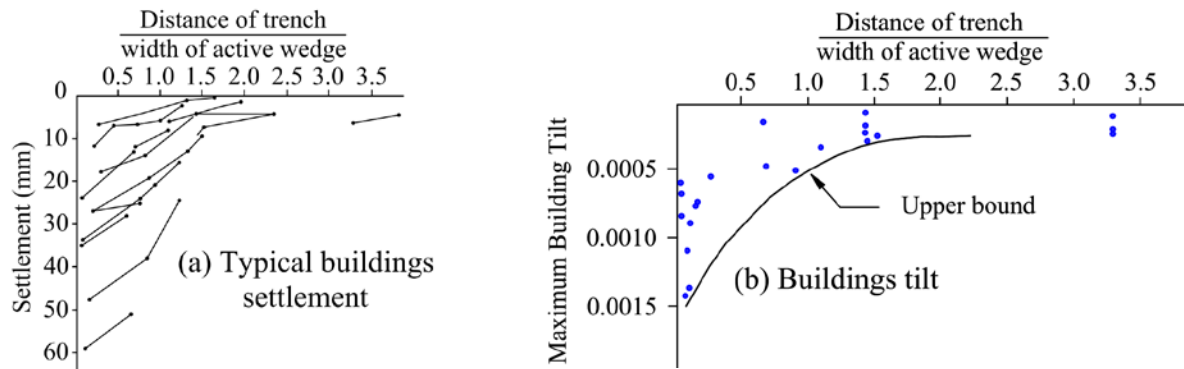


Fig. 3-5: Effect of slurry trenching on building (Cowland and Thorley, 1985)

Field monitoring results of diaphragm and bored pile walls for three different sites were presented by Symons and Carder (1993). They measured the stress distribution and water pressure. Diaphragm walls were used in two sites and it was T shape section with thickness of 0.8m, length of 4m and 2.7m and depth of 13.5m. The lateral stress was not measured for one of them but the pore water pressure was measured for both. The measurement of the lateral earth pressure was at a distance of 1.5m from the front face of the T-section diaphragm wall using spade shaped pressure cells during construction of different panels. The drop in lateral stress was around 50kN/m<sup>2</sup> and 160kN/m<sup>2</sup> during the trenching process. The effect of wall installation on coefficient of earth pressure (K-values) is presented in Table 3-1, the values decrease with depth. The pore water pressure decreased during excavation and then it increased during concreting to values slightly greater than the original normal values, while it returns back to its normal values after more than one month from time of excavation.

Table 3-1: Effect of wall installation on K-value (Symons and Carder, 1993)

Spade Cell	Depth (m)	K-value before	K-value after	Decrease Ratio
SC8	8	1.6	1.5	94%
SC9	10	2.3	2.0	87%
SC10	12	2.2	1.3	59%

Tse, C.M. and Nicholson, D.P. (1993) also present the monitoring resulting of the diaphragm wall installation on clayey soil (London Clay). The monitored project contained 140 diaphragm wall rectangular panels with a length of 3.75 m, a thickness of 0.8m and a depth of about 23.5 m, which was mainly governed by its bearing function. The maximum recorded horizontal displacement due to diaphragm wall trenching was 3mm.

Monitoring of a multi-propped diaphragm wall in Lion Yard, Cambridge with a typical length of 8.5 m and a thickness of 0.6 m with a depth approximately of 16m was presented by Lings et al. (1993). The soil was mainly Gault Clay overlaying a greensand layer while the upper layer was a Fill layer. The main focus of their work was to study the effect of main excavation on ground deformation and the behavior of a single panel (bending moment and deflection). However, the discussion was directed toward understanding the effect of trenching on the lateral earth pressure. A decrease up to 50% in the lateral earth pressure was recorded. On the contrary, the settlement was almost negligible.

Hamza et al. (1999) studied three different cases of diaphragm wall installation for different underground metro stations in Cairo. The idealized soil profile consisted of mainly sandy soil under 5 m layers of fill and clay. The water table was 2m under the ground surface. The average depth of the diaphragm wall was 50 m. The average settlement to trench depth ratio was about 0.031% with a maximum value of 0.052%. They confirmed an equation for settlement calculation due to the diaphragm wall installation as following:

$$S_o(x) = S_t \left(1 - \frac{x}{x_o}\right)^m \quad 3.2$$

where:  $S_t$  is the maximum settlement just near the wall,  $x$  is the distance from the wall,  $x_o$  is the distance from the wall at which settlement is equal to zero, and  $m$  is an empirical exponent.

Poh et al. (2001) discussed four different case histories in Singapore considering the effect of different diaphragm walls installation. The diaphragm walls were part of a deep excavation project of four different deep basement construction buildings inside the city of Singapore with an average excavation depth of 15 m. The diaphragm wall panels lengths were between 2.4 and 7.5 m while their average thickness was 0.8 m, except for some panels the thickness reached 1.5m. Trenches depth were not less than 13.1 m and it were not exceeding 30.7 m. The first 20 m were mainly cohesive soil and consisted of silt or clay and its shallower depth was soft and it becomes stiff and hard with depth. A layer of weathered granite appeared under the cohesive layers for the first case history (Lot one shoppers' Mall) and the wall almost did not penetrate in this layer. In the second case history (Jurong point building) a layer of limestone appeared under the cohesive layers and the walls did not penetrate in this layer as well. On the other hand, two case histories (Capital tower and cantonment complex building) a layer of siltstone was located under the cohesive soil layers and the walls have partially penetrated in this layer. The settlement from the first and second case studies was higher than the third as well as the horizontal displacement due to the penetration of the wall in the limestone layer in the third case study. However, in the fourth case study the horizontal displacement was very high because the water level and slurry level were almost the same.

Abdel Rahman (2007) studied the effect of constructing diaphragm walls as a part of an underground garage in Cairo. The deep excavation was about 10 m and the used diaphragm wall was 27 m in depth. The thickness and length of the wall were 0.8 and 2.8 m, respectively. A fill layer was found in the surface with thickness ranges between 4.5 and 6 m followed by a layer of dense to very dense sand to the reached boreholes depth of 48 m below the ground surface. The ground water level was about 3m from the ground surface. The measured settlement due to diaphragm wall installation was 2.0mm, which was less than predicted.

A 50m deep T-shape diaphragm wall was used in Bari, Italy as a part of a 26 m underground metro station. The soil was mainly sand, and deep mixing was used in the first 6 to 10 m to support the surrounding soil during trenching. The horizontal displacement with depth during different stages of diaphragm wall construction was measured and presented by L'Amante et al. (2012). The maximum horizontal displacement was 8 mm.

The effect of slurry trenching on soft clay in Shanghai, China was discussed in two different case histories by (Chen et al. 2014; Shi et al. 2015). The depth of the diaphragm wall panels were between 20 and 26 m. The maximum recorded settlement and horizontal displacement were 9 mm and 4 mm, respectively.

### 3.3.2 FIELD TESTS (TESTED PANELS)

The construction purpose of the tested panels was normally conducted before beginning of construction to find out the effect of the trenching on such a soil. However, some of them were conducted for research purposes by some researchers such as (DiBiagio and Myrvoll 1972; Tsai et al 2000; Ng et al, 1999) . In both cases, the tested panel(s) was heavily instrumented and monitored.

DiBiagio and Myrvoll (1972) studied a trench of length 5 m, width 1 m and depth of 28 m in soft clayey soil. The purpose of their study is to find out the effect of slurry density, slurry level and time on the ground deformation. The trench was excavated and kept by the slurry with an initially density equal to  $12.4 \text{ kN/m}^3$  for 12 days. Thereafter that it was reduced to  $11 \text{ kN/m}^3$  for 8 days and then the slurry was replaced with water for 11 days. The slurry was finally replaced by the concrete after this stage. The trench width was measured using hydraulic gages during the 31 days and it was reduced by 5.5 cm during this duration. The width was decreased with time and its value was higher in the middle than at the edges, as was presented previously in Figure 2-21a. The maximum decrease in width was 5.5 cm at a depth of 15.5 m (the lower third) and that was just before concreting. The settlement around the trench was measured at different stages using twenty-three settlement points. The settlement increased with time independent on the slurry density. In general, the values of settlement decrease with distance



and it becomes negligible at about 10 m from the trench face. The horizontal displacement was measured using inclinometers. There was almost no horizontal movement at the first upper 8 meters while the maximum displacement was detected near the end and was about 10 mm. The change of the slurry density did not affect also the horizontal displacement; however, it changes the creep rate. The pore pressure decreased near the wall before concreting, while it increased after concreting.

Farmer and Attewell (1973) used inclinometers and magnetic ring settlement gauges to find the ground response that was caused by the installation of slurry trench in London clay. The slurry trench was 6.1 m in length, 0.8 m in width and 15 m in deep and it was constructed in three stages. The inclinometers were located at different distances from the edge of the trench in four boreholes. The results showed a sudden increase in the horizontal displacement just after excavating the middle panel. This displacement was inversely proportional to the distance from the trench and it continued to increase with time until the trench was filled with concrete. The maximum horizontal displacement was 16 mm located at a depth of 5 m. The maximum settlement was 6 mm at a depth of 7.7 m. However, the surface settlement was almost negligible.

The effect of the slurry level inside the trench on the ground deformation was the main focus of the field experiment conducted by Stround and Sweeney (1977) in Hong Kong. They monitored excavating a trench of length 6.1 m, width 1.2 m and depth of 36m. The upper 3 to 5 m of the soil was a Fill layer which overlies about 3.5 m layer of marine deposit. The rest of the soil was weathered granite. The trench full length was achieved by excavating it in three bites. Then the slurry was lowered gradually from 0.5 m below ground surface until it collapses at slurry level of 2.67 m below ground surface. A heavily instrumentation system was implemented around the trench; including inclinometers, settlement survey points (surface and deep) and pneumatic piezometers as shown in Figure 3-6. Generally, the slurry level affected greatly the soil deformation; such lowering caused the maximum horizontal displacement to be doubled. The horizontal displacement and settlement results are to be used in the numerical verification.

A trench of 1.0 m width, 9.5 m length and depth of 21 m in normally consolidated soft clay in Japan was discussed by Tamano et al (1996). Soil cement piles with a small diameter of 0.46 m were installed in the upper 11 m to avoid any possible trench collapse in the upper sand and reclaimed layers. Inclinometers and pore water pressure cells were installed at different distances from the trench face. The test was focused on studying the horizontal displacement and earth pressure at different slurry density and levels. In the beginning of the test the slurry unit weight was  $10.2 \text{ kN/m}^3$ , then it was increased to  $10.6 \text{ kN/m}^3$  and reduced back again to

10.2 kN/m<sup>3</sup>. The slurry level was remaining constant; however, in the 18<sup>th</sup> day of the experiment the slurry level was reduced in stages from G.L. -0.3 m to -3.5 m which causes a high increase in horizontal displacement that indicated instability of the trench, so the slurry level was increased again to the original level and the displacement was reversed. The maximum horizontal displacement increased from 13 mm to 18 mm due to such lowering. In general, the soil deformation was greatly affected by the change in slurry level; however, the change in slurry density has a negligible effect. The lateral earth pressure was measured before and after excavating and placing the concrete. The values of the earth pressure after placing the concrete is almost between the values of at rest earth pressure and the pressure of the slurry.

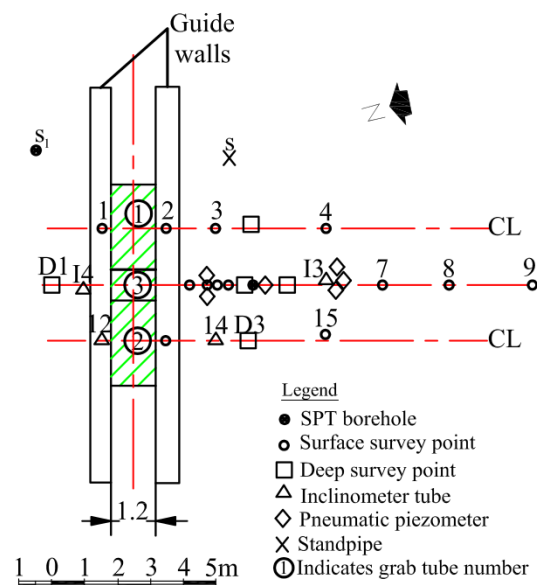


Fig. 3-6: Instrumentation plane for tested panel (after Stround and Sweeney, 1977)

Field monitoring was conducted and discussed by Poh and Wong (1998) for a rectangle diaphragm wall trench (6 x 1.2 x 55 m) in cohesive soil in Singapore. The soil consisted of three main layers, upper marine clay (very soft to soft), lower marine clay (soft to medium) and a stiff clay layer at the very low depth. The test was also conducted to understand the effect of lowering the slurry level. The horizontal displacement, soil settlement and pore water pressure were measured at different depths and distances from the trench. Before lowering the slurry, the maximum horizontal displacement measured from the nearest inclinometer (1.5 m from the trench) at the upper marine clay was 21.5 mm, while another peak (9.5 mm) was found at the lower marine clay layer. The horizontal displacement at the panel center is higher than that at the edges. It decreased with distance from the trench. It could be 45 mm at the panel edge by applying interpolation. The maximum recorded settlement was about 23.5mm at the center of the panel. The ground water level shows a decrease of about 0.5 m just after trenching. The holding period effect was insignificant regarding soil deformation. Lowering the slurry level of

1m causes the maximum horizontal displacement and settlement to increase 60% and 28%, respectively. The concreting of the trench decreased soil deformation.

Ng et al (1999) observed the deformation of a short diaphragm wall panel (Barrette) in Hong Kong. The panel was 2.8 m long, 0.8 m width and 40 m deep. A layer of Fill, Marine deposits, alluvium Clay, alluvium Sand and weathered granite was located in the site. The ground water was found at a depth of 3 m from the ground surface. The slurry density was  $10.8 \text{ kN/m}^3$ . Pressure cells, Piezometers, magnetic extensometers, inclinometers and settlement markers were used for observing the panel during trenching process. The maximum settlement and horizontal displacement were less than 3 mm. The limited difference between the bentonite pressure and initial horizontal stress could be the reason for the very low deformation values. The lateral pressure distribution with depth is shown in Figure 3-7.

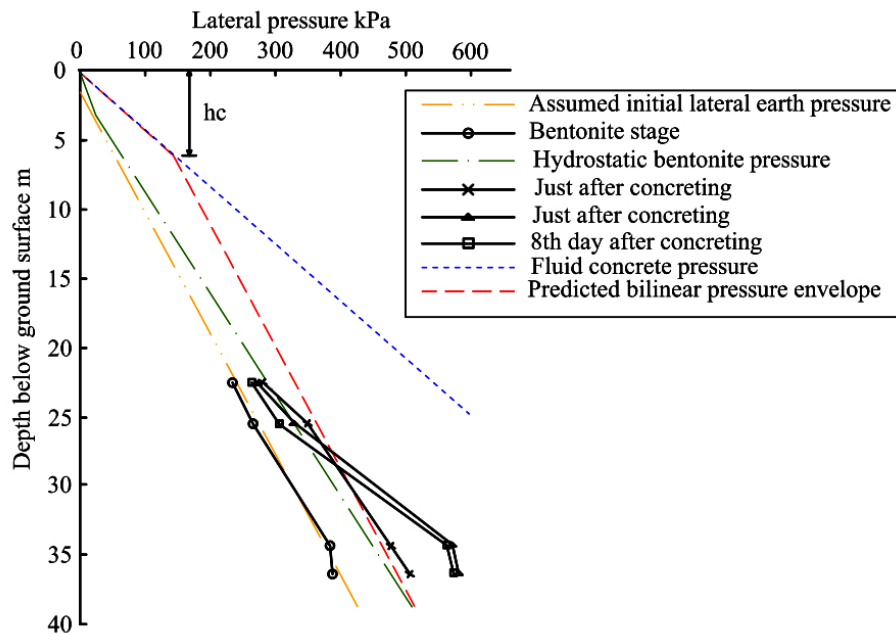
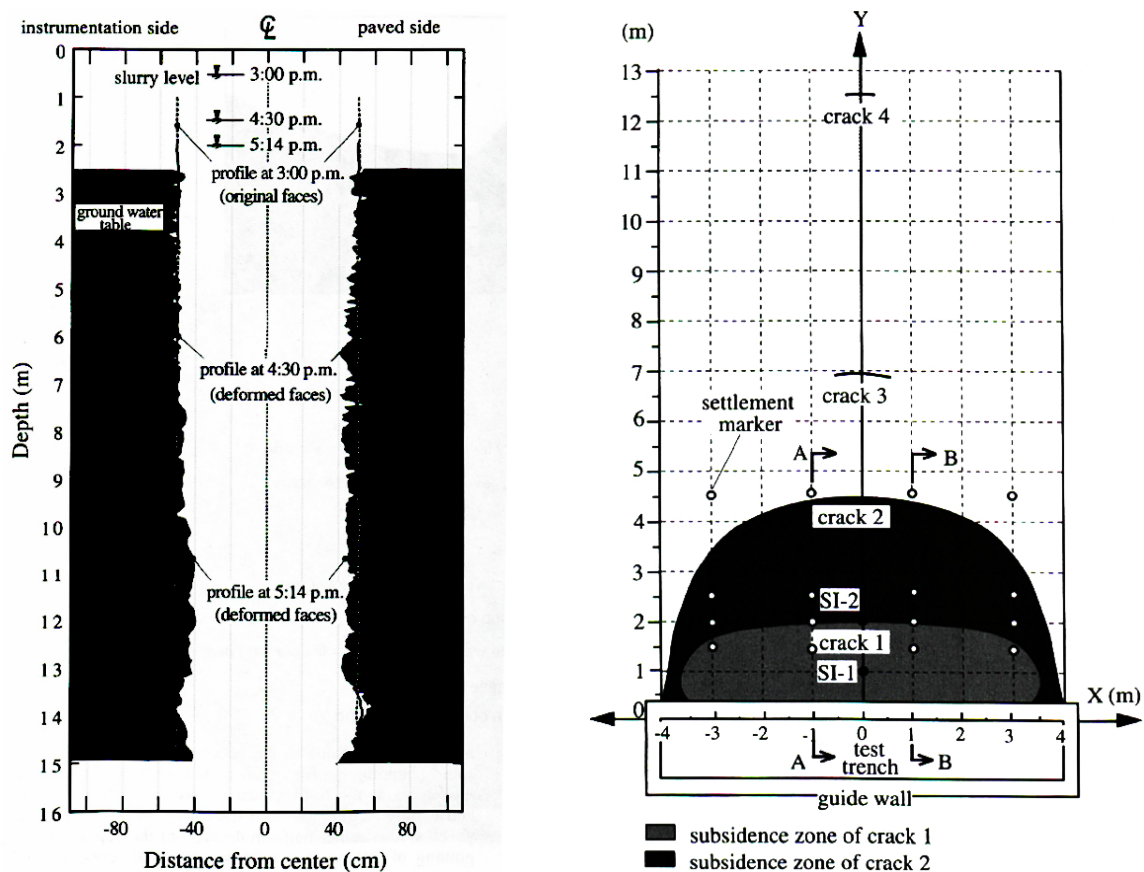


Fig. 3-7: lateral pressure distribution with depth (Ng et al, 1999)

In order to understand the failure mechanism of slurry trenching and proofing the analytical method by Tsai and Chang (1996), a full field experiment in sandy soil in Taiwan was discussed by Tsai et al. (2000). The monitored trench was 8 m length, 0.9 m thickness and 15 m depth. The ground water level was 3 m below ground surface. The guide wall was 0.3 m width and 1 m depth. The slurry in the trench was lowered in stages of 0.5 m until a failure was observed. Settlement marks, inclinometers and ultrasonic soundings were used to monitor the trench during construction. The monitoring system was placed in one side of the trench while the other side was paved with 30cm concrete slab in order to carry the machine. Lowering the slurry level showed a big variation in the horizontal displacement and settlement. The slurry level at 1.5 m below ground surface caused settlement of 7.2 mm. The settlement increased to

90 mm and the horizontal displacement was 13mm, when the slurry level was at 2.0 m below ground surface, after half an hour the settlement and horizontal displacement increased dramatically to 500 mm and 63mm, respectively. A 2 mm wide crack at a distance of about 2 m from the trench was appeared in the surface when the slurry level was 1.5 m. The ultrasonic sounding was then used and showed signs of failure at some depths as shown in Figure 3-8a. Three other cracks were observed by reduction of the slurry as shown in Figure 3-8b. The ultrasonic sounding was able to detect the failure surface, while the inclinometer didn't show any indication of failure.

Another experiment was also conducted in Taipei, Taiwan to study the effect of one/multiple diaphragm wall panels on the ground surface by Ou and Yang (2011). The soil was mixed between silty sand and clay. They found out that ground settlement from the tested panel was less than that from the construction of the entire diaphragm wall panels for the project.



(a) ultrasonic sounding profile  
 (b) Plan view of the cave in rough  
 Fig. 3-8: Failure surface detection (Tsai et al., 2000)

### 3.3.3 LABORATORY WORKS

The slurry trench field tests are expensive and they are limited to some situations. The laboratory simulation of slurry trenching process considered less expensive, can be made for many situations, and could provide better understanding of the soil deformation and earth pressure.

The effect of slurry trenching in cohesion-less soil was discussed by Elson (1968) through a series of small scale laboratory experiments. A steel tank 2.44 x 1.22 x 1.22 m filled with sand was used in the experiments. The trench width was variable, while its depth and length were 0.914 m and 1.98 m, respectively. The purpose of the study was to investigate the effect of slurry hydrostatic pressure, slurry passive resistance, filter cake characteristic and shear resistance of the soil zone infiltrated by slurry. The trench was constructed as a framework by insertion of six plywood sheets vertically to form the trench length, while its distance from the tank wall defines the trench width. Polythene sheets as shown in Figure 3-9 covered the outer face of the trench framework. The framework was slowly removed section by section during slurry pumping into the trench. In this case, the slurry was allowed to penetrate into the soil. Rising the water level was not enough to achieve failure; accordingly, a surcharge load was added at the top of the sand layer until failure. The shape of the failure zone was then recorded and measured. The experiment showed that the slurry hydrostatic pressure, its passive resistance and the shear strength of the soil zone saturated by the slurry are major factors that affect the trench stability. The measured settlement was small until the factor of safety was 1.1 and it increased rapidly after this value and until failure. The shear strength of the sand was increased due to the flow of the slurry into the sand.

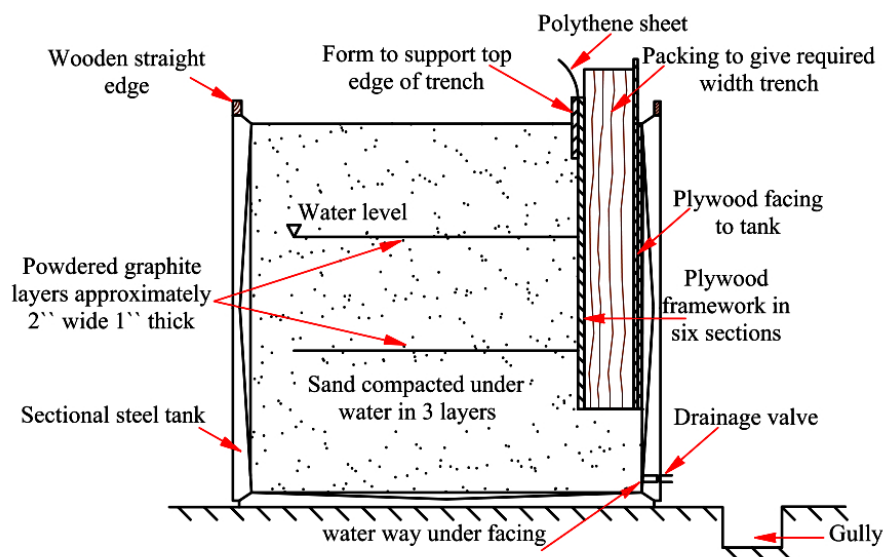


Fig. 3-9: Section of the tank showing the Framework (Elson, 1968)

Hajnal et al. (1984) discussed an experiment performed by the Research Center of Water Resources Development in Hungary in 1971. The aim of the experiment was to understand the effect of trench length and width in addition to the effect of groundwater and slurry levels. The experiment consisted of four test series. The first two series were considered to be preliminary experiments and they were conducted in a glass box filled with sand with a surface dimension of 0.3 x 0.5 m and a depth of 0.3 m. A temporary stabilizing plate was used to simulate the

trench inside the box which was removed to achieve failure. A crack with an arch-like curve was observed at the surface during the failure. The third and fourth series were conducted in a larger box with a depth of 1.0 m and a surface dimension of 1.0 x 0.6 m filled with river gravel. A slot was made and filled with bentonite slurry with a width of 45mm, length varies between 200 and 700mm and depth in range 200 to 670mm. A gradual inundation was made in steps until failure. The surface settlement and variations in slurry and groundwater levels were recorded for the successful nine tests. The trench stability is decreased linearly by increasing its length for the same depth. The stability decreased with increasing depth.

The implementation of the small scale tests could be useful to give indication of the general behavior of the trench, but indeed they cannot provide real deformation values because they used to model the trench dimensions with small values compared to the field. The centrifuge experiments could be the other best alternative. It was used by (Kantartzi 1993; Powrie, Kantartzi 1996) to study the effect of slurry trenches in clay. The purpose of the test was to find out the effect of trench geometry and ground water level on the ground deformation and earth pressure. The simulation was made with a strongbox of dimension 550 x 200 x 285 mm. A slot of 185mm was simulating the diaphragm wall. A rubber bag filled with a sodium chloride solution of a density equal to  $1.16 \text{ kN/m}^3$  was replacing the clay to simulate the slurry trench. This solution was 85 mm higher than the soil surface to model the initial high lateral stress of the over-consolidated clay and adjusting the value of earth pressure coefficient  $k_0$ . Half of the required width was simulated i.e. 5mm in the model scale. The diaphragm wall equivalent dimension was then 18.5m depth and 1m width in a 1:100 centrifuge scale. The panel length was 5, 10 m and infinity (plane strain). The simulation of the trenching process was conducted by reducing the sodium chloride solution level to the soil surface. The final density of the solution was then  $11 \text{ kN/m}^3$ . The concreting process was simulated by adding a mixture of iron powder, cement and fine sand to solution inside the rubber and then the final density was  $24.5 \text{ kN/m}^3$ . The time of trenching process was 60-100 seconds which corresponds to 7-11 days from the field time scale; however, in reality it just takes one day. The concreting process took in experiment until hardening from 7 to 10 minutes which is equivalent to 50 to 70 days; in reality it normally needed 30 days. The time difference indicated that excess pore water pressure from the laboratory should be higher than that from the field. The water table in all the tests was at the ground surface except one test it was 10m under the ground surface. The changes in pore water pressure and ground deformation during the installation of the diaphragm wall were observed. Generally, the pore water pressure reduced during trenching and increased again during concreting almost to its original value. However, a slight increase in pore water pressure during trenching in some locations was noticed. This may be due to the

increase of total horizontal stress under the trench bottom as the soil in this place was prevented from moving. The change in pore water pressure was also affected by the arching effect of the trench with finite length. The deformation of soil due to diaphragm wall installation is presented in Figure 3-10 (a). The arching and ground water effect on the ground deformation can be noticed from the Figure. Test 3 showed the lowest values of settlement, because the ground water level in this test was 10m below surface. The settlement just near the trench is considered to be greater than that from the field data because the guide wall was not simulated in the model. The trench height to length value with the normalized settlement is presented in Figure 3-10 (b). The authors recommended an idealized trench length to depth ratio between 0.25 and 0.3.

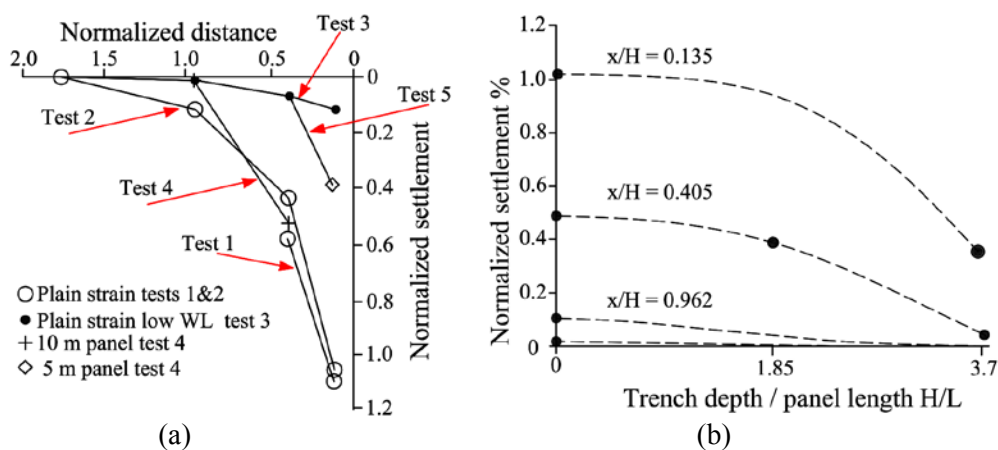


Fig. 3-10: normalized Settlement due to diaphragm wall installation with (a) normalized distance (b) normalized height to trench length (after Powrie and Kantartzi, 1996)

Katagiri et al. (1997) studied the failure behavior and deformation of slurry trenches in sand using centrifuge model tests under the 2D and 3D conditions. The trench shape effect and surcharge load were the main factors of investigation. The strongbox dimension was 800 x 250 x 400 mm. The used scale for the centrifuge model was 1:60. Saline water with density of 10.5 kN/m<sup>3</sup> was used to fill a rubber bag that simulates quarter of the prototype trench. The field scale of the used diaphragm wall was 15 m depth and 1m width with variable length between 3 and 6 m or infinity in case of 2D analysis (plane strain). In all tests, the groundwater level was at the surface. A 34 kPa surcharge load was applied in some tests with different length ranges between 3.78 and 7.56 m. The slurry level was lowered until failure. The stability condition was defined by the difference between the slurry and water levels at yield point. The stability condition was directly proportional to the panel length to width ratio and the surcharge load. The change in groundwater level in the unstable zone was in contrast to the soil settlement. The deforming zone size is directly proportional to the panel length and is also greatly affected by the presence of surcharge load. The settlement reduced with distance from the trench.

### 3.4 DIAPHRAGM WALL INSTALLATION ADJACENT TO DEEP FOUNDATION

The installation of the diaphragm wall adjacent to deep foundations had happened in limited projects around the world; however, it is expected to be in more projects in the future specially in the crowded developed cities. This section discusses some case histories and one centrifuge model test related to the construction of diaphragm wall near deep foundations.

#### 3.4.1 CASE HISTORIES

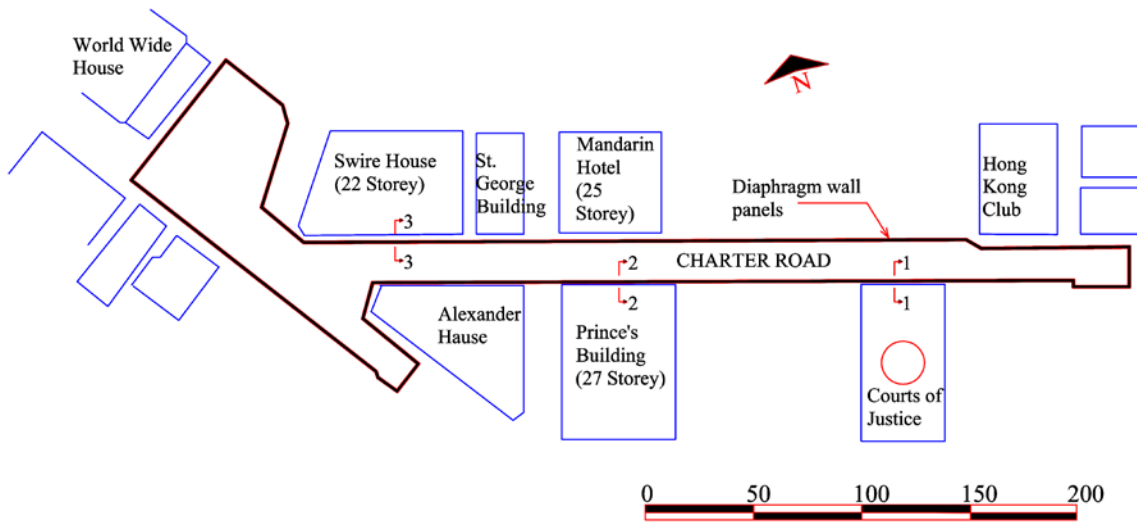
This section discusses four case histories in four different countries. Soil deformation was the only available output from the projects. The behavior of pile itself was not discussed, as it was quite difficult to investigate the existing piles.

##### **3.4.1.1 Charter underground station (Hong Kong)**

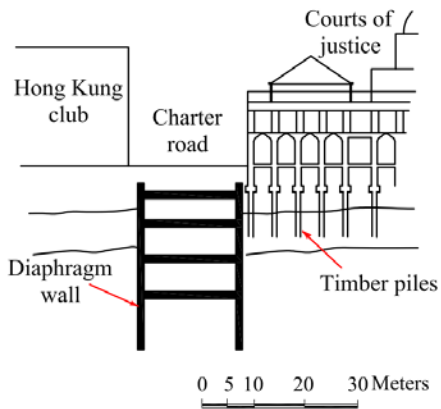
The construction of Charter Station in Hong Kong included installing diaphragm walls in a crowded area containing buildings on piled foundation as shown in Figure 3-11. The effect of station construction on adjacent ground surface and adjacent building was presented and discussed by Davies and Henkel (1982). The depth of the deep excavation was 27 m. The main construction operation of the project started in October 1976. The diaphragm wall was 1.2 m in thickness, 37 m depth and length varying between 2.7 and 6.1 m. The installation of the diaphragm walls near the Courts of Justice, Hong Kong Club and Princes building caused a maximum settlement of 78, 38 and 21 mm, respectively. These settlement values were considered to be high in comparison with similar other projects. Cracks were observed in the Courts of Justice building due to the differential settlement. The large settlement values were due to the swelling of the decomposed granite during panels construction.

The length of the used diaphragm walls near all buildings was in the range between 4.8 and 6.1 m. To avoid large settlement, the length used for the diaphragm wall panels near Swire House was 2.7 m. The slurry level was increased to 0.3 m above the ground level using a higher guide wall as shown in Figure 3-12. The settlement was measured for each column for the Swire house. The maximum settlement was about 15 mm and horizontal displacement was 14 mm. The three sections were used in the next chapter for numerical verification.

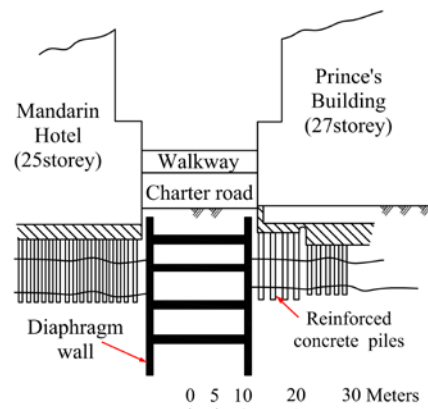




(a) Plan



(b) Section 1-1



(c) Section 2-2

Fig. 3-11: Charter Station and adjacent building (after Davies and Henkel, 1982)

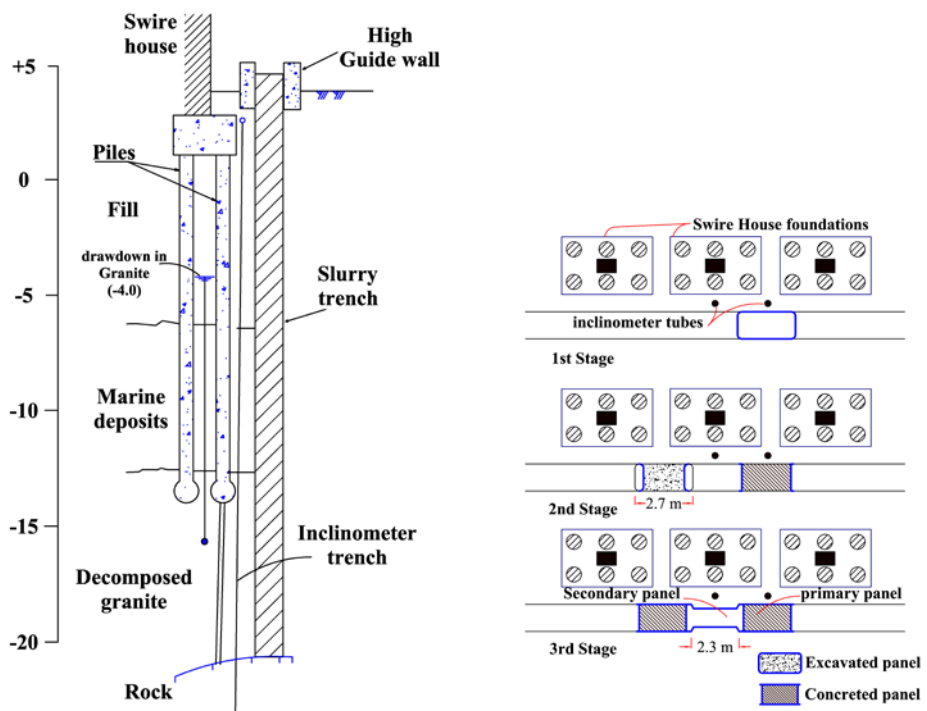


Fig. 3-12: Diaphragm wall near Swire House (after Davies and Henkel, 1982)

### 3.4.1.2 Full scale field test (Amsterdam)

The 30 m deep underground metro stations for the North/ South line in Amsterdam were constructed using the diaphragm wall in urban area. Mixed soil layers were found in the area and consist of Fill, Clay, Peat and Sand. Wit, de et al (2000) and Wit, de & Lengkeek (2002) were curious about the effect of the diaphragm wall construction on the nearby piled foundations. They conducted a full scale test as shown in Figure 3-13 using diaphragm walls with dimensions were 2.7 x 0.8 x 35 m. The adjacent tested steel piles were 3 piles with 11 cm in diameter and driven at a distance of about one panel width from the trench. Before installing the diaphragm wall, the tested piles were subjected to load equivalent to normal housing load. The monitoring system included measuring the vertical and horizontal displacement and pore water pressure. The stress was indicated by measuring the CPT's (cone pressure meter test) after and before the diaphragm wall installation. The maximum recorded vertical deformation was only 4 mm during excavation, and during concreting it was the same but upwards (heave). The maximum horizontal displacement during excavation was only 10 mm in the trench direction; however, during concreting a very high value of horizontal displacement was noticed at the soft clay soil layer and it was about 150 mm.

The ground deformation was greatly affected by the panels' shape and construction sequence. The effect of trenching process on pile bearing capacity was low due to the small relative displacement between the pile and the soil during trenching.

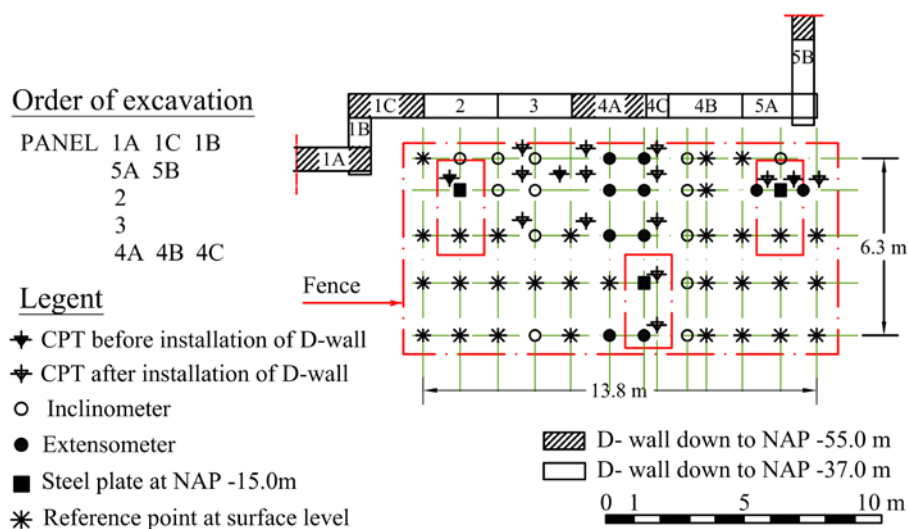


Fig. 3-13: Instrumentation layout of the test (Wit de and Lengkeek, 2002)

### 3.4.1.3 Underground basement (Giza, Egypt)

The effect of constructing an underground 10.8 m deep basement surround by five buildings in Giza was presented and discussed by (Abdel-Rahman, El-Sayed 2002a, 2002b, 2009). The diaphragm wall consisted of 20 panels with variable length ranges between 2.7 and 6.72 m, while their width was 0.6 m and depth reaches 21 m. Settlement points were used to measure

the buildings settlement. It was found that settlement due to trenching near deep foundation is less than that near shallow foundations. The settlement from diaphragm wall installation was about 80% in average from total settlement. Based on the monitoring results, the following Equation 3.3 was introduced for calculating the settlement due to trenching:

$$S_{trenching} = S_{max}^{trenching} \left[ \frac{2H - x}{2H} \right]^6 \quad 3.3$$

where:  $x$  is the distance from the trench and  $S_{max}^{trenching}$  is the settlement that is adjacent to the trench, which can be taken as 0.045% from the trench depth. The results of this fieldwork are discussed in detail with the numerical analysis in the next chapter.

#### 3.4.1.4 Underground stations (Amsterdam)

Korff (2013) studied the effect of constructing three underground metro stations on the adjacent buildings in Amsterdam. The soil was formed from mixed layers of Holocene, Sand, marine Eemclay and glacial Clay. The buildings in the area were almost 70 to 100 years old constructed on timber piled foundations. Pile load tests were performed on piles from a demolished house in the area. The tests results allow to calculate the bearing capacity of the piles in the area. The pile diameters ranged between 0.22 and 0.25 m while its toe was 0.11 m in diameter. The piles length was 12 m in average. The realistic capacity of the piles was considered to be 90 kN. The monitoring for the buildings and ground surface was made for all the construction stages. Generally, the settlement from primary activities that includes site preparation, diaphragm wall installation and pumping test was more than the half of the total settlement as shown in Table 3-2. Generally, The piled buildings settlement was smaller than the ground displacement.

Table 3-2: Ground displacement from primary activities (Korff, 2013)

Station	Diaphragm wall depth (m)	Excavation depth (m)	Surface displacements caused by preliminary work/total displacements
Ceintuurbaan	39	26	70%
Vijzelgracht	44.5	29.5	55%
Rokin	46	31	74%

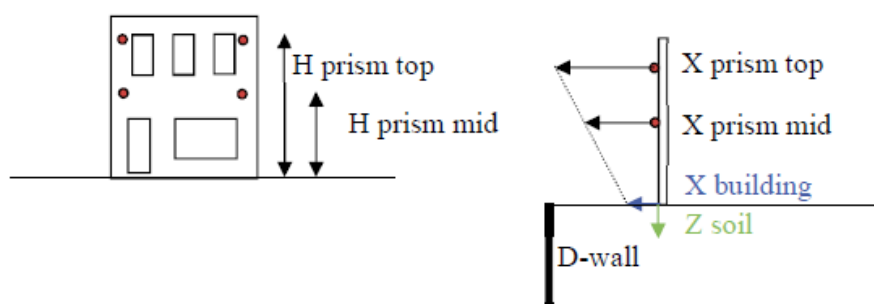


Fig. 3-14: Buildings horizontal displacement measuring method (Korff, 2013)

The buildings tilt was indicated by measuring the differential settlement of the building and the horizontal displacement from its top and bottom as shown in Figure 3-14. The horizontal displacement at the street level was about 50% of the settlement and it didn't exceed 10 mm. Korff (2013) assumed that one third of the horizontal displacement could be transferred to the piles. That means the piles in this case to have a maximum horizontal top displacement of 4 mm.

### 3.4.2 LABORATORY TEST

The pile or pile groups subjected to excavation or tunneling was modeled in laboratory by several researchers such as Leung et al. (2000), Loganathan et al. (2000) and Ong et al. (2009). However, the study of trenching process and its effect on piled foundation was only conducted and discussed by (Choy, 2004; Choy et al., 2007).

#### 3.4.2.1 Test description

A series of eight centrifuge model tests were made to study the effect of constructing single/multi panel diaphragm wall on adjacent single driven pile. The centrifuge strongbox dimension was 700 x 400 x 470 mm, while the used acceleration was 75g. Dry sandy soil was used in the study with friction angle of 32°. The pile was simulated using aluminum tube with a diameter of 12 mm and length of 250 mm, which represent a pile of diameter 0.9 m and length 18.75 m in the field scale. The pile was chosen to be at offset distance of 3.5D, 5.6D and 7.7D where D is the pile diameter. Latex membrane was used to simulate the diaphragm wall panel(s) slot. The simulated panel(s) was 1.2 m in thickness (B) and 26.25 m in depth (H), while the length was 3 or 6 m. Two tests simulated the multiple panels. One test included single concrete panel, while another test included two concrete panels. Summary of the successful tests is presented in Table 3-3. The guide wall was simulated with rectangle aluminum plate with equivalent field depth of 1.5 m.

Table 3-3: Summary of successful centrifuge tests (Choy, 2004)

Test	Panel length (m)	Pile offset distance (m)	Number of Concrete panels	Slurry density (kN/m <sup>3</sup> )	segmental pile response	d/H at failure (%)
CKC1	6.0	6.93	-	10.97	N/A	80 %
CKC3	6.0	3.15	-	10.95	N/A	45 %
CKC6	6.0	3.15	-	10.89	N/A	45 %
CKC7	6.0	5.04	-	10.92	N/A	80 %
CKC13	3.0	3.15	1	10.92	A	82 %
CKC14	3.0	3.15	2	10.91	A	90 %
CKC15	3.0	3.15	-	10.92	A	80 %
CKC16	6.0	3.15	-	10.93	A	60 %

Note : The dimension is in the prototype scale  
d/H : slurry level to trench depth at failure

### 3.4.2.2 Test procedure

The first step was to fill the strongbox with sand while the latex membrane is placed as shown in Figure 3-15. The water was used first to fill the latex membrane to support the soil during accelerating. The pile was also placed in position of 10 mm (75cm field scale) above its final level as shown in the figure. During centrifuging, the pile penetrated into its final level. Then the sodium polytungstate with density of  $11 \text{ kN/m}^3$  was used to simulate the slurry in the trench. The concreting process for tests CKC13 and 14 was made by adding a mixture of coarse sand and a powder of stainless steel. The slurry was reduced in stages until soil failure but before the pile damaged.

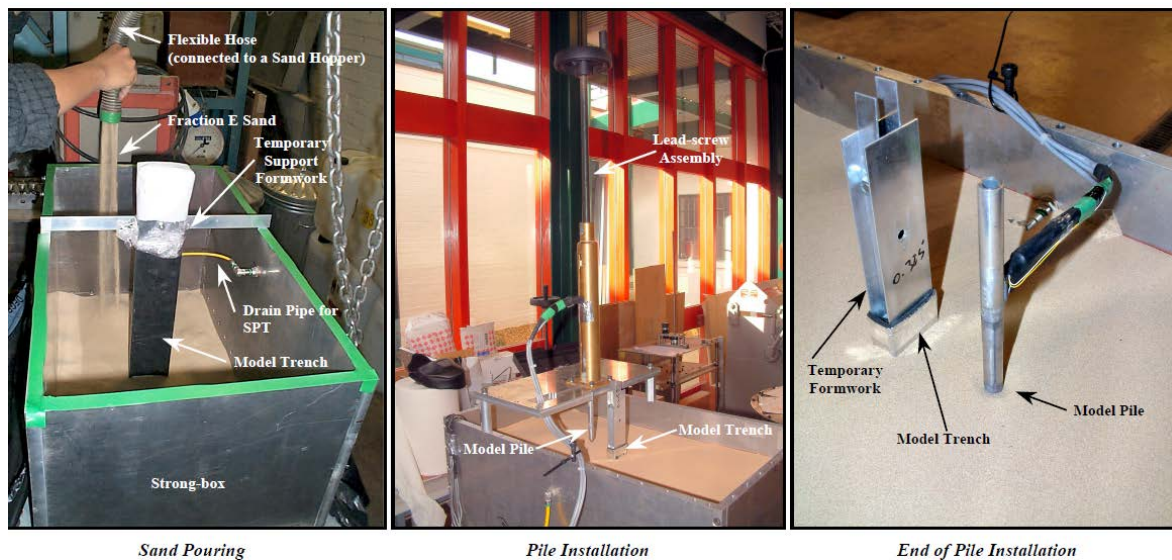


Fig. 3-15: Test preparation and sequence (Choy, 2004)

### 3.4.2.3 Test results

The stress and deformation of the soil and the pile deflection, settlement, bending moment and shear stress were monitored during the different stages of the test.

Generally, the soil horizontal stress increased with pile installation, while during excavation the horizontal soil strength increased near the center of the trench and decreased near the edge as shown in Figure 3-16. On the other hand, during the slurry reduction, the relation is reversed, as the horizontal stress near center decreased while it increased near the edge.

The effect of slurry trenching (change the water to the slurry) on the ground surface deformation was almost negligible. The pile installation effect on the ground surface deformation had the same trend for all the experiments with a maximum settlement of no more than 1mm (field scale). The reduction of the slurry causes noticeable deformation and it was huge at failure as shown in the picture taken just after failure in Figure 3-18. The shape of failure surface at the pile side was different from that at the soil side as shown in Figure 3-19. The pile deflection and bending moment increased with the advance of reduction in slurry.

The deflection and bending moment increased greatly at failure. The pile shear stress was increased with slurry reduction. The results are presented in the next chapter for numerical verification.

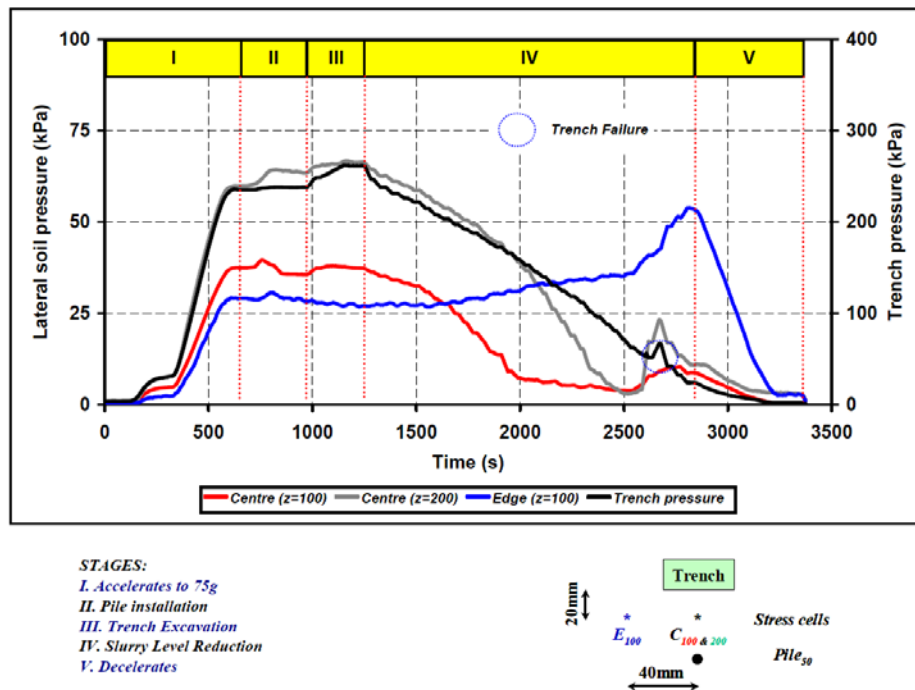


Fig. 3-16: Soil and trench pressure with time during testing (3.0m width diaphragm wall) (Choy, 2004)

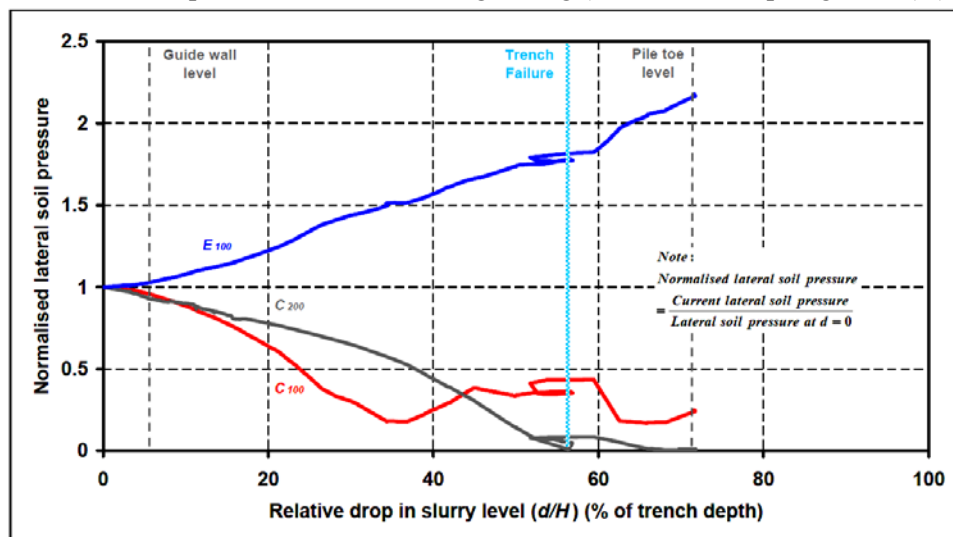


Fig. 3-17: Change in soil stress during slurry reduction (6.0m width diaphragm wall) (Choy, 2004)

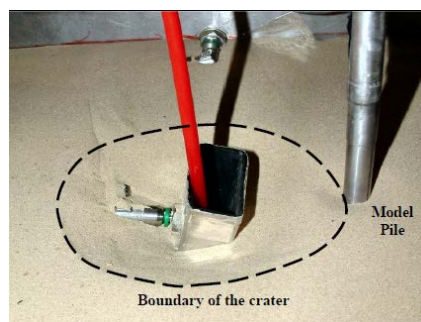


Fig. 3-18: Soil deformation after test (Choy, 2004)

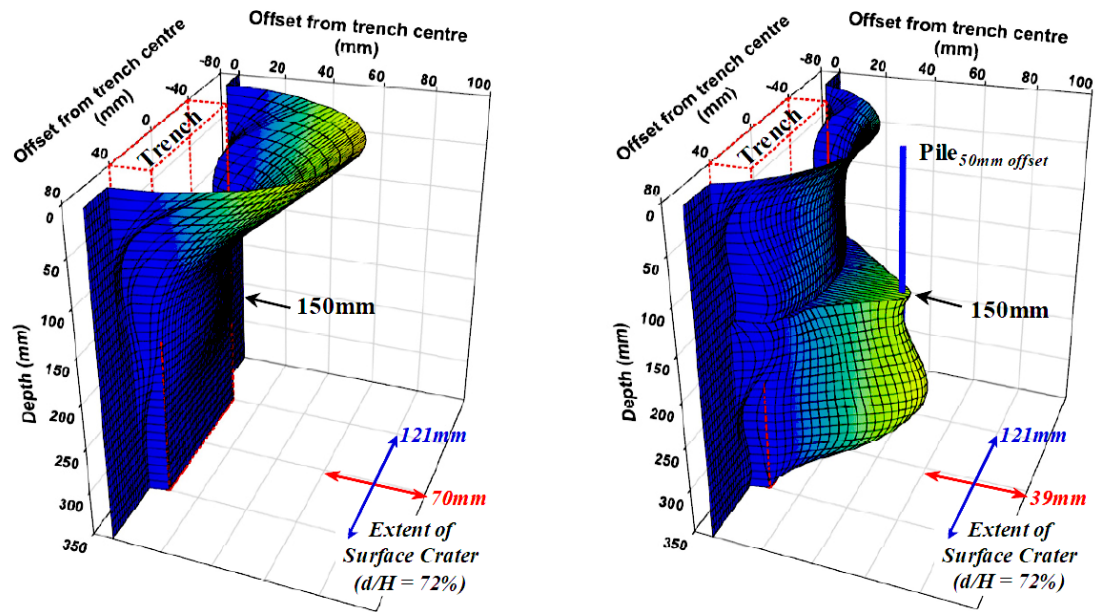


Fig. 3-19: Failure surface recorded on both sides of the 6m trench CKC16 (Choy, 2004)

### 3.4.2.4 General conclusion and comments

The soil used in the experiments was dry sand; however, the groundwater is normally found in most engineering projects. The initial stress state was affected by filling the trench with water in the beginning of the experiment as was described. The water inside the trench causes the horizontal pressure to be  $\gamma_w z$  ( $9.8z$ ) instead of  $k_s \gamma_s z$  ( $7.3z$ ). Replacement of the water with the slurry (sodium polytungstate) causes the horizontal pressure to be  $\gamma_{slurry} z$  ( $11.0z$ ). This stress difference caused a slight horizontal movement towards the trench and small heave during trench excavation (change water with slurry). This contradicts with the fact that during slurry trenching the soil moves horizontally towards the trench and the settlement could be observed in the soil surface instead of heave, as discussed in the previous chapter. Generally, the absence of water causes the soil pressure to be less than the slurry pressure, which is not common in the real engineering projects. The failure in the experiment was based on the reduction in the slurry. The maximum allowable depth of slurry reduction can be calculated by back stability calculations. The factor of safety can be calculated by applying Morgenstern and Amir-Tahmassebi (1965) two dimension stability analysis method as follows:

$$FS = P_s / P_f \quad 3.4$$

The slurry force  $P_s$  calculated as

$$P_s = \gamma_s Z_s^2 / 2 \quad 3.5$$

Where,  $\gamma_s$  and  $Z_s$  are the slurry density and depth, respectively. While, the horizontal acting force  $P_f$  is calculated from Equation 3.6.

$$P_f = [\gamma H^2 / 2 (\sin \theta - \cos \theta \tan \phi) + U \tan \phi] / (\cos \theta + \sin \theta \tan \phi) \quad 3.6$$

Where,  $\gamma$  is the soil density and  $H$  is the trench depth. The value of  $\theta$  (the inclination of the plane of failure) was used as  $45^\circ + \phi/2$ . While, the water pressure  $U$  is equal to zero and friction angle  $\phi$  equal  $32^\circ$  the horizontal acting force  $P_f$  equal  $62.7 \text{ kN/m}$ . In this case the slurry level could be only 3.5m high inside the trench to achieve a factor of safety equal unity, it means the slurry could be reduced 87 % of the total trench depth. This solution is considered to be conservative, as it didn't take into consideration the arching effect.

By conducting Fox (2004) three dimension analytical approach for such case the factor of safety equal 1.35 for the 6m length trench and 2.35 for the 3 m length trench. The trench could theoretically sustain global failure if the slurry reduced up to about 90 %. Back to Table 3-3 The failure was observed for most of the tests at 80 % or higher even for the 6m panel length such as CKC1 and CKC7. However, it was less than 60 % for tests CKC3, 6 and 16. The only logical reason is the location of pile very close to the trench (i.e. 3.15 m). In this case, the load from the pile could have probably increased the load on the slurry wall edges. The diagram movement pattern at failure presented in Figure 3-19 shows that the soil deformation under the pile tip was great. The failure in this case happened in place below the pile toe, while in the other tests it was at the upper part. Choy (2004) suggested that a base wedge under the pile tip should be added as a pressure force acting on the slurry trench wall. It can be clear, that the failure happened when the slurry reduced near the pile tip level (i.e. 60% = 18 m) and that only for the large panels. In reality, the slurry never reduced to such level but the slurry pressure could be reduced at some depths due to coarse materials or lenses.

The settlement due to slurry reduction at the pile side is higher than that at the soil side. This match with the results of Abdel-Rahman, El-Sayed (2002a).

The used latex membrane should have played the role of the filter cake but indeed it could provide some additional strength for the trench wall surface. In reality, filter cake is formed during trenching but it is not strong enough to form a structural membrane; it only prevents grains' penetration inside the trench. It is possible that the pattern of soil deformation was affected by the presence of such a membrane. However, the tests provide a very good overview of the effect of slurry trenching on piles.

### 3.5 DATA COLLECTION AND DISCUSSION

Many researchers have presented the monitoring results of slurry trenching. The presented results are varying according to the project natural and soil type. The summary of literature work regarding the diaphragm wall installation effect on the ground surface deformation and stress are presented in Table 3-4. In the table, the maximum settlement and horizontal displacement are presented. The normalized horizontal stress percentage (i.e. horizontal stress



after trenching ( $\sigma_h$ ) / initial horizontal stress ( $\sigma_{hi}$ ) %) was presented as well. The following subsections describe the effect of trenching on soil deformation and stresses based on the literature.

### 3.5.1 STRESS CHANGE

Few researchers recorded the horizontal stress from several sites all over the world. The normalized horizontal stress percentage from the literature is plotted in Figure 3-20. All the results were related to cohesive soil except Ng et al (1999) it was mixed soil. The values from Ng et al. (1995) considered to be very low compared to the others. If these values ignored, the average normalized horizontal stress could range between 70 % and 90 %. The normalized horizontal stress values are higher at the shallower depths and it even can reach 100 %. In general, the trenching process causes the horizontal earth pressure to decrease with values ranging between 10 % and 30 %, which means the average value of earth pressure coefficient can be used as 80 % of the at rest earth pressure coefficient during the trenching process.

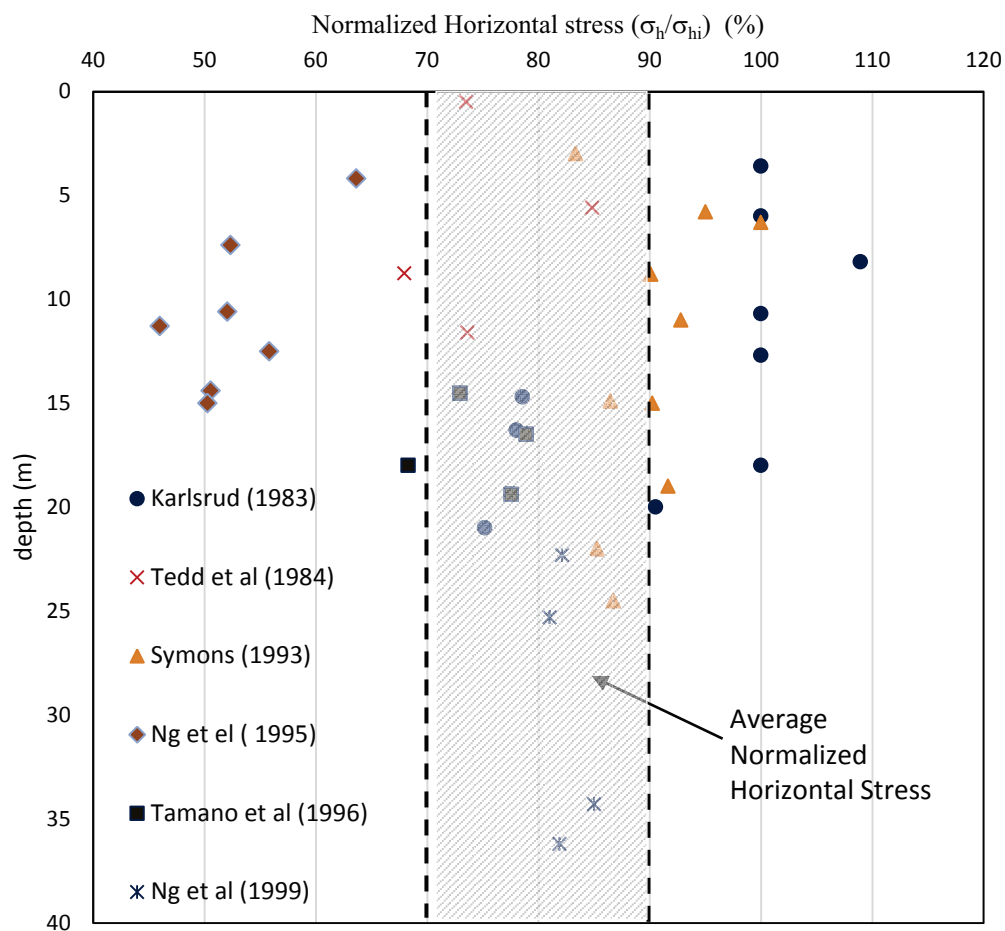


Fig. 3-20: Normalized horizontal stress with depth

Table 3-4: Summary of diaphragm wall installation field results

Researcher	Type of work	Panels dimension (L x T x H) m	Main Soil type/ location	Max. Settlement (mm)/distance (m)	Max. Horizontal disp. (mm)/ depth (m)	$\sigma_h/\sigma_{hi}$ % Equivalent to $K/K_o$ %
Dibiagio & Myrvoll (1972)	Tested panel	5x1x28	Soft clay / Norway (Oslo)	8.0/0	10.5/30	N/A
Farmer (1973)	Tested panel	6.1x1x15	London Clay / England	6 /0.6	16/5	N/A
(Stround and Sweeney 1977)	Tested panel	6.1x1.2x36	Mixed soil /Hong Kong	Working 6/3.5 Lowering 22/2.0	Working 29/17 Lowering 59/11	N/A
(Davies and Henkel 1982)	Case history Near Piled foundation	2.7to6.6x1.2x37	Mixed soil /Hong Kong	Building1: 78/1 Building2:21/1 Building3: 15/1	Building1: 100/? Building2:100/? Building3: 14/17.5	N/A
Karlsrud (1983)	2 Case histories	S.L. 4.5x1x21	Soft clay / Norway (Oslo)	5/3	10/3	80%
		J.B.T 4.5x1x15		N/A	13/7.5	95%
Tedd et al. (1984)	Case history (secant pile)	1.18x1.18x21	London clay	9/2.6	15/2	≈80%
(Cowland, Thorley 1985)	7 Case histories	Varies x0.8to1.2 x20to50	Mixed soils /Hong kong	Chart Ground s/H =0.12% Building s/H =0.15%	N/A	N/A
(Clough and O'Rourke 1990)	Collection of work from (Cowland, Thorley 1985; Tedd et al. 1984; Karlsrud 1983) and others			Curve	N/A	N/A
Symons and Carder (1993)	Several projects	T-sec 2.7to4x0.8x13.5	London clay /England	N/A	N/A	≈80%
(Tse and Nicholson 1993)	Case history several panels	3.75x0.8x23.5	London clay /England (London)	N/A	3/7	N/A
(Lings et al. 1993a; Ng et al. 1995; Ng 1998)	Case history several panels	8.5x0.6x17	Gault Clay /England (Cambridge, Lion Yard)	Without piling: 2/7.5 With piling: 6/8	N/A	≈50%

Researcher	Type of work	Panels dimension (L x T x H) m	Main Soil type/ location	Max. Settlement (mm)/distance (m)	Max. Horizontal disp. (mm)/ depth (m)	$\sigma_h/\sigma_{hi}$ % Equivalent to $K/K_o$ %
Tamano et al (1996)	Tested panel	9.5x1x21.0	Soft clay /Japan	N/A	(SL*=-0.3)13/13 (SL=-3.5)18/13	90% to 80%
Poh and Wong (1998)	Tested panel	6x1.2x55	marine Clay /Singapore	(SL=+0.1) 23.5/0 (SL=-0.9) 30.0/0	(SL=+0.1)21.5/10 (SL=-0.9)33/10	N/A
Ng et al (1999)	Tested panel (19.5m Casing)	2.8x0.8x40	mixed soil / HongKong	1.5/2.6 2.5/6.4	2.6/1.5	100% to 80%
Hamza et al (1999)	several projects	50m in depth	Sand/ Egypt	Equation	N/A	N/A
(Tsai et al., 2000)	Tested panel	8x0.9x15	Sand/ Taiwan(Tainan)	(SL= -1.5) 7.2/2.5 (SL= -2.0) 90/2.0 (SL= -2.0) 500/2.0	(SL= -2.0) 13/1.0 (SL= -2.0) 63/2.5	N/A
(Poh et al. 2001)	Case history 1	2.8to5.5x0.6to0.8 x17.2to28.1	Silt /Singapore	25/2.5	8.2/14	N/A
	Case history 2	2.4to6.3x0.6to0.8 x13.1to25	Silty Clay /Singapore	11/1.0	-15/3 9/11.2	
	Case history 3	Varies x0.8to1.5 x25to45	Mixed soil /Singapore	4/5	-5.5/4 5/8	
	Case history 4	2.7to7.5x1.0 x23.8to30.7	Silt /Singapore	N/A	21.5/12.5 SL $\approx$ WL	
(Thorley and Forth 2002)	Case History	3to5x1.2x40to50	Weather granite /Hong Kong	78/3	N/A	N/A
Wit de & Lengkeek (2002)	Case history Tested panel Near Piled foundation	2.7x0.8x35	mixed soil	4.5/2	9/10 Trenching -100/9! (Concreting)	N/A
(Abdel-Rahman, El-Sayed 2002b, 2002a, 2009)	Case history Near Piled foundation	2.7to6.7x0.6x21	Sand /Egypt (Cairo)	(Building A) 8.6/1.8 (Building B) 8.0/3.1 (Building D) 6.5/3.2 (Building E) 6.7/3.2	N/A	N/A
(Abdel Rahman 2007)	Case history	2.8x0.8x27	Sand /Egypt (Cairo)	2.5/5.0	N/A	N/A

Researcher	Type of work		Panels dimension (L x T x H) m	Main Soil type/ location	Max. Settlement (mm)/distance (m)	Max. Horizontal disp. (mm)/ depth (m)	$\sigma_h/\sigma_{hi}$ % Equivalent to $K/K_o$ %
(Ou and Yang, 2011)	CN253B	First tested panel	3.4to5.5x1.0x35.5	Mixed layer of Sand and Clay / Taiwan (Taipei)	11.5/4.0	4.6/2.5	N/A
		Multiple panels			20/2.0	12.1/3	
	CN255	Tested panel	3.6to5.0x1.0x41		16/1.0	N/A	
		completed wall			40.5/14.0		
(L'Amante et al. 2012)	Case history		T-Shape X1.2x50	Sand /Italy (Bari)	N/A	8/0	N/A
(Korff, 2013)	Rokin		2.8to5.2x1.2x39	mixed soil / Netherland (Amsterdam)	10/10	N/A	N/A
	Vijzelgracht		2.6to3.7x1.2x44.5		20/55		
	Ceintuurbaan		2.6to3.8x1.2x46		20/3		
(Chen et al., 2014)	Case history		4.05x0.8x20.5	Soft clay /China (Shanghai)	9/3.4	N/A	Decrease in stress
(Shi et al., 2015)	Case history		Unknown x0.8to1.0x26	Soft clay /China (Shanghai)	N/A	4/0	N/A
(Rotisciani et al., 2016)	Case history		0.6to1.0 x 10to22 (Piles)	Sand and silt/ Italy (Rome)	7/1m	N/A	N/A

\* (SL) slurry level

### 3.5.2 SETTLEMENT

In general, the settlement decreased with distance from the trench. The maximum surface settlement presented in the table varies greatly. A value of 25 mm could be considered as the maximum recorded settlement value in normal trenching situation. However, a value of 78 mm was found and it was due to large horizontal movement of the weathered granite during trenching in Hong Kong. Lowering the slurry in the tested panels shows a relatively large amount of settlement, the maximum recorded value due to lowering the slurry was 500 mm. The values of settlement from literature were within the curve suggested by Clough and O'Rourke (1990) except the trenching process in Hong Kong as shown in Figure 3-21. The settlement values for the points above the suggested curve in the figure are low due to the small value of panel length and high level of the slurry. While the other points between the suggested curve and Clough curve have either a longer panel length or low slurry level. However, the settlement could be low with a low slurry level value if the water table was low.

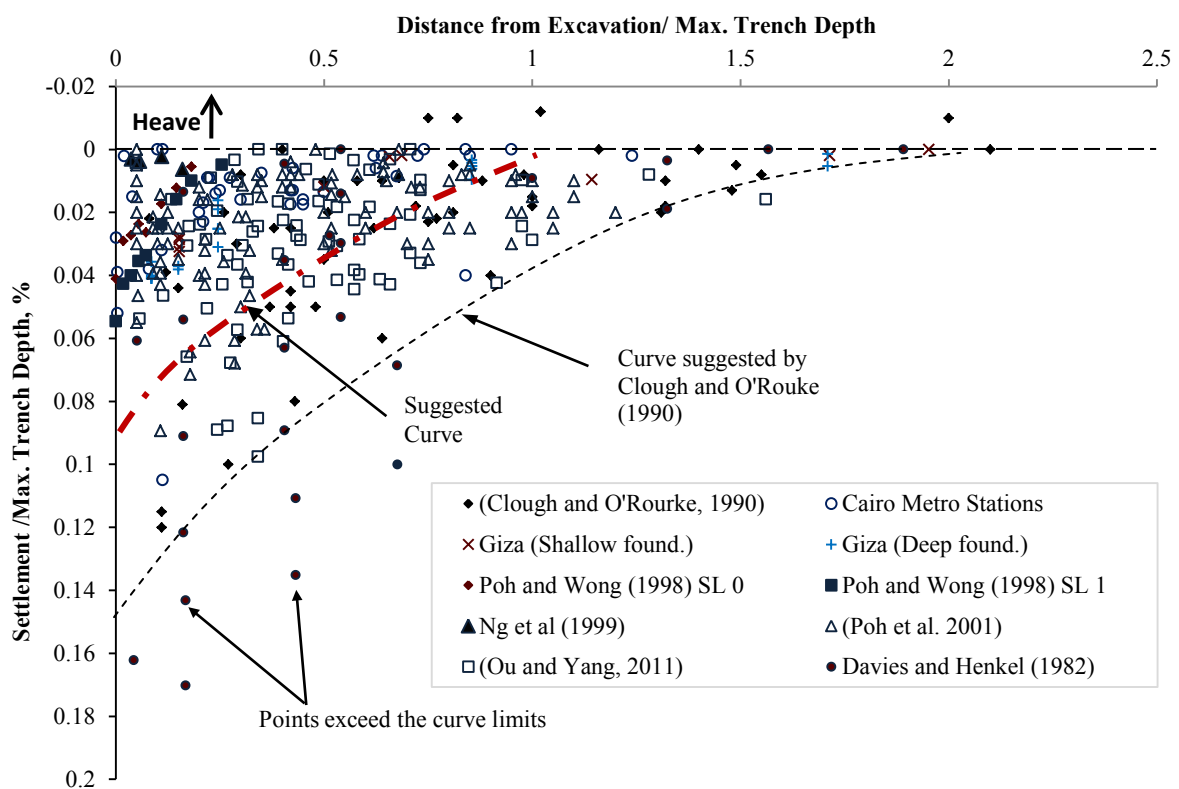


Fig. 3-21: Normalized settlement to normalized distance from the trench due to the diaphragm walls installation

Since the trench depth is not the only covering parameter the settlement from case histories is plotted versus distance from the trench as shown in Figure 3-22. The settlement values are divided into three main groups divided by bounds as shown in the Figure. Each bound group is depending on the volume loss of soil during trenching but not necessary on trench dimension. The lower bound is limited the soil settlement values for good soil condition, skilled contractor and an appropriate slurry level (higher than water level). The middle bound shows the

settlement from several panels in project or lowering slurry for a single panel in a test. The expansion of weathered granite causes a huge settlement that can be confined by the higher bound; however, some data from Taiwan and Egypt are also found within this bound.

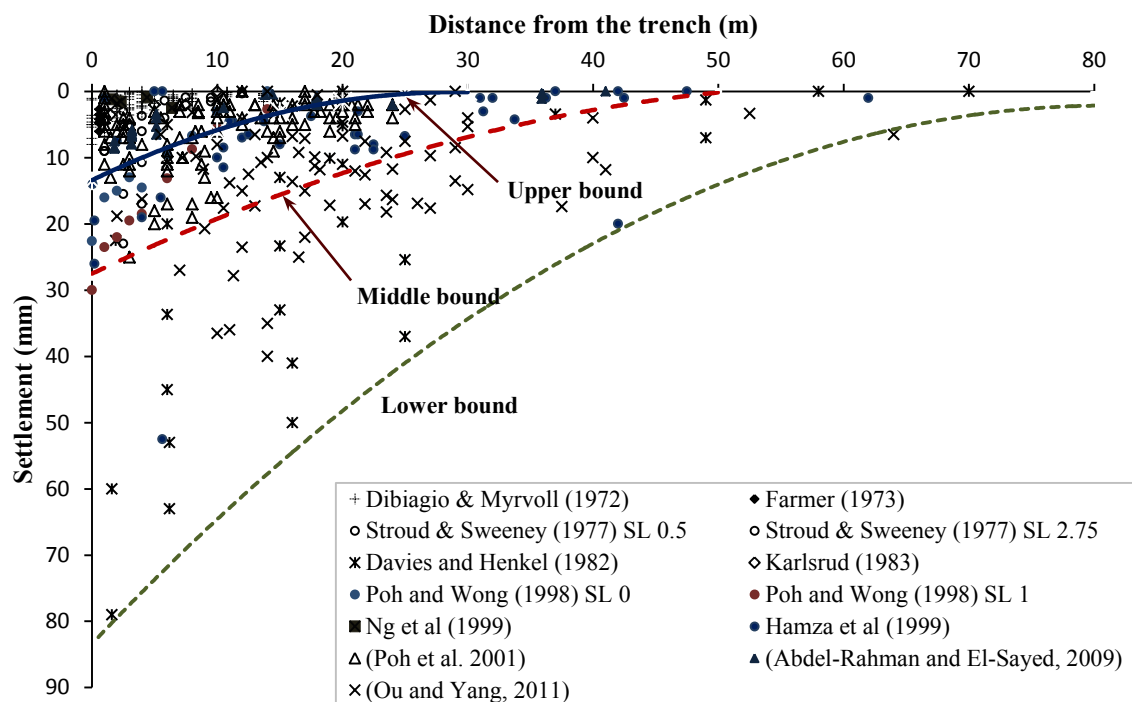


Fig. 3-22: Settlement to distance from the trench due to the diaphragm walls installation

The higher bound is considered to be very conservative. The middle bound is recommended to be used for the normal project with panel lengths more than 4.8 m and depth more than 30 m. The upper bound could be carefully used for trenches with lengths less than 4.8 m and depth less than 30 m. The settlement at a distance  $x_t$  from the trench for each bound could be calculated as following:

$$S_{Lower\ bound} = \frac{x_t^2}{64} - 0.9x_t + 14 \quad x_t < 30 \quad 3.7$$

$$S_{middle\ bound} = \frac{x_t^2}{143} - 0.9x_t + 28 \quad x_t < 50 \quad 3.8$$

$$S_{Higher\ bound} = \frac{x_t^2}{80} - 2.0x_t + 84 \quad x_t < 80 \quad 3.9$$

### 3.5.3 HORIZONTAL DISPLACEMENT

The horizontal displacement decreased with the distance from the trench; however, its trend shape with depth varies according to the soil layers. The values of horizontal displacement vary greatly according to the slurry level and trench length. The soil type is also governing the horizontal displacement values. Figure 3-23 is a collection of horizontal displacement values from twelve documented literatures. The horizontal displacement values were plotted in the x-axis, while the normalized trench depth (i.e. trench depth / maximum trench depth) in the y-axis. The higher the slurry level than ground surface level and the low groundwater table

cause the horizontal displacement to be negative at the top of the trench in some readings. The values of horizontal displacement decrease after about 60 % of the trench depth, and it could extend to depth below the trench tip level. It could be divided into three groups as well as the settlement values.

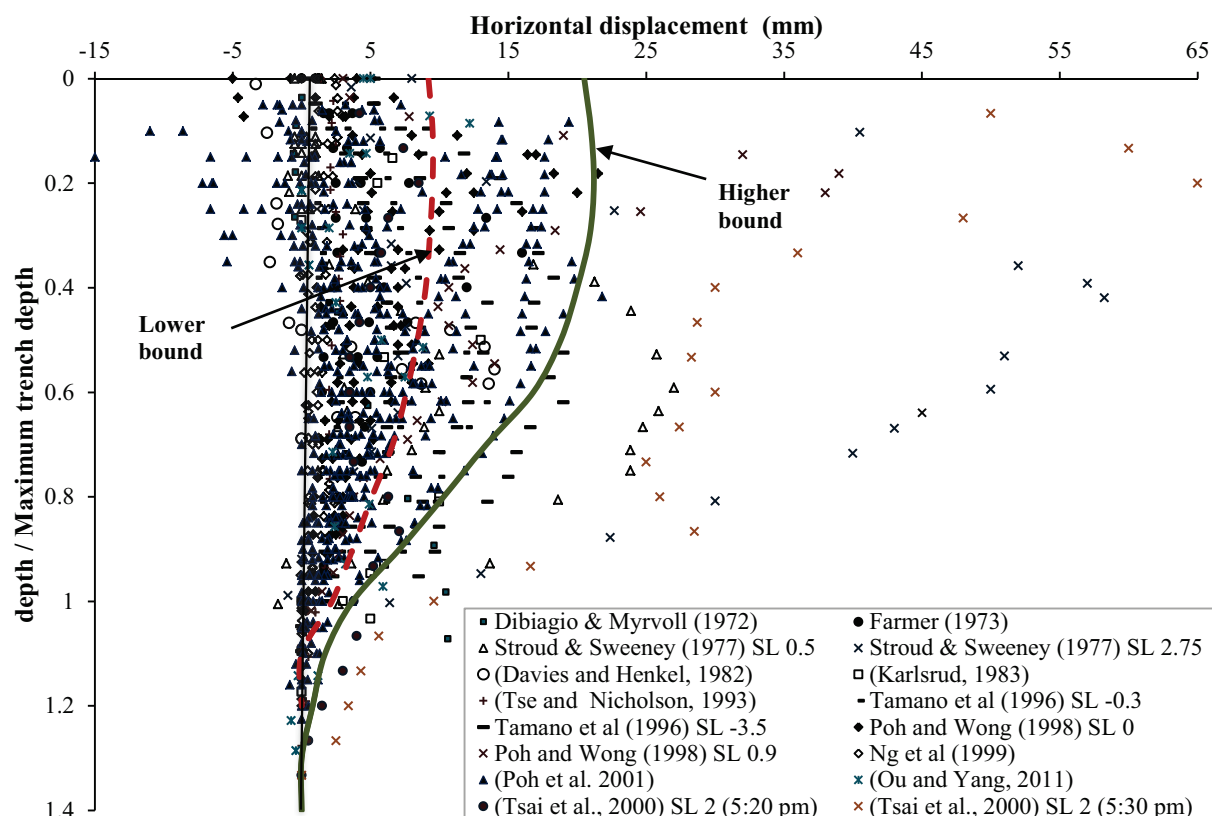


Fig. 3-23: Horizontal displacement with normalized depth

Two boundary curves are suggested as shown in the figure. The values that are greater than the higher boundary considered an exception and they were found due to the low slurry level or reduction of slurry pressure at some levels. The displacement values taken near the trench were normally between the lower and higher bounds, whereas, the values below lower boundary were measured far from the trench face. The height of slurry level indicates the bound type as well. The values confined by the lower bound were for a relatively high slurry level, which may be higher than the ground surface level. In normal cases, the values of horizontal displacement could be less than 20 mm; however, most of the recorded values were below 10 mm. The lower and higher horizontal displacement values for a maximum trench depth  $H_{max}$  and at any trench depth  $H$  could be calculated from the following equations:

$$\delta_{Lower} = 9.2 + 3.7 \frac{H}{H_{max}} - 10.8 \frac{H^2}{H_{max}^2} \quad 3.10$$

$$\delta_{Higher} = \frac{19.5H}{H_{max}} \left( 24 - \frac{68H}{H_{max}} - \frac{10.8H^2}{H_{max}^2} \right) \quad 3.11$$

### 3.6 SUMMARY

This chapter discussed the different results of field data and laboratory testing regarding slurry trenching. The field data values were found from the full scale panel tests and from case histories. The values of settlement and horizontal displacement were varying significantly. Some contractors and design engineers would ignore the deformation due to trenching. They suggested that the deformation values from trenching process could be very small compared to the main excavation. On the contrary, some researchers showed that deformation due to trenching process could be higher than the main excavation activates and can not be simply ignored. Accordingly, it was important to collect the available field data in one plot to give an indication of the deformation values.

The available values of lateral earth pressure due to trenching were plotted. The plot allowed to understand the range of reduction in earth pressure coefficient due to trenching. The soil settlement was plotted in one chart allowing to understand the settlement limits. An equation was suggested for each limit. The equations allowed to understand the maximum settlement for each case. The same idea was applied for the horizontal displacement. The horizontal displacement values ranges were varying mainly according to the trench length and slurry level. It was reduced with distance from the trench.

The pile near the trench excavation will be definitely affected by the trenching process. The reduction on the earth pressure coefficient could affect the skin friction of the pile. The soil movement will be transferred to the pile. The amount of transferred displacement to the pile will be discussed in the next chapters.



## CHAPTER 4: NUMERICAL ANALYSIS AND VERIFICATION

### 4.1 INTRODUCTION

The numerical modeling is now a very useful tool that can be used for simulation of different geotechnical engineering problems. Since the start of using numerical analysis in soil mechanics, soil models were greatly developed. In general, the problem geometry and soil type controls the choice of soil model. The numerical analysis could be conducted in two or three dimensions based on the geotechnical problem characteristics. The main aim of this chapter is to find out the best possible way to model numerically the slurry wall trenching process near piled foundation, because the trench is a three-dimensional problem as illustrated in chapter 2. Numerical verification using 3D finite difference method was implemented in order to find out the best simulation method and soil model. A full-scale tested panel, a centrifuge laboratory experiment and two case histories were simulated numerically in this chapter.

A well instrumented full-scale tested trench was initially simulated. The soil horizontal displacement and settlement from the full-scale test were used to verify the used numerical analysis method and soil model. In the centrifuge laboratory experiment the pile deflection, bending moment and shaft friction as well as soil settlement were recorded and compared to the results of the numerical analysis. Finally, two case histories were simulated numerically with the same concept. They include piled foundation near the diaphragm wall. The outputs from the projects were limited to soil deformation and there were no available data about the existing pile behavior during trenching due to technical difficulties; however, the available data are suitable for numerical verification.

These different verification models allow understanding the numerical modeling of the trench problem near piled foundation and they allow to verify the approximation used in the numerical modeling process using FLAC<sup>3D</sup>.

### 4.2 NUMERICAL ANALYSIS AND THEORETICAL BACKGROUND

The numerical analysis was conducted using one of Itasca commercial software “FLAC 3D” which is based on the finite difference analysis method. The term FLAC is shorted from Fast Lagrangian Analysis of Continua. The use of Lagrangian coordinates in analyzing continuum mechanics problems is called Lagrangian analysis. This kind of analysis is suitable for the non-use of global stiffness matrix. Adding the incremental displacements to the coordinates allows the grid to move with the material (Itasca, 2011). The following subsections discuss the sequence used in finite difference and the equation of motion.

#### 4.2.1 FINITE DIFFERENCE SEQUENCE

The explicit calculation method is used in FLAC, which depends on calculating the system state after the current system time. The basic cycle of explicit calculation is presented in Figure 4.1. The approach of finite difference is described in the following sequences.

1. Discretization: The continuum is discretizing into a number of “quadrilateral elements”. These elements are triangle and connected with nodal points. The velocity at nodal points and stress in triangle element are known at certain time; however, an initial condition for the velocity and stress should be defined.
2. FD Compatibility equations: Strain rates in triangle elements are defined by finite different compatibility equations which use nodal velocities.
3. Incremental FD constitutive relationships: define stress rates by using strain rates, while the stresses for the current time step could be updated by the stress rates.
4. FD Equilibrium equations for triangular elements: used to calculate “nodal forces” that are used for quadrilateral element’s nodal force vector producing.
5. Equations of equilibrium for each node: calculate the vector of unbalanced force by the summation the nodal forces.
6. Static boundary conditions control nodal force vector, while the kinematic boundary conditions reduce the calculated number of unbalanced forces.
7. Nodal velocities updated by the FD equations of motion for each node.
8. Solution: repeating the steps from 2 to 5 until the unbalanced force becomes very small.

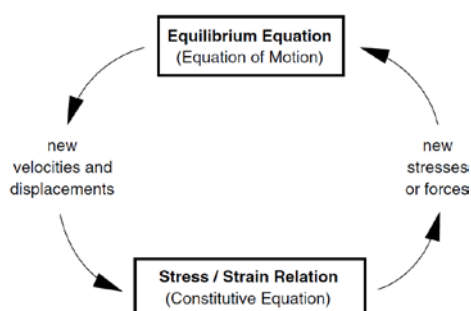


Fig. 4-1: Basic cycle of explicit calculation method (Itasca, 2013)

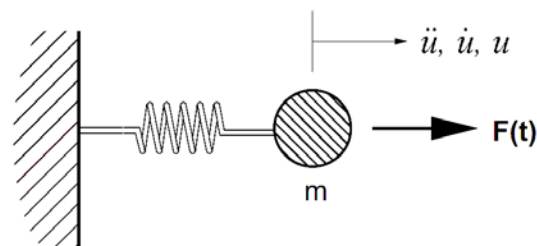


Fig. 4-2: mass subjected to time-varying force (Itasca, 2013)

It could be a common question whether the finite different is better in plasticity analysis than finite element. This question can't be directly answered. The plastic flow in FE is represented by a series of static equilibrium solutions, while in FD plastic flow is solved in one step. However, the good algorithm used in some FE programs could give same results like in FD. Frydman and Burd (1997) showed that FD could be better than FE with respect to smooth footings problems, as it doesn't require to inverse the system stiffness equations for each time step.

#### 4.2.2 EQUATION OF MOTION AND CONSTITUTIVE RELATION

The relation between the applied forces on a mass with the acceleration  $d\dot{u}/dt$  is the equation of motion. If force,  $F$  acting on a mass,  $m$ , causes motion as presented in Figure 4-2, Newton's law of motion then solved the mass-spring system as following:

$$F = m \frac{d\dot{u}}{dt} \quad 4.1$$

Continuum form of the momentum principle applied in FLAC 3D Itasca (2013) and the equation of motion is then:

$$\frac{d\sigma_{ij}}{dx_j} + \rho g_i = \rho \frac{d\dot{u}}{dt} \quad 4.2$$

where  $\rho$  is the mass density;  
 $t$  is the time;  
 $x_i$  are the components of coordinate vector;  
 $g_i$  are the body forces (gravitational acceleration); and  
 $\sigma_{ij}$  are the stress tensor components.

The strain rate can be derived from the following body move equation with velocity  $\dot{u}$ .

$$\varepsilon_{ij} = \frac{1}{2} \left[ \frac{d\dot{u}_i}{dx_j} + \frac{d\dot{u}_j}{dx_i} \right] \quad 4.3$$

The constitutive equations define the stress and strain relation through the following equation:

$$[\dot{\sigma}]_{ij} = H_{ij}(\sigma_{ij}, \varepsilon_{ij}, k) \quad 4.4$$

where  $[\dot{\sigma}]_{ij}$  is the co-rotational stress = material derivative of stress;  
 $H$  is any constitutive law given function; and  
 $k$  is a history parameter(s).

The co-rotational stress components which seem to be rotating with and attached to the material point, can be calculated as

$$[\dot{\sigma}]_{ij} = \frac{d\sigma_{ij}}{dt} - \omega_{ik}\sigma_{kj} + \sigma_{ik}\omega_{kj} \quad 4.5$$

where  $d[\sigma]/dt$  is the material time derivative of  $\sigma$ ; and  
 $\omega$  rate of rotation tensor.

#### 4.2.3 CONSTITUTIVE MODEL

There are several available constitutive models for dealing with the different soil problems. Two main constitutive model groups are in FLAC<sup>3D</sup>. The first is the elastic model group which deals with the material as its deformation is reversible with unloading. Its stress path could be linear or independent. Isotropic and anisotropic elastic models are also included. The second group is the plastic model group which deals with the material in its elastic and plastic behavior. The strain in this case could be the summation of the elastic and plastic strain. The different plastic models are characterized by yield function, flow rule, hardening/softening

functions. The following subsections describe the Mohr-coulomb model and strain hardening softening soil models.

#### 4.2.3.1 Mohr-Coulomb model

The failure envelope in Mohr-coulomb model in FLAC is corresponding to shear and tension yield functions. The principal stress space is shown in Figure 4-3. The stress point position in the failure envelope is controlled by the non-associated flow rule for the shear and associated flow rule for the tension failure(s). The principal stresses and strains were used to express the criterion. The form of Hooke's law incremental expression of generalized and incremental stresses was represented as a factor of the shear and bulk modulus.

The tension cutoff with the Mohr-Coulomb criterion used in FLAC<sup>3D</sup> is defining the failure criterion (i.e.  $\sigma_1 \leq \sigma_2 \leq \sigma_3$ ). It can be represented in the plane  $(\sigma_1, \sigma_3)$  as shown in Figure 4-4.

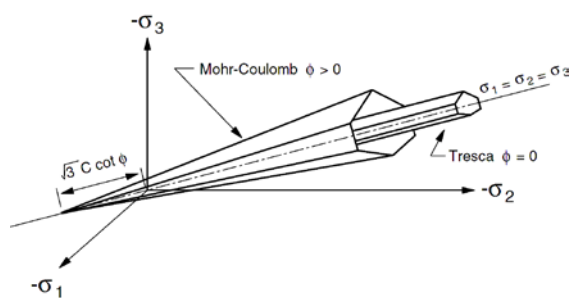


Fig. 4-3: Mohr-Coulomb yield surface in principal stress space. (Itasca, 2013)

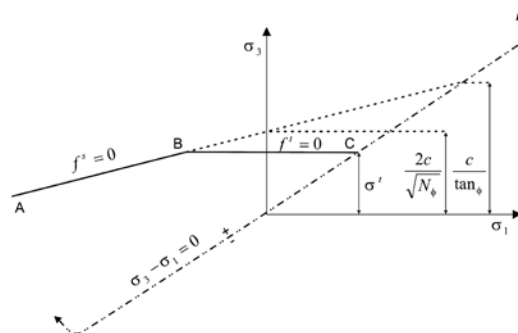


Fig. 4-4: Mohr-Coulomb failure criterion (Itasca, 2013)

The Mohr-Coulomb failure criterion  $f^s = 0$  defines the failure envelope from point A to B with

$$f^s = \sigma_1 - \sigma_3 N_\phi + 2c\sqrt{N_\phi} \quad 4.6$$

A tension failure criterion from B to C of the form  $f^t = 0$

$$f^t = \sigma_3 - \sigma^t \quad 4.7$$

where  $\phi$  is the friction angle,  $\sigma^t$  is the tensile strength,  $c$  is the cohesion while

$$N_\phi = \frac{1 + \sin(\phi)}{1 - \sin(\phi)} \quad 4.8$$

The maximum tensile strength is limited by  $\sigma_3$  and given by

$$\sigma_{max}^t = \frac{c}{\tan \phi} \quad 4.9$$

The shear ( $g^s$ ) and tension ( $g^t$ ) plastic flow define the potential function with the form

$$g^s = \sigma_1 - \sigma_3 N_\psi \quad 4.10$$

$$g^t = -\sigma_3 \quad 4.11$$

where  $\psi$  is the dilation angle and

$$N_\psi = \frac{1 + \sin(\psi)}{1 - \sin(\psi)} \quad 4.12$$

A diagonal at point B can be determined whether the failure is shear ( $f^s, g^s$ ) or tension ( $f^t, g^t$ ).

### 4.2.3.2 Hardening soil model

The strain hardening softening soil model in FLAC<sup>3D</sup> is based on the Mohr-Coulomb model. In addition, it allows hardening or softening of the friction, cohesion, dilation and tensile strength after onset of plastic yielding. The dilation, friction and cohesion could be defined as a function of a hardening parameter measuring the plastic shear strain.

The sum of some incremental measures of plastic shear and tensile strain defines the hardening parameters  $k^s$  and  $k^t$ . The shear hardening increment can be calculated based on plastic shear strain as

$$\Delta k^s = \frac{1}{\sqrt{2}} \sqrt{(\Delta \epsilon_1^{Ps} - \Delta \epsilon_m^{Ps})^2 + (\Delta \epsilon_m^{Ps})^2 + (\Delta \epsilon_3^{Ps} - \Delta \epsilon_m^{Ps})^2} \quad 4.13$$

The plastic shear strain

$$\Delta \epsilon_m^{Ps} = \frac{1}{3} (\Delta \epsilon_1^{Ps} + \Delta \epsilon_3^{Ps}) \quad 4.14$$

where  $\Delta \epsilon_1^{Ps} = \lambda^s$  and  $\Delta \epsilon_3^{Ps} = -\lambda^s N_\psi$

The tetrahedron tensile-hardening increment is calculated as

$$\Delta k^s = |\Delta \epsilon_3^{Pt}| \quad 4.15$$

where  $\Delta \epsilon_3^{Pt} = \lambda^t$

The values of  $\lambda^s$  and  $\lambda^t$  are calculated in the plastic correction stage in the Mohr-Coulomb model.

This model is considered to be more advanced and suitable than the Mohr-Coulomb model in simulating the trenching problems in cohesion-less soils.

## 4.3 SIMULATION OF FULL-SCALE FIELD TEST AND SOIL MODEL

Generally, the full-scale field tests provide detailed data of the settlement and horizontal displacement from different locations from the trench. The numerical simulation was made for a 36 m deep tested trench discussed by Stround and Sweeney (1977), which was shortly described in the previous chapter.

### 4.3.1 SOIL PROPERTIES

The soil layers are Fill, marine deposits, decomposed Granite and strong Granite. Table 1 shows the soil properties that could be used in the analysis. they were determined based on SPT values. The groundwater level was 2.3 m below the ground surface.

Table 4-1: Field test soil properties

Soil layer	Bottom Level	SPT	$\gamma$ (kN/m <sup>3</sup> )	$c'/cu$ (kN/m <sup>2</sup> )	$\phi$ (°)	E (kN/m <sup>2</sup> )
Fill	1.0	5-30	17.0	0	27	10000
Marine Deposits	-2.6	5-30	17.0	5/35	15	10000

Soil layer	Bottom Level	SPT	$\gamma$ (kN/m <sup>3</sup> )	$c'/c_u$ (kN/m <sup>2</sup> )	$\phi$ (°)	E (kN/m <sup>2</sup> )
Highly Weathered Decomposed Granite	-11.0	10-20	17.62	0	30	40000
Decomposed Granite	-31.75	>40	20.0	0	36	85000
Granite	-	-	22.2	0	40	100000

#### 4.3.2 SOIL MODELING

The strain hardening softening soil model was used in modeling the soil. As was previously mentioned this model is based on the Mohr-coulomb model. The hardening shear parameters were deduced from empirical equations based on the reference deformation modulus through the following set of equations:

$$E_{oed} = \frac{(1 - \nu) \times E}{(1 - 2\nu)(1 + \nu)} \quad 4.16$$

$$E_{oed}^{ref} = \frac{E_{oed}}{\left(\frac{\sigma}{p_{ref}}\right)^m} = \frac{p_{ref}}{\lambda^*} \quad 4.17$$

$$\lambda^* = \frac{\lambda}{(1 + e_0)} \quad 4.18$$

$$E_{50}^{ref} = E_{oed}^{ref} \quad 4.19$$

$$E_{ur}^{ref} = 3E_{50}^{ref} \quad 4.20$$

where:

- m                      power of stress-level dependency of stiffness
- $E_{oed}$                       oedometer stiffness modulus
- $E_{oed}^{ref}$                       tangent stiffness for primary oedometer loading
- $E_{50}^{ref}$                       secant stiffness in standard drained triaxial test
- $E_{ur}^{ref}$                       reference stiffness for unloading-reloading corresponding to reference pressure  $p_{ref}$
- $\sigma$                       vertical stress
- $\lambda$                       compression index.

In addition to the Mohr Coulomb parameters, a relation between the mobilized friction angle and plastic shear strain was provided in the model to simulate the friction hardening which reproduces the hyperbolic stress-strain relation. Vermeer and de Borst (1984) present a friction hardening relation as follows:

$$\sin\phi_m = 2 \frac{\sqrt{\varepsilon_p \varepsilon_f}}{\varepsilon_p + \varepsilon_f} \sin\phi \quad \text{for} \quad \varepsilon_p \leq \varepsilon_f \quad 4.21$$

$$\sin\phi_m = \sin\phi \quad \text{for} \quad \varepsilon_p > \varepsilon_f \quad 4.22$$

where:

- $\phi_m$                       mobilized friction angle
- $\phi$                       ultimate friction angle

$\varepsilon_p$	plastic strain
$\varepsilon_f$	strain needed to mobilize the limit friction angle

The relation between the plastic strain and the mobilized friction angle according to Byrne et al. (2003) can be written as:

$$\varepsilon_p = \frac{P_{ref}}{\beta G_{ref}^e} \times \frac{\sin\phi}{R_f} \left( \frac{1}{1 - \frac{\sin\phi_m}{\sin\phi} R_f} - 1 \right) \quad 4.23$$

$$G_{ref}^e = \frac{E_{ur}^{ref}}{2(1 + \nu_{ur})} \quad 4.24$$

where:

$P_{ref}$	reference pressure (can be taken as 100 kN)
$R_f$	failure ratio (can be taken as 0.9)
$\beta$	calibration factor (equal to 1)
$G_{ref}^e$	elastic tangent shear modulus
$\nu_{ur}$	undrained Poisson's ratio.

The relations between the plastic shear strain and mobilized friction angle for the different soil layers are shown in the Figure 4-5.

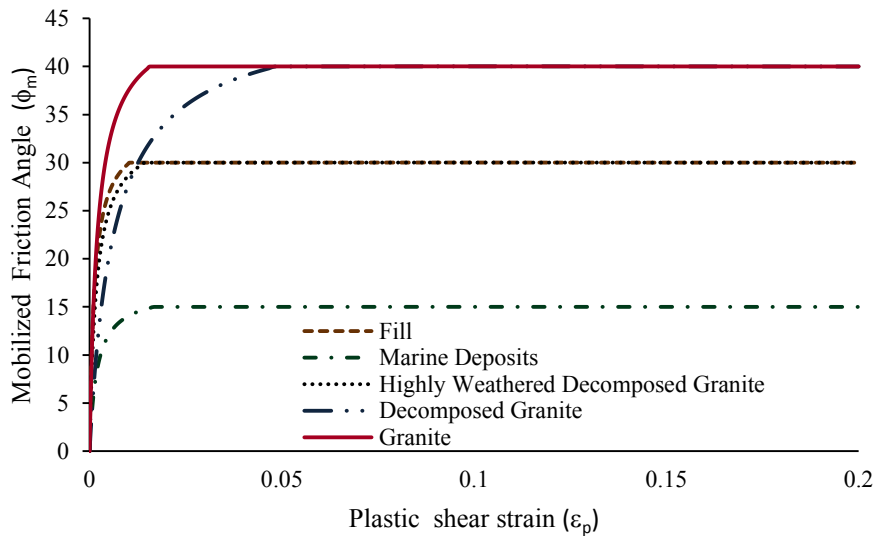


Fig. 4-5: Relation between mobilized friction angle and plastic shear strain for different soil layers

#### 4.3.3 GEOMETRY MODELING AND MESHING

The test panel geometry was described in the previous chapter. The conducting of the trench in three bits and reduction of the slurry were simulated with FLAC<sup>3D</sup> in the same procedure as in the field. The model mesh geometry is shown in Figure 4-6. The mesh was 40 x 40 m in the surface, while its depth was 50 m. The mesh was dense near the trench and it becomes coarse far from the trench. The zone depths in z direction slightly increased with depth and they ranges between 0.513 to 1.72 m. The surface area of the zones ranges between 0.0465 and 1 m<sup>2</sup>. The

total number of zones is 126800 and the nodes are connecting them. The small strain model was adopted in the analysis.

The mesh model was fixed in all directions at the bottom, while it was fixed in x only for the y-z plans and fixed in y only for the x-z plans. The slurry bites were simulated in stages. The soil elements at the slurry location were replaced by the null element and then pressure was applied at the trench sides and bottom equivalent to the slurry pressure as shown in Figure 4-7.

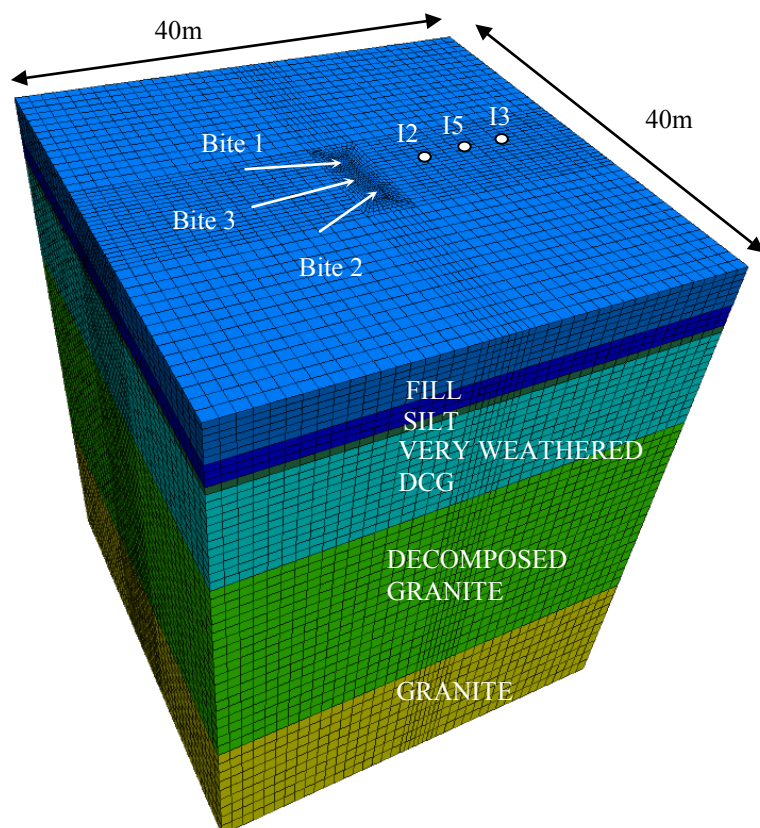


Fig. 4-6: Mesh geometry of the tested panel

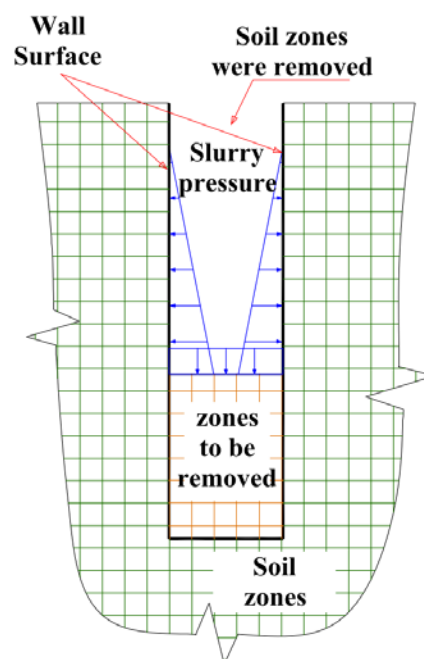


Fig. 4-7: Trench modeling

#### 4.3.4 RESULTS AND COMPARISON

The values of horizontal displacement and settlement from the field data and numerical modeling were plotted together for comparison in Figure 4-8 and Figure 4-9, respectively. The horizontal displacement was plotted at the three inclinometers I2, I5 and I3 located at a distance of 1 m, 2.4 m and 5.4m from the trench edge, respectively, and for the slurry levels 0.5 and 2.17 m defined by the two conditions C1 and C2, respectively. The settlement was measured for a distance up to 12 m from the trench at the center line of the middle bite (TCL) and side bites (BCL). It was measured for the conditions C1 and C2 as well. A FLAC 3D -Fish function was used to predict the settlement and horizontal displacement at the different locations. The typical soil modeling code used in FLAC 3D is presented in Appendix A.

The horizontal displacement calculated with numerical analysis was almost identical with that measured in the field. Its maximum peak was generally at depth ranges between 15 and 25 m, while another small peak appeared at higher levels for the cases of a lower slurry level. The



values of horizontal displacement decreased with distance from the trench and increased with lowering the slurry level. The reading of nearest inclinometer I2 was exceeding the lower limit defined in chapter 3 while the values of I3 were almost between the lower and upper limit. The values of I5 were within the upper limit. The numerical analysis values were noticeably different for inclinometer I5; the reason is probably due to the reported problem about such an inclinometer during the field experiment. If the numerical analysis results for it could be considered the values should be then exceeding the lower bound.

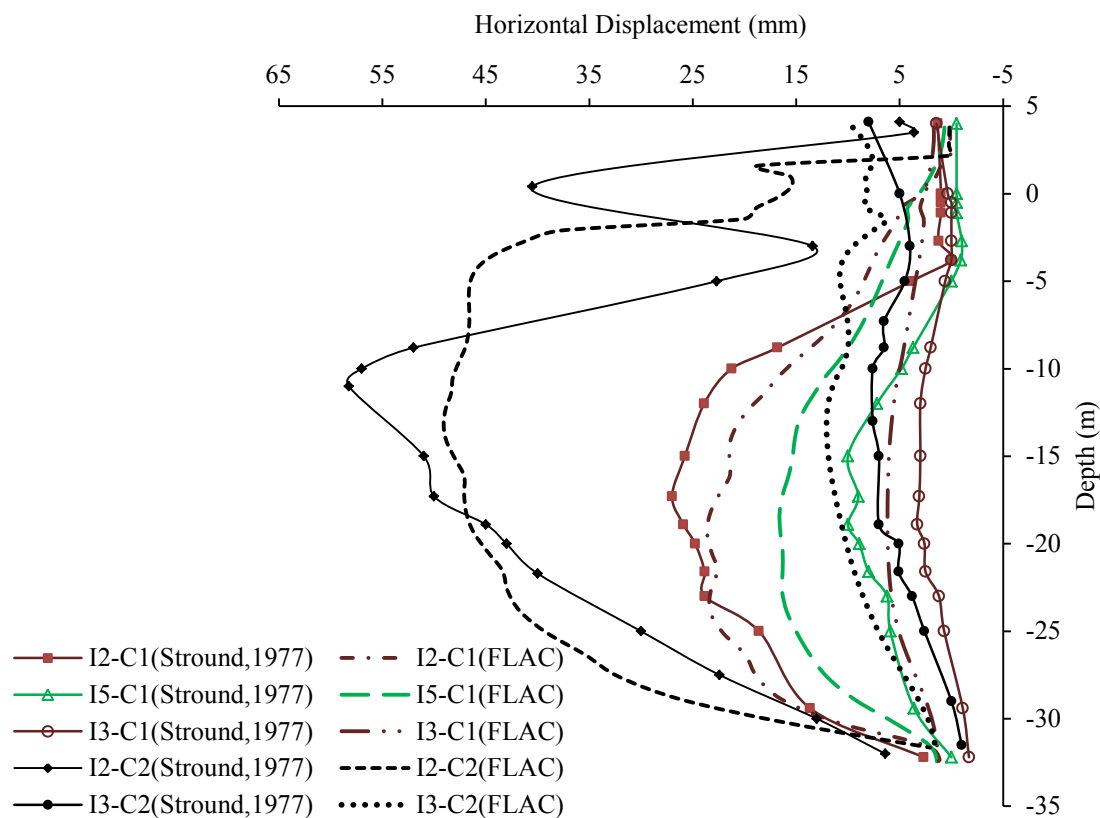


Fig. 4-8: Soil horizontal displacement

The values of the settlement from finite difference are close to the values of field data for the first approximately 5m from the trench. The settlement values from the field decreased and reach almost zero at a distance of 8 m from the trench (0.22 trench depth) unlike the found results in the literature (Figure 3-21). The reduction of the slurry causes a high decrease in settlement. The settlement values from the field settlement points at the center were noticeably higher than those from the other panels center. However, this difference was not great in the numerical analysis results.

The comparison between the numerical analysis and field data regarding deformation for this test was generally acceptable. The field settlement values after 5 m away from the trench were not in the same trend as that from the literature. It might be affected by other activities in the

site. The values from the numerical analysis were more in contrast with the literature values in the general trend.

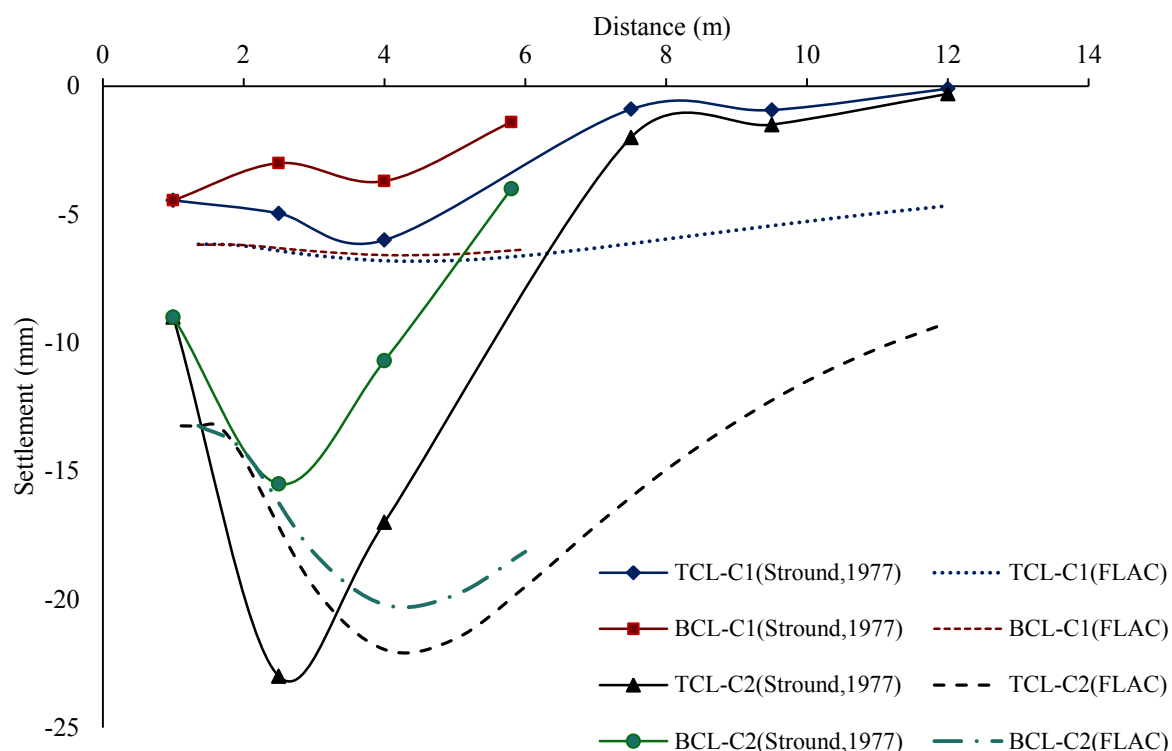


Fig. 4-9: Soil settlement

#### 4.4 LABORATORY WORK MODELING

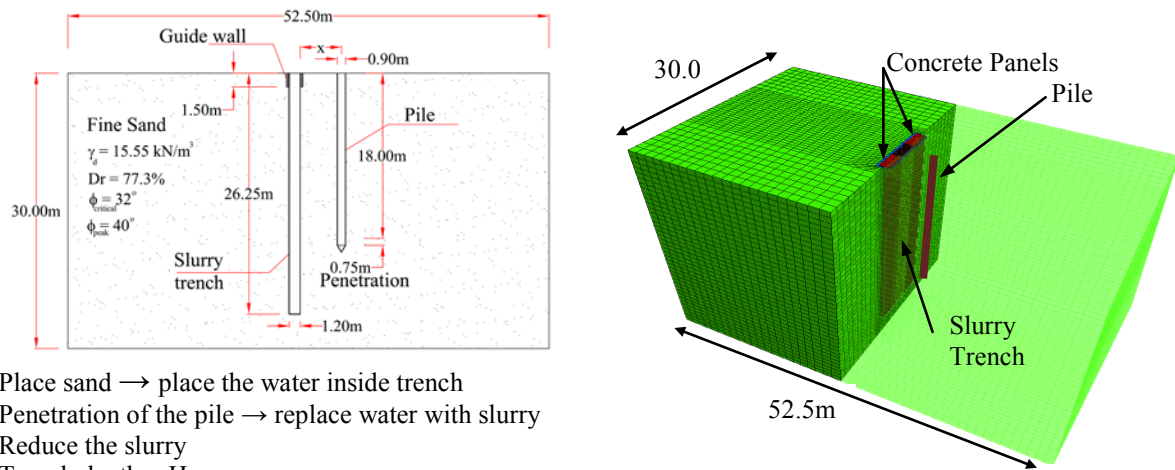
This section concerns on modeling the centrifuge model test of a single pile near trench excavation that was discussed in the previous chapter by Choy (2004). The purpose of modeling is to verify the numerical analysis method.

##### 4.4.1 NUMERICAL MODELING OF THE EXPERIMENT

The numerical simulation of the experiment included modeling of the soil, the pile, the concrete panel (in case of multiple panels), guide wall and the trench with the latex membrane.

##### 4.4.1.1 Model Geometry

The model was chosen with a dimension equivalent to the prototype strongbox dimension. The dimension of the model was 30 x 52.5 m for the surface area, while the depth was 30 m. The sketch of the geometry, construction sequence and modeled mesh are presented in Figure 4-10. The mesh was made of 75520 zone elements. The mesh was denser around the trench and become coarser at the edges of the model. The depth of each element was 0.75 m while the surface area was ranging between 0.15 x 0.375 m and 1.063 x 1.1 m. The bottom was fixed in all directions, while the edges were fixed in the two directions only.



Place sand → place the water inside trench  
 Penetration of the pile → replace water with slurry  
 Reduce the slurry  
 Trench depth = H  
 , Slurry depth = d

Fig. 4-10: General geometry, construction stages and typical mesh used for simulation.

#### 4.4.1.2 Soil modeling

The soil used in the experiment was dry dense sand and modeled using the strain hardening softening soil model. The friction angle, density and deformation modulus were  $32^\circ$ ,  $15.55 \text{ kN/m}^3$  and  $50 \text{ MPa}$ , respectively. The friction angle peak was  $40^\circ$ . The same equations between 4.16 and 4.24 were used to define the strain hardening softening parameters and the relation between plastic shear strain and mobilized friction angle.

#### 4.4.1.3 Guide wall modeling

The guide wall was modelled as an elastic soil element in order to simulate the 1.5 mm (11.5 cm – prototype scale) thick aluminum plate, while its depth was 1.5 m in the prototype scale. The real thickness of the guide wall was not simulated, because the mesh thickness near the trench was 0.322 m; accordingly, the used deformation modulus of the aluminum guide wall was  $0.115/0.332 \times E_{\text{aluminum}} = 25 \text{ GPa}$ .

#### 4.4.1.4 Pile modeling

The pile structural element defined in  $\text{FLAC}^{3D}$  was used to simulate the pile. Indeed, the simulation of pile using solid element (i.e. soil element with the pile properties) could provide a better accuracy but mesh difficulties between the pile and the trench were expected to cause numerical errors. Accordingly, it was more convenient with an acceptable accuracy to use the pile structural element. It consists of finite elements between two nodes with six degrees of freedom per node. It has the same beam stiffness matrix. The pile element is defined by its geometric and material properties such as its cross section area, inertia, perimeter, modulus of elasticity and Poisson ratio etc... In addition, it is defined also by its coupling spring properties. The coupling spring properties are divided into shear and normal coupling. The shear and normal behavior of the pile-grid interface is represented numerically as a spring-slider system at each node along the pile axis as shown in Figure 4-11. The relative shear displacement

between pile and soil is defined numerically by its shear stiffness  $k_s$ , friction angle  $\phi_s$ , cohesion  $c_s$  and exposed perimeter. Similarly, the relative normal displacement between pile and soil is defined by normal stiffness  $k_n$ , friction angle  $\phi_n$ , cohesion  $c_n$ , exposed perimeter and gap  $g$ . These parameters with effective confining stress define the pile mechanical behavior in shear and normal, respectively.

The gap that could occur due to lateral loading of pile in the host medium is simulated numerically as a parallelogram with its sides parallel to the  $y'z'$  - axis as shown in Figure 4-12. The shear and normal stiffness could be calculated empirically from the following equation:

$$K_n = K_s = 10 \max [k+4G/\Delta z_{\min}] \quad 4.25$$

- where:
- $k$  is the bulk modulus of the soil
  - $G$  is the shear modulus of the soil
  - $\Delta z_{\min}$  is the minimum distance in the vertical direction of the mesh

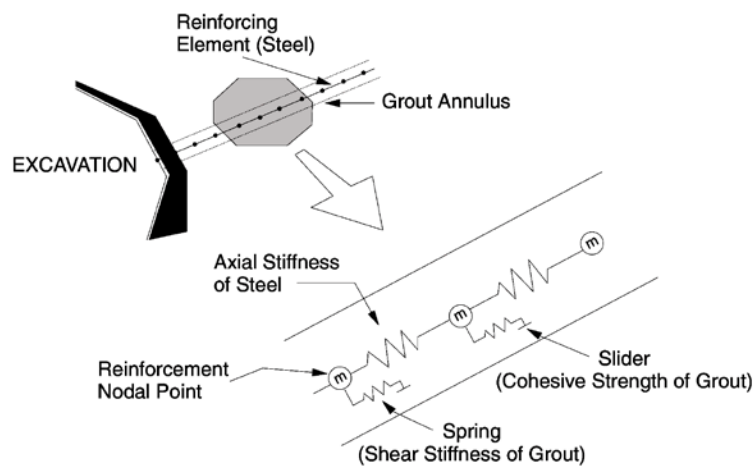


Fig. 4-11: Fully bonded reinforcement mechanical representation (Itasca, 2013)

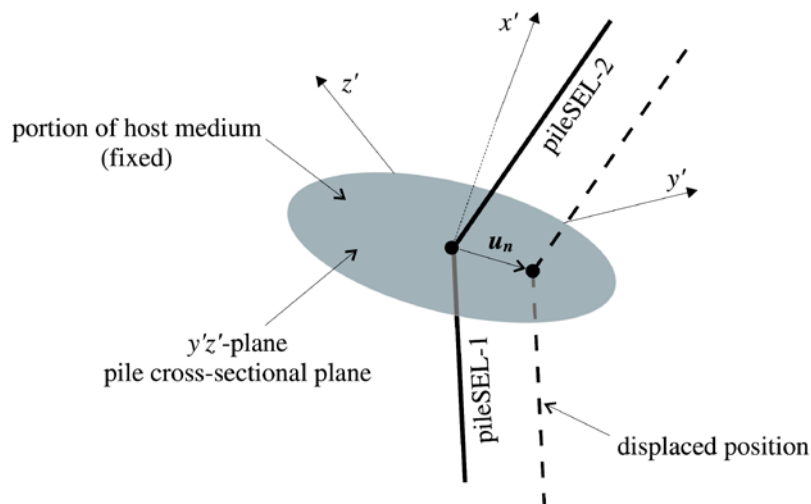


Fig. 4-12: Behavior of pile in normal direction ( $u_n$  is the relative normal displacement between pile and host medium) (Itasca, 2013)

The pile cross-section was a cylinder tube of aluminum and consisted of different segments. It was simulated with an equivalent dimension and properties. The pile properties used in the analysis are presented in Table 4-2. Each pile segment shows different values of friction recorded during pile installation. The interface friction angles  $\phi_s$  and  $\phi_h$  were varying according to the different pile segments. The values of the interface friction angles are presented in Table 4-3.

Table 4-2: Laboratory test pile properties

Parameter	Pile				Interface		
	Area (m <sup>2</sup> )	Inertia (m <sup>4</sup> )	Perimeter (m)	E (kN/m <sup>2</sup> )	k <sub>s</sub> (kN/m <sup>3</sup> )	k <sub>n</sub> (kN/m <sup>3</sup> )	$\phi_s, \phi_h$ degree
Used Value	0.636	0.0322	2.826	4.3e7	1.0e6	1.0e6	see Table 4-3

Table 4-3: Interface friction angles of the different pile segments

Segment*	$\phi_s$ (degree)	$\phi_h$ (degree)
2	14.0	6.0
3	11.0	4.0
4	13.0	8.4
5	3.0	1.0

\* The segments are from almost the top to the bottom with an average length of 20 mm

#### 4.4.1.5 Latex membrane and trench modeling

In the experiment, the latex membrane was used to prevent liquids from penetration into the soil during the different stages. However, it has also some stiffness that provides local stability and prevents possible local failure during slurry reduction. The shell structural element implemented in FLAC3D was used to simulate the membrane. This element is a three-nodded flat finite element with a local coordinate system shown in Figure 4-13a. It behaves as an isotropic linear elastic material without a failure limit and is connected rigidly with the grids. The shell within the zone grid is presented in Figure 4-13b.

The shell element is defined by its stiffness and thickness. The thickness of the used latex membrane was about 0.5 mm (about 4mm in the prototype scale). Its stiffness equal to 20 MPa. Modeling of the trench was made in the same way as discussed in section 4.2.4 and Figure 4-7, while the pressure was distributed on the shell element and not in the zones. The shell elements transfer the pressure to the soil zones. The concrete panels were modeled by replacing the null zones by linear elastic model zones with the concrete properties. The applied pressure was removed gradually during the concreting process.

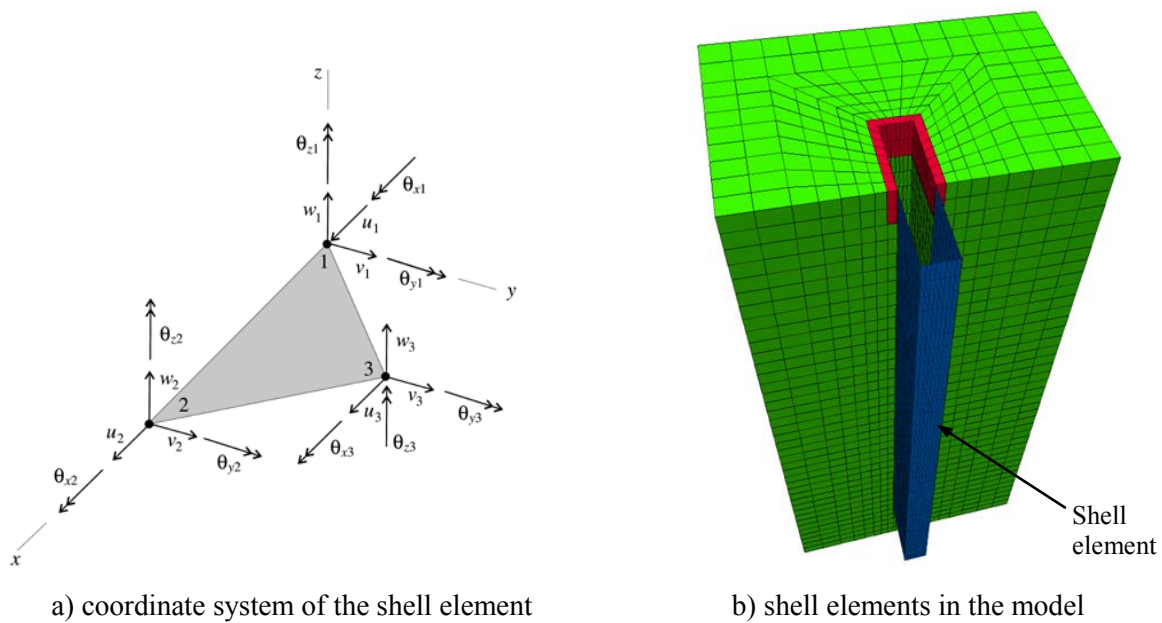


Fig. 4-13: Shell element used in simulating the latex membrane

#### 4.4.2 RESULTS FROM THE EXPERIMENT NUMERICAL MODELING

This section discusses the results from finite difference and laboratory experiments regarding the surface soil settlement and pile behavior (i.e. deflection, bending moment, friction and end bearing). Six numerical models were conducted for the eight experiments, because three of the experiments have the same parameters and dimensions as discussed in the previous chapter in Table 3-3.

##### 4.4.2.1 Surface soil settlement

The surface soil was measured in the eight experiments during pile installation and slurry reduction. The settlement due to pile installation from laboratory compared to numerical analysis in all tests has shown almost the same trend and values. Figure 4-14 shows a typical comparison between numerical analysis and laboratory work regarding pile installation process.

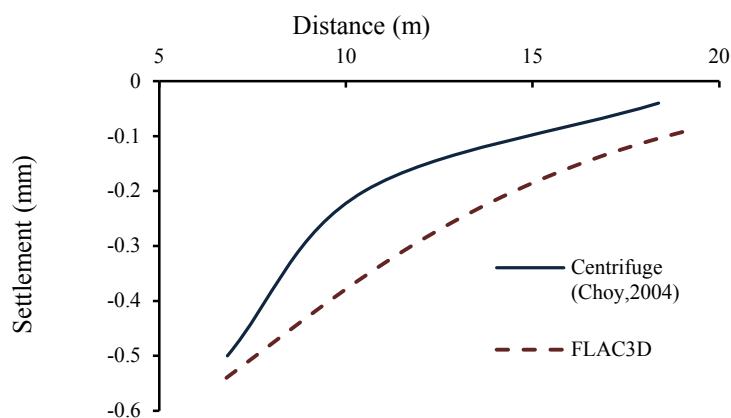


Fig. 4-14: Typical effect of pile installation on soil settlement

The surface settlement due to replacing the water with the slurry liquid was almost unnoticeable. The settlement from the slurry reduction compared to numerical analysis is presented in Figure 4-15 for a single panel trench, while multiple panels are shown in Figure 4-16.

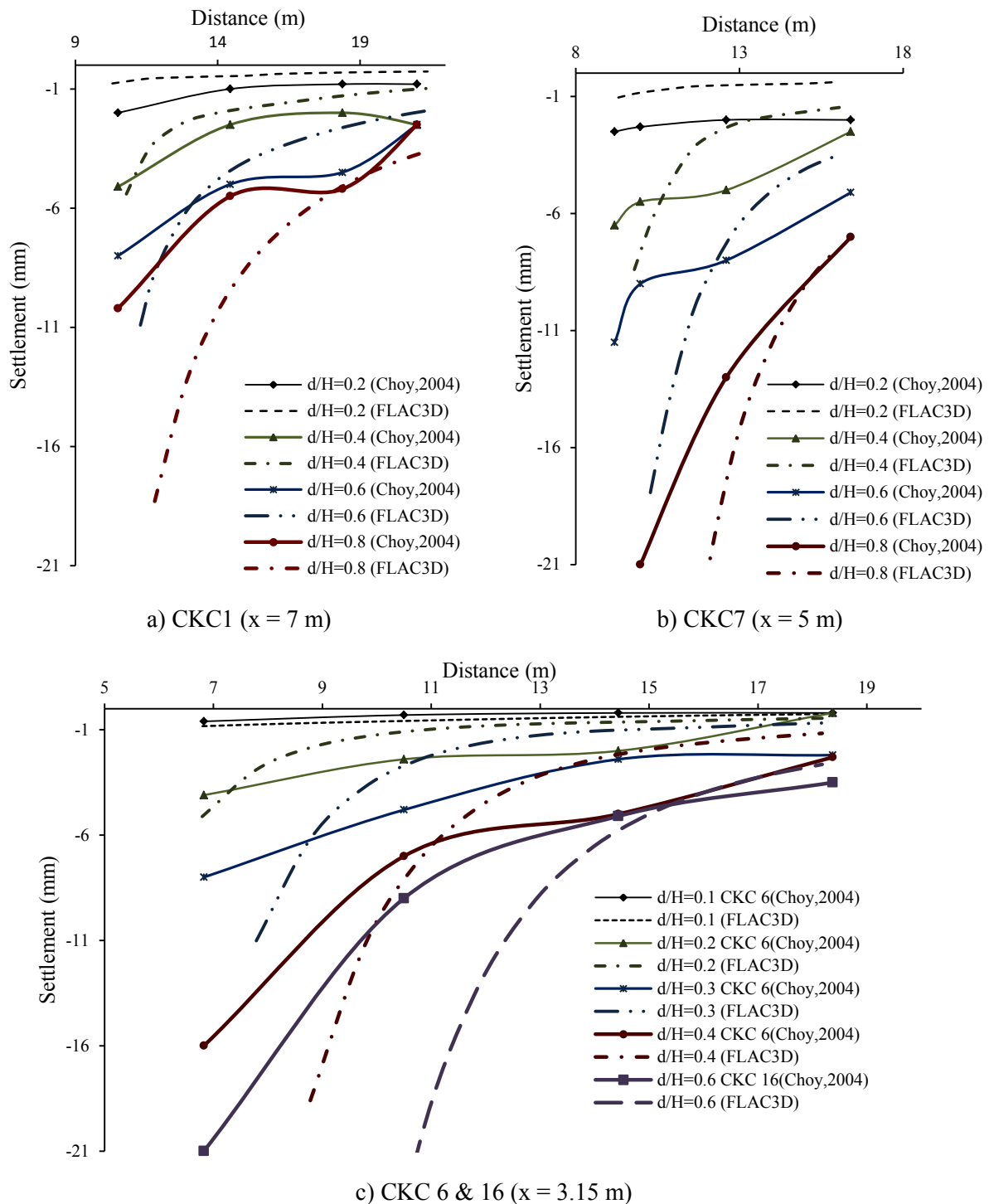


Fig. 4-15: Soil settlement due to slurry reduction for 6 m length single panel

In general, the settlement from CKC1 (i.e.  $x=7$  m) was less than that from CKC7 (i.e.  $x=5$  m) and both were less than those from CKC 6 and 16 (i.e.  $x=3.15$  m). This indicated that the pile distance from the trench has a great effect on the settlement. The settlement from the single

6.0 m length panel was double the values taken for the 3.0 m length multi-panels trench. Generally, it decreased with distance from the trench.

The settlement due to slurry reduction from numerical analysis was quite in a good contrast with laboratory work. However, there was some big difference for some cases. The pile installation from numerical analysis was slightly higher than the results from the laboratory. This difference could be acceptable for the verification purposes.

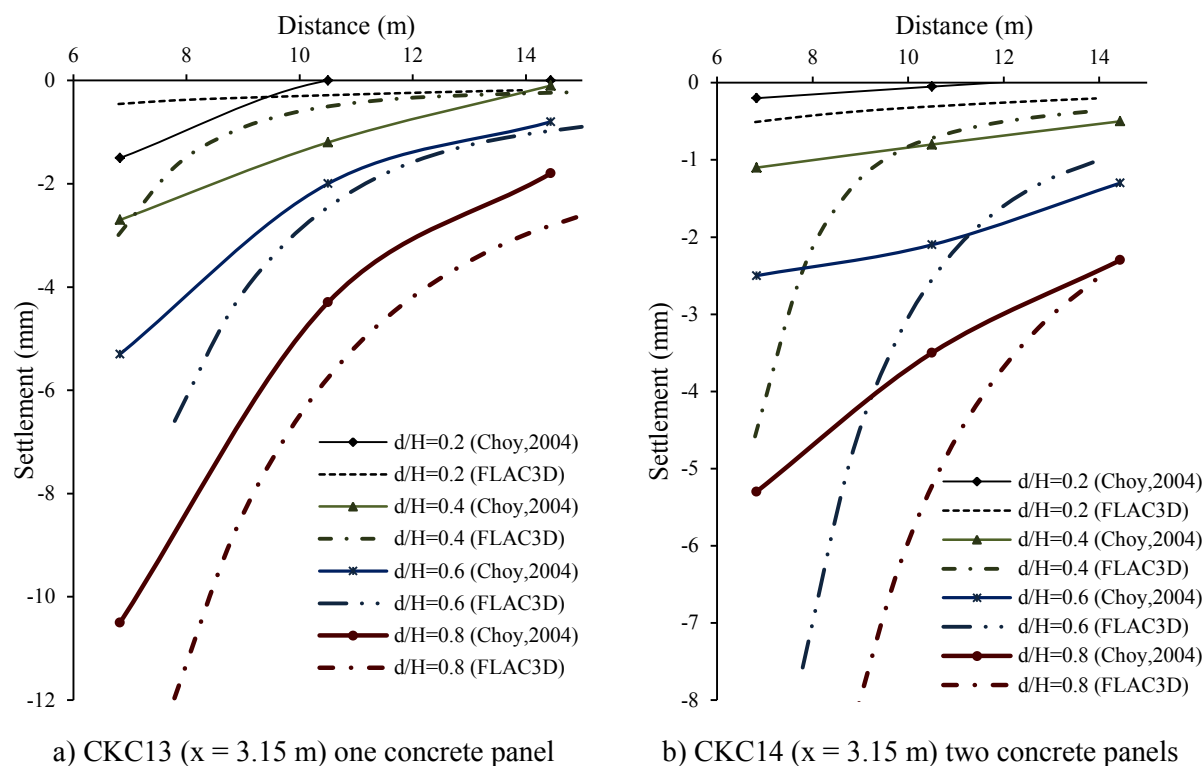


Fig. 4-16: Soil settlement due to slurry reduction for 3.0 m length multiple panels

The settlement from the numerical analysis for the CKC 1 showed a very low difference for the slurry to depth ratios between 0.2 and 0.6, while it showed almost double the settlement values for  $d/H = 0.8$ . The settlement difference was great for  $d/H = 0.6$  and it was not so great for the other levels in the CKC 7 experiment. The settlement difference between numerical and laboratory results of CKC 16 was noticeable at  $d/H = 0.6$ , while it was quite low for CKC 6 in most of the slurry levels. In general, the difference between the settlement values from the numerical analysis and CKC 13 laboratory results was very low, but it was high in CKC 14 for most of the slurry levels.

The general settlement trend from the finite was high near the trench and increased greatly by distance. In other hand, not all of the laboratory tests results showed the same trend. The settlement shape from the numerical analysis is considered to be reliable compared to the general trend discussed and suggested in Figure 3-22. The settlement values for the single 6 m length panel and slurry reduction less than 30 % were within the upper bound, while the slurry level could be reduced to 60 % and still in the upper bound for the short panel. The rest of the



values were within the upper and middle bounds. Only the slurry reduction of 60 % in the case of the single 6 m long panel passed the middle bound, because the trench was unstable and almost collapsed in this case.

#### 4.4.2.2 Pile deflection and bending moment

The deflection and bending moment of the pile due to slurry reduction were recorded in the experiments CKC 15 and CKC 16. The comparison between the results from numerical analysis and laboratory is presented in Figures 4-17 and 4-18. The laboratory data results were recorded and plotted for limited values of slurry reduction levels. However, the numerical analysis results were plotted for more levels in order to better understand the slurry reduction effect on the pile. The laboratory results are presented in the solid lines, while the numerical analysis results are presented in non-solid lines.

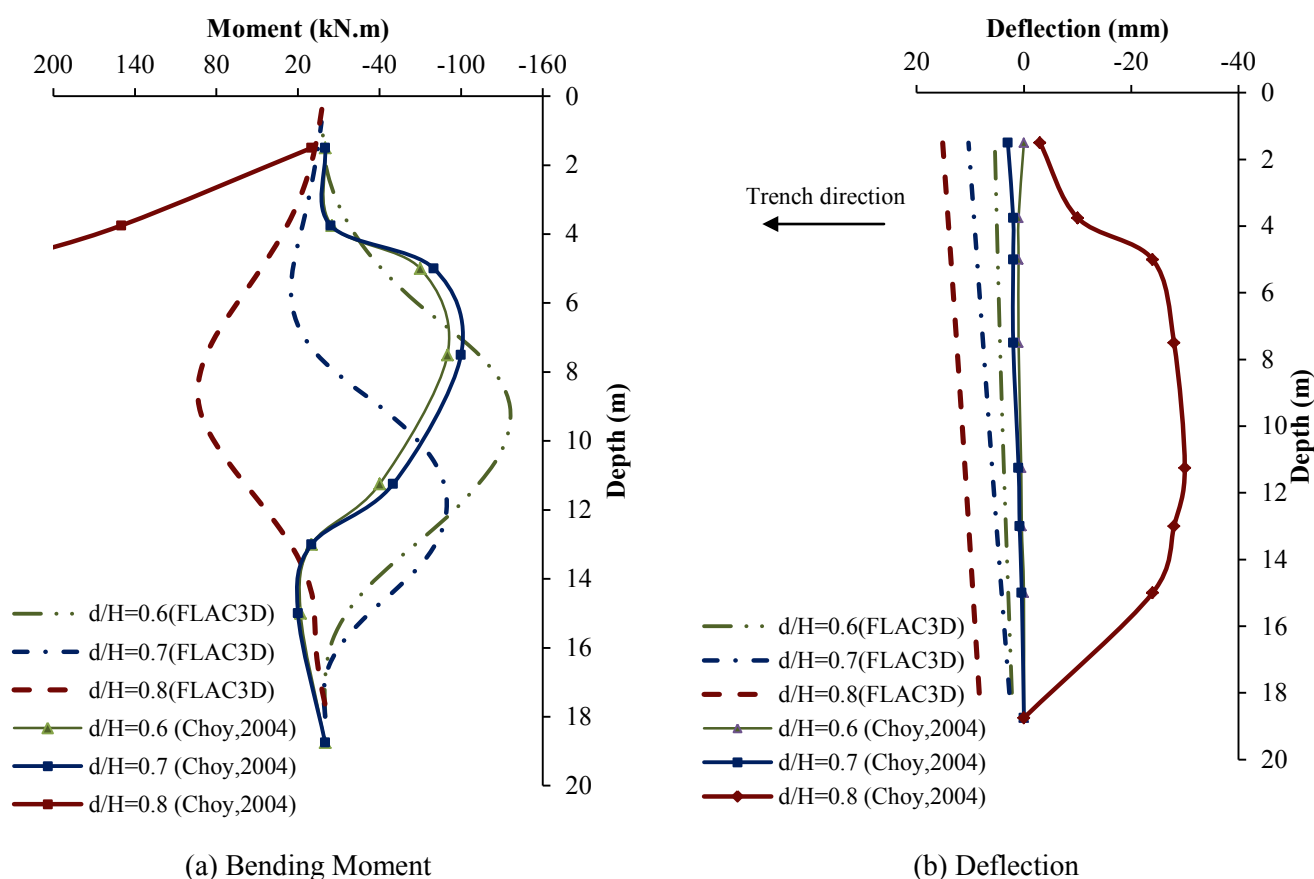


Fig. 4-17: Pile bending moment and deflection due to slurry reduction (CKC15)

The pile deflection and bending moment were affected during slurry reduction but the effect was high at a certain level of the slurry. At such a level the failure could have occurred and causes huge displacement and bending moment for the pile.

In the laboratory experiment CKC15 the laboratory results showed that the failure probably happened at  $d/H = 0.8$ , the bending moment increased to almost 1000 kN.m, while the deflection showed an illogical behavior of movement which was against the trench as shown in Figure 4-17(b). The results for the same

experiment from the numerical analysis showed that the pile deflection increased gradually with slurry reduction but it greatly increased at  $d/H = 0.8$ , which indicates that the trench had failed at this slurry level as well. The laboratory results showed that, the bending moment shape and values were changing during the reduction of the slurry. The numerical analysis showed the same trend with a high increase at  $d/H = 0.8$ . The high laboratory result values of deflection and bending moment at  $d/H = 0.6$  in the laboratory experiment CKC16 indicated that failure happened at this level. The numerical analysis results showed a little different behavior. The pile deflects almost gradually until  $d/H = 0.5$  and at  $d/H = 0.57$  it showed a very high increase which indicates that failure most probably happened at this level. The numerical analysis showed a high change of bending moment values from positive to negative at  $d/H = 0.57$  and  $0.6$ . The pile deflection values from numerical analysis were higher than those from the laboratory before failure but slightly less after failure, while the bending moment values after failure were less than those from the laboratory. Generally, the numerical analysis provides logical and reliable deflection and bending moment values.

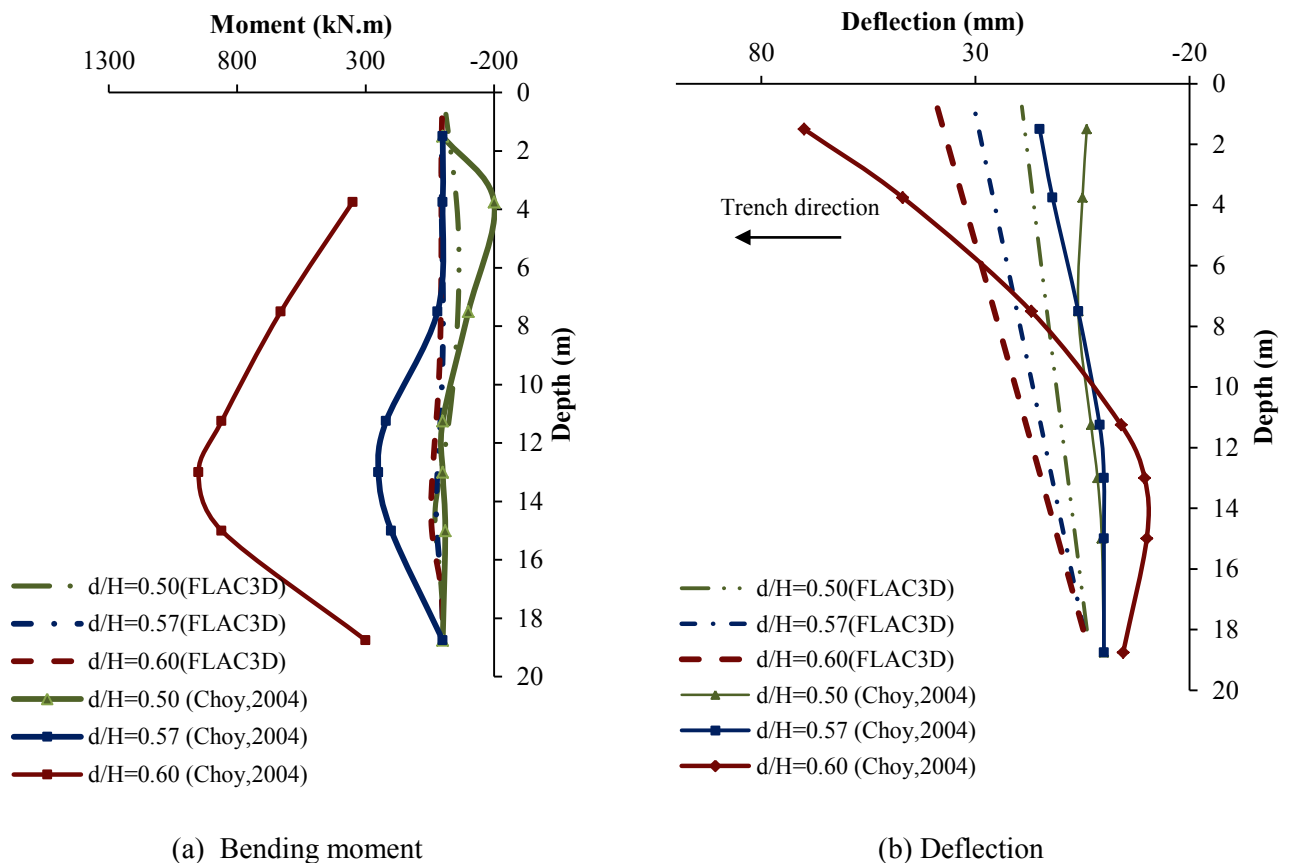
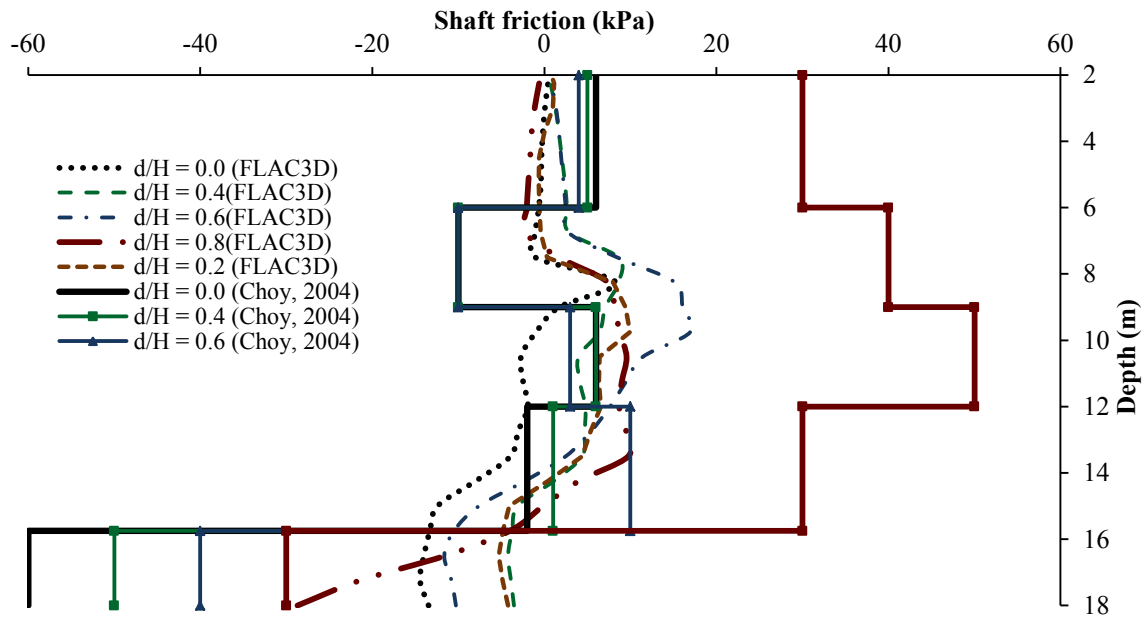


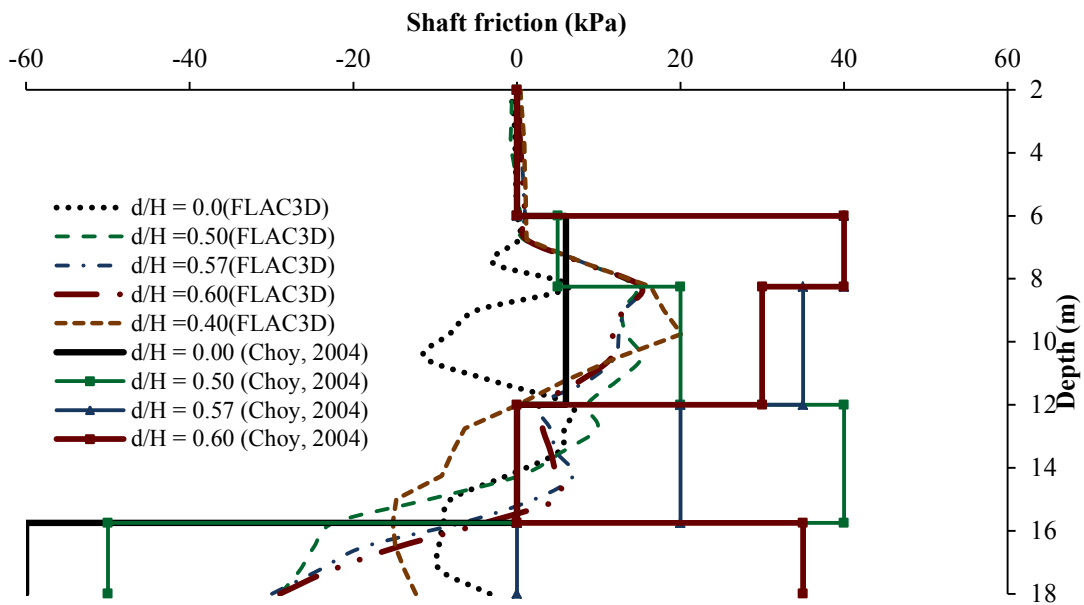
Fig. 4-18: Pile bending moment and deflection due to slurry reduction (CKC16)

#### 4.4.2.3 Pile shear friction and bearing capacity

The reduction of slurry causes a change in the pile shear friction and bearing capacity. Its effect on shear friction from the numerical analysis compared to field data is presented in Figures 4-19 (a) and (b) for CKC 15 and CKC 16, respectively. The reduction in bearing capacity at different slurry levels is presented in Figure 4-20.



(a) CKC 15



(b) CKC 16

Fig. 4-19: Pile shaft friction during slurry reduction

The values from the laboratory test and numerical analysis showed that shaft friction shape and values changed during slurry reduction. The shaft friction values were plotted for  $d/H = 0.0$  just before slurry reduction and for different  $d/H$  values. The solid lines in Figures 4-19 and 4-20 are related to the laboratory results while the non-solid lines are the results from numerical analysis. The laboratory results are in the form of vertical straight lines because they were measured using strain gages at five locations (segments) on the pile, while the numerical analysis was measured at the pile coupling springs (section 4.3.1.4) which are located every 1 m along the pile length.

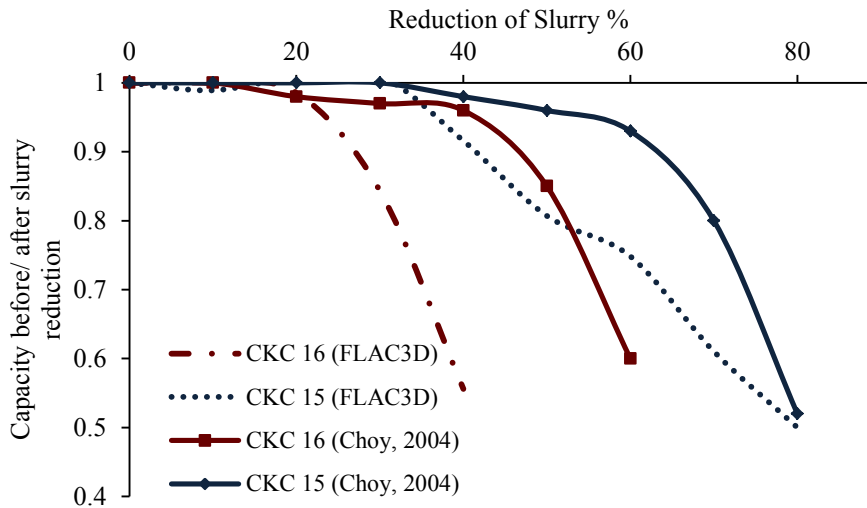


Fig. 4-20: Reduction of pile end bearing at different slurry levels

The CKC15 laboratory results of the shaft friction did not show a big change at the upper 12 m for  $d/H$  less than 0.8 (i.e. failure). However, at the lower part a decrease of shaft friction was observed, the increase of shaft friction at  $d/H = 0.8$  was great in the whole pile length. A different trend was recorded from the numerical analysis results. The shear friction increased for the different slurry levels and below the pile depth of 6.0 m. The value of change from numerical analysis at  $d/H = 0.8$  was not as great as that from the laboratory results.

The shaft friction from the experiment CKC 16 results did not show any change during slurry reduction in the upper 6 m of the pile, while it increased below this depth without any fixed relation with  $d/H$  values. The greatest increase was not necessary always at failure (i.e.  $d/H = 0.6$ ). However, the increase of the lowest 2 m of the pile was great at  $d/H = 0.6$ . The numerical analysis showed also no change in shaft friction for the upper 6 m of the pile. It increased at depths below 6 m. The maximum increase was recorded for  $d/H = 0.4$ . The increase of shaft friction from the laboratory and numerical analysis was not fully related to the slurry level, except for laboratory results of  $d/H = 0.8$  in experiment CKC 15. This high increase is an exception and could be an error in the laboratory reading caused by the collapse of the trench at this level.

The bearing capacity was calculated in the laboratory using four strain gages at the pile conical tip. It was measured from the numerical analysis by replacing the lower link with another one that contains a normal yield spring in the axial direction. The normal yield compression of the spring was chosen to be 1.8 MPa.

In test CKC 15, the laboratory results showed that pile bearing capacity decreased after 30% reduction of the slurry. It was above 0.9 at a slurry level below 60%, while it decreased greatly after that and was 0.52 at 80% slurry reduction. The numerical analysis showed also a decrease in bearing capacity after 30% of slurry level, but this decrease was higher at slurry levels of

40 %, 60 % and 70 % than laboratory results. However, at slurry level of 80 % the numerical analysis showed almost the same value of the laboratory results.

The laboratory and numerical analysis results showed a reduction of bearing capacity at a slurry level below 20 % for the test CKC 16. However, the numerical analysis showed a high reduction in bearing capacity values than laboratory test. The bearing capacity values from laboratory decreased below 0.9 after slurry reduction level of 40 %, while it decreased below this value at 30 % from numerical analysis.

#### **4.4.2.4 General discussion of the results**

It is not always easy to predict the soil behavior in the laboratory, especially in the centrifuge model tests because it needs very small sensitive devices with limited errors. The engineering logic and sense should be a main factor in judging the laboratory results. The pile deflection, bending moment and axial forces measurements in the laboratory are subjected to error. On the other hand, the surface settlement was measured using laser-beam, which should be more accurate than those measured from the strain gages.

The surface settlement results from numerical analysis are more close to those from laboratory compared to the results of pile behavior. The numerical analysis should not necessarily provide a full contrast with the laboratory results, especially if the possibility of error from the laboratory measurements is expected.

Generally, the behavior of the pile from the numerical analysis was logical as well as from laboratory tests except pile deflection at  $d/H = 0.8$  for experiment CKC 15. The trench failure from numerical analysis has happened almost at the same slurry level in the laboratory for both tests. Indeed, the surface settlement for the same tests or the similar tests was in a high contrast with the laboratory results. This means that the difference in results regarding pile behavior is not always indicating that the numerical analysis is inaccurate.

### **4.5 MODELING OF PREVIOUS WORKING PROJECTS**

There are limited monitored projects for a slurry trench near deep foundations. The settlement and horizontal soil deformation were the only available data from such projects. In this section two projects were modeled using the numerical analysis. The comparison was made with the available field data for each project. The first project is an underground metro station in Hong Kong near several high-rise buildings located in deep foundations. The second project is an underground basement in a crowded area in Cairo.

#### 4.5.1 NUMERICAL MODELING OF CHARTER UNDERGROUND STATION (HONG KONG)

This project was discussed in the previous chapter. Two sections that were presented in Figure 3-11 will be modeled in this section. The available data for section 1-1 and 2-2 are the soil settlement, while for section 3-3 is the soil horizontal displacement. Section 1-1 refers to the Courts of Justice, section 2-2 refers to Prince's building and section 3-3 refers to Swire House. The soil properties and soil modeling are the same for the full-scale field test discussed in section 4.2, because the tested panel was conducted close to the project area. Accordingly, the soil profile and properties are assumed to be the same for the project area and test panel.

##### 4.5.1.1 Diaphragm wall panels near Courts of Justice

The panels were constructed in three main stages as shown in Figure 4-21. The panels length are varying between 4.8 and 6.2 m. The individual panels were modeled as discussed in section 4.2.4, while the concreting of the panel was simulated by replacing the zones in the previous excavated panel with concrete properties as shown in Figure 4-22 a. The linear elastic model was used for modeling the concrete. The bulk and shear modulus for the concrete were equal to 11.8 and 10.8 GPa, respectively, while the density equals to  $20 \text{ kN/m}^3$ .

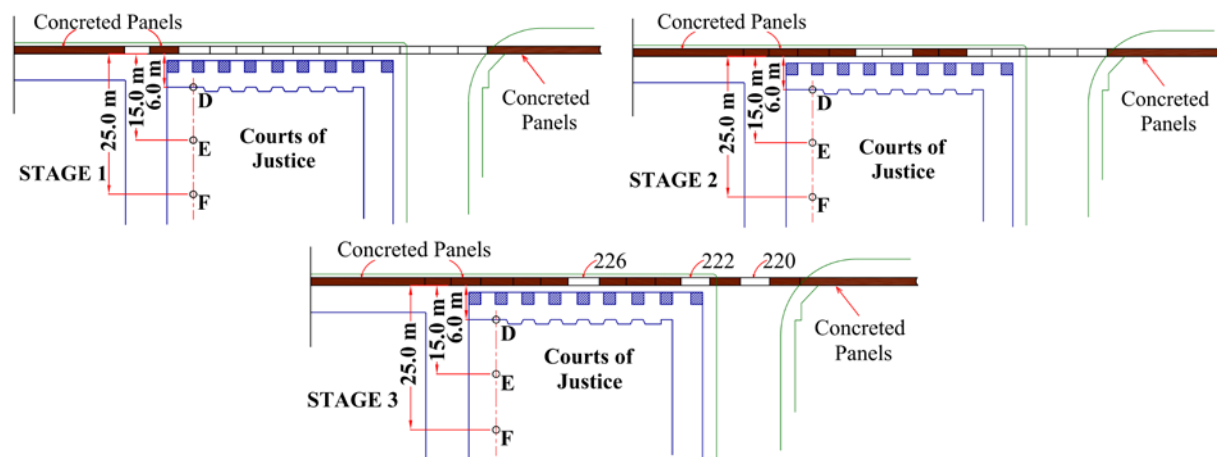


Fig. 4-21: Diaphragm wall construction stages near Courts of Justice (Davies and Henkel, 1982)

The large recorded settlement was assumed to be due to the squeezing of the weathered granite during trenching at a certain depth. Such a depth can be found in Figure 3-12. This squeezing was simulated approximately by reducing the slurry pressure and the soil strength parameters at such a location as shown in Figure 4-22b. The reason for reducing the slurry pressure is due to the possibility that the filter cake was dysfunctional due to the squeezing process. Accordingly, the penetration of the slurry in the surrounding medium reduces the bentonite effective pressure. It is very difficult to define accurately the reduction value, so an approximate reduction of 20 % was made to the slurry pressure at this location.

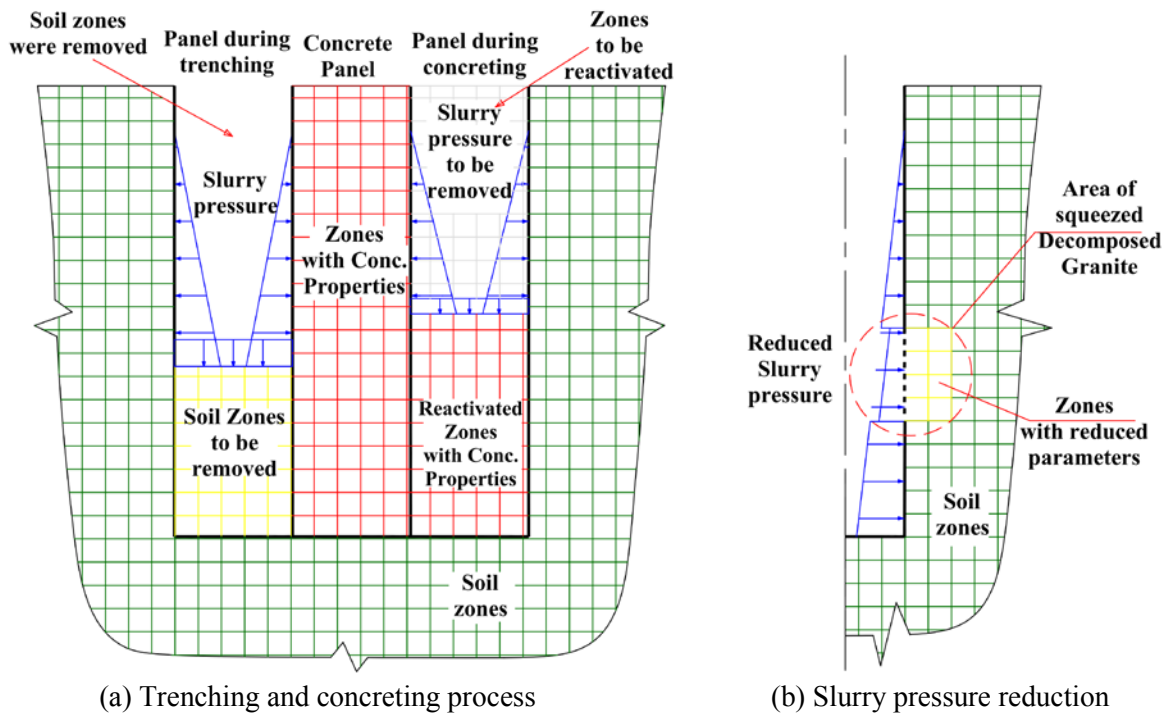


Fig. 4-22: Trench modeling

The Courts of Justice was found on timber piles with a length of 12 m. The Piles cross section area was approximately  $0.0254 \text{ m}^2$  and separated by a distance of about 4.5 m. Grade beams that carry a wall or columns connect each pile. The area method was used to calculate the load above the grade beams which transfer the load to the piles. The building consisted of two floors with an upper floor of a big dome and several decorated inclined surface roofs. Each floor is expected to apply a surface vertical load of about  $12 \text{ kN/m}^2$ . The distance between the diaphragm wall and the building timber foundation is about 2.2 m.

Beam elements were used to model the grade beams. The building load was simulated by applying a distributed line load on the beam elements. The beams were connected to the piles and transfer the load to them. The connection between the beam nodes and pile nodes was a hinged connection.

The model contained 157800 zones. Their sizes were smaller near the trench panels. They become slightly larger under the building and much larger for the rest of the model. The dimension of the model was chosen in order to have a negligible deformation at the mesh edges. The length and the width of the mesh were  $120 \times 120 \text{ m}$ , while the depth was 60 m. The model mesh and dimension are presented in Figure 4-23.

The settlement was measured at the points E, D and F for the different construction stages as shown in Figure 4-21. The maximum settlement was recorded at the nearest point (D) during constructing panels 220, 222 and 226. The settlement from numerical analysis and field data at the different construction stages is presented in Figure 4-24.

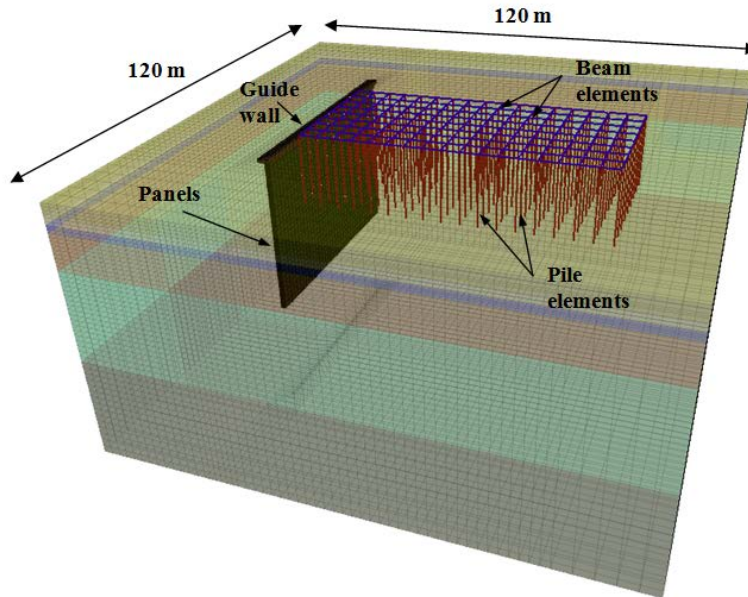


Fig. 4-23: Trench mesh modeling

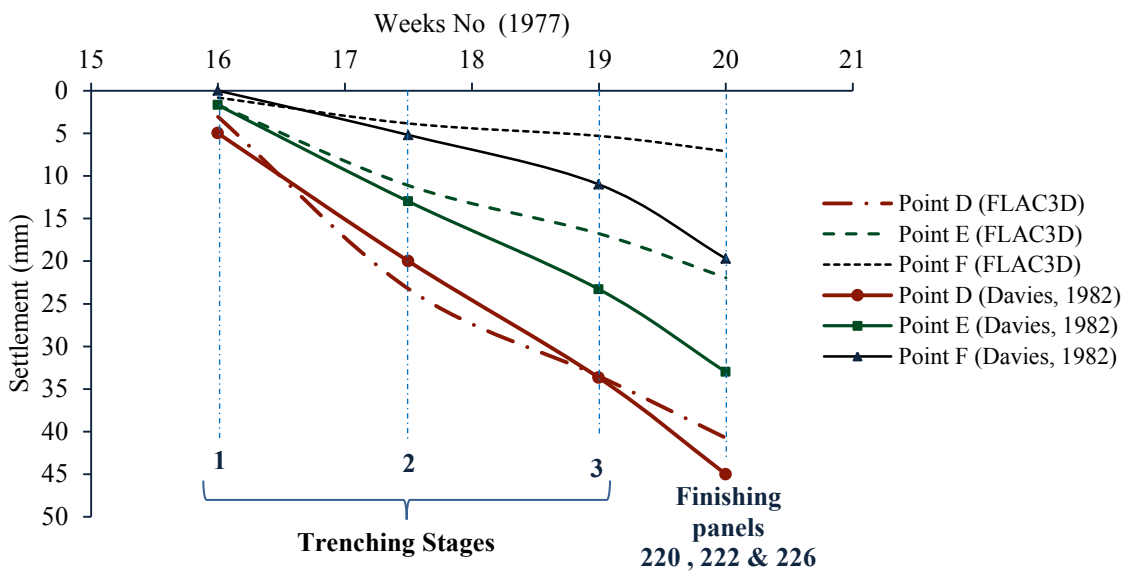


Fig. 4-24: Settlement at different stages

The settlement values decreased with distance from the trench, while they increased with advancing in the construction stages. The settlement results from the numerical analysis were almost identical with the field data results for the nearest point D, but it was different for points E and F. These points were probably affected by other construction activities which were not possible to be numerically simulated. Accordingly, the difference in values is considered to be acceptable. However, this comparison indicated that the assumptions used in the numerical analysis method are valid. The values of settlement after the third stage were critical as they are between the middle and the lower bounds in Figure 3-22.

The results of horizontal displacement from the numerical analysis at the same points (D, E and F) are presented in Figure 4-25. They were not compared to field data because no field data are



available for horizontal soil displacement. However, it is considered reliable based on the numerical verification with settlement results.

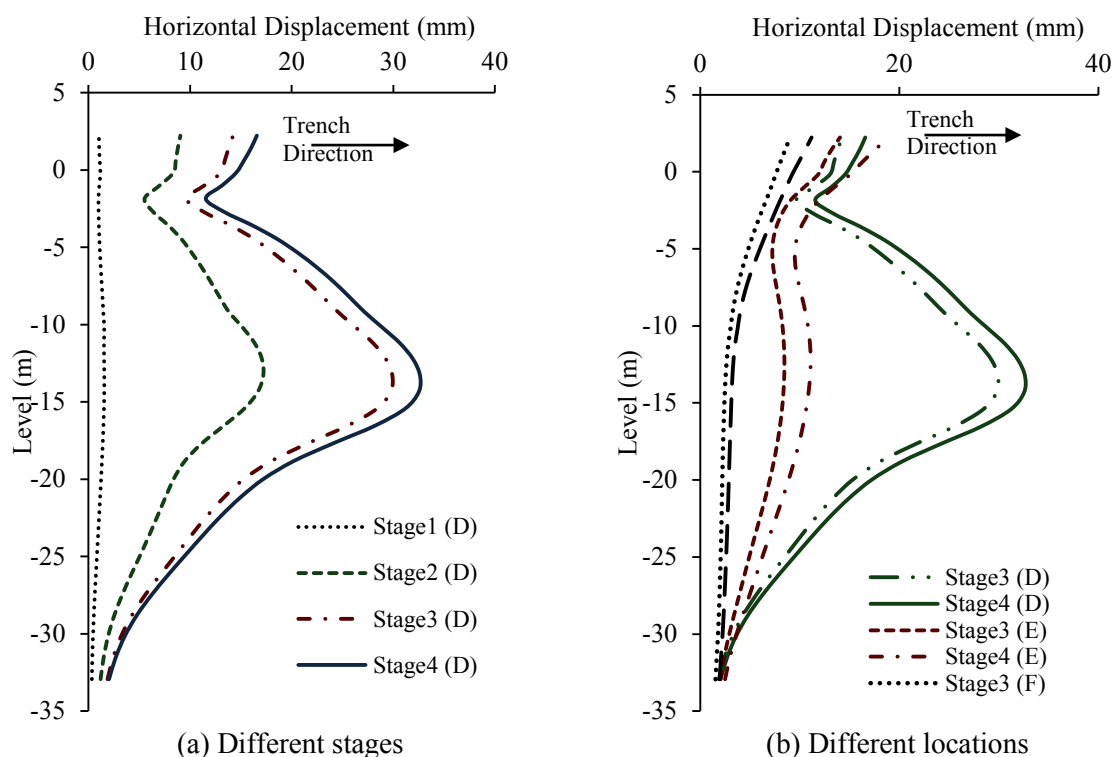


Fig. 4-25: Horizontal displacement from different stages and locations

The horizontal displacement of the soil increased with advancing on the stages, and it decreased with distance from the trench. The shape of the displacement is different according to the distance from the trench. The values of the horizontal displacement measured 6 m from the trench (i.e. point D) were maximum at the location of the squeezed decomposed granite. The maximum horizontal displacement was at the top at points E and F, while it was relatively high at the squeezed area at point E. This indicates that the effect of the squeezed decomposed granite decreased greatly with distance and its effect was almost negligible at 25 m away from the trench (i.e. point F). The same concept was presented previously for the same area in Figure 4-8 with respect to one panel only, where the horizontal displacement for the tested panel showed a different shape with distance from the trench.

The deflection and bending moment of three piles from numerical analysis near points D, E and F are presented in Figure 4-26. Again, there are no field data available for the piles but the numerical analysis could indicate the behavior of piles during such a high soil deformation.

Comparing the soil movement at point D and pile P1 deflection in the third and last stage showed that the piles have the same soil movement. In general, the piles deflected with the values of soil movement due to the high flexibility of the pile (i.e. low stiffness). Accordingly, the change in bending moment values was very low and even becomes almost zero for the most distant pile (P3). The pile movement illustrates the reason for the building minor damages

without partial collapse. If the piles were rigid and subjected to high soil deformation, their bending moment could highly increase and some of them may damage. The shaft friction in average slightly increased because it was fully mobilized during different trenching stages. Its change was not great because the pile moved the same value as the soil.

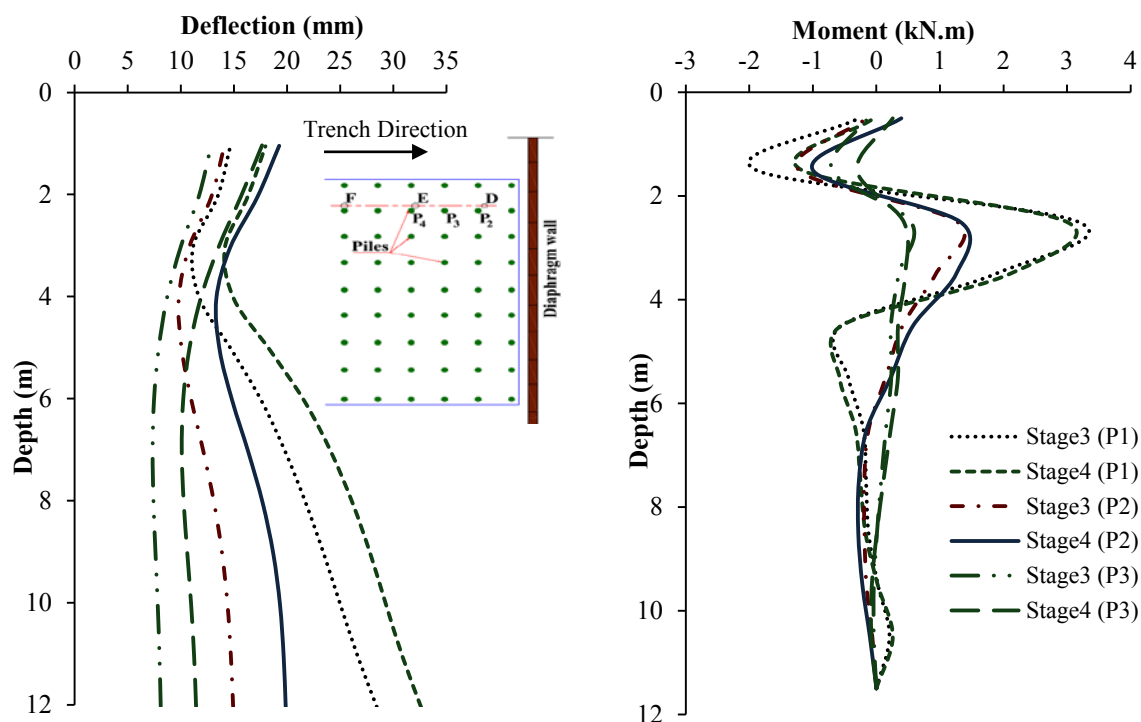


Fig. 4-26: Piles deflection and bending moment

#### 4.5.1.2 Diaphragm wall panels near Swire House

The Swire house is a 22 multi-story building located in deep foundations. This building deep foundation system was consisted of reinforced concrete piles carry individual pile caps. The piles diameter was 0.6 m. The high settlement values for this building were avoided by increasing the slurry level 0.7 m above the ground and using a panel length of 2.7 m. The numerical simulation was made for part of the building foundation and only for three panels, because the readings were taken for only three panels as previously presented in Figure 3.12. The soil is considered to be the same as the tested panel discussed in section 4.2. The panels and squeezed decomposed granite were simulated as described previously in Figure 4-22b. The shell elements were used to simulate the individual pile caps that carry the building columns. The load of the column was approximately distributed over the shell element. The dead and live loads of each floor could be taken approximately as  $11 \text{ kN/m}^2$ . The area method was used to calculate the stress above the pile caps by considering the distance between the columns is 5 m. In this case, the edge columns could carry a load equal to  $5 \text{ m} \times 2.5 \text{ m} \times 11 \text{ kN/m}^2 \times 22 \text{ floors} = 3025 \text{ kN}$ . Similarly, a load of 6050 kN is expected to be carried by the center columns. The columns loads are distributed on the surface area of the pile cap.

Pile elements were used to model the piles as previously used. Only 20 pile caps of the building were modeled. The geometric mesh showing diaphragm wall, piles, pile caps and squeezed zone is presented in Figure 4-27.

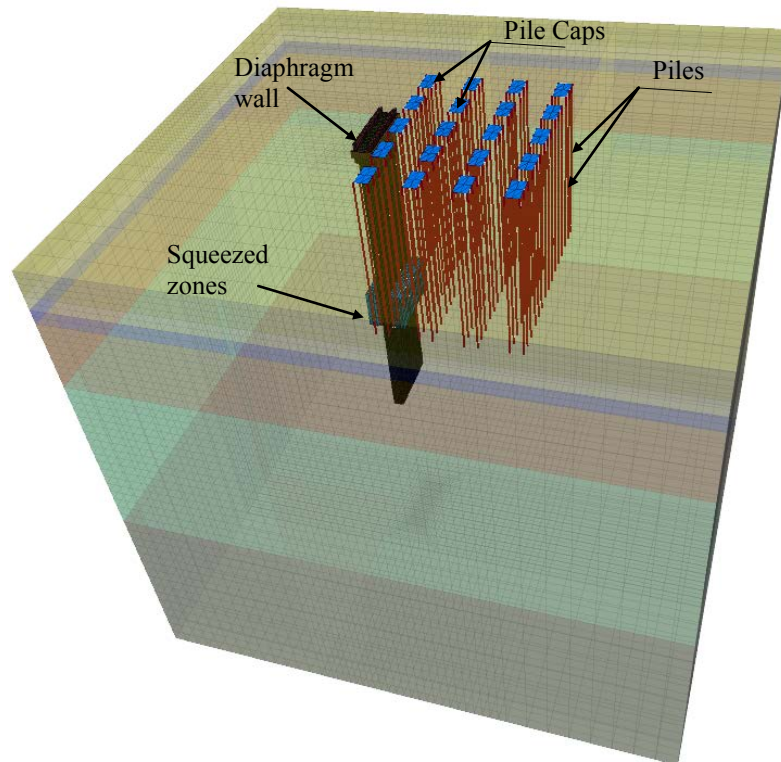


Fig. 4-27: Mesh geometry and pile caps

The graphical representation of soil horizontal displacement and pile movement at the last construction stage (i.e. secondary panel) is shown in Figure 4-28 (a), while Figure 4-28 (b) presents the horizontal soil displacement compared to field data measured with the inclinometers described in the previous chapter and located as shown in Figure 3-12. The deflection and bending moment for pile row perpendicular to the trench are presented in Figure 4-29. There are no data available about the pile behavior. However, the results from the numerical analysis regarding the pile behavior are considered to be acceptable based on the verification of soil displacement. The values of horizontal soil displacement from numerical analysis presented in Figure 4-28 were close to the values from field observation for the lower 10 m. In the upper 10 m the horizontal displacement values from numerical analysis showed a zero value while the field data showed negative values (i.e. opposite to trench direction). The high level of the guide wall than the ground surface causes the slurry pressure to be higher than earth pressure at the top of the trench. Accordingly, the horizontal displacement values at the top were negative.

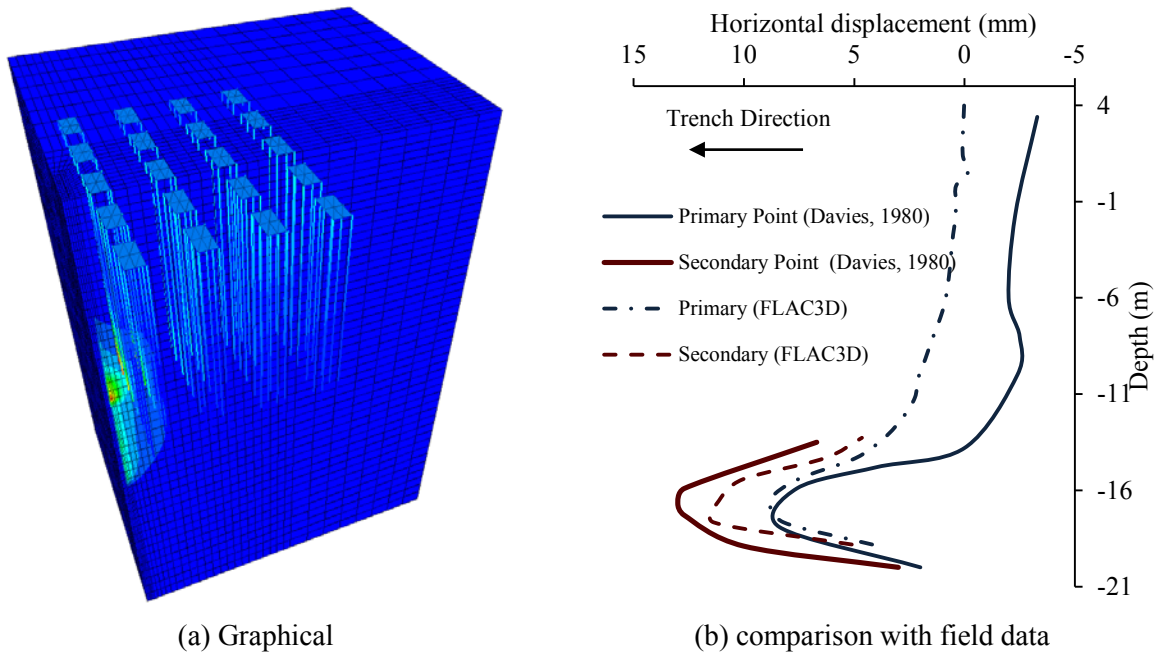


Fig. 4-28: Horizontal soil displacement

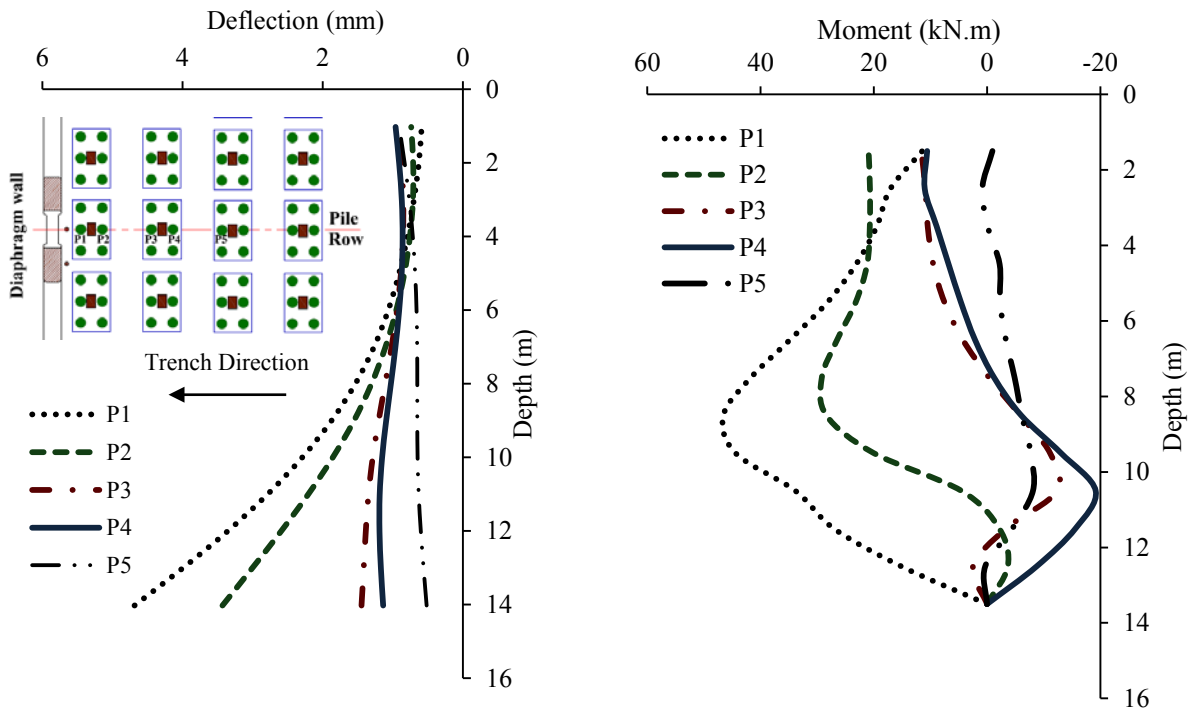


Fig. 4-29: Piles row deflection and bending moment

The location of pile from the trench defines its behavior during the trenching process as can be noticed in Figure 4-29. The nearest pile P1 to the trench showed the highest deflection and bending moment values; while the distant pile P5 showed the lowest values. The piles moved with the soil but with less values due to the relatively high stiffness of the piles. Accordingly, the bending moment change was relatively high. The shaft friction of the piles increased for the upper 10 m and then it decreased. The amount of change was relatively high compared to that found in the Court of Justice because the relative settlement between soil and pile was high in the Swire house due to pile rigidity.

#### 4.5.2 NUMERICAL MODELING OF TWO STORY BASEMENT (GIZA)

The construction of the diaphragm wall panels in Giza, Egypt discussed in the previous chapter is modelled herein for numerical verification.

##### 4.5.2.1 Diaphragm wall panels and adjacent building characteristics

The construction site plane and the section of the studied building are shown in Figure 4-30 while the panels chosen to be modeled and monitoring system for the building are shown in Figure 4-30. These panels were only chosen to be modeled because they are the nearest to the piled foundation, and the rest of the panels effect on that building will be minimum.

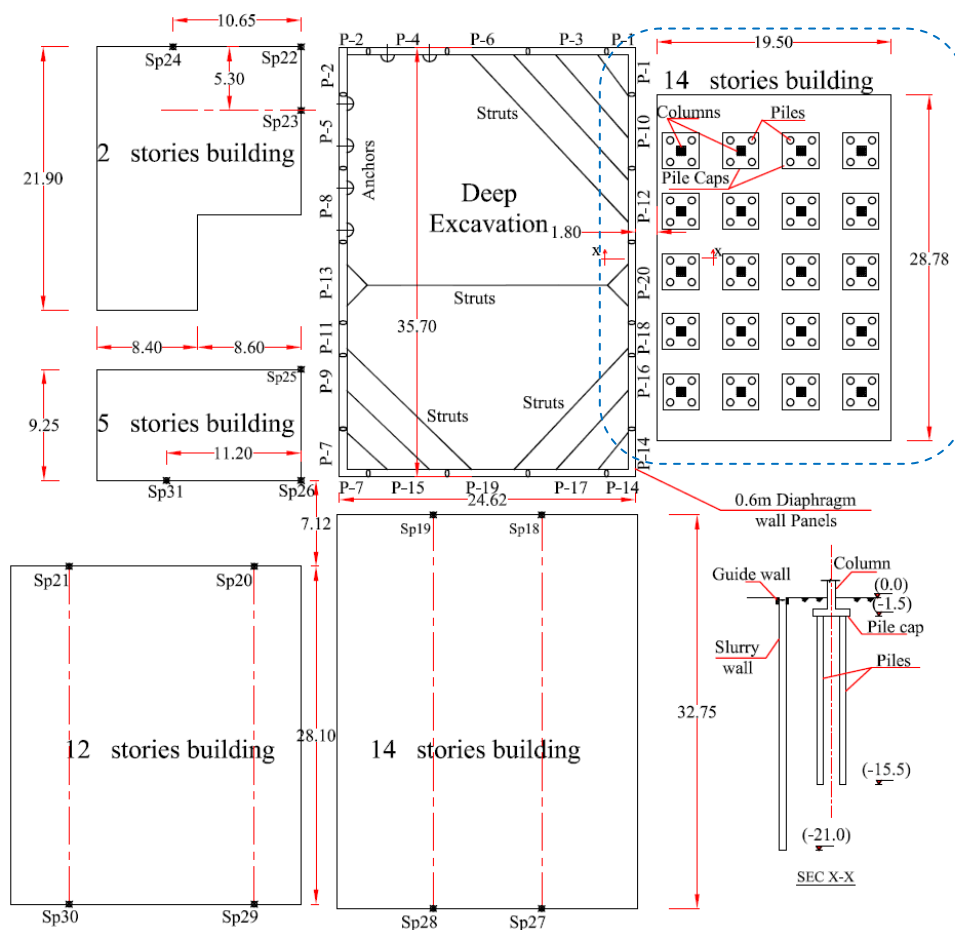


Fig. 4-30: Construction site plane and section of the studied building

The building adjacent to the diaphragm wall is a 14 story building located in piled foundations. The tip level of the building piles is 15.5 m below ground surface as shown in sec x-x. The piles have a circular diameter equal to 0.6 m. Pile caps of 0.7 m thickness were used to carry the column loads and transfer them to a group of four piles. The column loads were transferred as a stress on the pile caps and calculated by considering the stress from each floor equal to  $11\text{kN/m}^2$ . The diaphragm wall was located just 1.8 m from the building and about 2.0 m from the first pile caps row. The diaphragm wall was 0.6 m in thickness and it extended to 21 m below ground surface. The slurry level was 0.5 m below ground surface and its density was  $10.7\text{ kN/m}^3$ .

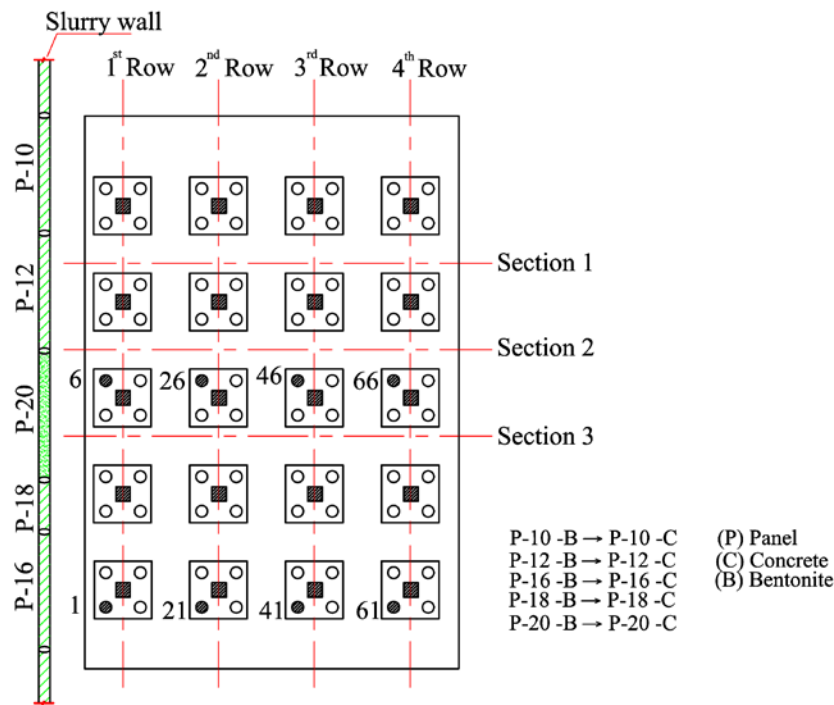


Fig. 4-31: The construction stages of the panels adjacent to the studied building

#### 4.5.2.2 Soil properties

The soil was mainly sand with different densities, friction angle and deformation modulus. The SPT and laboratory tests were used to predict the soil properties. Table 1 is a summary of the soil properties in the project area. The ground water level was found at a depth of 2.0 m below the ground surface.

Table 4-4: Soil properties at the basement location

Soil type	Bottom level (m)	SPT	$\gamma_b$ (kN/m <sup>2</sup> )	$\phi^\circ$	$E_{oed}$ (MPa)	$E_{50}$ (MPa)	$E_{ur}$ (MPa)
Fill	2.0	-	17.0	28	16.0	16.0	48.0
Silty Sand	5.0	12	18.0	30	17.0	17.0	49.0
Medium Sand	11.0	20	19.0	33.5	36.0	36.0	108.0
Dense sand	25.0	42	20.0	36	42.0	42.0	124.0

#### 4.5.2.3 Numerical modeling

The soil was modeled using the strain hardening softening soil model with the same concept discussed in section 4.2.2. The relation between the plastic shear strain and mobilized friction angle is presented in Figure 4-32. The construction of the diaphragm wall panels was simulated using FLAC 3D with the same construction sequence presented in Figure 4-31. The model mesh geometry is shown in Figure 4-33. The trenching and concreting process for each panel were modeled as previously presented in Figure 4-22 a. The pile was modeled using the pile element while the pile caps were modeled using shell elements. Beam elements were used to model the grade beams that connected the pile caps. The building was simulated first by

placing the piles, pile caps and beams. Then pressure was applied to the pile caps. The trenching process then was started.

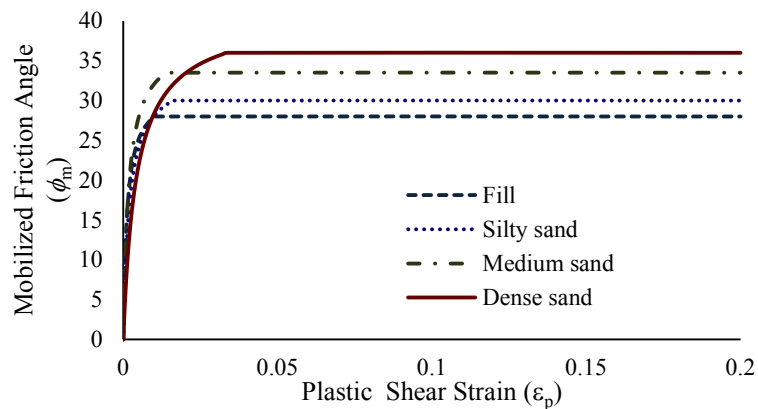


Fig. 4-32: Plastic shear strain and mobilized friction angle

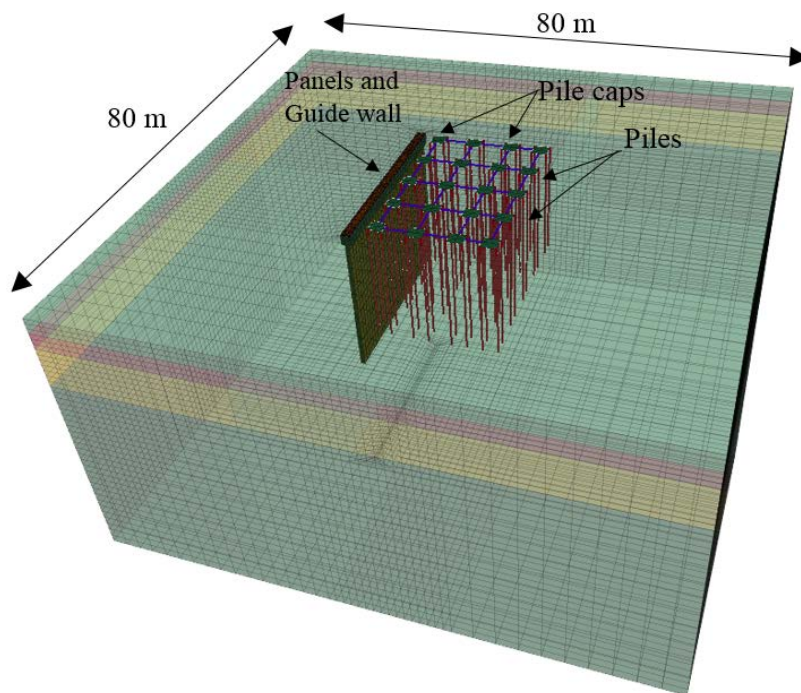
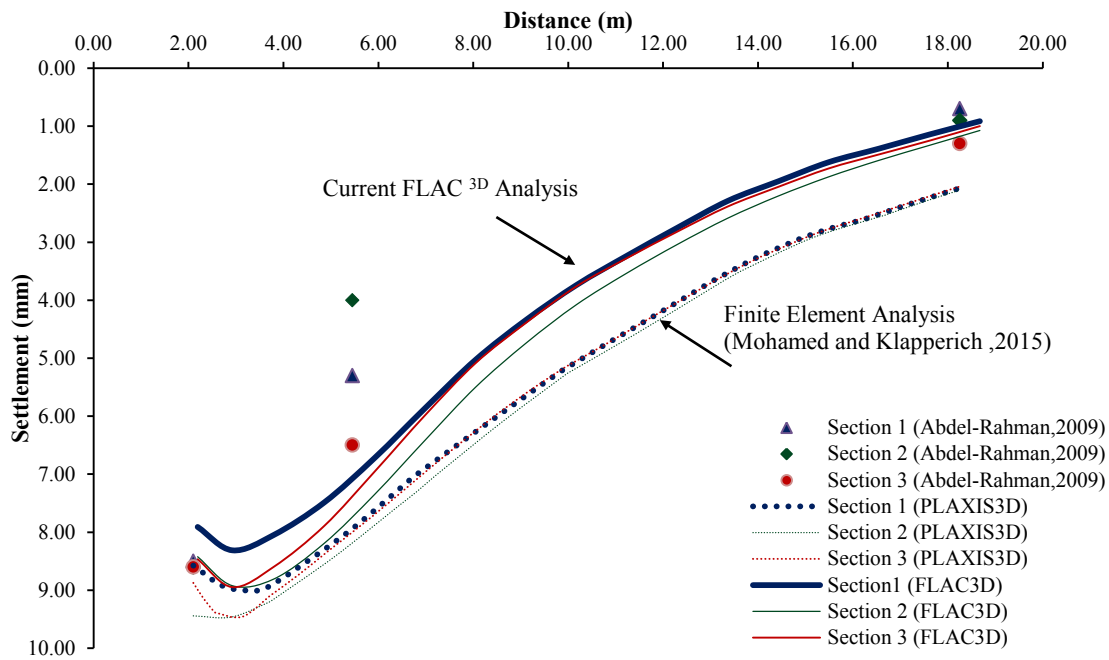


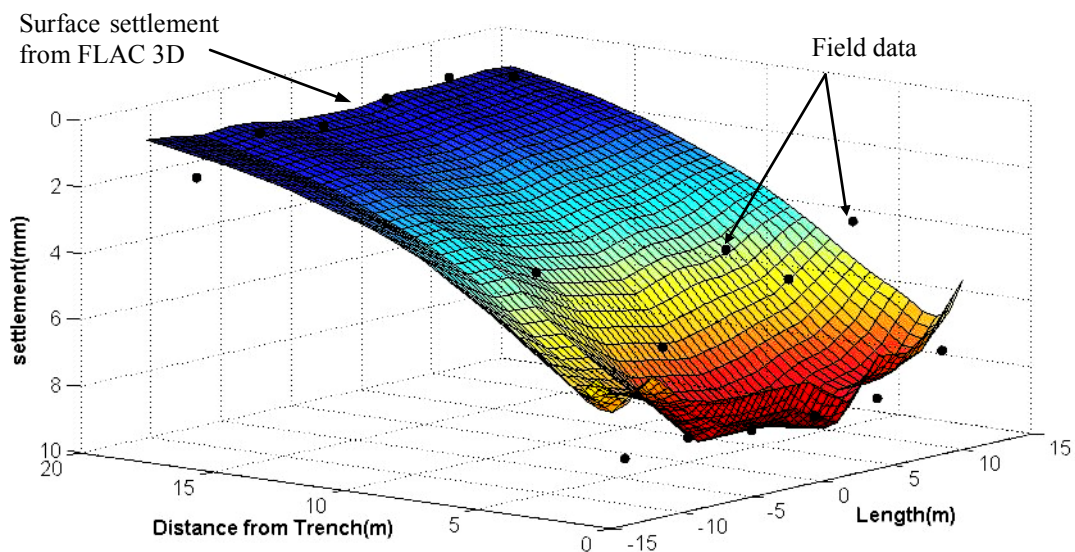
Fig. 4-33: Model Geometry

#### 4.5.2.4 Numerical results and comparison

The soil settlement from field data and numerical analysis methods is presented in Figure 4-34. In Figure 4-34a the current FLAC 3D analysis is plotted by solid lines while the previous finite element analysis conducted by Mohamed and Klapperich (2015) is shown by the non-solid lines. The field data were three points at three different locations and plotted as points. The soil surface settlement from FLAC analysis is shown in Figure 4-34b as a mesh grid while the field data results were plotted as dots. All the data were plotted after construction of the last panel. The settlement results from the FLAC analysis were closer to the field data than finite element analysis. The field settlement values located at a distance of 5m from the trench were lower than the FLAC analysis results but the values in the other locations were almost identical with the numerical analysis.



(a) Comparison at different sections



(b) Surface soil settlement

Fig. 4-34: Soil settlement

The pile deflection and bending moment values for some piles are presented in Figure 4-35. These data were not verified because no measurements were taken for the existing piles due to the technical difficulties.

The deflection and bending moment values of piles in the row at the center of panel 20 (i.e. Pile 6, 26, 46 and 66) were presented in the single line while the other values were presented in the double line.

Generally, the deflection of the piles in the center was higher than that at the edge. The piles close to the trench (i.e. Pile 1, 6 and 26) deflect slightly higher at the bottom while the other



piles deflect higher at the top. The piles far from the trench were not affected directly by the trenching process. They were dragged by the piles near the trench.

The trenching process causes additional bending moment in the piles. The bending moment values of the piles before trenching were almost zero. The change in bending moment was almost zero for the piles 41, 46 and 61. The piles near the trench showed a high increase in bending moment values which reach about 60 kN.m; however, these values are still within the carrying capacity of the reinforced concrete pile section.

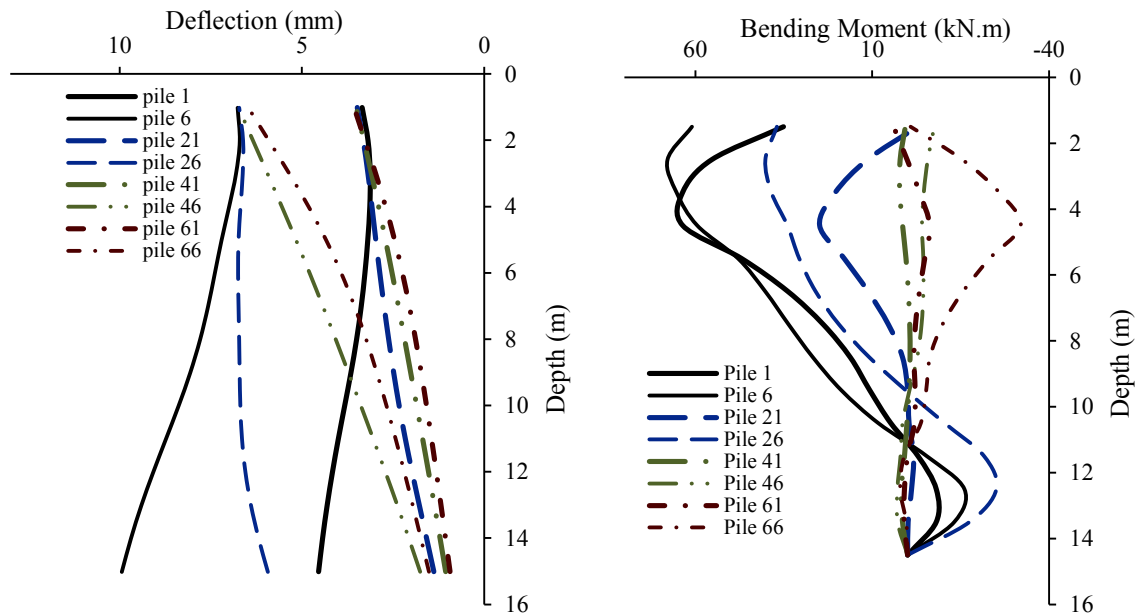


Fig. 4-35: Piles deflection and bending moment

#### 4.6 SUMMARY

In this chapter, the numerical simulation of the field and laboratory works has been conducted. It was done using FLAC 3D software which based on the finite difference analysis method. The strain hardening softening soil model was used in the analysis. The numerical analysis results were compared to the field and laboratory results to verify the analysis approach and approximation that have been used.

The results from the field test were in a contrast with the numerical analysis with respect to the horizontal displacement but it was not in such a contrast with the settlement. Some assumptions were used to model the centrifuge laboratory experiment. The settlement results from the experiment and the numerical analysis showed some differences due to the homogeneous nature of the numerical analysis results. On the other hand, the pile behavior results were not in such good agreement but it has almost the same trend except for one result which was considered to be an error in the centrifuge model test. The results of pile deflection from the numerical analysis were in a better contrast with the laboratory results than bending moment

values. Generally, this difference between values was not high and it indicate that numerical analysis had provided reliable results.

The case histories were successfully simulated numerically. The results from the numerical analysis were quite in a good contrast with the different field results. However, some differences were found due to the random nature of the field data results, while the numerical analysis showed a fixed trend of deformation based on mathematical equations.

Generally, the soil deformation predicted from the numerical analysis method used in this chapter was logic and within the deformation values discussed in the previous chapter. Indeed, the numerical analysis can't provide fully accurate results but it can draw a full picture of the problem with an acceptable accuracy. Accordingly, this numerical analysis method will be adopted for the parametric study in the next chapter.

## **CHAPTER 5: PARAMETRIC STUDY**

### **5.1 INTRODUCTION**

The soil deformation caused by construction activities is a reason for passive load on nearby existing piled foundations as discussed in Chapter 2. The trenching process of the diaphragm walls near piles is considered to be a source of such a passive load as well. Chapter 3 and 4 discussed the effect of the trenching process on the nearby piles behavior. However, the discussed cases were considered to be limited for some conditions. The parametric study that was conducted by Choy (2004) using eight centrifuge model tests was limited only to single pile and the ground water table was not taken into consideration. He studied the slurry level reduction but not the trenching process itself. However, the results of his parametric study showed the effect of the pile location and panel length on the pile behavior.

This chapter tries to draw a clear picture of the slurry trenching effect on piled foundation in a wider view. In order to provide such a picture more parameters should be investigated. The flexible nature of the numerical analysis allows to investigate more parameters and parameter combinations which are not easy to investigate using the laboratory tests. Accordingly, in this chapter the numerical analysis method with FLAC3D that was verified in the previous chapter was adopted in the current parametric study.

This study is divided into three main parts. The first part concerns the effect of single and double trench panel(s) on isolated pile group. The effect of multiple panels on connected pile groups is presented in the second part. The last part is discussing the effect of several panels on piled raft foundation. In each part, a combination of several parameters such as panel dimension, water level, soil properties, slurry level and pile properties was adopted. The pile deformation, bending moment and shaft friction were the main outputs from the analysis.

### **5.2 MODELING OF STUDIED PARAMETERS**

The idea behind conducting the parametric study was to provide a practical understanding of realistic cases of trenching near a piled foundation. The parameters were chosen to simulate real cases and some extreme situations that might happen in real engineering projects. The following sections show the chosen parameters used in the parametric study.

#### **5.2.1 SOIL PROFILE AND PROPERTIES**

The soil used in the parametric study was cohesion-less with different values of friction angle, density and deformation modulus as shown in Table 5-1. The soil profile was homogeneous for simplification. It was not necessary to model layered soil, because the layers are varying greatly and the aim of the parametric study was to understand the behavior of pile during

trenching with a general overview. However, the effect of a weak layer such as the coarse soil or the squeezed decomposed granite that might cause the slurry liquid to penetrate into the soil was modelled by reducing the slurry pressure at some levels.

The water table was chosen at five different depth ranges between 1 and 5 m below ground surface with 1m interval. The variation of the groundwater table that could happen during the trenching process itself was not taken into consideration.

Table 5-1: Soil properties used in the parametric study

Soil	$\gamma_b^*$ (kN/m <sup>3</sup> )	$\phi^o$	G (MPa)	K (MPa)	$E_{oed}^{ref}$ (MPa)	$E_{ur}^{ref}$ (MPa)
1	16.0/18.0	30	7.7	16.7	5.9	17.7
2	16.0/18.0	32	9.6	20.8	7.4	22.0
3	18.0/20.0	34	17.3	37.5	12.67	36.7
4	18.0/20.0	36	19.2	41.66	13.4	40.25
5	18.0/20.0	40	28.84	62.5	20.12	60.38

\* The density above/below ground water table

The soil was modeled using the strain hardening softening soil model that was discussed in the previous chapter. The relation between the plastic shear strain and mobilized friction angle is plotted in Figure 5-1.

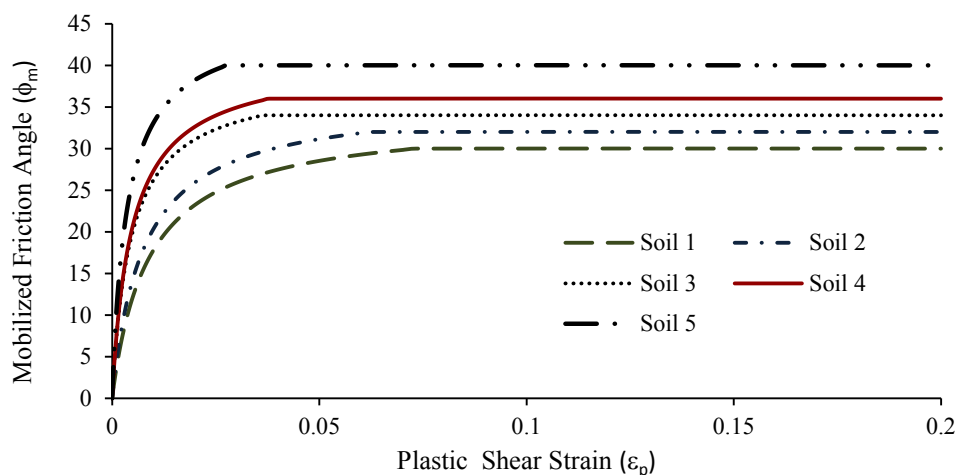


Figure 5-1: Relation between plastic shear strain and mobilized friction angle

### 5.2.2 GUIDE WALL, DIAPHRAGM WALL PANELS AND SLURRY

The guide wall used in the proposed study had a depth of 1.5m and a thickness of around 0.3 m depending on the mesh size. It was modeled by changing the zones properties to concrete properties. The concrete properties are defined by the linear elastic model with density, bulk modulus and shear modulus equal to 22 kN/m<sup>3</sup>, 11.8 and 10.8 GPa, respectively.

Generally, the dimension of the diaphragm wall is considered to effect the ground deformation. The trench panels have a common dimension which is influenced by the project requirement

and the equipment used for trenching process such as hydraulic clamshells (grab) or hydro-fraise (hydraulic cutter).

Theoretically, the diaphragm wall panel length cannot be less than 2.4 m while its length can be unlimited. Practically, the average minimum length is ranging between 2.8 and 3 m which considered the minimum grab length, while the maximum average length is 6 m. the used panel lengths in the parametric study were 3 and 6 m.

The thickness of the diaphragm wall cannot be less than 0.6 m and it can reach 1.5 m as a maximum value. In normal cases, the maximum thickness is 1.2 m. In the parametric study, the used thicknesses were 0.6 and 1.2 m.

The used equipment limits the maximum trench depth. It can reach a depth more than 100 m, but on average it ranges between 15 m and 60 m. Generally, it is not common to conduct a diaphragm wall trench deeper than 60 m inside cities. Accordingly, the average depths used in this study are between 20 and 50m.

The number of panels in any project is variable due to the required total length of the diaphragm wall. A single panel and two panels were used to study the effect on a single pile group, while nine and seventeen panels were used to study the effect of multiple panels on connected pile groups and piled-raft foundation.

The slurry level inside the trench is normally located about 0.5 m below ground surface, but it can be decreased during construction below that level. In this study, the slurry level was ranged between 0.5 m and 2.5 m below ground surface. The density of slurry liquid is limited by a value of around  $13 \text{ kN/m}^3$  as discussed in Chapter 2, while its minimum value could be slightly higher than the water density. The value used in this analysis was  $10.9 \text{ kN/m}^3$ .

The null element was used to define the zones at the trench location and a pressure equivalent to the slurry pressure was applied on the trench wall surface as described previously in Figure 4-22a. The slurry reduction at some location was done in the same concept described in Figure 4-22b but without reduce the shear strength of the nearby zones. The concrete panels, if any, were modeled using the linear elastic model with the same properties of the guide wall.

### 5.2.3 PILED FOUNDATION AND OFFSET DISTANCE

The piles under existing structures are the scope of this study. The piles in this cohesion-less (sandy) soils are normally used to support the high-rise buildings. Accordingly, the reinforced concrete piles should be modelled using an element that can carry such high loads, because timber piles cannot carry such high loads. The piles in the cohesion-less soil normally extend to reach a denser soil or extend to a depth that can achieve the pile design capacity. On average, the piles could extend 12 m in such soil. The number and capacity of piles affect the choice of pile diameter. It normally ranges between 0.6 and 1.5 m or equivalent for case of using

rectangular piles. Reinforced concrete circular piles were assumed in the parametric study with length ranges between 12 and 20 m, while the used diameter was 0.2, 0.4, 0.6, 0.8, 1.0 and 1.2 m. They were modeled using the pile element implemented in FLAC 3D. The properties of the investigated pile are presented in Table 5-2.

Table 5-2: Piles properties used in the parametric study

Pile Diameter	Pile				Interface			
	Area (m <sup>2</sup> )	Inertia (m <sup>4</sup> )	Perimeter (m)	E (kN/m <sup>2</sup> )	k <sub>s</sub>	k <sub>n</sub>	φ <sub>s</sub>	φ <sub>n</sub>
					(kN/m <sup>3</sup> )		(degree)	
0.2	0.0314	0.00015	0.6283	2.5x10 <sup>7</sup>	Equation 4.25	2/3 φ		
0.4	0.125	0.0025	1.25					
0.6	0.283	0.0120	1.88					
0.8	0.502	0.0402	2.51					
1.0	0.785	0.0981	3.14					
1.2	1.131	0.203	3.77					

The piles normally exist in a group carried by a pile cap to support the building columns. The group could contain different number of piles. Groups of four, five and six piles connected with pile caps were simulated in the study. The study included also connected pile groups and piled raft foundation. The shell element was used to model the reinforced concrete pile caps or the raft. The used thickness for the shell element was 0.7 m, while its elastic deformation modulus and Poisson's ratio equal 25 GPa and 0.3, respectively.

The reinforced concrete grade beams are used to connect the pile caps. Their depth and thickness are 0.7 and 0.3, respectively. They were modeled using the beam element implemented in FLAC. The linear elastic model was chosen to define such an element.

The offsite distance between the trench excavation and any existing buildings varies according to the project. The chosen distances in this research were 2, 3.5, 5.5 and 7.5 m.

### 5.3 PARAMETERIC STUDY PLAN

This section discusses the different parameters used in the parametric study and is divided into three main parts. Each part is divided into several model groups (MG) and each model group is again divided into several parameters combination (C). The following subsections discuss the parametric study parts with the different model groups and combinations.

#### 5.3.1 PART I - THE EFFECT OF SINGLE OR DOUBLE TRENCH PANELS ON ISOLATED PILE GROUP

This part of the parametric study concerns understanding the local effect of constructing a single or double panel(s) on isolated pile group. The pile group was modeled with different pile numbers and formations in order to understand the different behavior of piles within the group.

### **5.3.1.1 Parameters and model groups of Part I**

Five different values of the groundwater table (WL) were considered, while the slurry level (SL) was in the range between 0.5 and 2.0 m. The slurry pressure was assumed to be reduced 1.0 m below seven different levels defined by (SP). This simulates a 1 m thick weak soil layer at these levels. The five different soil types mentioned in section 5.2.1 were used only in the first model group. The trench depth (H) was varying for several model groups while its length (L) and thickness (T) were varying only for the first model group. The distance between the trench and the first pile centerline (x) varies between 2.0 and 7.5 m. The effect of pile diameter (D) and depth ( $h_p$ ) only were studied for the first model group. Figure 5-2 shows the summary of the studied parameters of this part.

### **5.3.1.2 Combination of the studied parameters**

The effect of each parameter combined with the other parameters in Part I is presented in Figure 5-3. Each model group is divided into several combinations. The symbols in each combination are defined first by the part number (P), model group (MG) and finally by the combination number (C).

The first combination of model group 1 (PI-MG1-C1) was directed to study the effect of ground water table, trench dimension and pile group distance from the trench at fixed slurry level, soil strength and pile dimensions. The second combination of the same model group (PI-MG1-C2) concerned the study of the different slurry levels and different values of soil strength, while all the other parameters were constant except for the trench length and width. The third combination (PI-MG1-C3) was considered to be the same as the second one, but it has concerned more about the different distances of the pile group from the slurry trench while soil properties were considered to be constant. The effect of slurry pressure reduction at some trench depths and two different slurry levels was discussed in the fourth and fifth combinations (PI-MG1-C4 & PI-MG1-C5). The pile depth and diameter were chosen to be varying at different trench depths in combinations (PI-MG1-C6) and (PI-MG1-C7), respectively.

Model groups 2, 3 and 4 have the same parameters combinations. The first parameters combinations for these groups (PI-MG2-C1, PI-MG3-C1 or PI-MG4-C1) took into consideration the effect of different slurry levels and trench depths, while the second parameters combination (PI-MG2-C2, PI-MG3-C2 or PI-MG4-C2) took into consideration the effect of slurry pressure reduction.

Model group 5 has the same two combinations as model group 2, but it modeled double panels. The trenching process was made in two main steps. The first panel was excavated first and then concreted, then the second panel was excavated.

Model group	Half Isometric / Plan	Parameters
1		<p>Trench:  <math>H = 20, 30, 40</math> and <math>50</math> m  <math>T = 0.6</math> and <math>1.2</math> m  <math>L = 3</math> and <math>6</math> m</p> <p>Pile:  <math>h_p = 12, 14, 16, 18</math> and <math>20</math> m  <math>D = 0.4, 0.6, 0.8</math> and <math>1.0</math> m</p> <p>Water Level:  <math>WL = 1, 2, 3, 4, 5</math> m</p> <p>Slurry level:  <math>SL = 0.5, 1.0, 1.5, 2.6</math> m</p> <p>Upper Levels of Reduced slurry pressure:  <math>SP = 9.0, 10, 11, 12, 13, 14</math> m</p> <p>Pile offsite distance:  <math>X = 2, 3.5, 5.5, 7.5</math> m</p>
2		<p>Trench:  <math>H = 20, 30, 40</math> and <math>50</math> m  <math>T = 1.2</math> m  <math>L = 6</math> m</p> <p>Pile:  <math>h_p = 12</math> m  <math>D = 0.8</math> m</p> <p>Water Level:  <math>WL = 2</math> m</p> <p>Slurry level:  <math>SL = 0.5, 1.0, 1.5</math> m</p> <p>Upper Levels of Reduced slurry pressure:  <math>SP = 9.0, 10, 11, 12, 13, 14</math> m</p> <p>Pile offsite distance:  <math>X = 3.5</math> m</p>
3		<p>Trench:  <math>H = 20, 30, 40</math> and <math>50</math> m  <math>T = 1.2</math> m  <math>L = 6</math> m</p> <p>Pile:  <math>h_p = 12</math> m  <math>D = 0.8</math> m</p> <p>Water Level:  <math>WL = 2</math> m</p> <p>Slurry level:  <math>SL = 0.5, 1.0, 1.5</math> m</p> <p>Upper Levels of Reduced slurry pressure:  <math>SP = 9.0, 10, 11, 12, 13, 14</math> m</p> <p>Pile offsite distance:  <math>X = 3.5</math> m</p>



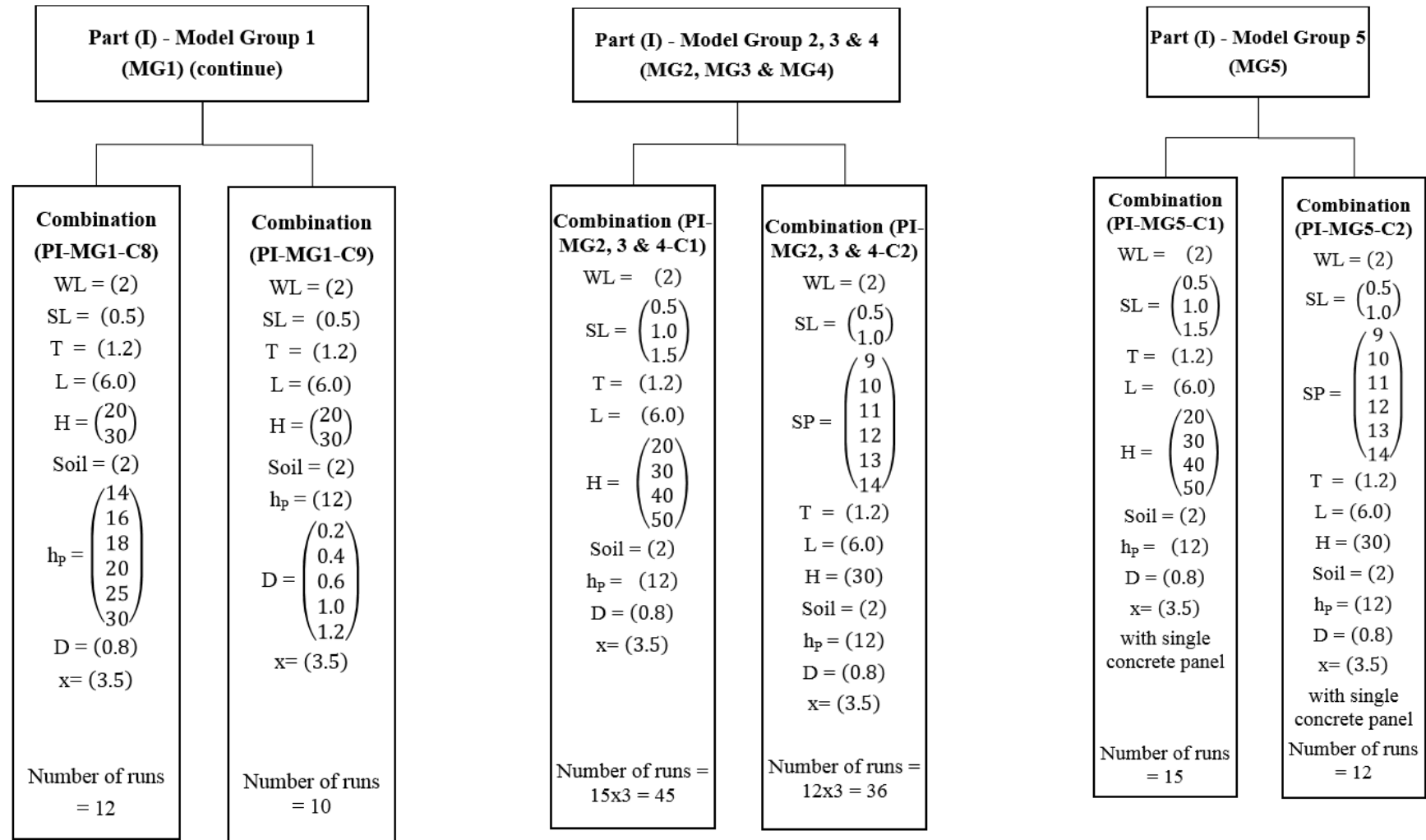
Model group	Half Isometric / Plan	Parameters
4		<p>Trench:  <math>H = 20, 30, 40</math> and <math>50</math> m  <math>T = 1.2</math> m  <math>L = 6</math> m</p> <p>Pile:  <math>h_p = 12</math> m  <math>D = 0.8</math> m</p> <p>Water Level:  <math>WL = 2</math> m</p> <p>Slurry level:  <math>SL = 0.5, 1.0, 1.5</math> m</p> <p>Upper Levels of Reduced slurry pressure:  <math>SP = 9.0, 10, 11, 12, 13, 14</math> m</p> <p>Pile offsite distance:  <math>X = 3.5</math> m</p>
5		<p>Trench:  <math>H = 20, 30, 40</math> and <math>50</math> m  <math>T = 1.2</math> m  <math>L = 6</math> m</p> <p>Pile:  <math>h_p = 12</math> m  <math>D = 0.8</math> m</p> <p>Water Level:  <math>WL = 2</math> m</p> <p>Slurry level:  <math>SL = 0.5, 1.0, 1.5</math> m</p> <p>Upper Levels of Reduced slurry pressure:  <math>SP = 9.0, 10, 11, 12, 13, 14</math> m</p> <p>Pile offsite distance:  <math>X = 3.5</math> m</p>

Figure 5-2: Model groups and parametric study parameters

**Part (I) -Model Group (1)**  
**(PI-MG1)**

<b>Combination (PI-MG1-C1)</b>	<b>Combination (PI-MG1-C2)</b>	<b>Combination (PI-MG1-C3)</b>	<b>Combination (PI-MG1-C4)</b>	<b>Combination (PI-MG1-C5)</b>	<b>Combination (PI-MG1-C6)</b>	<b>Combination (PI-MG1-C7)</b>
$WL = \begin{pmatrix} 1 \\ 3.0 \end{pmatrix}$ $SL = (0.5)$ $T = (1.2)$ $L = (6.0)$ $H = \begin{pmatrix} 20 \\ 30 \\ 40 \\ 50 \end{pmatrix}$ $Soil = (2)$ $h_p = (12)$ $D = (0.8)$ $x = \begin{pmatrix} 2.0 \\ 3.5 \end{pmatrix}$	$WL = (1.0)$ $SL = (0.5)$ $T = \begin{pmatrix} 1.2 \\ 0.6 \end{pmatrix}$ $L = \begin{pmatrix} 6.0 \\ 3.0 \end{pmatrix}$ $H = (30)$ $Soil = (2)$ $h_p = (12)$ $D = (0.8)$ $x = \begin{pmatrix} 2.0 \\ 3.5 \end{pmatrix}$	$WL = (2)$ $SL = (0.5)$ $T = (1.2)$ $L = \begin{pmatrix} 6.0 \\ 3.0 \end{pmatrix}$ $H = (30)$ $Soil = (2)$ $h_p = (12)$ $D = (0.8)$ $x = \begin{pmatrix} 2 \\ 3.5 \\ 5.5 \\ 7.5 \end{pmatrix}$	$WL = \begin{pmatrix} 1.0 \\ 2.0 \\ 3.0 \\ 4.0 \\ 5.0 \end{pmatrix}$ $SL = \begin{pmatrix} 0.5 \\ 1.5 \end{pmatrix}$ $T = (1.2)$ $L = \begin{pmatrix} 6.0 \\ 3.0 \end{pmatrix}$ $H = (30)$ $Soil = (2)$ $h_p = (12)$ $D = (0.8)$ $x = (3.5)$	$WL = (2)$ $SL = \begin{pmatrix} 1.0 \\ 1.5 \\ 2.0 \end{pmatrix}$ $T = (1.2)$ $L = \begin{pmatrix} 6.0 \\ 3.0 \end{pmatrix}$ $H = (30)$ $Soil = (2)$ $h_p = (12)$ $D = (0.8)$ $x = \begin{pmatrix} 2.0 \\ 3.5 \\ 5.5 \end{pmatrix}$	$WL = (2)$ $SL = \begin{pmatrix} 0.5 \\ 1.0 \end{pmatrix}$ $T = (1.2)$ $L = (6.0)$ $H = (30)$ $Soil = \begin{pmatrix} 1 \\ 2 \\ 3 \\ 4 \end{pmatrix}$ $h_p = (12)$ $D = (0.8)$ $x = (3.5)$	$WL = (2)$ $SL = \begin{pmatrix} 0.5 \\ 1.0 \end{pmatrix}$ $SP = \begin{pmatrix} 9 \\ 10 \\ 11 \\ 13 \\ 14 \\ 21 \end{pmatrix}$ $T = (1.2)$ $L = \begin{pmatrix} 6.0 \\ 3.0 \end{pmatrix}$ $H = (30)$ $Soil = (2)$ $h_p = (12)$ $D = (0.8)$ $x = \begin{pmatrix} 2.0 \\ 3.5 \\ 5.5 \end{pmatrix}$
Number of runs = 10.0	Number of runs = 8.0	Number of runs = 8.0	Number of runs = 20.0	Number of runs = 18.0	Number of runs = 8.0	Number of runs = 72.0

(a) Model Group 1



(b) Model Group 1 (continued)

(c) Model groups 2, 3 and 4

(d) Model group 5

Figure 5-3: Parameters combinations of Part I

### 5.3.1.3 Typical mesh model of Part I

The size of the mesh model was the same for all the models in this part. The difference was in the pile group formations and locations. Modeling of each element was made as described before in section 5.2, as well as simulation of the trenching process. The mesh model contained 114480 zone. The mesh surface area was small near the trench and it increased gradually far from the trench. It was 0.15 x 0.375 m exactly at the trench location and 1.812 x 1.88 m at the corner of the mesh and it was between these two values at the edges parallel and perpendicular to the trench location. The piles were divided into equal segments of 1 m in length and they were connected in the group with a shell element. The typical mesh used in the analysis is presented in Figure 5-4.

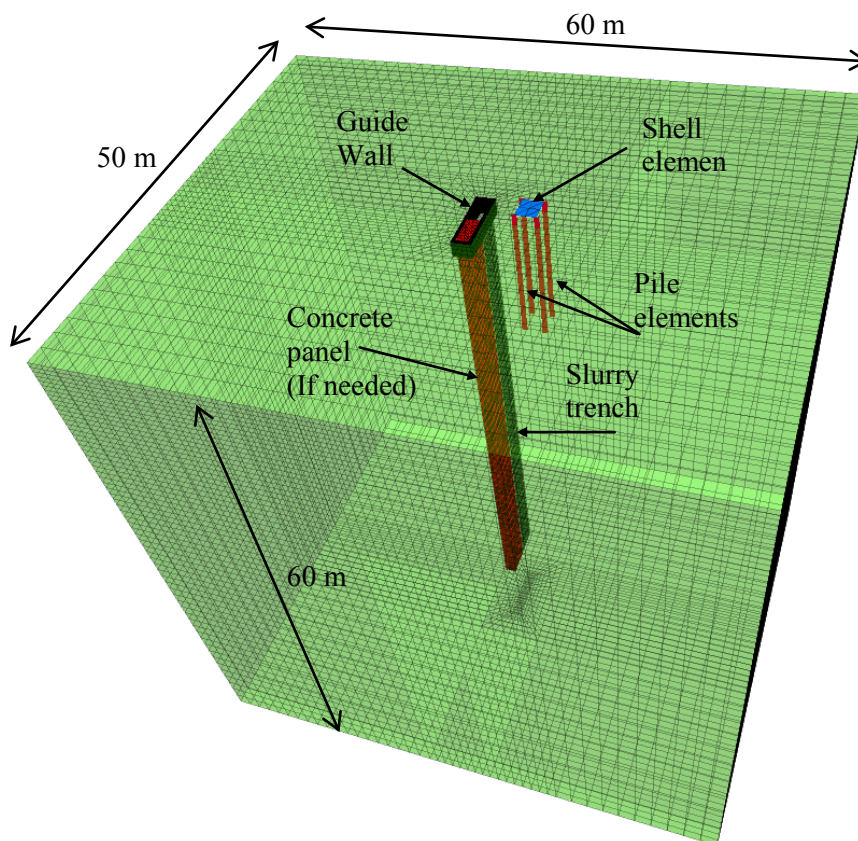


Figure 5-4: Parameters combination of Part I

### 5.3.2 PART II - MULTIPLE PANELS EFFECT ON SEVERAL CONNECTED PILE GROUPS

The previous part was limited to study single and double panel(s) effect on a single pile group. In reality, the trench wall is made of several panels which may extend to several tenth of meters, also the piled foundation is consisting of several pile groups connected with each other by grade beams. The large-scale effect of multiple panels on the piles behavior within several connected pile groups is discussed in this part (Part II).

### 5.3.2.1 Geometry and model groups of Part II

The total wall length was chosen to be 54 and 51 m in the case of using 6 and 3 m length panels, respectively. The panels were trenched in stages to simulate the common construction sequence of the diaphragm wall excavation. The spacing between the columns was assumed to be 5 m and 7 m for the 4 and 6 piled groups, respectively. The first row of pile groups was located just 2 m from the trench center line. The piles tips were located 15 m below the group surface. The pile diameter was assumed to be equal to 0.8 m in all the cases.

Two main model groups were assumed for this study. The main difference is related to the spacing between columns and pile arrangement. The spacing between the columns for the first model group was assumed to be 5 m and four piles were within each pile group. The columns spacing in the second model group was 7 m and each pile group contains six piles. The ground water table, slurry level and panel lengths were the major studied parameters. The panel construction stages of the 6 and 3 m panels of model group 1 are described in the planes in Figure 5-5 (a) and (b), respectively. The pile arrangement of model group 2 is shown in Figure 5-6.

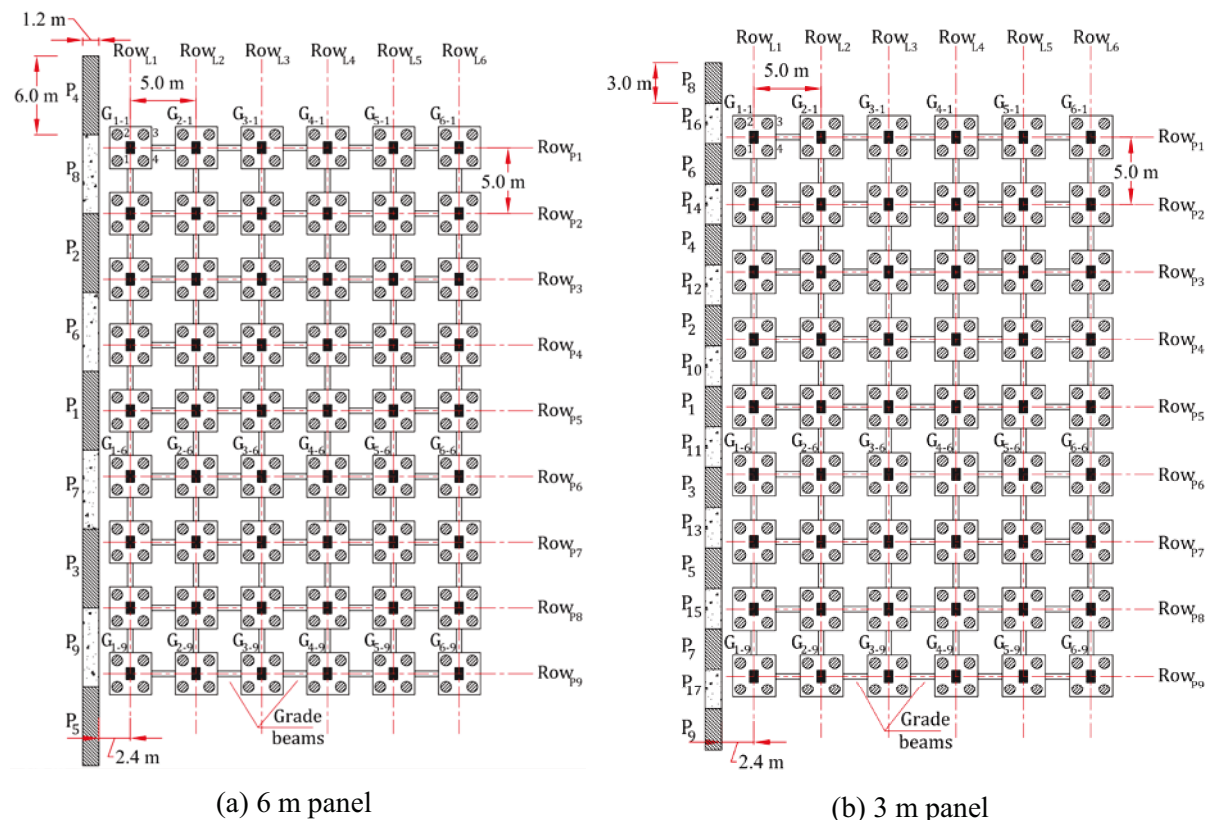


Figure 5-5: Planes of model group 1

The panel length was only 6 m for the second model group. The panel is represented by the letter P and the number located near this letter is describing the panel number, so the first, second and n panels are  $P_1$ ,  $P_2$ , ...  $P_n$ , respectively. The panels were constructed in ascending order according to their number. Each panel was trenched first and then concreted, the

following panel can be trenched after that. The pile groups were represented by the symbol G followed by the vertical and horizontal row number. The first vertical row is the nearest to the trench. The first horizontal row is assumed to be at the top. The piles within the group were also numbered in the first pile group ( $G_{1-1}$ ) in each plane.

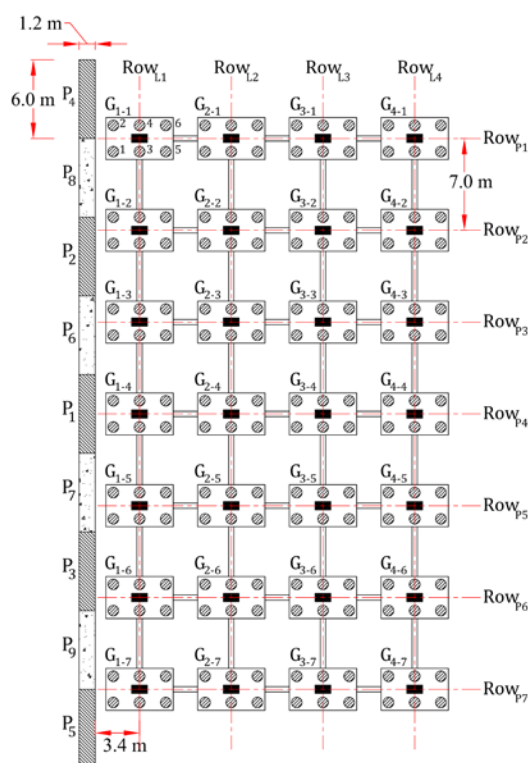


Figure 5-6: Plane of model group 2

### 5.3.2.2 Parameters combination of Part II

The parameters combinations of each model group are shown in Figure 5-7. The first combination in the first model group (PII-MG1-C1) concerns the groundwater level and trench length effect, while the second (PII-MG1-C2) shows the effect of reducing the slurry level, and finally the reduction of slurry pressure at some levels was discussed in the third combination (PII-MG1-C3). Model group 2 has only one combination that is similar to the first combination of the first model group but the groundwater level and panel length were constant.

### 5.3.2.3 Mesh models of Part II

The mesh model of this part is larger than the previous part because it modeled multiple panels that simulated a trench wall with a normal length. The simulation of the panels and piles is similar to that discussed in the previous chapter in Section 4.4, specifically the simulation of the two-story basement in Giza, where the beam elements were used to simulate the grade beams. The mesh surface area at the location of the panels was  $1.5 \times 0.2 \text{ m}^2$ , under the piles it was  $2 \times 2 \text{ m}^2$ , while at the corner it reached  $4 \times 4 \text{ m}^2$ . The rest of the mesh size was between these values with a total number of zones of 157800. Figure 5-8 shows the typical mesh geometry.

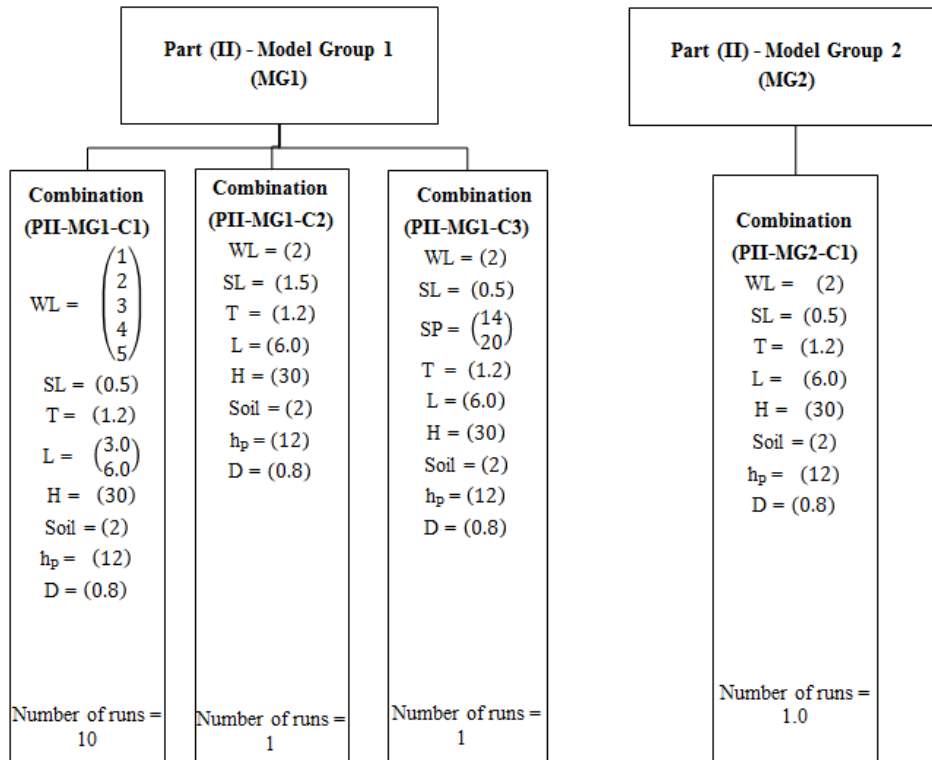
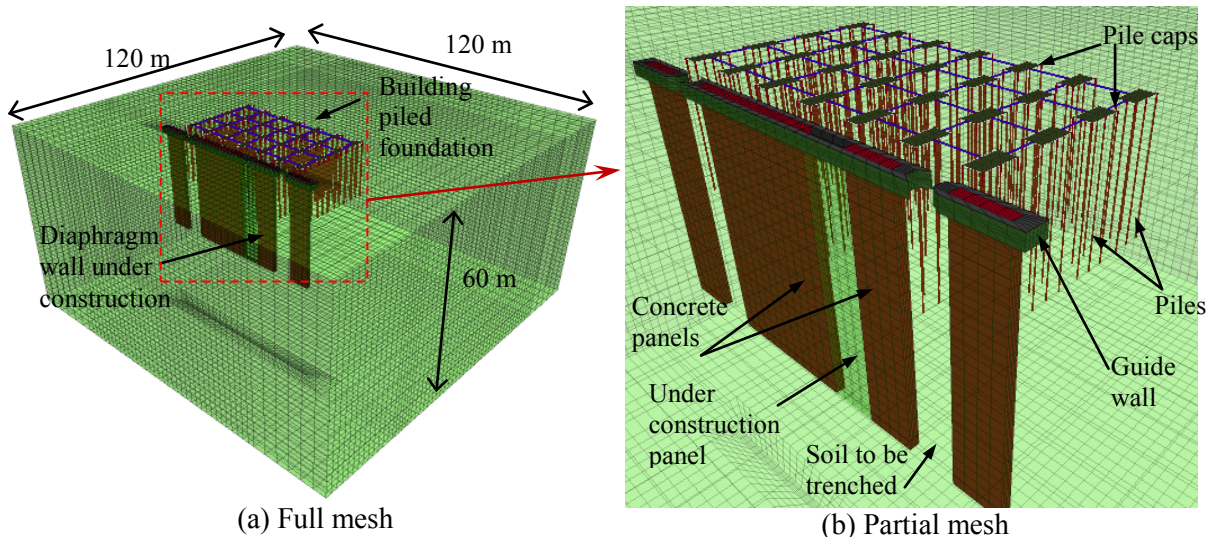


Figure 5-7: Parameters combination of Part II



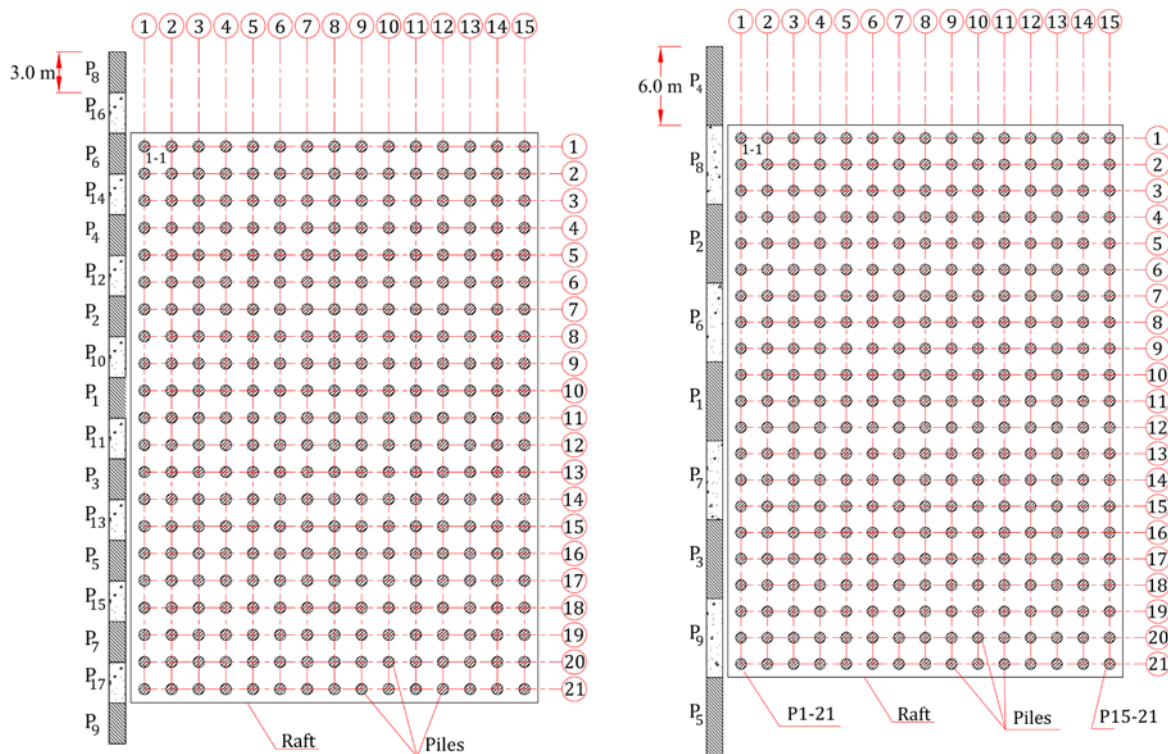
(a) Full mesh  
(b) Partial mesh  
Figure 5-8: Typical mesh geometry of Part II model groups

### 5.3.3 PART III - MULTIPLE PANELS EFFECT ON PILED RAFT FOUNDATION

The building inside the cities could be also located on piled raft foundation. The pile in this case the pile is carrying a large raft footing that carries the building columns. The behavior of piles within the raft foundation is expected to be different from that of the pile cap. This part is almost similar to the previous part (Part II) but the nearby building to the trench is assumed to be supported by piled raft foundation, in order to show the different behavior of piles in case of raft foundation rather than connected pile caps due to nearby slurry trenching.

### 5.3.3.1 Geometry of Part III

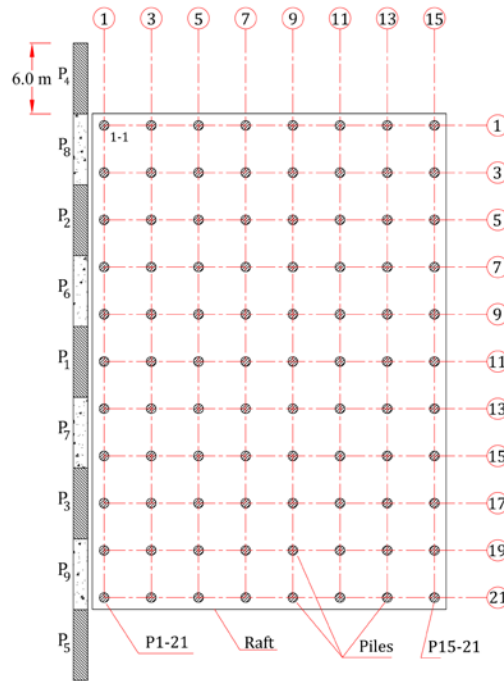
The total diaphragm wall length and its construction stages are similar to the previous part. The suggested panel lengths were also three and six meters for the first model group, while in the second model group only the six meter panels were used. The piles tip levels and diameters were similar to the previous part. The spacing between piles was assumed to be 2 m (2.5D) and 4 m (5.0D) for the first and second model groups, respectively. The nearest pile row parallel to the trench was located 2.0 m from the trench centerline. The plane of the panels and the piled raft foundation of both models are presented in Figure 5-9. The panels were numbered as explained in the previous part. The total number of piles in the first and second model groups is 315 and 88, respectively. The piles were numbered according to the horizontal and vertical axes. For example, the pile in the top left corner is numbered by the first vertical row and horizontal row as 1-1. The raft supported by the piles assumed to be 0.7 m in thickness and the pile is connected directly to the raft. Accordingly, the load is transferred from the building to the piles through the raft and it is assumed to be distributed equally on the raft. The values of groundwater level, slurry level and panel lengths were chosen to be variables while the piles properties and spacing were not variables. The trench depth was fixed to be 30 m below the ground surface and soil number 2 was chosen for this study.



(a) Model group 1 - 6 m panel

(b) Model group 1 - 3 m panel





(c) Model group 2 - 6 m panel

Figure 5-9: Planes of Part III model

### 5.3.3.2 Parameters combination of Part III

In this part, there are only two combinations for each model group. The first combination of the first model group (PIII-MG1-C1) discussed the effect of groundwater table and the second (PIII-MG1-C2) concerned the effect of the panel length. The first combination of model group 2 (PIII-MG2-C1) is similar to that of model group 1 but the second combination (PIII-MG2-C2) of model group 2 concerned the effect of slurry level. The parameters combinations of this part are explained by the flow chart in Figure 5-10.

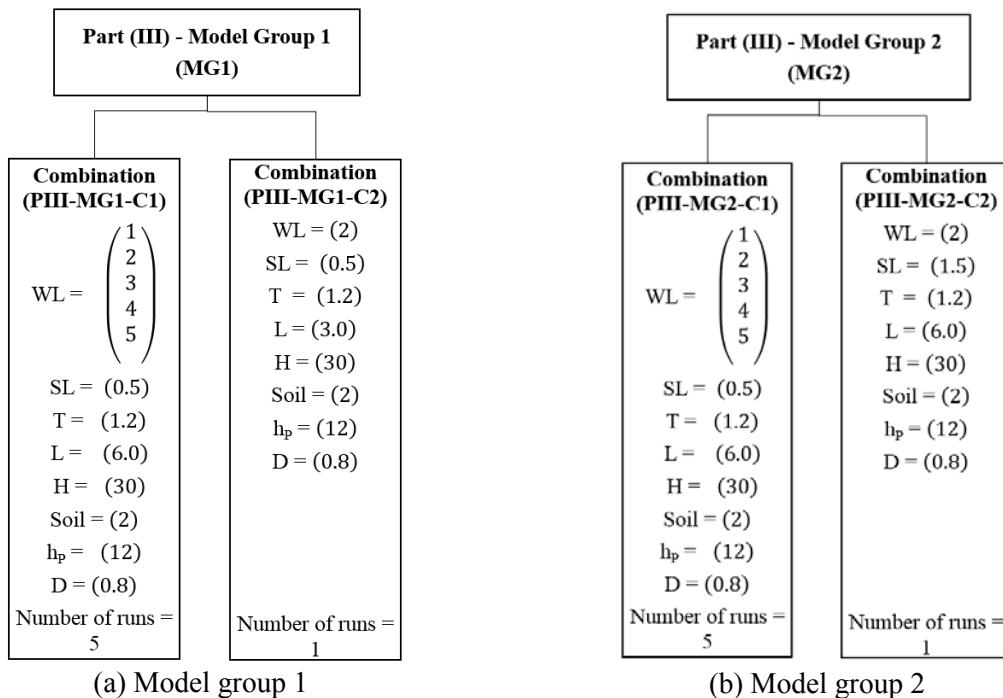


Figure 5-10: Parameters combination of Part III

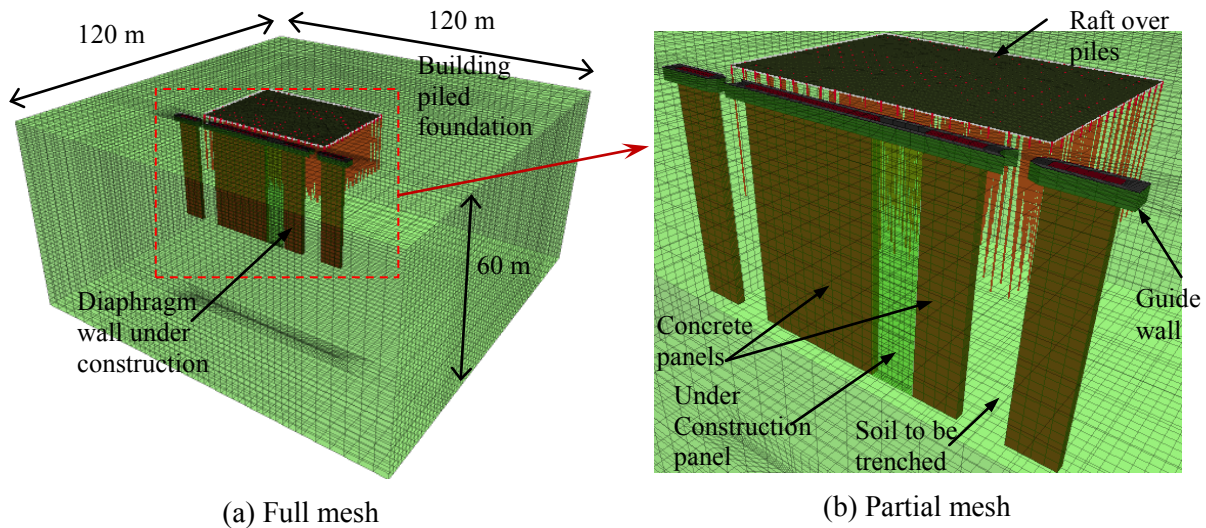


Figure 5-11: Typical mesh geometry of Part III model groups

### 5.3.3.3 Mesh model of Part III

The zones size and number of the modeled mesh are exactly similar to that of the mesh model in Part II. One shell element was used to simulate the raft. This element was divided into 2399 sub-elements. The load of the building was distributed on the shell element. The piles transfer the load from the shell element to the soil through the friction and end bearing. The load transfer process from the pile to the soil elements (zones) was described in the previous chapter. The typical mesh geometry is shown in Figure 5-11.

## 5.4 RESULTS AND DISCUSSION

The results of the parametric study concern the pile behavior during the slurry trenching just before concreting in case of a single panel but in the case of the double or multiple panels the concreting process is conducted as a part of the wall construction stages. The presented pile behavior is characterized by its deflection, bending moment and shaft friction. The following subsections show the results of each part separately, while the last section gives an overview of all the results from the parts.

### 5.4.1 PART I- RESULTS

This part contains 274 model runs. It discusses a wide variety of parameters. The results of the parameters combination are presented herein and the separate effect of each of them is presented in the following subsections.

#### 5.4.1.1 Trench dimension (PI-MG1-C1 and C2)

The influence of the trench dimension that includes trench depth (H), length (L) and thickness (T) on a piled foundation is presented based on parameter combination (PI-MG1-C1). The first

pile in the model group was chosen to show the deflection and bending moment differences due to the assumed values of trench depths (H) and such results are presented in Figures 5-12 and B-1 for pile offset distances  $x = 2.0$  m and  $x = 3.5$  m, respectively. The shaft friction is presented for both offsite distances in Figure 5-13. Two values of water level (WL) were assumed in order to show the behavior of pile under several conditions.

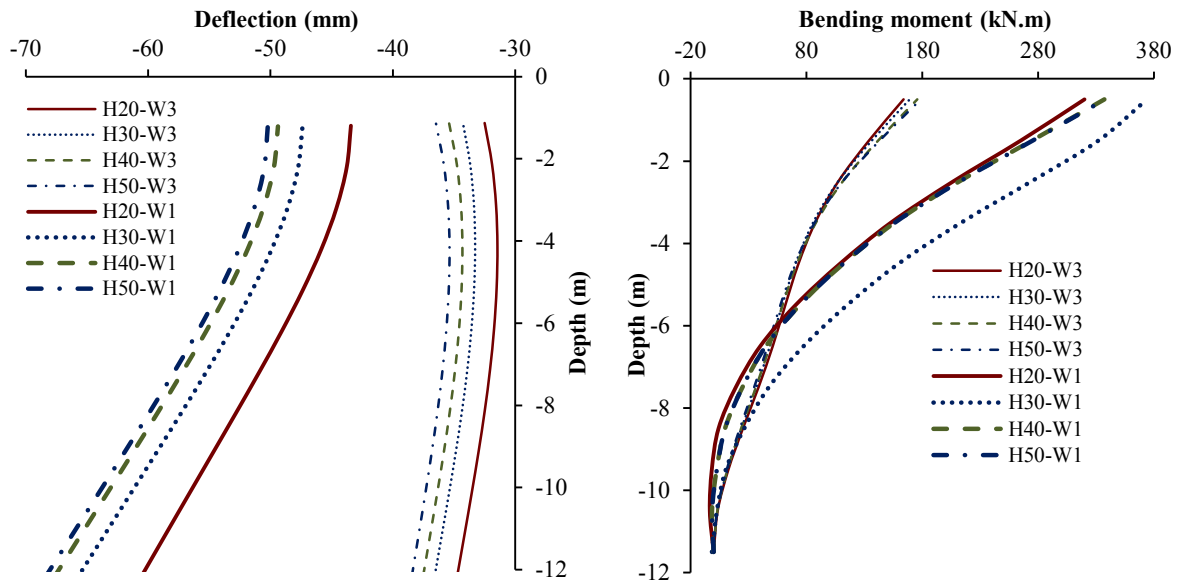


Figure 5-12: Pile deflection and bending moment for parameter combination (PI-MG1-C1) at pile offset distance ( $x$ ) = 2.0 m

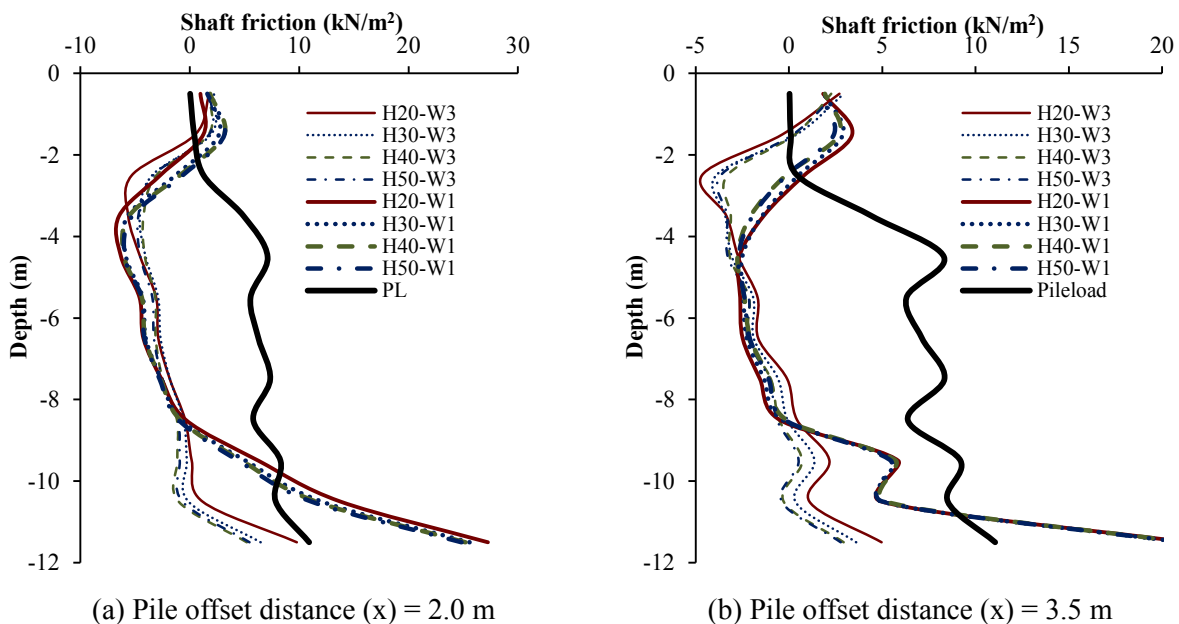


Figure 5-13: Pile shaft friction for parameter combination (PI-MG1-C1)

The effect of trench length (L) and thickness (T) on pile deflection and bending moment at different pile offset distances is presented in Figure 5-14 and Figure B-2, while their effect on shaft friction is presented in Figure 5-15. The other parameters were remaining constant as described by parameter combination (PI-MG1-C2).

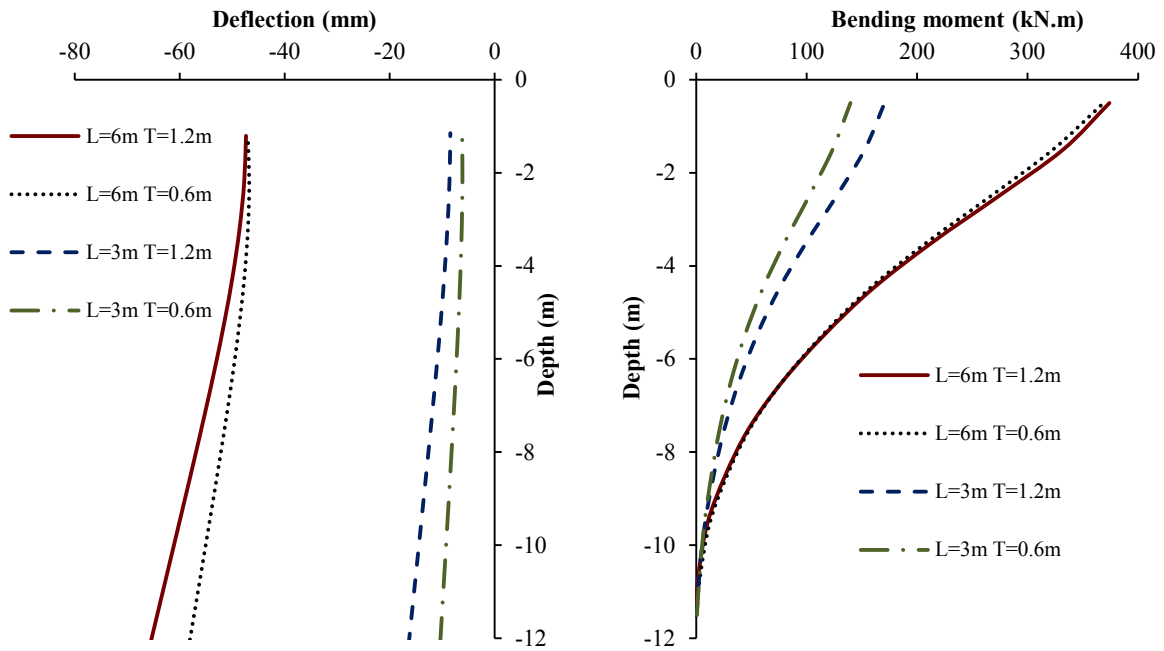


Figure 5-14: Pile deflection and bending moment for parameter combination (PI-MG1-C2) at pile offset distance ( $x$ ) = 2.0 m

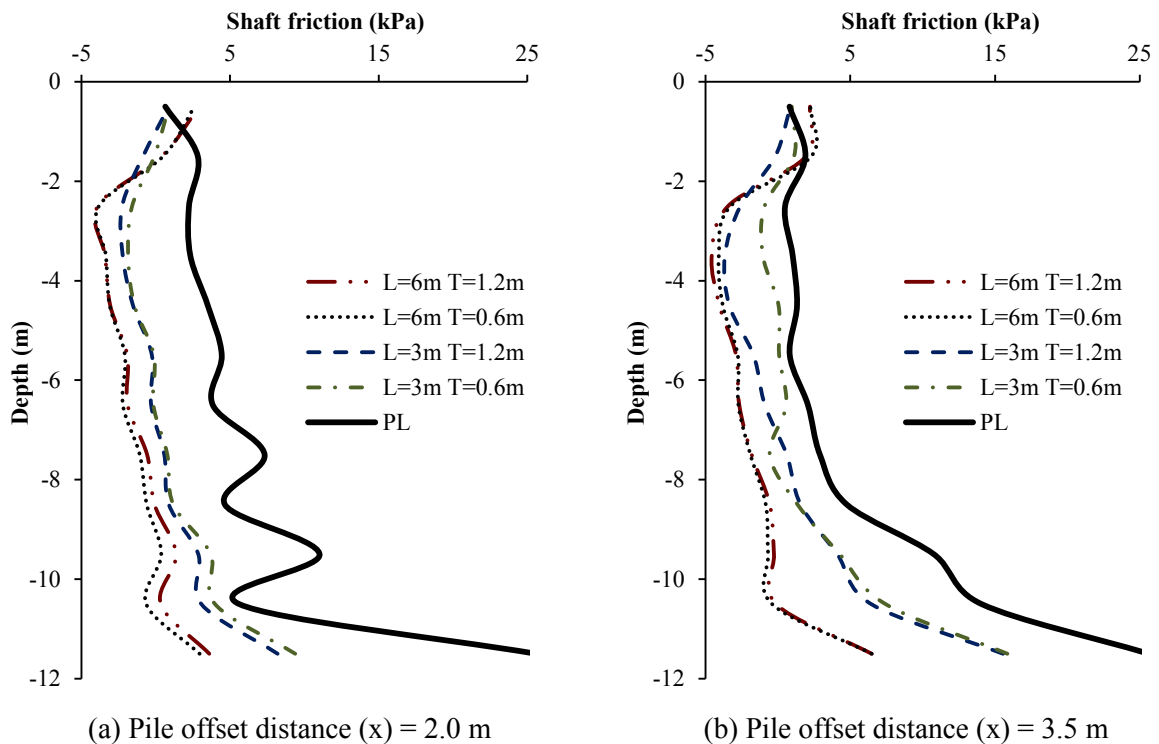


Figure 5-15: Pile shaft friction for parameter combination (PI-MG1-C2)

The deflection of the pile in all conditions increases by an average value of 8 % when the trench depth increased from 20 m to 30 m. However, this increase was low when the trench was deeper than 30 m. The deflection increased less than 3% when the trench depth increased between 40 and 50 m. The bending moment did not show any change with different values of trench depth at groundwater level ( $WL = 3.0$  m), while it showed relatively higher positive

values at a trench depth ( $H = 30$  m) when the groundwater level (WL) was 1.0 m below ground surface. The increase of trench depth causes a limited decrease for the shaft friction values. Generally, the effect of trench depth on the pile general behavior is limited if the trench depth was lower than 30 m.

The effect of trench thickness and length was studied at a trench depth of 30 m and groundwater level (WL = 2.0m). The increase in trench thickness from 0.6 m to 1.2 m causes the deflection of the pile to increase in a wide range between 0.1 % and 30 %. However, this increase in deflection values is considered to be very low compared to the deflection due to the difference in trench length. The increase of deflection due to increase of trench length from 3 m to 6 m was greater than 300 % and it even reaches 650 %. Similarly, the increase of panel thickness causes a slight increase in the bending moment values. The bending moment difference between the 0.6 m and 1.2 m thick panels for a trench length ( $L = 6.0$  m) was less than 2 % while for the trench length ( $L=3.0$  m) it reaches an increase of 40 %. The increase of trench length from 3.0 m to 6.0 m causes the pile bending moment to increase between 120 % and 260 %. The shaft friction values were not almost effected by the trench thickness, but they were reduced to an average value of 80 % with the increase of trench length values.

The general conclusion showed that the pile behavior is greatly affected by the trench length. However, it was not greatly affected by its depth or thickness.

#### **5.4.1.2 Pile group location and the pile position within the group (PI-MG1-C3)**

The individual pile within the pile group is affected during trenching in relation to its position within the pile group and the distance between the pile group and the trench ( $x$ ). Figure 5-16 shows the different values of pile deflection and bending moment within the pile group at  $x = 3.5$  m, while pile shaft friction is presented for the same group in Figure 5-17. The pile groups at  $x = 2.0, 5.5$  and  $7.5$  m are presented in Figures B-3 and B-4 in Appendix B. The first pile (P1) deflection, bending moment and shaft friction at four different locations from the trench (distance:  $x$ ) are presented in Figures 5-18, B-5 and 5-19.

As presented in Figures 5-16 and B-3, in all cases the first pile P1 which is the nearest to the trench and located on its centerline showed the highest deflection than the other piles. The deflection of the pile P2 was greater than that of pile P4 at the pile tip but it was less at the top because the deflection of the pile P2 was directly affected by the soil displacement near the trench, and this soil displacement is mainly high in the lower part of the trench. The pulling out of pile P1 effected the deflection of the pile P4. The deflection of pile P3 was the lowest because it is located in the corner and it is affected mainly by the pulling force of pile P2. Generally, the piles near the trench (i.e. P1 and P2) show a higher deflection in their tip than at the top while the other two piles showed a higher deflection at the top. This makes the

difference between the deflection values of the piles at the top to be less than 12 % while it reaches 50 % at the bottom of the piles.

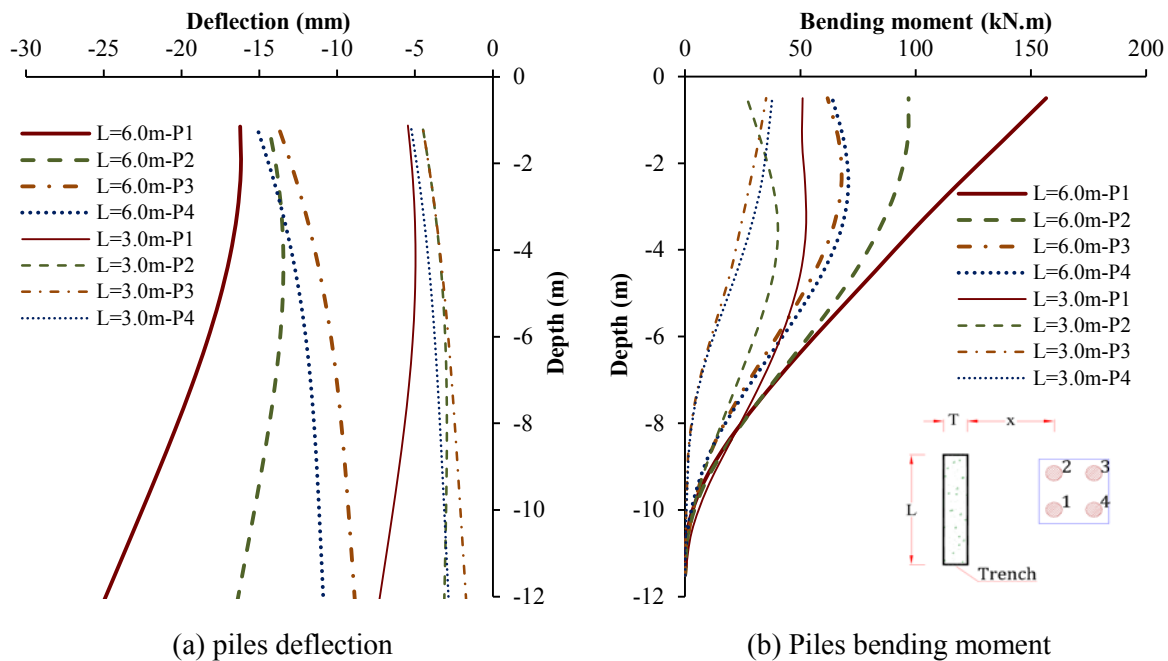


Figure 5-16: Piles deflection and bending moment for parameter combination (PI-MG1-C3) at  $x = 3.5$  m (in the same pile group)

In general, the increase of bending moment of the front piles (P1 and P2) was greater than that of the back piles (P3 and P4) and the trench length affects the bending moment difference. On average, the bending moment of pile P1 was 60 % greater than that of pile P2 in case of 6 m trench length but it was only 36 % greater in the case of 3 m trench length. The difference in bending moment values between piles P3 and P4 was less than 5 % in both cases. The bending moment value of pile P2 was about 50 % higher than that of P3 and P4 in case of 6 m panel length but it was less than 3 % in case of 3 m panel length.

The shaft friction of all the piles before trenching was coincident and plotted as PL (i.e. pile load stage). The shaft friction decreased due to trenching at the upper part of the pile and increased again with depth because each individual pile is intended to carry the same load during trenching. The pile group is formed from connected piles that tries to balance the effect of trenching by rearranging the pile load on different piles within the group. Accordingly, the reduction of the shaft friction of the piles near the trench is balanced by a relative increase of the two piles far from it. Accordingly, it can be seen in Figure 5-17 (a) that the shaft friction decreased for piles P1 and P2, while it relatively increased for piles P3 and P4. However, that was not the case for the trench with a panel length of 3.0 m as there was a reduction for all the piles in this case. The shaft friction of the lower part of the front piles that is near a 3.0 m panel length increased to balance the decrease of the shaft friction of the upper part as shown in Figure 5-17(b).

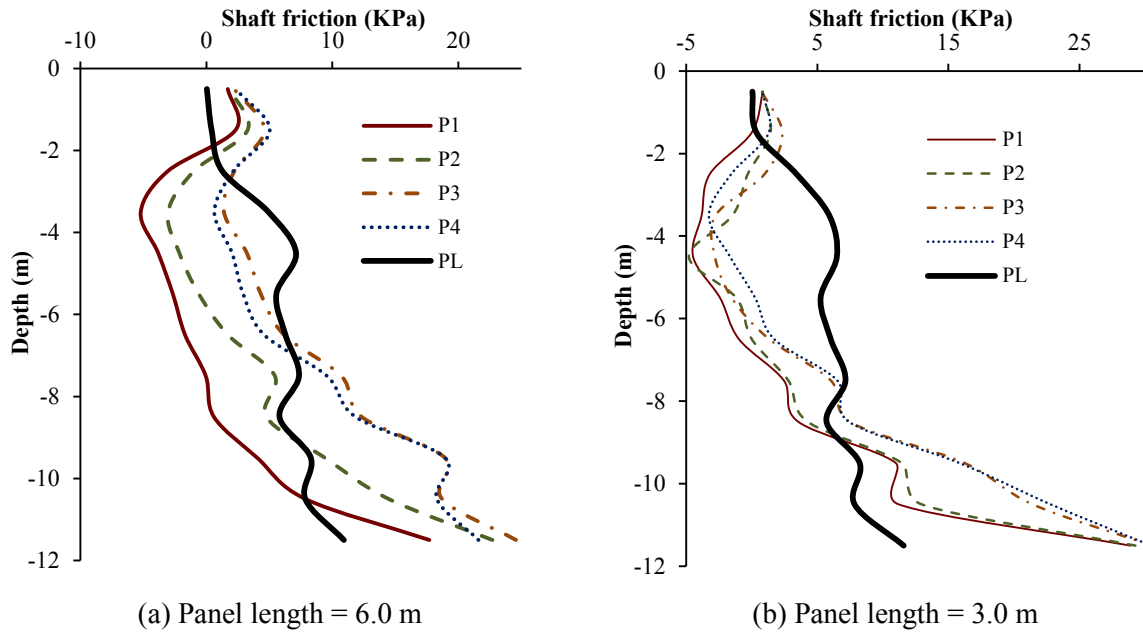


Figure 5-17: Pile shaft friction for parameter combination (PI-MG1-C3) at  $x = 3.5$  m

The deflection of the individual pile within the group is affected by the location of the pile group from the trench. Figure 5-18 shows that the pile deflection increased greatly when the pile located in a closer distance from the trench. The shape of the deflection was also influenced by the pile distance from the trench. The pile at a distance  $x = 2.0$  and  $3.5$  m moves from its tip greater than the top while the opposite was found for the other two studied distances. The differences between the deflection values at the top were lower than those at the piles tip. Such differences did not exceed 20 % at the top of the pile while they were 50 % on average at the pile tip.

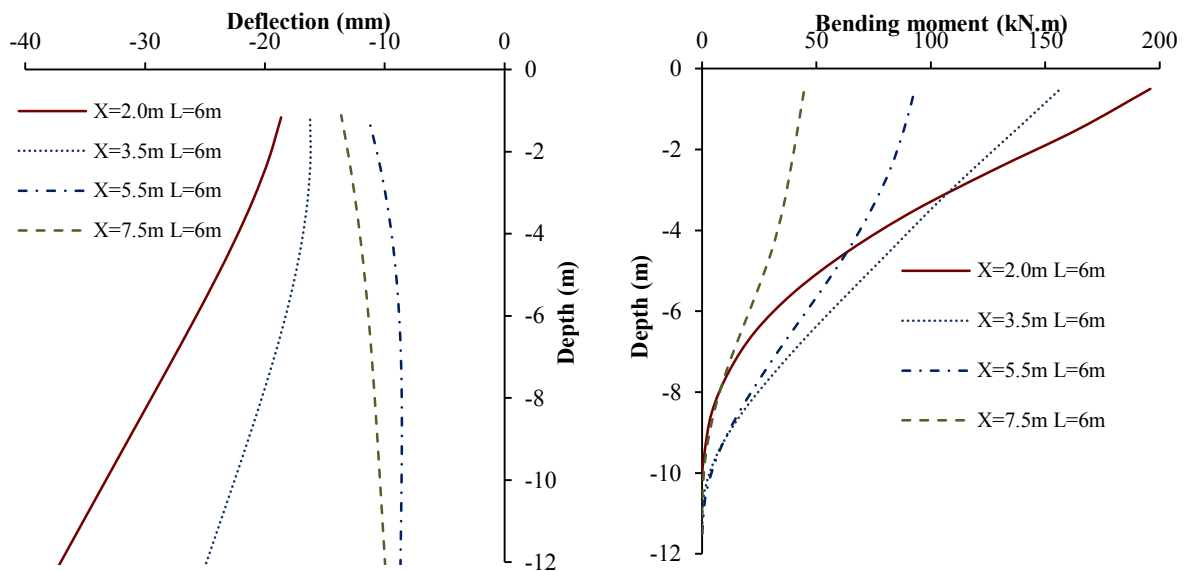


Figure 5-18: Pile deflection and bending moment at different offsite distances for parameter combination (PI-MG1-C3) for Panel length ( $L = 6.0$  m) and Pile (P1)

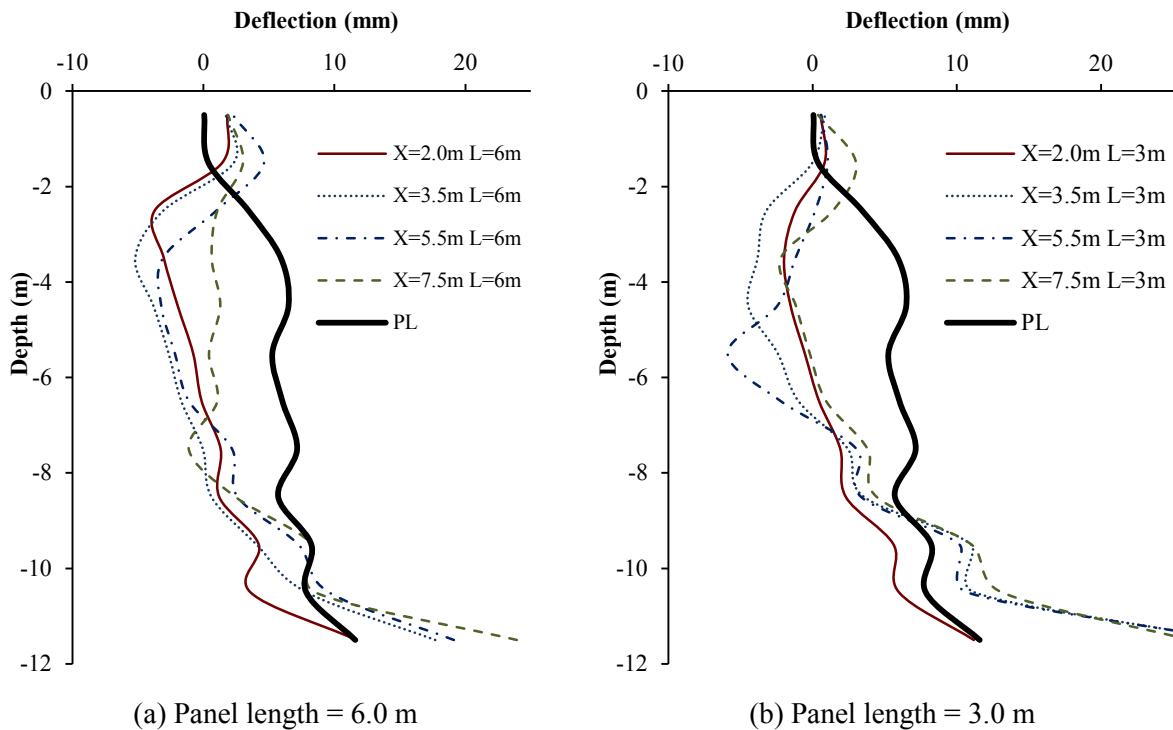


Figure 5-19: Pile shaft friction for parameter combination (PI-MG1-C3)

The bending moment was higher for the pile groups near to the trench. The bending moment at the pile tip was zero in all cases and it shows the higher value at the top where it is considered to be fixed. The value of bending moment at  $x = 3.5$  m was about 25 % lower than that at  $x = 2.0$  m and it was about 60 % higher than that at  $x = 5.5$  m. The values of bending moment decreased more than 100 % when the pile group was at distance  $x = 7.5$  m compared to the pile group at  $x = 5.5$  m.

The shaft friction was decreasing with trenches at all the values of  $x$  but it increased again near the pile tip except for the pile at  $x = 2.0$  m. This indicates that this pile was not able to balance the shaft friction and its bearing capacity could be possibly reduced.

#### 5.4.1.3 Groundwater level (PI-MG1-C4)

In the engineering projects, the groundwater level is an important parameter that should be taken into consideration in the initial design and during construction. The effect of groundwater level on the stability of the slurry trench was discussed previously in Chapter 2. The rising of groundwater level could cause a collapse to the slurry trench. In order to understand the separate effect of the groundwater level on the pile behavior the other parameters were assumed to be constant. In Figures 5-20 and 5-21 several curves are plotted for the different values of groundwater level as described in the parameter combination (PI-MG1-C4).



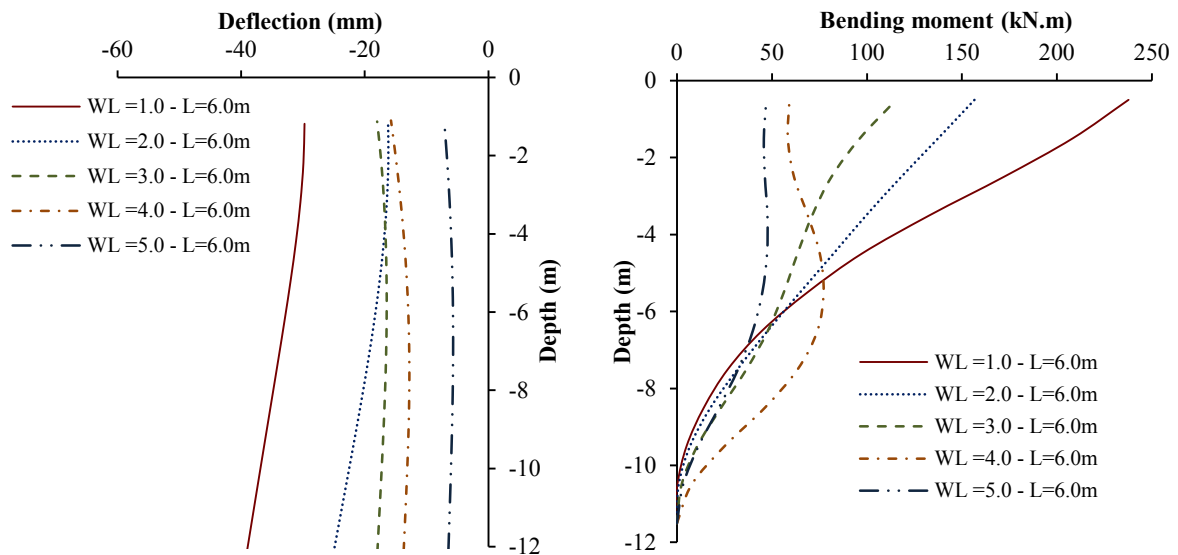


Figure 5-20: Pile deflection and bending moment at different groundwater levels for parameter combination (PI-MG1-C4)

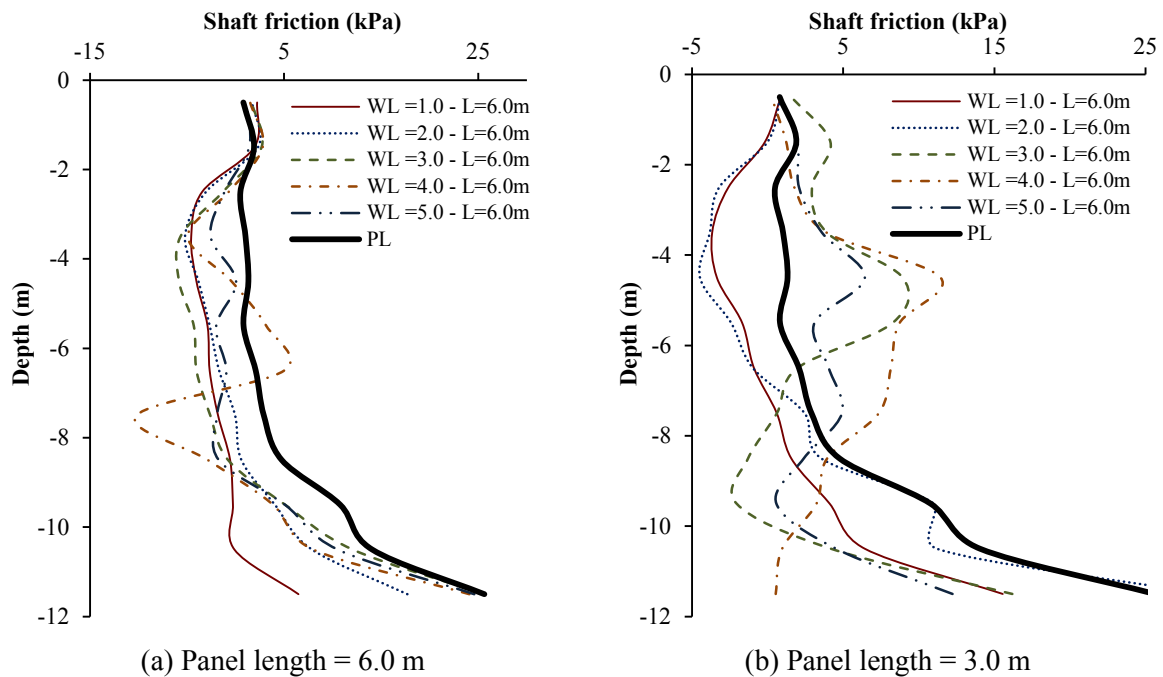


Figure 5-21: Pile shaft friction at different groundwater levels for parameter combination (PI-MG1-C4)

Generally, the shallower the groundwater level the higher the values of the pile deflection and bending moment. The average difference of the pile deflection values between the groundwater levels WL = 2.0, 3.0 and 4.0 m was 20 % but it was more than 50 % between the groundwater levels WL = 1.0 and 2.0 m. The minimum deflection value was at WL = 5.0 m and it was about half the value at WL = 4.0 m. The average increase of the pile bending moment between the different groundwater levels was 45 %. The maximum bending moment was higher at the top of the pile for the shallower groundwater levels, while it was in the middle for the deeper water levels. The shaft friction of the pile decreases with the shallower water depths.

#### 5.4.1.4 Slurry level (PI-MG1-C5)

Controlling the slurry level in the field may not always be achieved and it could be possible to have lower values of slurry level. Accordingly, a comparison between the different effects of slurry level values on pile deflection, bending moment and shaft friction was plotted in Figures 5-22, 5-23 and B-7. Such a comparison was plotted for three different slurry levels at different pile distances (x) from the trench. It was plotted for two different panel lengths.

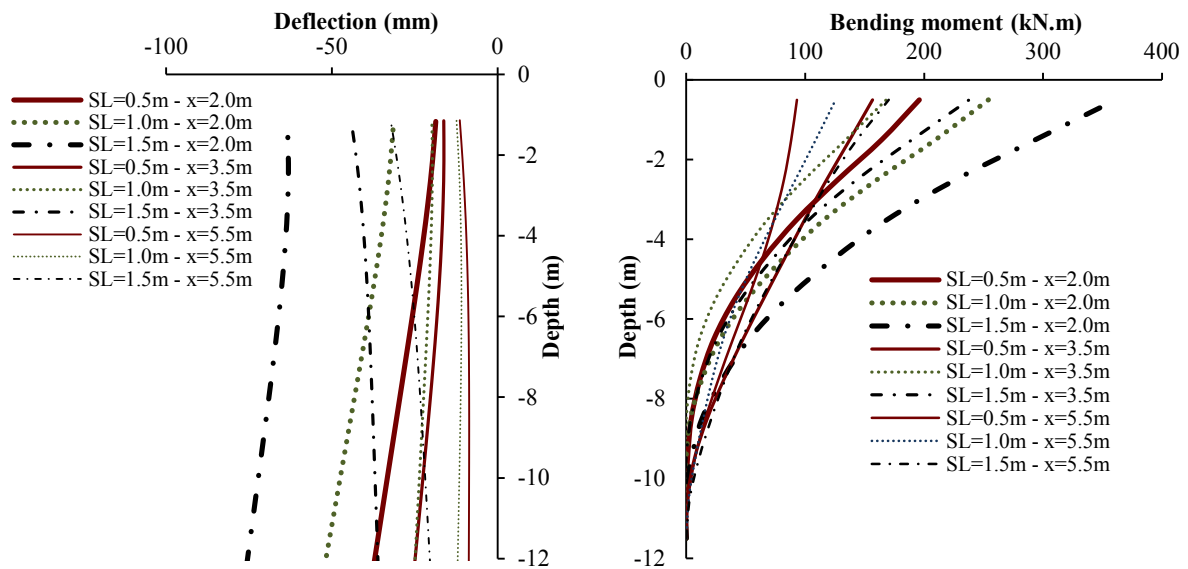
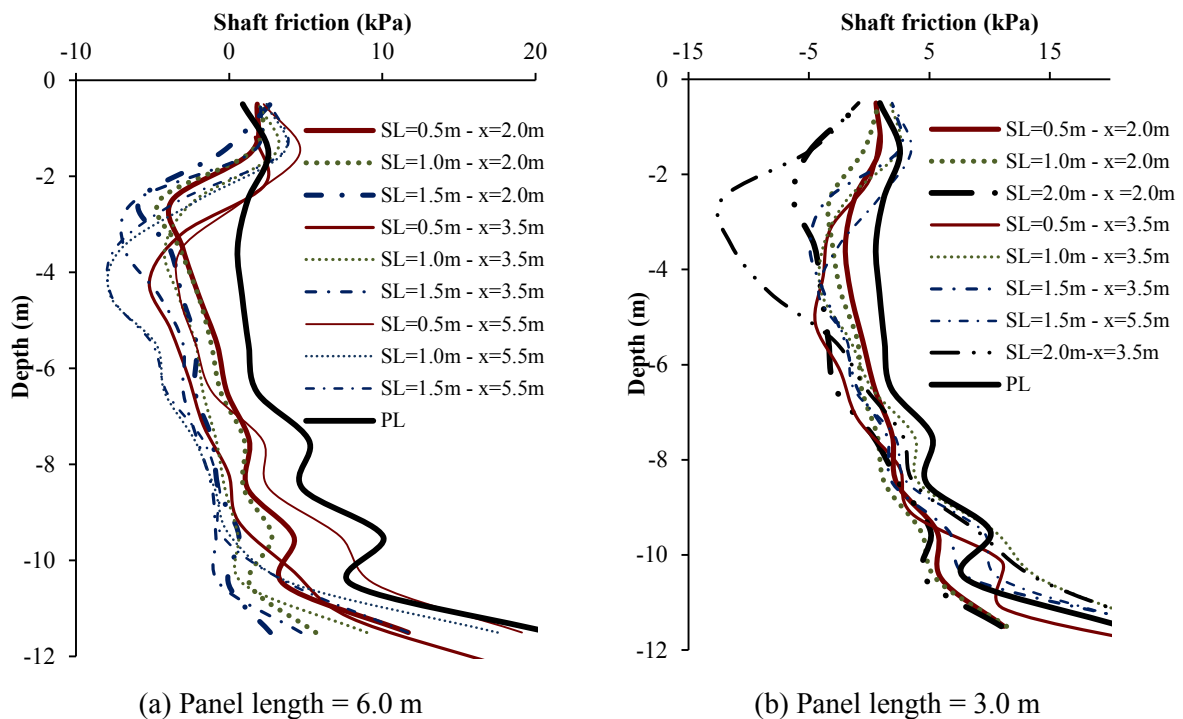


Figure 5-22: Pile deflection and bending moment at different slurry levels for parameter combination (PI-MG1-C5) for panel length = 6.0 m



(a) Panel length = 6.0 m

(b) Panel length = 3.0 m

Figure 5-23: Pile shaft friction at different slurry levels for parameter combination (PI-MG1-C5)

The comparison showed that the behavior of the pile was greatly affected at a slurry level of 1.5 and 2.0 m. The deflection of pile increased less than 50 % between the trench of slurry level of 0.5 and 1.0 m, while it increased with an average value of 80 % when the slurry decreased from 1.0 to 1.5 m and it increased with an average value over 100 % when the slurry level decreased from 1.5 to 2.0 m. The bending moment increased almost gradually with the increase of slurry level values from the ground surface. The average increase of the bending moment values was about 40 %. The shaft friction did not show a fixed ratio of change with the change of slurry level. However, the shaft friction decreased in the lower part when the slurry level is low.

#### 5.4.1.5 Soil properties (PI-MG1-C6)

The ground deformation during the trenching process is affected by the properties of the soil. Accordingly, the pile behavior is affected by it as well. The deflection and bending moment of the pile show higher values when the soil type was Soil1 while the lowest values were at Soil5 as shown in Figures 5-24 and B-7.

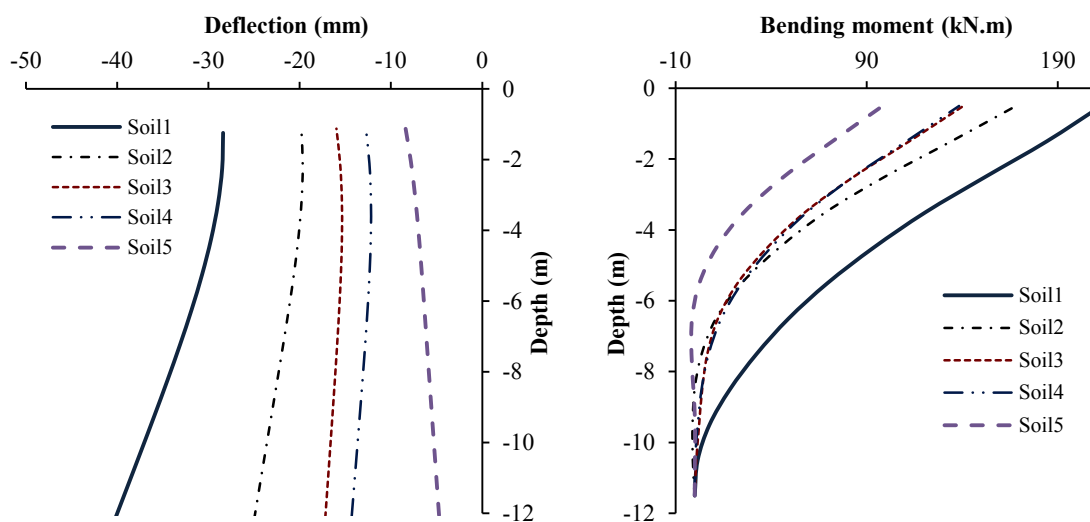


Figure 5-24: Pile deflection and bending moment at different groundwater levels for parameter combination (PI-MG1-C6) at slurry level (SL = 1.0 m)

The difference in deflection was not constant between the different soil types and it shows a wide range between 5 % and 200 % with a mathematical average for all the values of 60 %. This difference was much less regarding the bending moment which was less than 40 % with an average value of 20 %. The bending moment was less effected than pile deflection because the pile is normally moving with the soil, which means that there is no difference in forces along the pile length. In case of a slurry level of 0.5 m the shaft friction values of the pile at all soil types decreased and then increased again near the pile tip except for Soil1 it was always lower than the initial value. In general, at slurry level of 1.0 m the shaft friction was decreasing with a higher value for the denser soils than the loose ones.

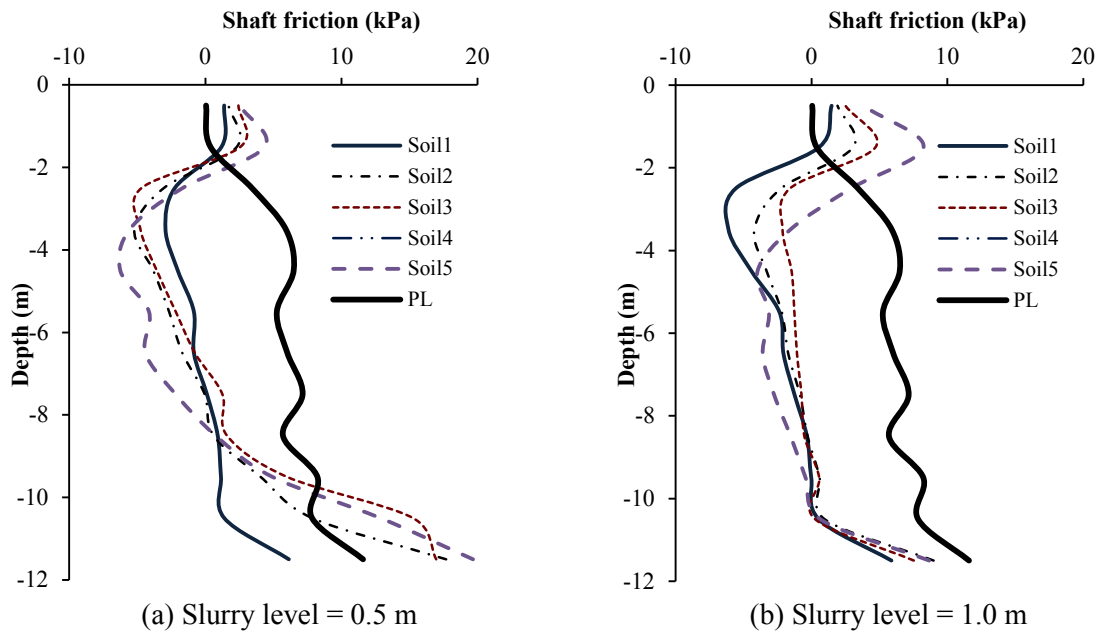


Figure 5-25: Pile shaft friction at different slurry levels for parameter combination (PI-MG1-C6)

#### 5.4.1.6 Slurry pressure reduction at some assumed levels (PI-MG1-C7)

The reduction of the slurry pressure for about 1.0 m thickness at some levels and its effect on pile deflection and bending moment is presented in Figures 5-26 and B-8. The solid line in the figures indicated the case with no slurry reduction (SP=0.0). The shaft friction is presented in Figures 5-27 and B-9. The thick solid line presents the stage of the pile loading, while the condition without any slurry reduction is presented again by a thinner solid line.

Generally, the deflection increased by reduction of slurry at any level. The increase was great when the slurry decreased near the pile tip. The average increase in deflection from the original value was 110% at slurry pressure reduction SP = 9.0 to 10.0 m and SP = 20.7 to 21.7 m, while it was 200 % as an average at the other slurry pressure reduction levels. The maximum deflection was found at SP = 11.5 to 12.5 m, where the pile tip is found at this level. The bending moment shows an increase of less than 50 % when the slurry pressure reduced at SP = 9.0 to 10.0 m and SP = 20.7 to 21.7 m, and it increased in average of 130 % at the other levels of slurry reduction. The maximum increase of bending moment values was found when the slurry was reduced at the pile tip location. The shaft friction was generally decreased by the reduction of slurry pressure at any level. However, this decrease was not influenced by the position of the slurry pressure reduction. In the middle third, the average reduction was found to be more than 300 % but it was almost zero at the top of the pile. The lower part of the pile showed different values with no constant behavior.

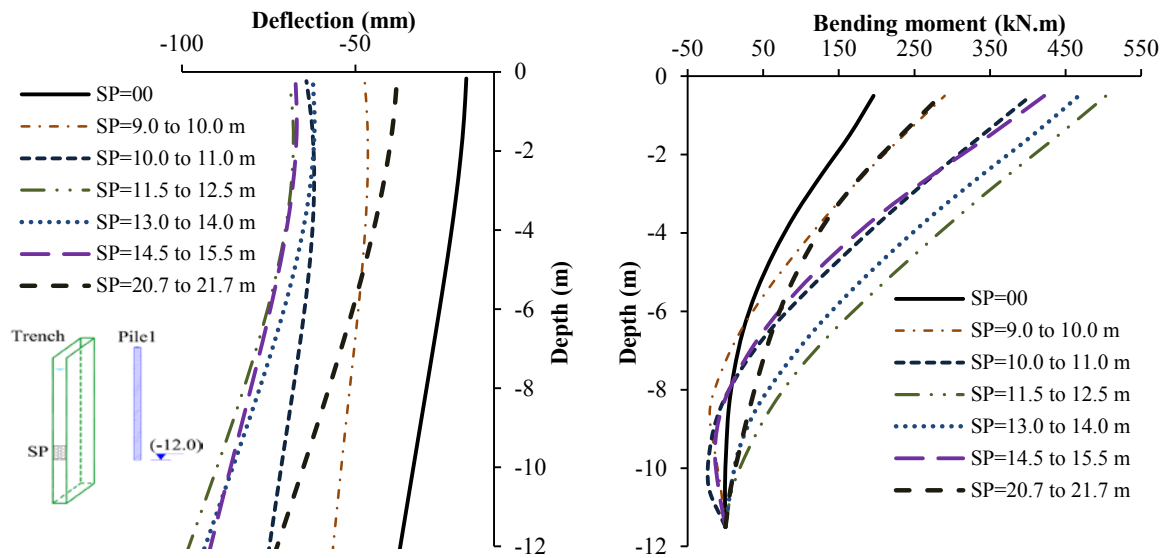


Figure 5-26: Pile deflection and bending moment at different slurry pressure reduction levels for parameter combination (PI-MG1-C7) at  $x = 2.0$  m and  $SL = 0.5$  m

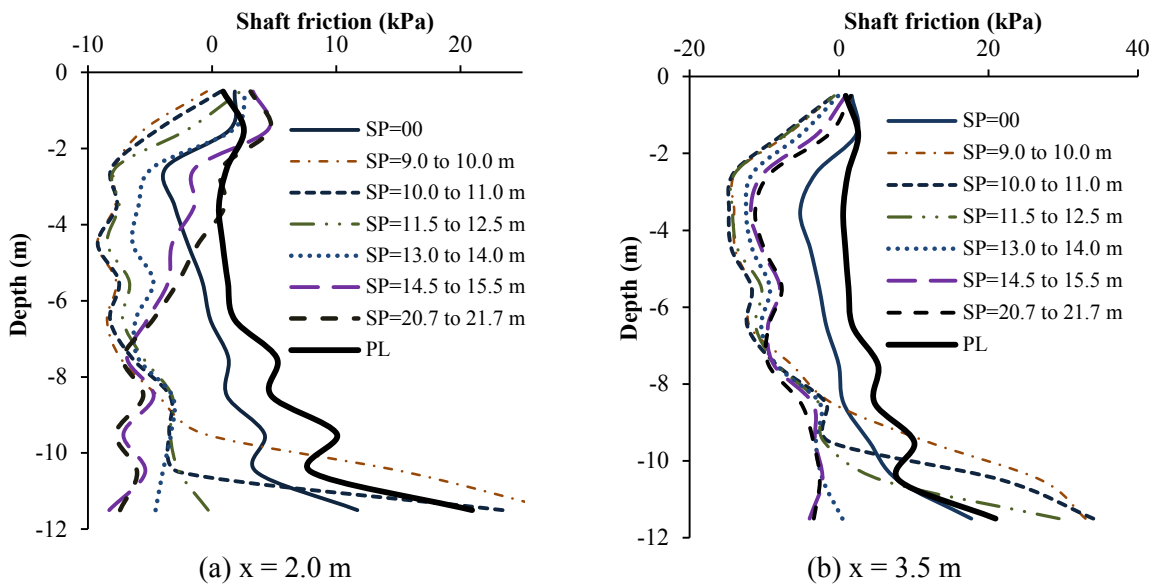


Figure 5-27: Pile shaft friction at different slurry pressure reduction levels for parameter combination (PI-MG1-C7) at  $SL = 0.5$  m

#### 5.4.1.7 Pile length (PI-MG1-C8)

The effect of the trenching process on piles with different penetration depths is presented in Figures 5-28 and 5-29 in this chapter and Figure B-7 in Appendix B. The first pile within the group was only presented in these figures. The pile penetration depth is indicated by (hp). Generally, the deflection of the pile is inversely proportional to its length. The shape of the pile deflection is also varying according to the embedded depth of the pile. If the pile tip is higher than or equal to the trench lower level it tends to move from its tip as shown in Figures 5-28 and B-10. The lower part of the pile below the trench tip is acts as a fixation to the pile and reduces its deflection.

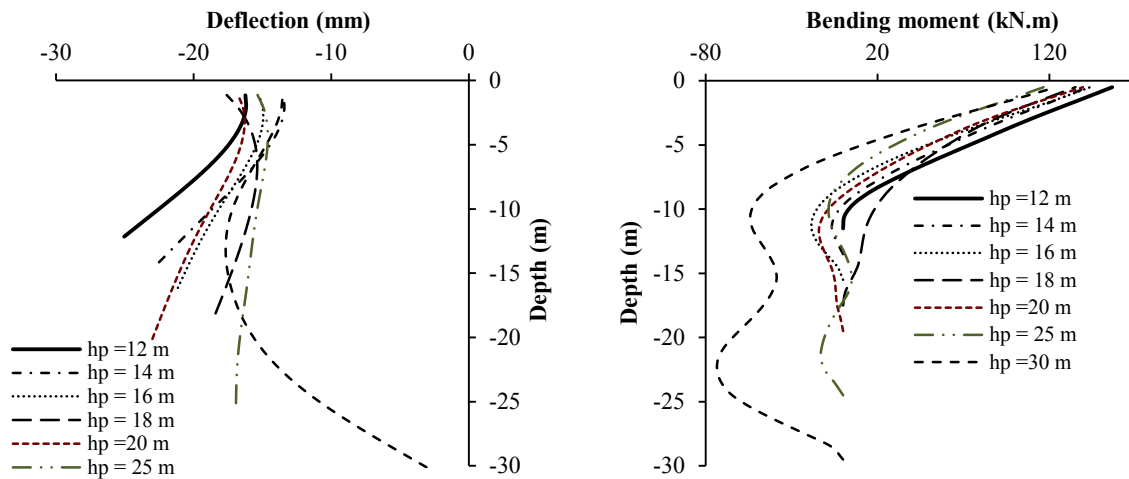


Figure 5-28: Pile deflection and bending moment at different values of pile impeded length for parameter combination (PI-MG1-C8) and trench depth (H=30m)

The positive bending moment is higher for the shorter piles while for the longer pile a negative moment appears in the lower part, because the lower part is considered to be a fixed support. The pile shaft friction tends to decrease in the middle third and increases again at the lower third. This increase in shaft friction is considered to balance the decrease.

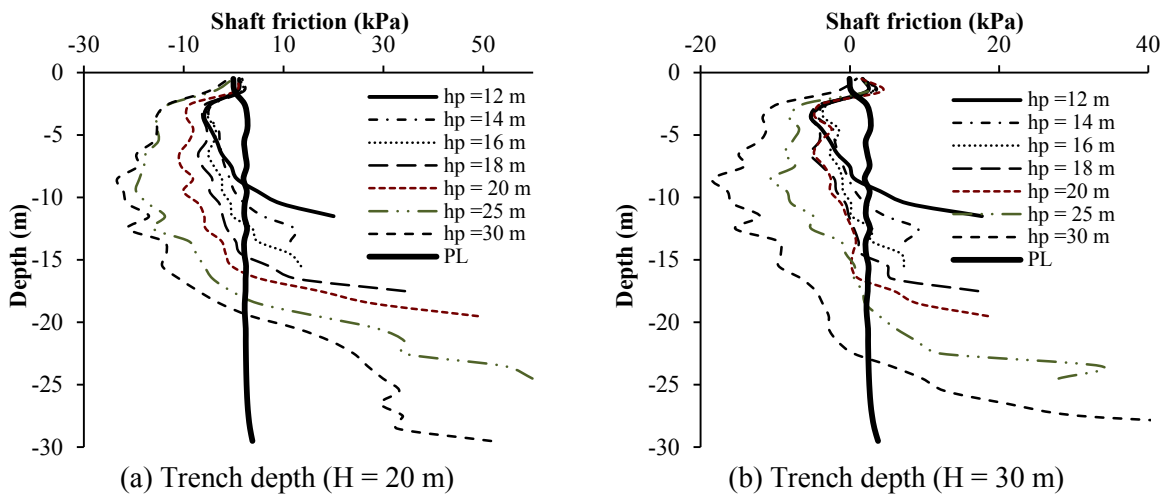


Figure 5-29: Pile shaft friction at different values of pile impeded length for parameter combination (PI-MG1-C8)

#### 5.4.1.8 Pile diameter (PI-MG1-C9)

The effect of trenching on piles with different diameters is described in Figures 5-30, 5-31 and B-11. The other parameters except of trench depth were considered to be constant as described by parameter combination PI-MG1-C9.

The highest value of deflection was at the smaller pile diameter value (i.e.  $D = 20$  cm) and the lowest deflection was at the pile with a diameter of 100 cm. The pile with the smallest diameter showed a low value of bending moment while the pile with a 120 cm diameter showed a higher value of bending moment. The difference in deflection between the largest and smallest diameter piles was about 45 % while the average difference between the other diameter piles was less than 10 %.

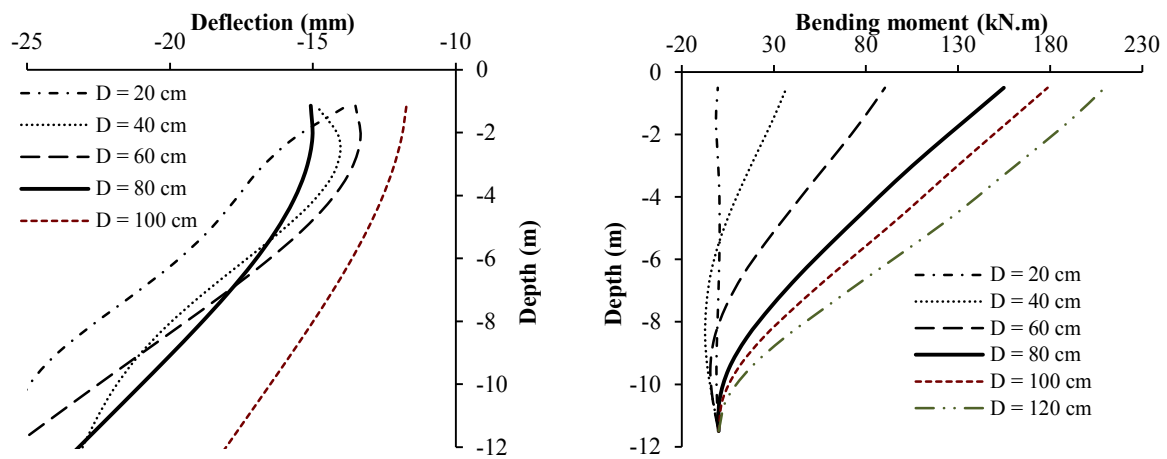


Figure 5-30: Pile deflection and bending moment at different pile diameter values (PI-MG1-C9) and at trench depth (H=30 m)

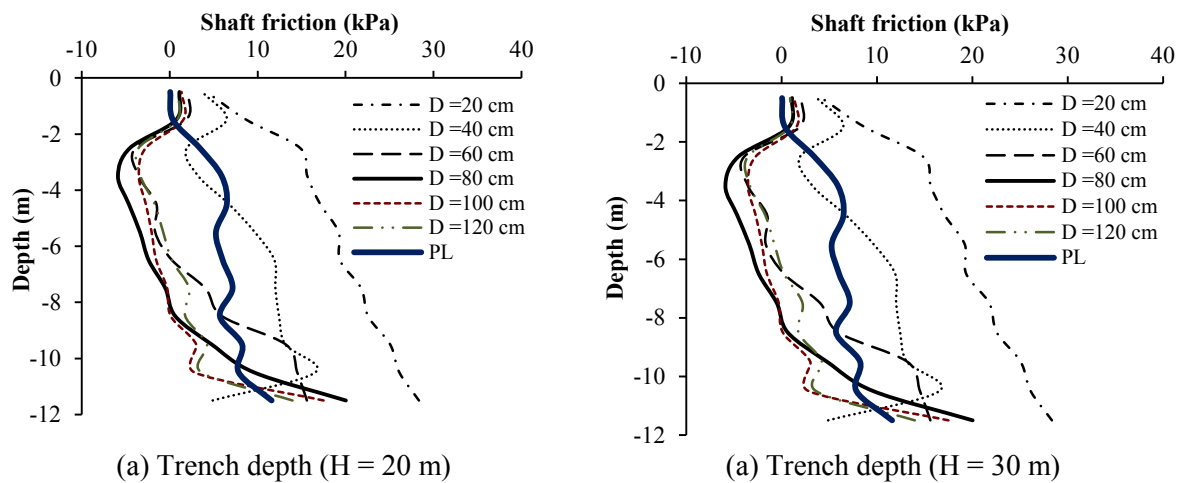


Figure 5-31: Pile shaft friction at different pile diameter values (PI-MG1-C9)

The increase of pile diameter below 80 cm causes the bending moment to increase with an average value greater than 100 %. However, this average increase was less than 20 % when the pile diameter increased above 80 cm, which indicates that the pile diameter did not play an effective role in bending moment when it is higher than 80 cm. The effect of trenching on shaft friction was found to be high on the smaller diameters (i.e. D = 20 and 40 cm). This effect was very low in case of the larger diameter piles (i.e. D > 60 cm). The small diameter piles showed higher values of shaft friction than large diameter piles because it moves with the soil and did not show a shaft friction resistance.

#### 5.4.1.9 Effect of slurry level and slurry pressure reduction on piles with different formation within model groups (MG 1, 2, 3 and 4)

Parameter combinations (PI-MG 2, 3 and 4 - C1) describe the effect of different slurry levels on piles within different pile group formations. Such an effect is presented in Figures 5-32 through 5-37 and in Appendix B from Figure B-12 through B-15.

The piles deflection and bending moment of model group MG2 are plotted together to show the behavior of each pile separately. The pile nearest to the trench in all cases showed the highest

deflection and bending moment values while the farthest showed the lowest values. The average difference between the highest and lowest deflection was greater than 100 % at the pile tip but it was less than 20 % at its top. The deflection difference between the other piles was low. The bending moment difference between the piles within the group was not great. The average difference between the piles was less than 15 %; however, the difference between the highest and lowest values was about 50 %.

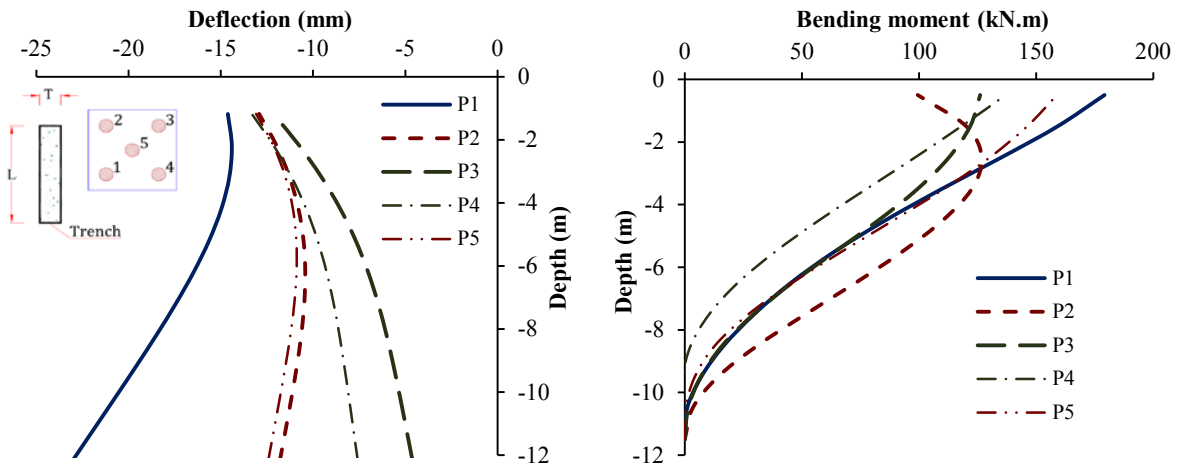


Figure 5-32: Pile deflection and bending moment of piles within model group (MG2) at slurry level (SL=0.5m)

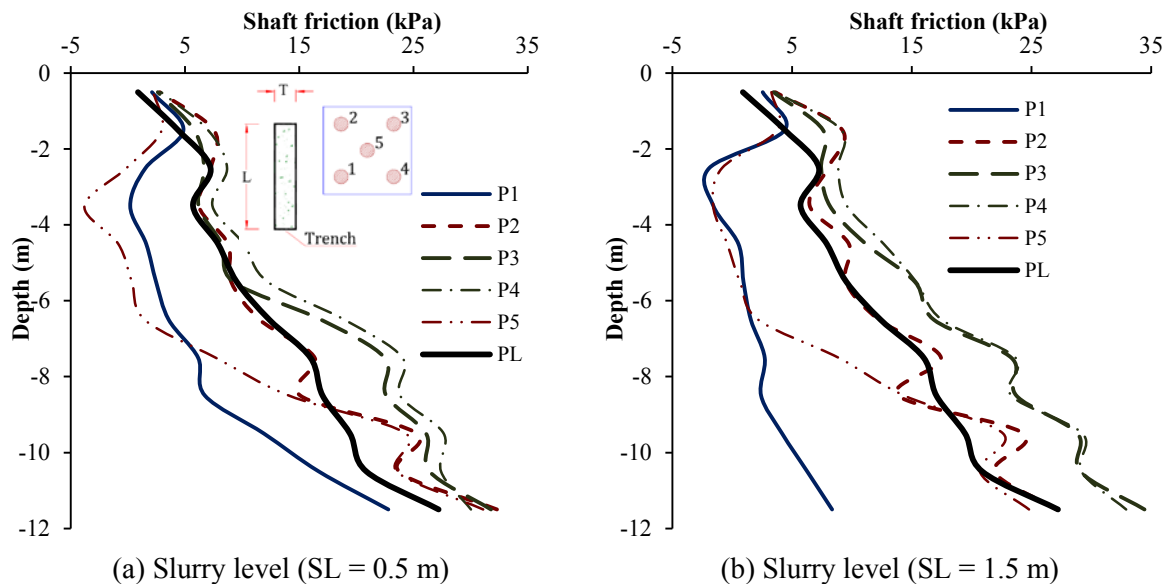


Figure 5-33: Pile shaft friction of piles within model group (MG2) at slurry level (SL = 0.5 m)

The shaft friction of the piles is plotted in Figure 5-33 showing the pile in the stage before trenching as well. The first and fifth pile showed a decrease in shaft friction while the second pile did not show any change. The rear piles (i.e. P3 and P4) showed an increase to balance the decrease of the front piles. However, the decrease was higher than the increase.

The behavior of the six piles of model group MG3 is shown in Figures 5-34, 5-35 and B-13. The piles nearest to the trench are P1, P2 and P3. The piles on the centerline of the trench are P1



and P6. The highest deflection was found for pile P1 that is located at the centerline of the trench followed by piles P2 and P6. Pile P2 showed a higher deflection from the bottom than pile P6 because it was nearest to the trench, while pile P6 was affected by the drag force of pile P1 which causes it to deflect from the top greater than pile P2. The effect of trenching on the farthest piles P3 and P4 was limited but not negligible. The average difference in deflection between the piles in their top was 20 %, while in the bottom it was 40 %, which indicates that the deflection difference in the bottom was almost double difference of the top values. The bending moment values of the piles near the trench (i.e. P1, P2 and P3) were higher than the farthest piles. The shaft friction decreased for the piles P1 and P2 while it showed an increase for the other piles.

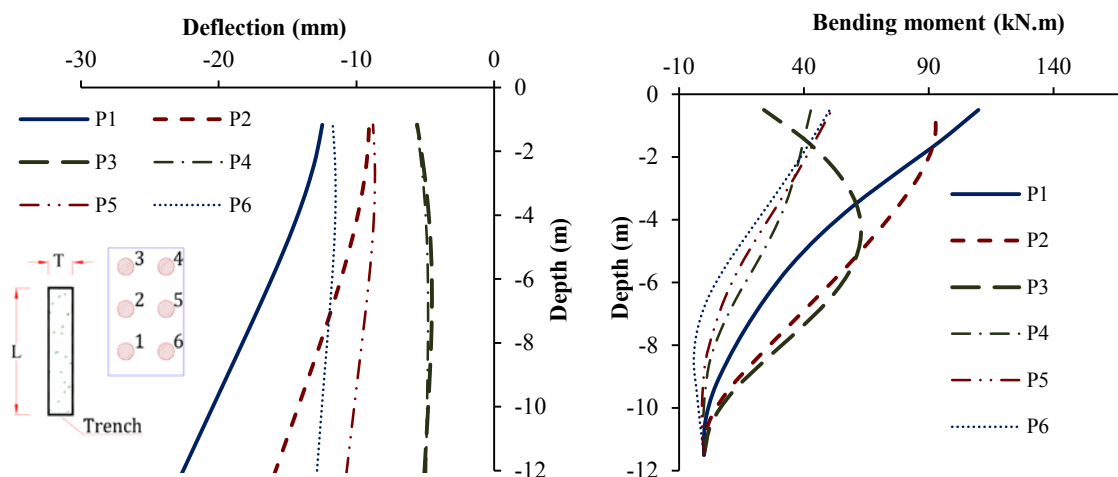


Figure 5-34: Pile deflection and bending moment within model group (MG3) at slurry level (SL = 0.5 m)

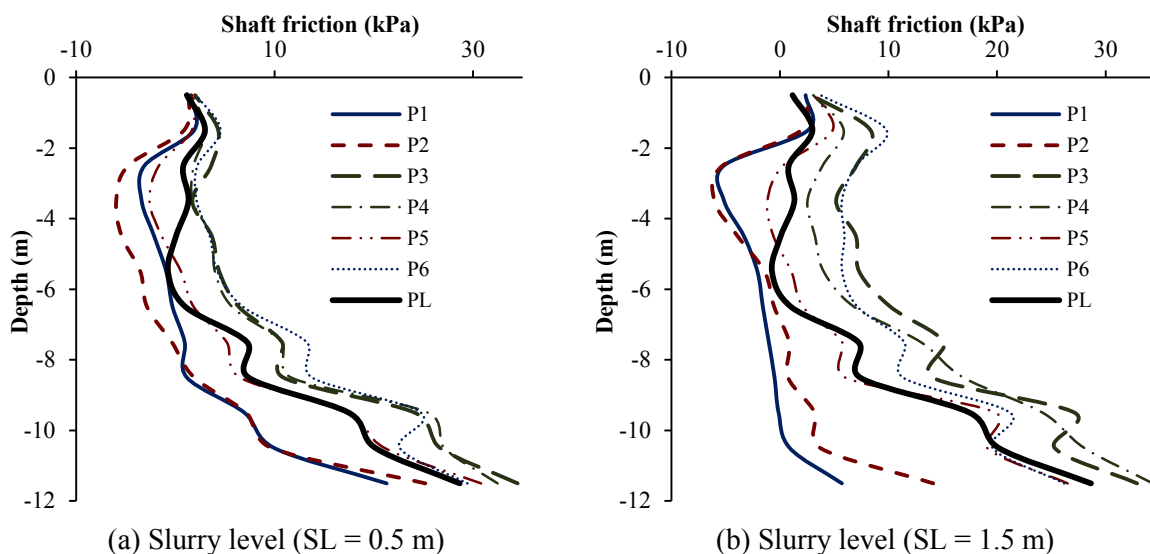


Figure 5-35: Pile shaft friction at different of piles within model group (MG3) at slurry level (SL = 0.5 m)

The piles deflection of model group MG4 is plotted in Figures 5-36 and B-14. The piles near the trench showed the highest deflection. They showed a higher movement at the top of the pile

than that at its tip. The other piles were affected by the drag forces of the front piles and were moving with higher values from the top than the tip. The average difference in deflection at the pile top was about 3 % while it was 40 % at its tip. The bending moment was almost the same for all the piles except for pile P1 which showed a relatively higher value. The difference in bending moment between pile P1 and P2 was 35 % while the average difference between the other piles was about 10 %.

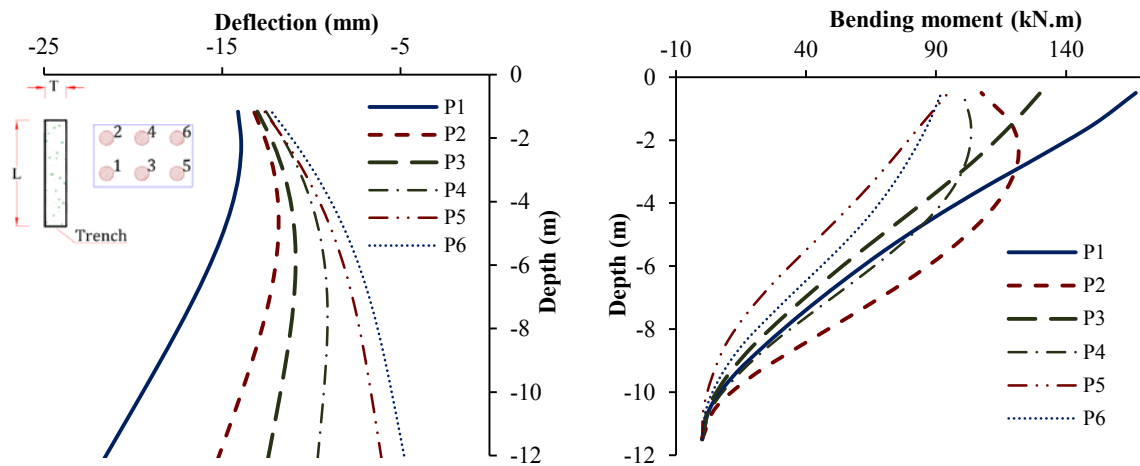


Figure 5-36: Pile deflection and bending moment of piles within model group (MG4) at slurry level (SL=0.5m)

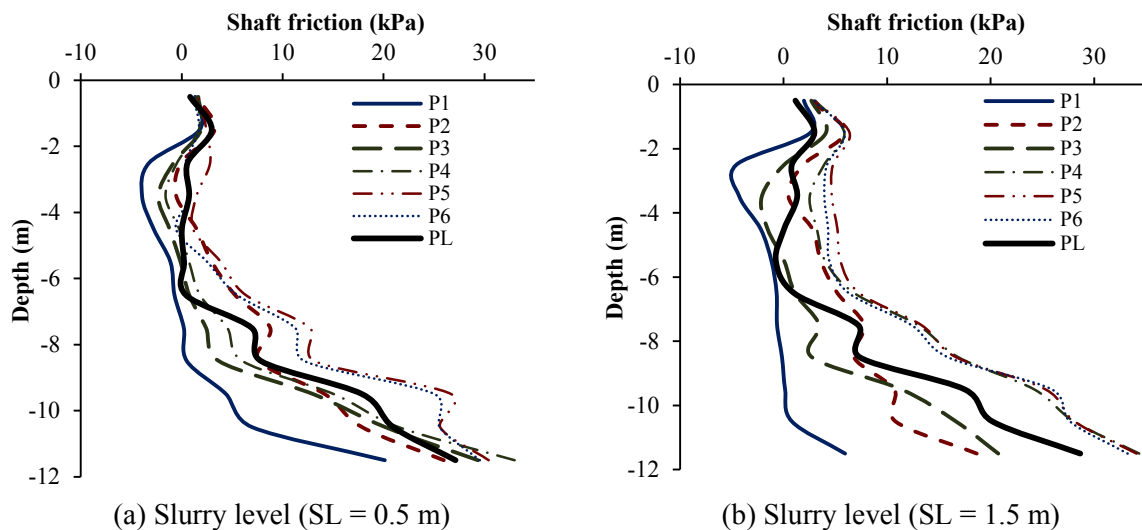


Figure 5-37: Shaft friction of piles within model group (MG4) at slurry level (SL = 0.5 m)

In order to understand the effect of different pile formation within the group, the deflection and bending moment of some piles within each pile group formation were plotted in Figures 5-38 and B-15, while the shaft friction was plotted in Figure 5-39. The piles nearest to the trench (P1) in each group were chosen for the comparison as well as the farthest piles.

The highest deflection was found for the first pile in model group MG1 because they were only four piles. The first pile in model group MG2 showed the second highest deflection values. The first pile in the other model group was almost the same. However, the pile P6 of model group

MG4 showed higher movement than the corresponding pile in model group MG3 because the piles in model group MG4 moved almost together, while in the model group MG3 there was a big difference between the deflection of the piles within the group as previously presented in Figure 5-34.

The bending moment showed the same trend of deflection but the first pile in the model group MG3 showed a low value compared to the first pile in the other model groups. The difference between bending moment values of the first pile within the model groups was very low but model group MG3 showed a relatively high difference of about 40 %.

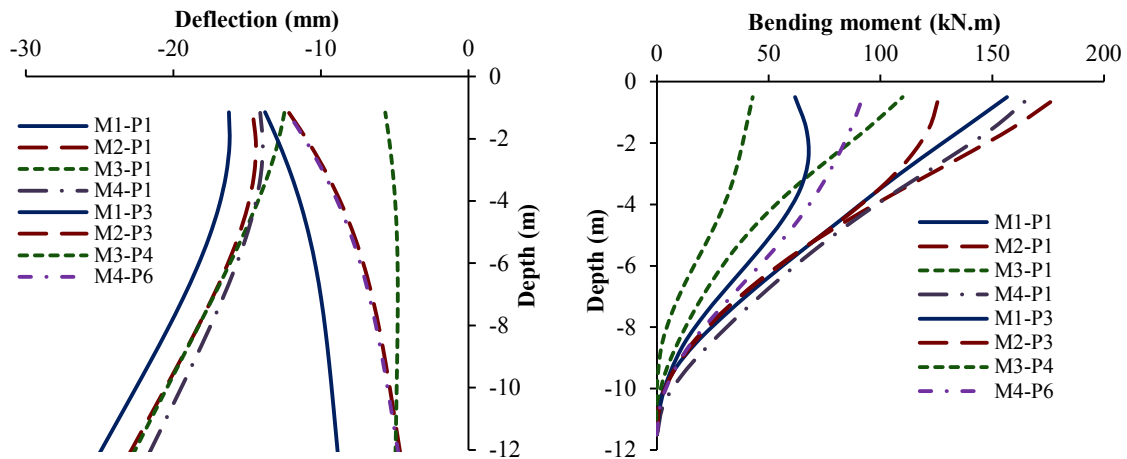


Figure 5-38: Pile deflection and bending moment at different formations

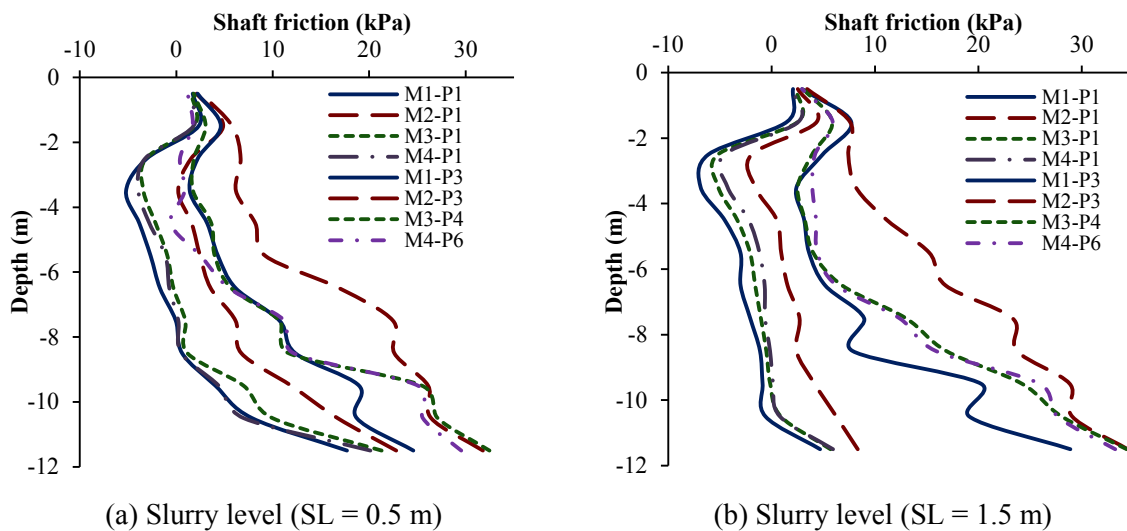


Figure 5-39: Shaft friction of piles at different formations

The shaft friction showed a decrease for the first pile in all models. Model group MG1 showed the greatest decrease while model group MG2 was the lowest. Generally, the difference in shaft friction values within the four model groups regarding the first pile was very low. It was also very low regarding the other piles except for the third pile in model group MG2.

The effect of reduction of the slurry pressure between levels 13.0 and 14.0 m on the piles was previously discussed in the parameter combinations (PI-MG 2, 3 and 4 – C2). The behavior of

piles due to such an effect is presented in Appendix B from Figure B-16 through Figure B-23. The pile behavior was the same as that from parameter combinations (PI-MG 2, 3 and 4-C1). The piles deflection and bending moment of parameter combination PI-MG2-C2 were presented in Figure B-16 and they showed that the difference between the piles within the model is almost the same as presented in the Figures 5-32 and B-12 except that piles P2 and P5 showed a larger difference regarding deflection. The shaft friction showed also the same trend but pile P3 showed a decrease in shaft friction as shown in Figure B-17.

The deflection, bending moment and shaft friction of model group MG3 are presented in Figures B-18 and B-19. The percentage of differences between the values of each pile is almost the same as that of parameter combination PI-MG3-C1.

The percentage of shaft friction differences of model MG4 was almost the same as that in the first combination but pile P2 showed a relatively higher trend of reduction as shown in Figure B-21. The two other parameter combinations also showed almost the same percentage of differences between piles regarding deflection and bending moment.

The comparison between the different model groups regarding slurry reduction was presented in Figures B-22 and B-23 in Appendix B. The percentage of difference between the first pile of each model group showed a very limited difference, while the other piles within the group showed a larger difference which could reach 50 %. The bending moment did not show a fixed trend of difference between the different models. The higher value was found to be for the first pile of model group MG2, while the lower value was found for rear pile of model group MG3. The shaft friction reduction of the first pile of all model groups was almost the same. However, the differences between the other piles reached about 20 %.

As a general conclusion, the number of piles within the group reduces the influence of trenching on the piles. The orientation of piles has an effect on the pile behavior as well. The pile group that contains 6 piles in a formation perpendicular to the trench shows less deflection regarding the middle piles than that parallel to the trench. However, the bending moment of the piles nearest to the trench was almost unaffected by the different piles formations, while the other piles were affected. The shaft friction of piles near the trench reduced relatively higher than the rear piles in order to balance the applied load above the pile cap.

#### **5.4.1.10 Double panel (MG 5-C1 and 2)**

The results in this section are focused on understanding the difference between the single and double panels effect on piles. The deflection, bending moment and shaft friction of the first and third piles within the pile group due to trenching of double and single panels are presented in this section from Figure 5-40 through 5-43 and in Appendix B in Figures B-24 and B-25.

The first pile P1 in all the figures is plotted with a single line while the third pile P3 was plotted with a double line. The effect of different slurry levels and slurry pressure reduction between levels 13.0 and 14.0 m are the main variables.

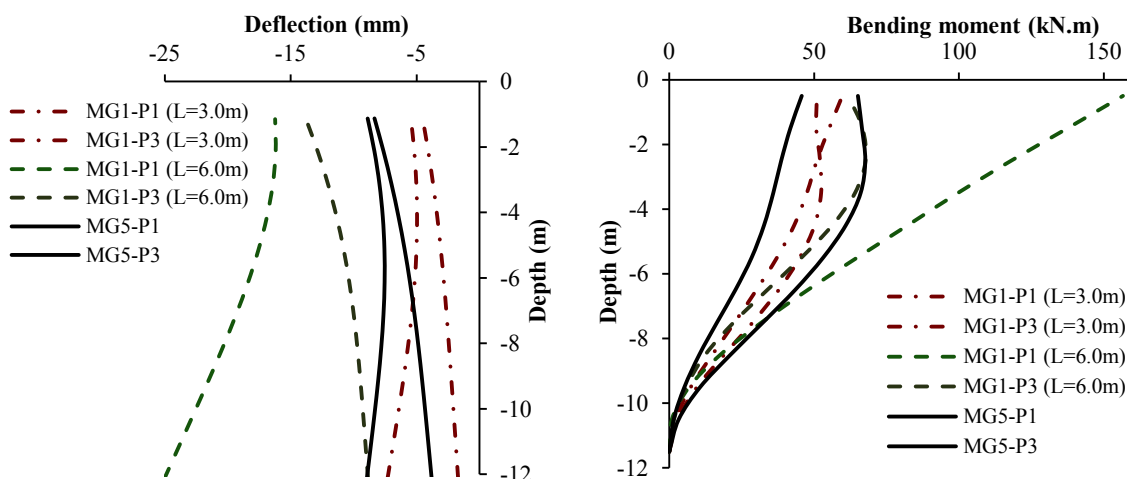


Figure 5-40: Deflection and bending moment of piles near double or single panel at slurry level (SL = 0.5 m)

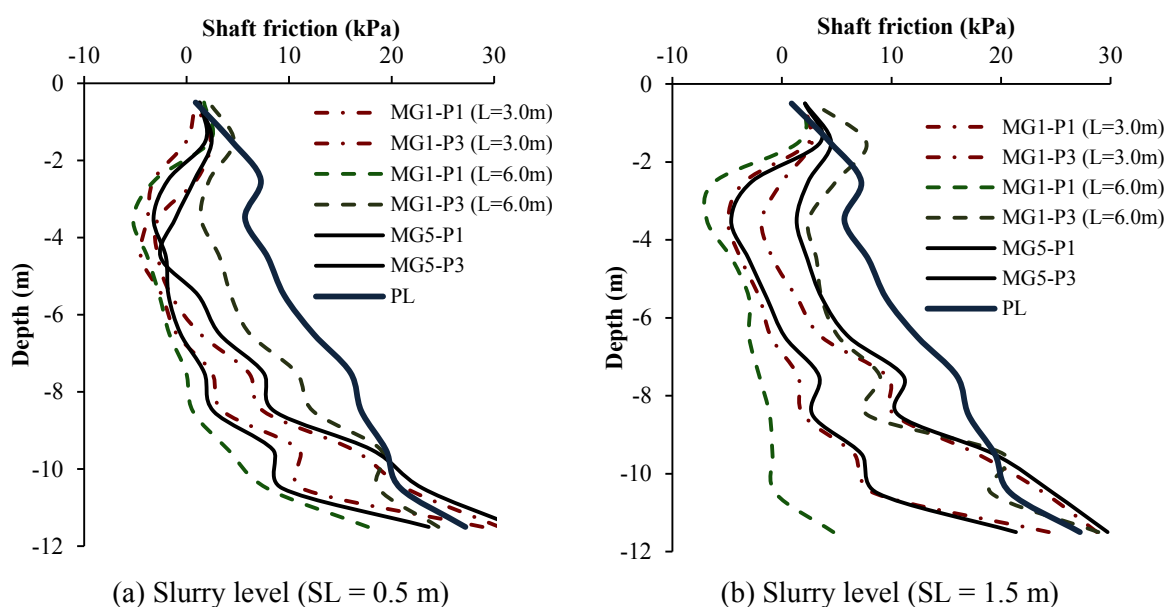


Figure 5-41: Shaft friction of piles near double or single panel

The plotted results showed that the maximum pile deflection and bending moment were found for the pile group near the 6 m long panel trench followed by the double panel. The minimum deflection and bending moment were near the trench with 3 m panel length. The average difference between the deflection of pile near the double panel and the 6 m panel was 140 % in case of a difference in slurry level and it reached 350 % in case of slurry pressure reduction. The difference of deflection between the piles near the double panel and the 3 m panel was 40 % in case of a different slurry level and it was higher in case of slurry reduction as it reaches 250 %.

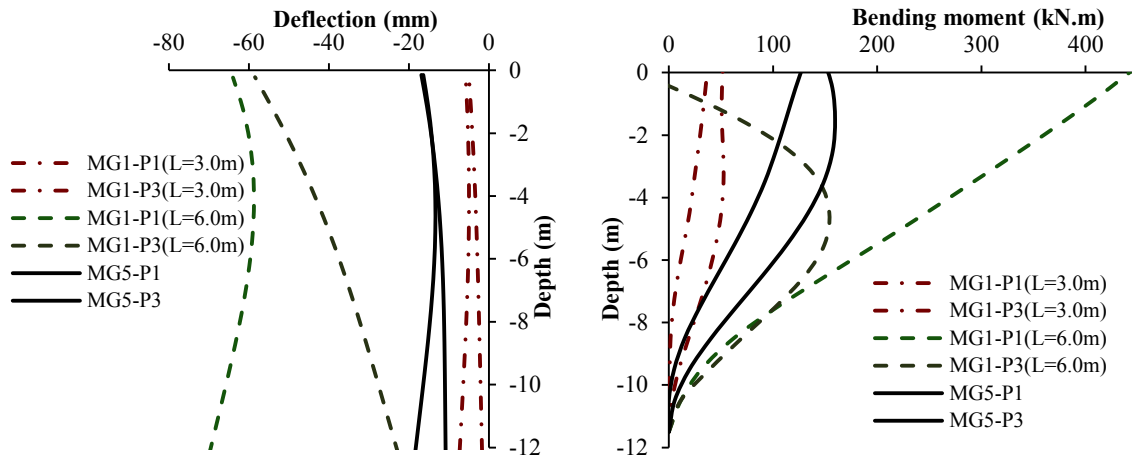


Figure 5-42: Deflection and bending moment of piles near double or single panel at slurry level (SL = 0.5 m) and at slurry reduction position (SP = 13.0 to 14.0 m)

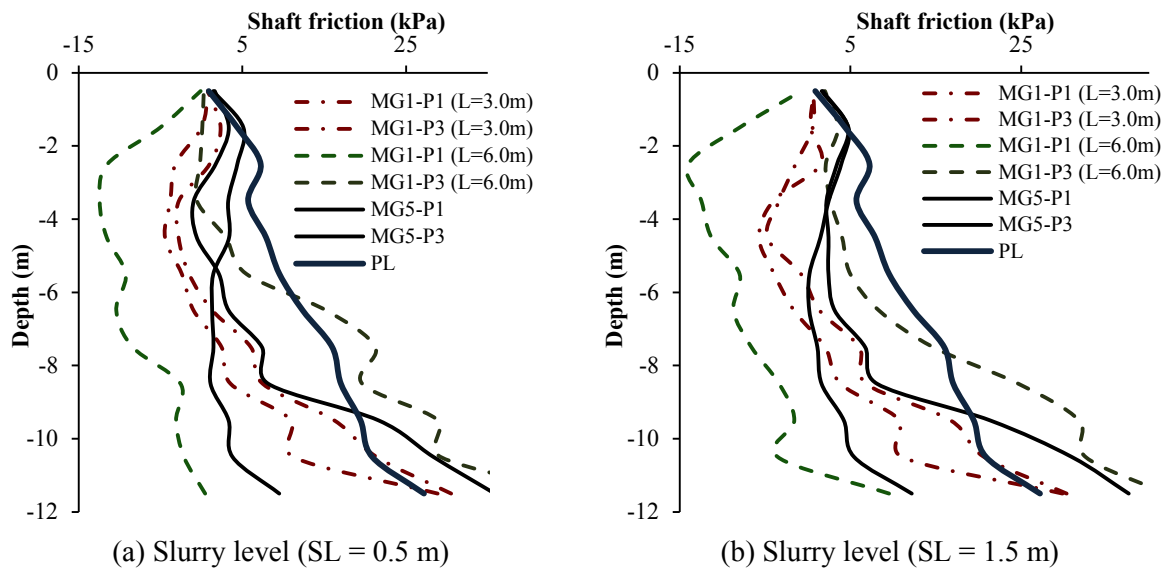


Figure 5-43: Pile shaft friction at slurry reduction position (SP = 13.0 to 14.0 m)

The difference in bending moment values has shown almost the same trend of deflection. It was about 130 % in case of comparing the results of the effect of the 6 m single and double panels, but it did not exceed 20 % between the double panel and the 3 m single panel. The difference due to slurry reduction was high and it reaches 200 % as an average difference between both cases.

The reduction of shaft friction for the first pile due to the 6m panel was higher than the double panel which was also slightly higher than the 3 m panel. The third pile showed an opposite behavior as the 6 m panel showed the lowest reduction. The effect due to different slurry level showed a less difference than the effect of slurry reduction at the pile tip level.

## 5.4.2 PART II- RESULTS

The previous section showed that some variables have a great influence on the pile group compared to other variables. Accordingly, the main focus in this section is to present the results of parameter combination shown in Figure 5-7. However, it is also necessary to present the effect of the panel stages of construction on some piles within the piled foundation at a certain water level.

### 5.4.2.1 Effect of panel construction stages

The effect of the 6m panels construction stages that was previously shown in Figures 5-5a on pile groups G1-1, G1-5, G1-9 and G6-5 is plotted in Figures 5-44 and B-26. The groundwater and slurry levels were constant and equal to 2.0 m and 0.5 m, respectively.

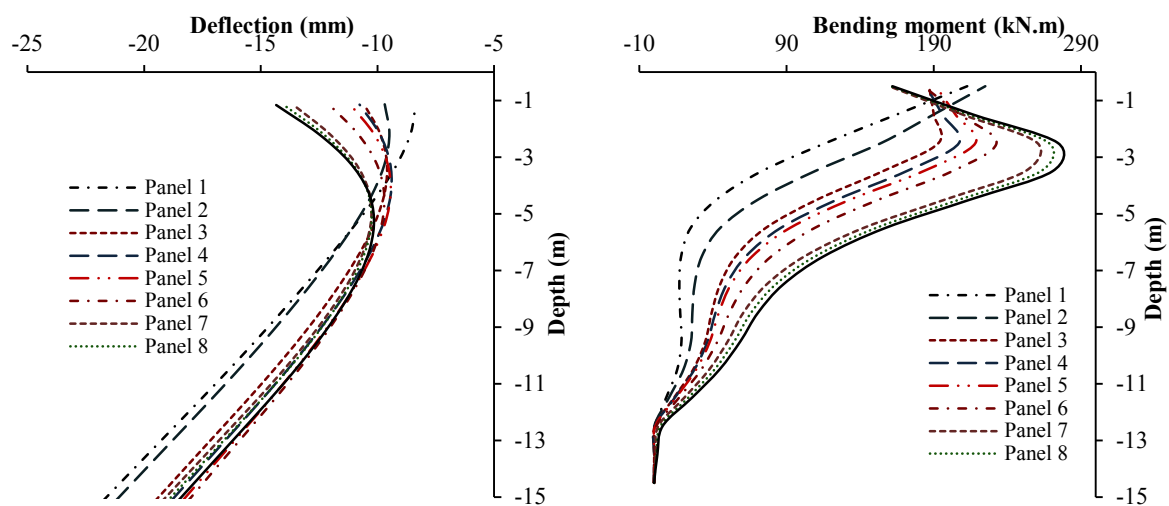


Figure 5-44: Pile deflection and bending moment for first pile within pile group (G<sub>1-5</sub>)

The effect of panels construction stages on piles is related to the pile group location. The deflection of pile group G1-1 was less influenced by the first seven panels construction but it relatively increased by the construction of the last two panels as shown in Figure B-26 (a). The first pile within model group G1-5 showed a different behavior during the construction of the panels. This group is located near the first panel which caused it to have a higher deflection values at the bottom with such panel construction. The deflection decreased from the bottom during construction of the other panels but it increased at the top as shown in Figure 5-44. The construction of the first four panels caused a less deflection difference on pile group G1-9, but by constructing the fifth panel the pile deflection relatively increased and no noticeable difference in deflection was found until the last panel (panel 9) was constructed as shown in Figure B-26 (b). The pile group G6-5 which located at the farthest distance from the trench was deflected gradually by advancing in the trenching stages as shown in Figure B-26 (c).

The positive value of the bending moment gradually increased for all pile groups with advancing in the trenching process except for pile group G6-5, which showed almost no

difference of bending moment during trenching stages as it was only effected by drag force from the other pile groups. The difference in bending moment values was affected by the pile group location. The pile group located far from the trench showed a negative value of bending moment because it acts as a fixed support from the bottom.

#### 5.4.2.2 The behavior of pile according to its location within the foundation

The effect of constructing the entire wall on individual pile groups defined by rows parallel and perpendicular to the trench is presented in this subsection. The deflection of the first row parallel to the trench is presented in Figure 5-45 while the third one is presented in Appendix B in Figure B-27. The shaft friction of both rows is presented in Figure 5-46.

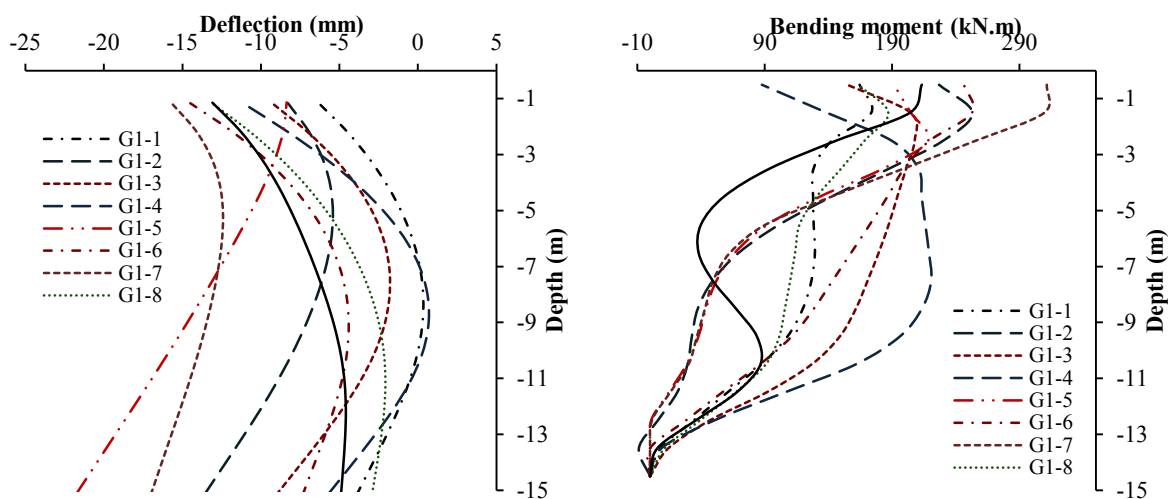


Figure 5-45: Pile deflection and bending moment for the first row of pile groups parallel to the trench (Row<sub>L1</sub>)

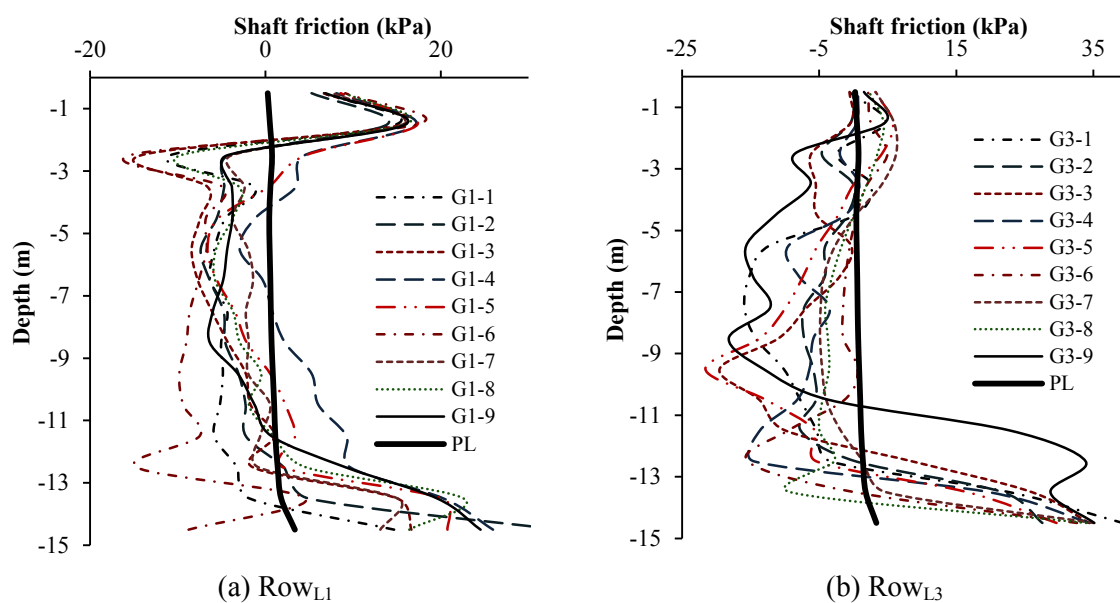


Figure 5-46: Pile shaft friction for the first and third pile groups rows parallel to the trench

There is a difference in deflection between the first and third row parallel to the trench but both of them showed that the maximum deflection was for the pile groups located near the centerline



of the entire trench wall. The pile group located at the edge of the raft showed the lowest value of deflection. The difference between the piles of the first row was between 1 % and 50 % while it ranged only between 1 % and 20 % for the piles within the third row. The first row showed a higher deflection at the top and tip of the piles than their middle. Because this row was affected by the general soil movement during the trenching process.

The bending moment results of the piles did not show a fixed noticeable difference because the whole system is acting together. However, the piles in the middle showed relatively larger values which were about 10 % higher than the average other piles values.

The shaft friction was relatively reduced in the middle of the piles for the pile groups located near the trench, but this reduction was accompanied by an increase at the pile tip.

The deflection and bending moment of the middle (fifth) row perpendicular to the trench are presented in Figure 5-47 while the last one (ninth row) is presented in the appendix in Figure B-28. The shaft friction of both rows is presented in Figure 5-48.

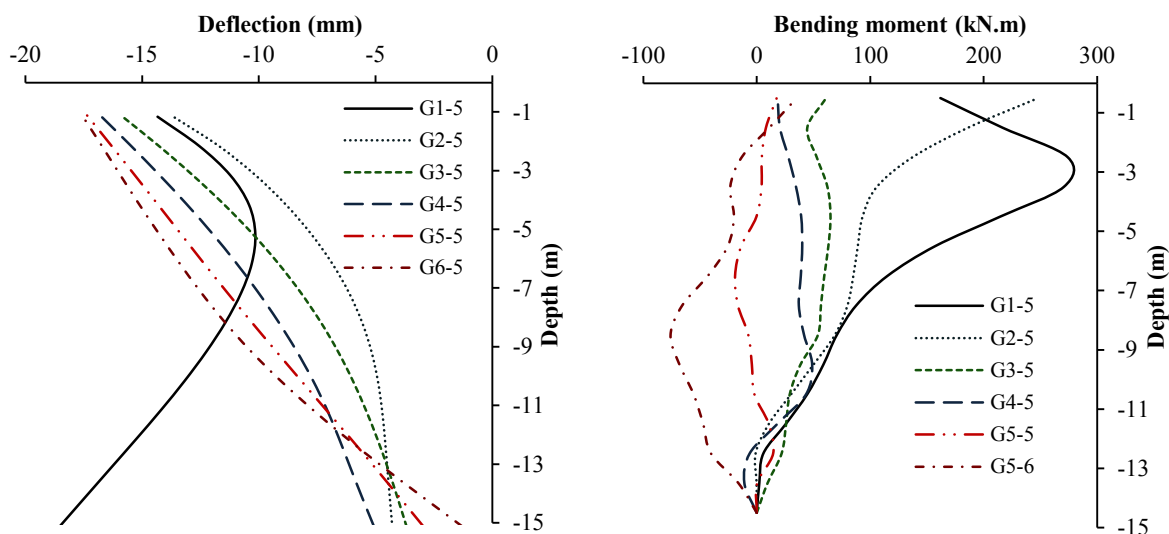


Figure 5-47: Pile deflection and bending moment for the first row of pile groups perpendicular to the trench ( $Row_{P5}$ )

The deflection of the first pile group within the middle pile row ( $Row_{P5}$ ) was much greater than that of the other piles regarding the pile tip. However, regarding the top of the pile there was no big difference between the piles and they almost move in the same way. This is because the soil movement affected the pile tip of the pile near to the trench while the other piles were only effected by the drag forces. The tip of the first pile showed higher movement values that reach about 250 % than the other piles. The variation of deflection piles of last row was less than 10 %.

The positive bending moment of the first two piles nearest to the trench was relatively greater than the other piles, while the last row showed only negative bending moment values because it

was effected by the drag force of the front piles. The difference in bending moment values in case of the middle row was relatively higher than that in the last row.

The shaft friction of all the piles has the same trend as it decreased at the middle of the pile and increased again at the pile tip in order to balance such a decrease. The maximum decrease was found at the pile within the second pile group (i.e. G2-5).

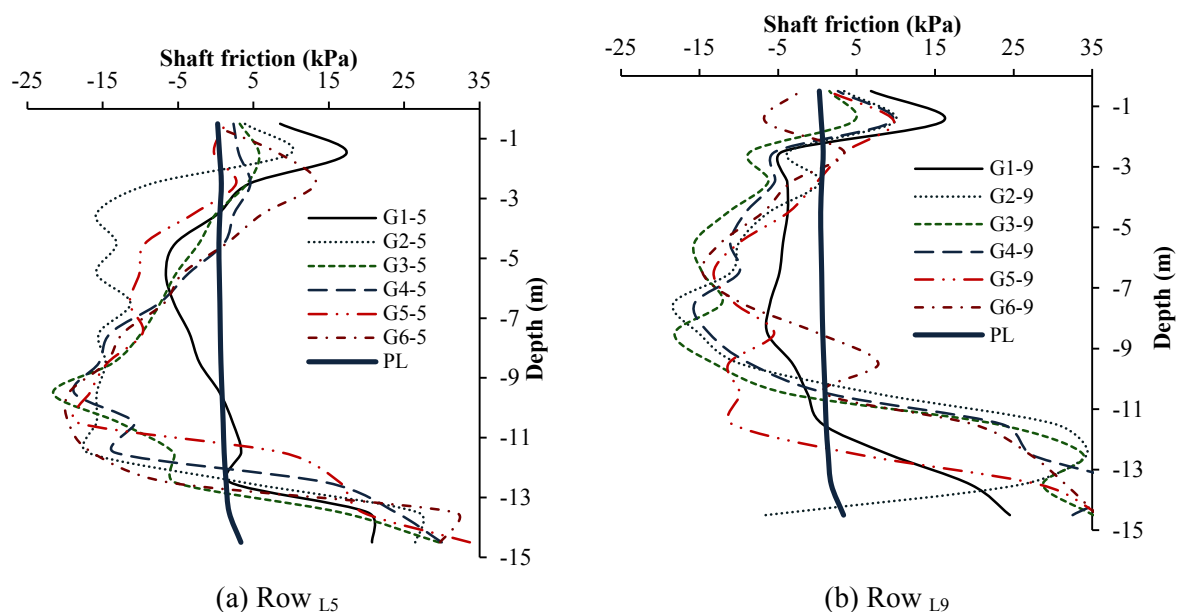


Figure 5-48: Pile shaft friction at slurry reduction position (SP = 13.0 to 14.0 m)

### 5.4.2.3 Effect of groundwater table, slurry level and slurry pressure reduction

The effect of different groundwater levels on the behavior of the first pile within the groups G<sub>1-5</sub> and G<sub>6-1</sub> is presented in Figures 5-49, 5-50 and B-29. Similarly, the effect of slurry pressure reduction and slurry level is presented in Figure 5-51, 5-52 and B-30 for the same pile groups.

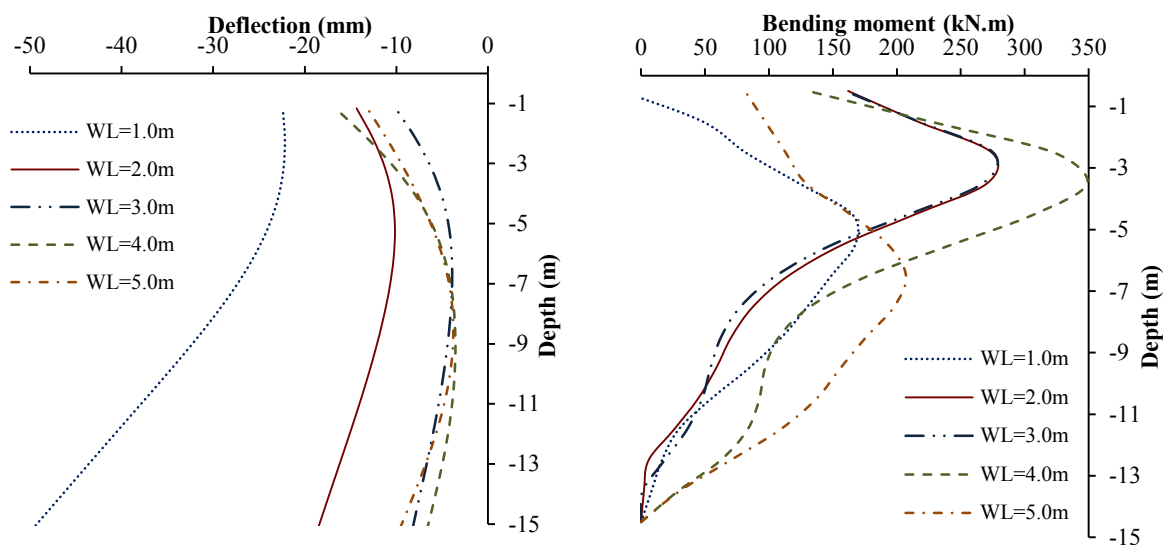


Figure 5-49: Pile deflection and bending moment for different groundwater levels at G1-5

The effect of the groundwater level on piles in the case of multiple panels is similar to single panel. The shallower the groundwater level the higher the deflection. However, the bending moment did not show the same trend that was presented in Figures 5-49 and B-29. The deflection of the pile at water level WL =1.0 m was between 50 % and 150 % higher than that by WL = 2.0 m, while the deflection at WL = 2.0 m was between 20 % and 80 % higher than WL = 3.0 m. The other deflection difference between the other water levels was less than 10%. The bending moment of the pile at WL =1.0 m was relatively low because the pile moved totally with the soil without producing a resisting force.

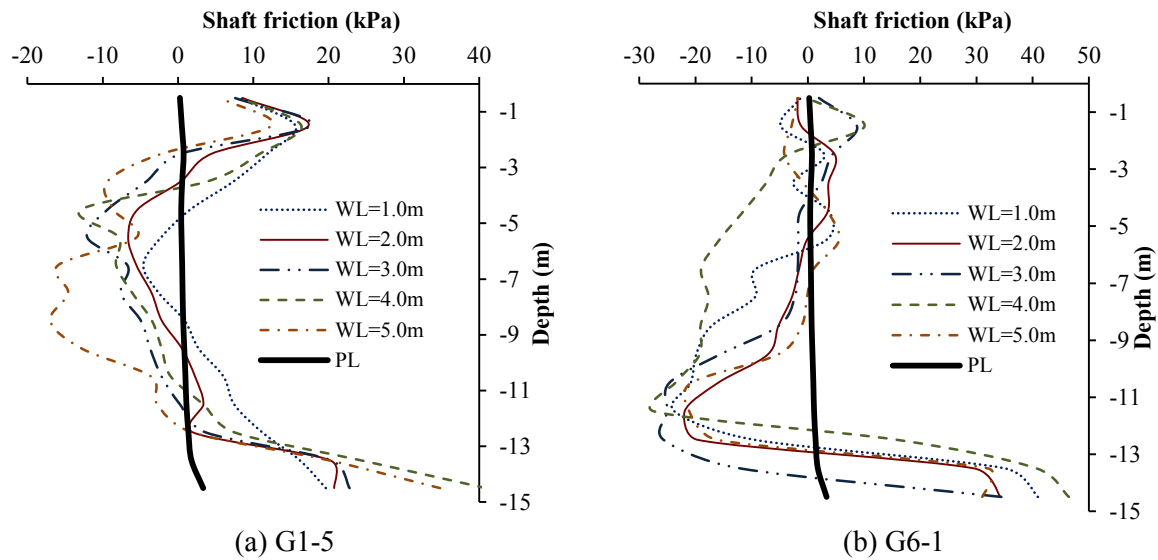


Figure 5-50: Pile shaft friction for different groundwater levels

The difference in shaft friction due to groundwater change was not high as shown in Figure 5-50. The reduction of shaft friction at shallower water level was not necessary the maximum because the pile in this case moved with the soil without resistance. The reduction at water levels WL 4 and 5 m was high but it was balanced by a high increase near the pile tip.

The effect of slurry level on pile deflection was greater than the effect of reduction on slurry pressure. The difference in deflection between slurry levels at (1.50) and (0.5) was 75 % in average. The effect of slurry pressure reduction on the pile tip movement was limited to less than 40 %. The bending moment did not show a noticeable difference due to slurry reduction but its shape was varying. Generally, the value of bending moment was not affected by trenching because the piles within the raft tend to rearrange the force between each other rather than a single pile group. Similarly, the effect of the slurry level and slurry pressure reduction on the piles was less than 10 %, but it reaches 30 % at the pile tip of pile group G<sub>1-5</sub>.

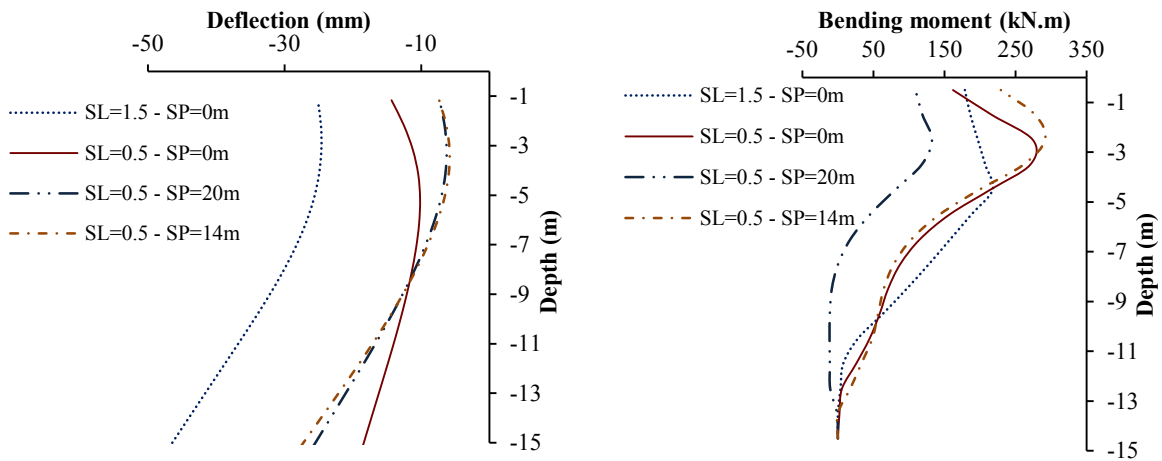


Figure 5-51: Pile deflection and bending moment at different slurry pressure reduction positions (SP) and at slurry levels for pile group  $G_{1-5}$

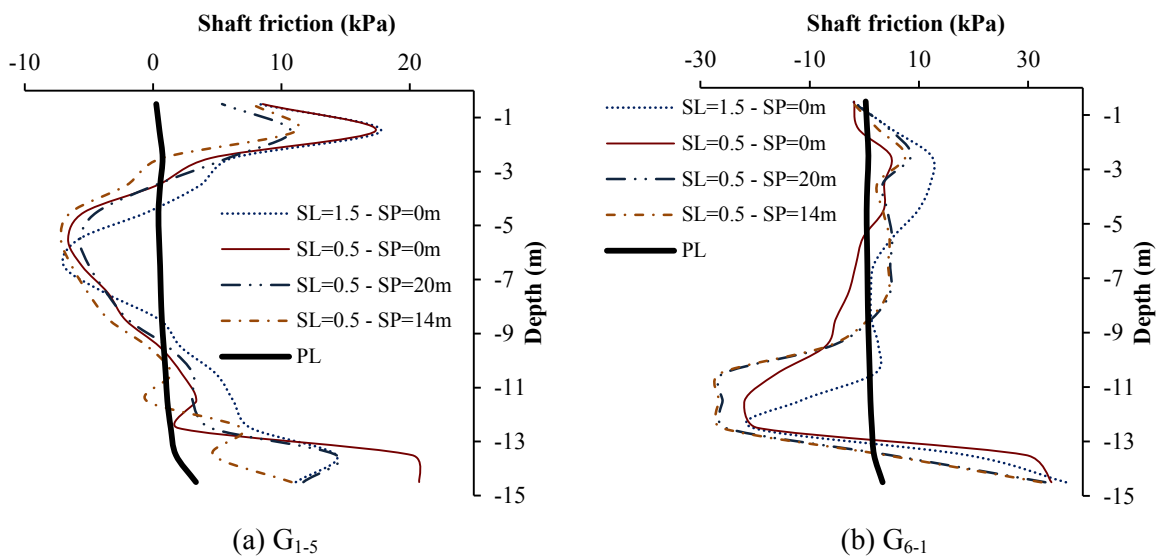


Figure 5-52: Pile shaft friction at different slurry pressure reduction positions (SP) and at slurry levels

#### 5.4.2.4 Effect of panel length

The effect of 3 m and 6 m panel length on the pile deflection and bending moment is presented in Figure 5-53. The plotted relations were made for the first pile within pile groups  $G_{1-1}$ ,  $G_{1-5}$  and  $G_{1-9}$  after finishing wall construction. These pile groups were chosen from the first row parallel to the trench (RL1).

The effect of the panel length on the pile tip deflection was greater than its top. The most effected pile group was the pile group at the centerline (i.e.  $G_{1-5}$ ) of the trench. The pile tip of such group deflects for the 6 m panel was 700 % greater than that of the 3 m panel length, while the difference of deflection due to panel length for the other pile groups was only about 75 %. The average increase of the pile positive bending moment due to the use of 6m panel was only 55 % greater than that of 3 m panel. This difference is lower than that of a single pile group (section 5.4.1.1) because the connected pile group rearranges the force between the pile groups and reduces the effect on pile bending.

### 5.4.2.5 Effect of pile group formation

In order to understand the effect of different pile group formation, a comparison was made between the piles in model groups MG1 and MG2 of part II. The comparison was for pile groups within the first and the last row parallel to the trench. The results of the first and last rows are presented in Figures 5-54 and B-31, respectively. The pile groups G1-1, G1-5 and G1-9 in model group MG1 are corresponding to pile groups G1-1, G1-4 and G1-7 in model group MG2, respectively.

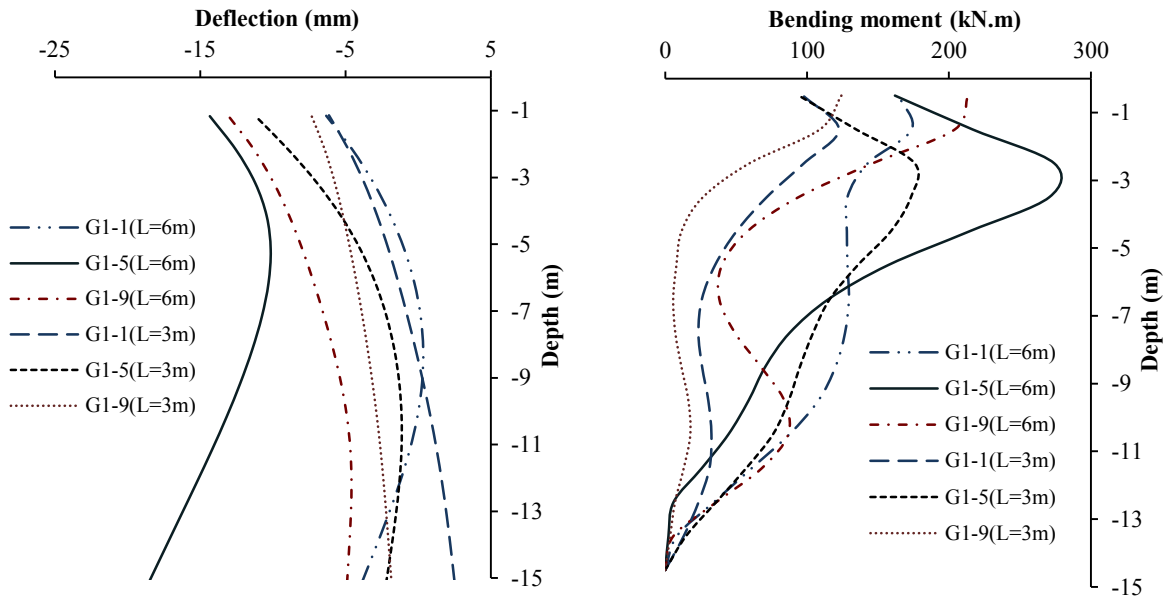


Figure 5-53: Pile deflection and bending moment at different panel lengths

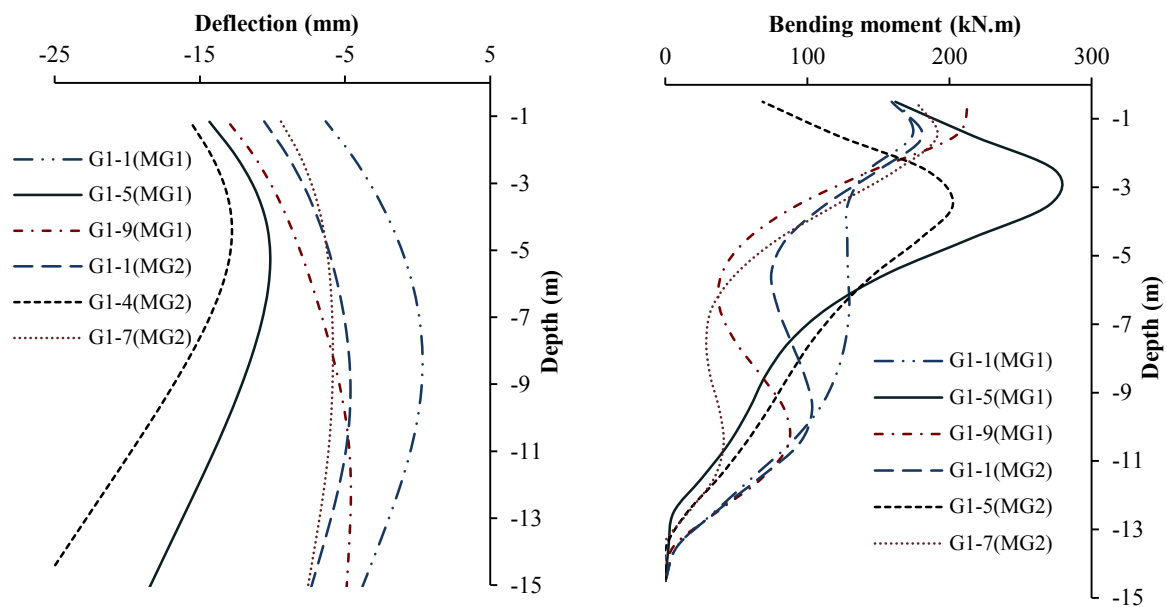


Figure 5-54: Pile deflection and bending moment for pile models MG1 and MG2 for the first row ( $R_{L1}$ )

The effect of slurry level on pile deflection was greater than the effect of reduction on slurry pressure. The difference in deflection between slurry levels at (1.50) and (0.5) was 75 % in average. The effect of slurry pressure reduction on the pile tip movement was limited to less than 40 %. The bending moment did not show a noticeable difference due to slurry reduction but its shape was varying. Generally, the value of bending moment was not affected by trenching because the piles within the raft tend to rearrange the force between each other rather than a single pile group. Similarly, the effect of the slurry level and slurry pressure reduction on the piles was less than 10 %, but it reaches 30 % at the pile tip of pile group  $G_{1-5}$ .

The deflection of the pile tip of model group MG2 was higher than that of MG1 with a range between 14 % and 200 %. On the other hand, the bending moment from MG2 was lower than that for MG1. The number of piles of MG1 was higher than MG2 which causes the resistance to be high and hence the bending moment was higher and deflection was lower.

### 5.4.3 PART III- RESULTS

This part is similar to Part II but it concerns about the pile raft foundation. The effect of stages on construction, water level, slurry level, panel length, and the number of piles within raft are the focus of the presented results.

#### 5.4.3.1 Panels construction stages effect on piles at different locations

The piles numbers within the raft and the panels construction stages were previously presented in Figure 5-9. The deflection, bending moment of the piles  $P_{1-11}$  and  $P_{15-11}$  at different panel construction stages are presented in Figures 5-55 and B-32, respectively, while their shaft friction is presented in Figure 5-56.

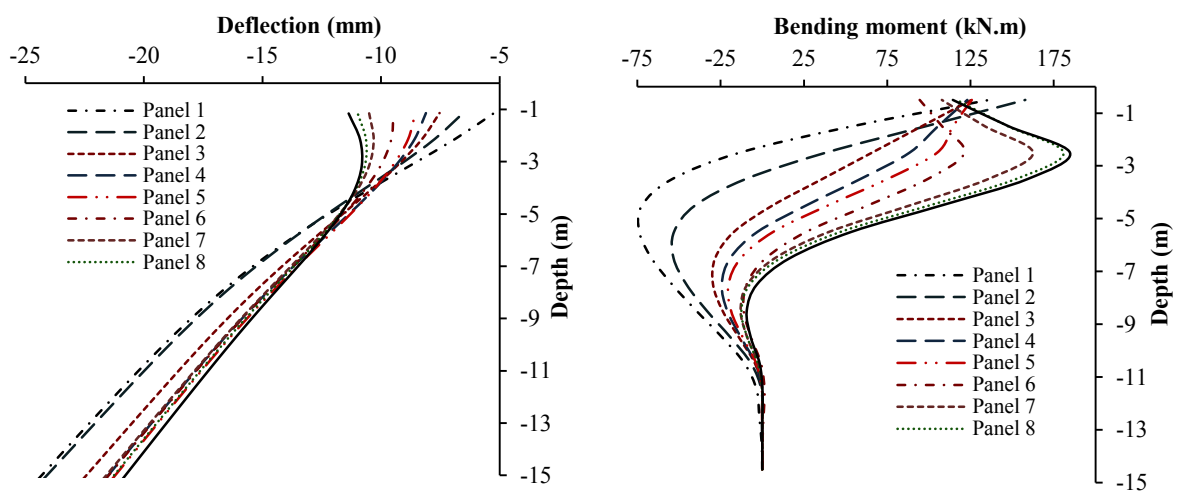


Figure 5-55: Pile deflection and bending moment at different panels construction stages for pile  $P_{1-11}$

The tip of the nearest pile to the trench (i.e.  $P_{1-11}$ ) deflects higher than its tip, while the farthest pile showed the opposite. The pile  $P_{1-11}$  showed a decrease in deflection at its tip with

advancing in panels' construction because it was close to the first panel. The pile top and the farthest piles showed an increase during construction of the panels because the whole movement of the raft is increased with advancing in construction. The average change in deflection for pile P1-11 was 6 % while for pile P1-15 was 20 %.

The bending moment showed a change from negative to positive values with panels' construction for pile P<sub>1-11</sub> and at the lower part of pile P<sub>15-11</sub>, while the positive value at the top of the pile P<sub>15-11</sub> decreased with advancing in construction. Generally, the average change in positive bending moment with panel construction is 15 %. This indicates that the change in deflection and bending moment values was great during constructing the initial panels.

The shaft friction showed a change during construction on the pile nearest to the trench while it shows no effect on the farthest pile (P<sub>1-15</sub>). The shaft friction decreased by the construction of the first panel and it increased gradually until it equals the shaft friction due to pile load by the end of the wall construction, because the panels nearest to the pile were filled with concrete, which cause the shaft friction to return almost to its original stage.

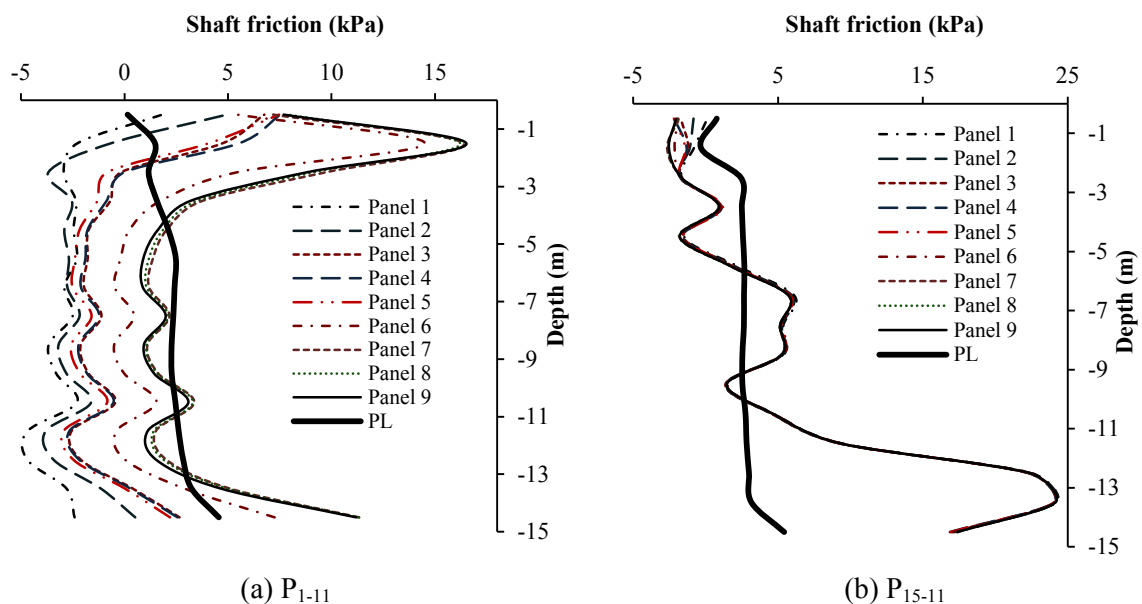


Figure 5-56: Pile shaft friction at different panels construction stages

#### 5.4.3.2 Comparison between different piles within the piled raft foundation

This section shows the different piles behavior according to their location within the raft foundation. The comparison between the different piles was made at the last construction stage for the first row parallel ( $R_{L1}$ ) to the trench and the one that is perpendicular ( $R_{P11}$ ) to the trench. The deflection and bending moment of row  $R_{L1}$  and  $R_{P11}$  are shown in Figures 5-57 and B-33, respectively. The shaft friction is presented in Figure 5-58.

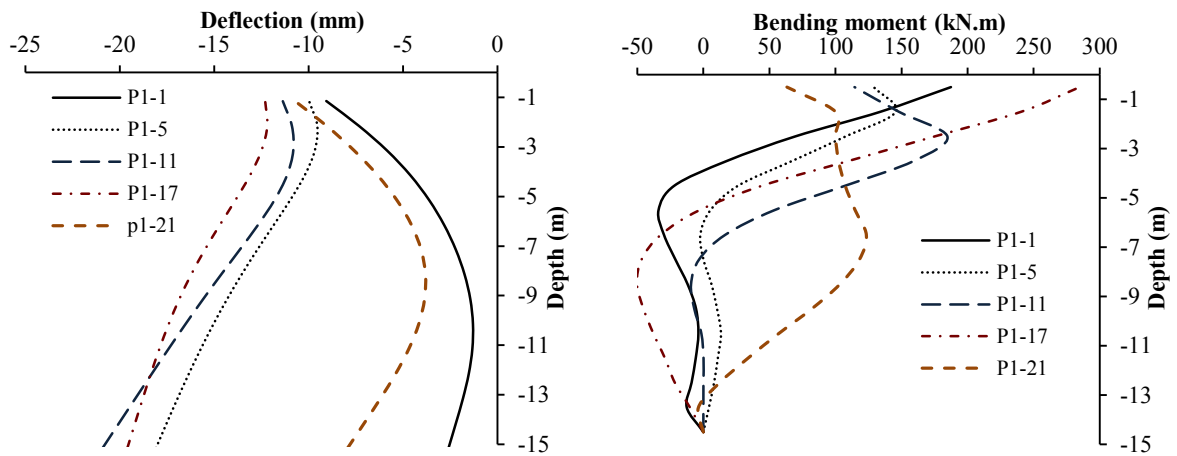


Figure 5-57: Pile deflection and bending moment for piles within the first row parallel to the trench (RL1)

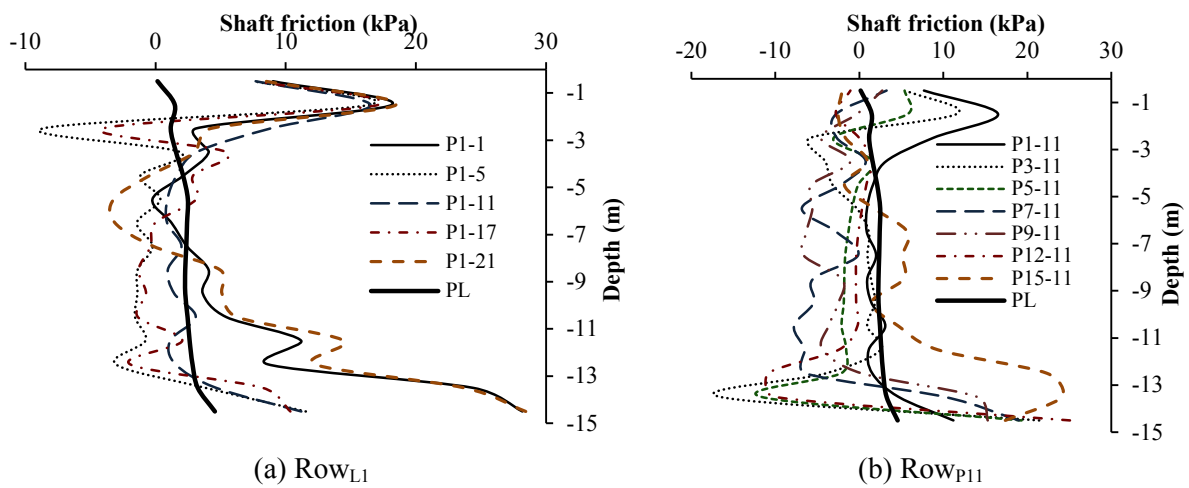


Figure 5-58: Pile shaft friction at different panels construction stages

The piles tip deflection, which is located within row RL1 and in the middle of the row, was more than 100 % higher than piles at the edges. However, the bending moment values did not show such a big difference which was less than 50 % as an average value. The piles around the middle showed a slight decrease in shaft friction while those in the edges showed a decrease. The piles within the row RP11 showed a higher deflection at their top than at the bottom except for the pile closest to the trench (i.e. P1-11). The deflection of the tip of such a pile was about 350 % higher than the average value of the other piles, while the average difference between the other piles regarding pile tip was less than 50 %. The average difference of deflection between the top of the piles was less than 6 %. The bending moment of the pile close to the trench was also about 350 % higher than the average value of the other piles. The last pile in the perpendicular row showed a relatively high deflection and bending moment because it carries less load and one of its sides is not fixed, while the other middle piles are considered to be fixed from all sides. The shaft friction did not show different values according to the pile position from the trench. The difference in such values was very low compared to the piles in the parallel row.



### 5.4.3.3 Effect of different groundwater tables and slurry levels

The previous subsections showed that the most effected pile within the pile raft is the pile in the middle P1-11, while the least effected one is that in the corner pile P15-21. The effect of groundwater and slurry level is presented for the two indicated piles. The pile deflection and bending moment for five different groundwater levels and at slurry level (SL = 0.5m) are presented in Figures 5-59 and B-34, while the slurry level SL=1.5m was plotted in the same figures for water level (WL =2.0m).

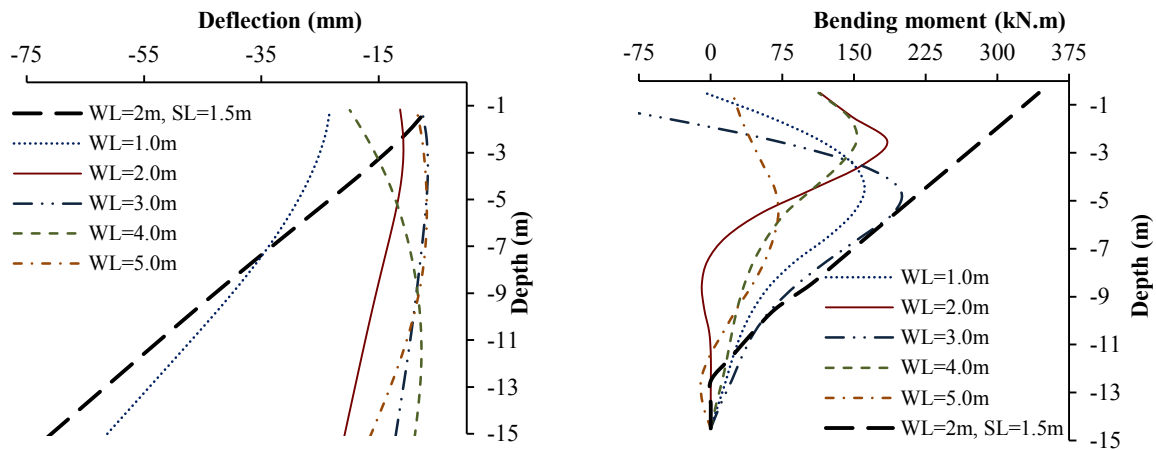


Figure 5-59: Pile deflection and bending moment of pile P1-11 for different groundwater levels

The deflection was noticeably high for pile P1-11 at its tip in case of water level of WL = 1.0 m and slurry level of SL = 1.50 m. The average difference in values between these two conditions and the other water levels was about 300 %. The other piles showed a difference of less than 30 %. The bending moment due to slurry reduction was about 200 % higher than the average value.

The slurry level did not show an effect on the farthest pile P15-21 as the deflection was not greatly changed with the slurry reduction. However, the pile deflection and bending moment were relatively high than average in case of water level equal 1.0 m while the slurry reduction did not show any great effect.

### 5.4.3.4 Panel length effect on the pile

In order to understand the effect of panel length on piled raft three piles were chosen. The chosen piles are one in the middle P<sub>1-11</sub>, another in the edge P<sub>15-11</sub> and the other in the corner P<sub>15-21</sub>. The calculation is made for the groundwater level (WL=2.0 m) and slurry level (SL=0.5m). The last stage of construction was considered in the analysis. The deflection and bending moment of the three piles are plotted for the two panel lengths 3.0 m and 6.0 m in Figure 5-60. The pile P<sub>1-11</sub> tip deflection in case of 6 m panel was 200 % higher than that at 3 m panel, while the piles top deflection difference was about 50 % as an average value between all the piles including P<sub>1-11</sub>.

The change in panel length showed a great difference in bending moment values for the pile P<sub>1-11</sub>, while this difference was less for the other piles. The panel length effect on pile behavior closest to the trench (i.e. P<sub>1-11</sub>) was greater than its effect on the other piles.

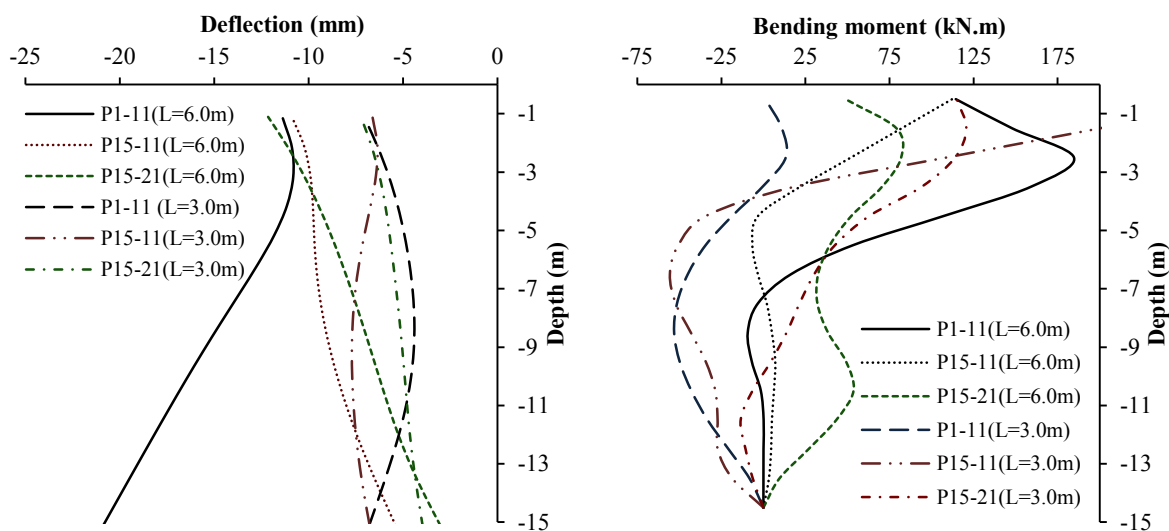


Figure 5-60: Pile deflection and bending moment for different panel lengths

#### 5.4.3.5 Effect of the number of piles within the raft

The influence of the number of piles within the raft on the pile behavior is presented in Figures 5-61 (row R<sub>L1</sub>) and B-35 (row R<sub>p11</sub>). In these figures, a comparison regarding pile deflection and bending moment was made between some piles within model group MG1 and piles in the same position in model group MG2.

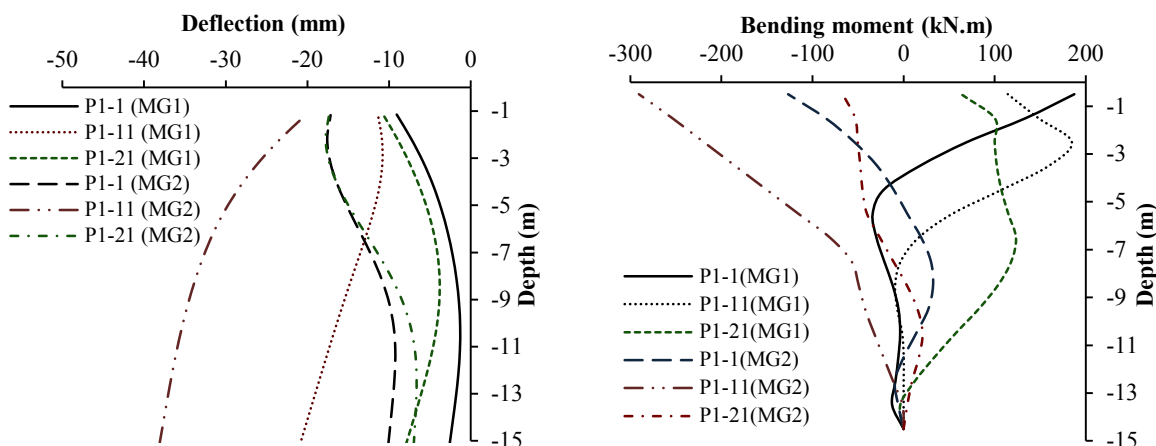


Figure 5-61: Pile deflection and bending moment for some piles within the first row parallel to the trench (R<sub>L1</sub>) in model group MG1 and corresponding piles in MG2

It is obvious from the figures that the pile deflection for the model group MG2 was higher than that from MG1. This difference was not the same for all piles within the raft. Accordingly, Table 5-3 shows the percentage of change in different piles deflection between the model groups MG1 and MG2. The table showed that there is a noticeable change on piles deflection values regarding the density of piles within the raft.

The bending moment of the piles in the first row parallel to the trench (i.e. P1-1, P1-11 and P1-21) showed a change from positive values in MG1 to negative values in MG2, while the other piles showed an increase in bending moment values between model group MG1 and MG2.

Table 5-3: Percentage of change in pile deflection between MG1 and MG2

Pile number	Average percentage change in deflection values between model groups MG1 and MG2
P <sub>1-1</sub>	>100 %
P <sub>1-11</sub>	80 %
P <sub>1-21</sub>	60 %
P <sub>3-11</sub>	>100 %
P <sub>7-11</sub>	30 %
P <sub>13-11</sub>	60 %

#### 5.4.3.6 Connected pile group in comparison with the pile raft foundation

The effect of the foundation type on the individual pile behavior during trenching is discussed in this section. The deflection, bending moment and shaft friction of piles within connected isolated footings (Part II) and corresponding piles within the piled raft foundation (Part III) are presented in Figures 5-62, 5-63 and B-36. The plotted results were made for two different slurry levels. The first pile was chosen from the pile group for the comparison with the piles within the raft foundation. The plot in the figures shows the pile or pile group number with the part number between brackets, the part number is written as PII for Part II and PIII for Part III. Pile group G1-1, G1-5 and G1-9 in Part II are corresponding to piles P1-1, P1-11 and P1-21 in Part III.

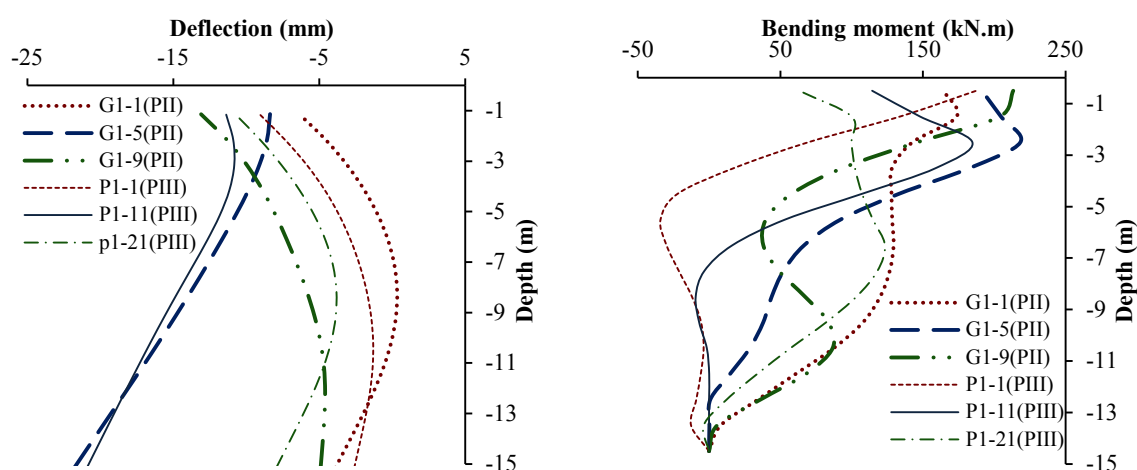


Figure 5-62: Pile deflection and bending moment for some piles in Part II compared to corresponding piles in Part III at slurry level (SL = 0.5 m)

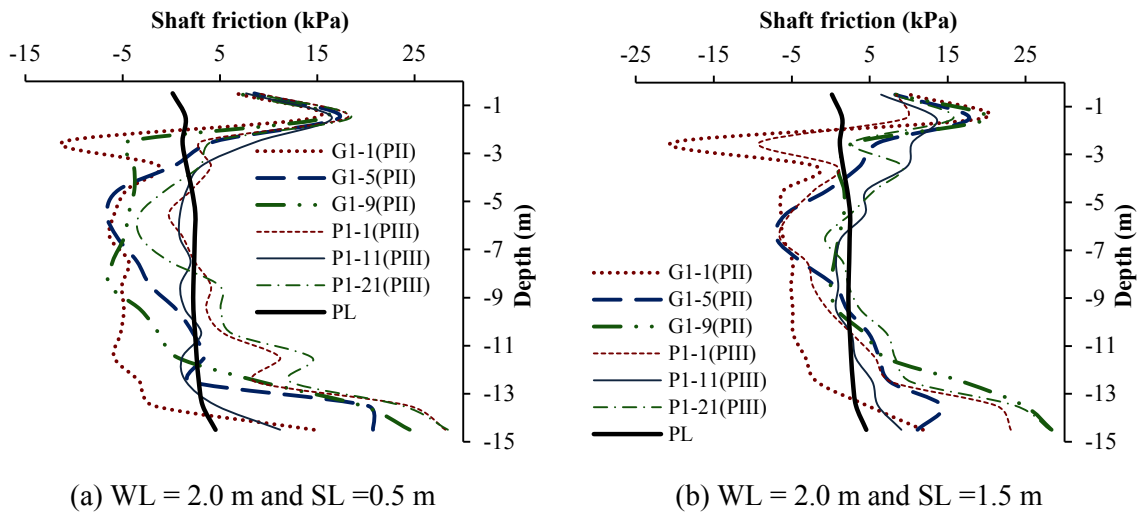


Figure 5-63: Pile shaft friction for some piles in Part II and corresponding piles in Part III

The deflection difference between the connected pile and piled raft foundation was noticeably low (less than 10 %) except for the case of slurry level (SL = 1.50 m). The deflection difference was higher at the pile tip of the middle pile within the raft foundation (P1-11) with a percentage of 35 % than the corresponding pile within the connected pile foundation (G1-5).

The connected pile groups also showed a slightly higher value of bending moment than the piles within the raft foundation. The connected pile group shows also a higher reduction in shaft friction than the piles within the raft.

#### 5.4.4 GENERAL OVERVIEW OF THE PARAMETRIC STUDY RESULTS

The parametric study provided an overview of the deflection, bending moment and shaft friction of the piles under different conditions. It may be important to point out which parameters have the greatest effect on the individual piles. The following Table 5-4 shows each parameter and its percentage of influence on the different pile behavior.

Table 5-4: Percentage of change in pile behavior due to all studied parameters

Parameter		Average percentage of change in			
		Deflection	Bending moment	Shaft friction	
Trench dimension	Panel depth (H)	3-8 % (< 10%)	< 10 %	< 10 %	
	Panel length (L)	Single	> 300 %	120 – 260 %	80 %
		Multiple	50-200 %		
	Panel thickness (T)	< 30 %	2-40 %	< 10 %	
Pile group location (x)		20-50 %	25-100 %		
Soil properties (Soil 1,2, ... n)		5-200 % (60 %)	< 40 %		
Slurry level (SL)		50 - 100 %	40 %		
Groundwater level (WL)	Single panel	20 – 50 %	45 %		
	Multiple panels	20 – 150 %	< 10 %		

Parameter		Average percentage of change in			
		Deflection	Bending moment	Shaft friction	
Pile position within a group	4-piles (MG1)		12 – 50 %	5 – 60 %	
	5-Piles (MG2)		20 - <b>100 %</b>	15 - 50 %	
	6-Piles (MG3)		20 – 40 %		
	6-Piles (MG4)		3 – 40 %	10 – 35 %	
Pile position within a group	Connected groups	Parallel*	1 - 50 %	5 - 10 %	
		Perpendicular	10 – <b>250 %</b>	Change signs**	
	Pile raft foundation	Parallel	6 – <b>100 %</b>	< 50 %	
		Perpendicular	6 - > <b>300 %</b>	> <b>300 %</b>	
Slurry reduction at some levels (SP)		<b>110 – 200 %</b>	50 – <b>130 %</b>	<b>300 %</b>	
Pile diameter (D)		10- 45 %	20 - <b>100 %</b>		
Pile within different group formation		5 -30 %	10 – 40 %	5 -50 %	
Double panel and single panel	6 m panel		<b>140 -&gt;300 %</b>	<b>130 %</b>	<b>200 %</b>
	3 m panel		40 – <b>250 %</b>	20 %	
Panel stages of construction	Pile raft foundation		4-80 % (20 %)		
Density of connected pile groups		14 – <b>200 %</b>			
Density of piles within raft		30 -> <b>100 %</b>	Change signs**		
Connected pile group and piled raft foundation		<10 - 35 %			

\*parallel to the trench or perpendicular to the trench

\*\*signs change from positive to negative and vice versa

The percentages of change presented in the table indicated that not all the parameters could have the same effect on the pile behavior. The numbers marked in bold indicate a high expected effect. The pile general behavior was affected by the change in panel length than the change on depth or thickness. The effect of different groundwater levels was less than that due to change of the slurry level. The position of the pile was more effective within a connected pile group or raft foundation than the isolated pile group. The effect of the number of piles within the foundation was great for some piles within the group. The stage of panel construction is effecting the pile behavior as well.

## 5.5 EFFECT OF TRENCHING ON THE PILE SHAFT FRICTION COEFFICIENT

The shaft friction capacity of the pile in cohesion-less soils is calculated from Equation 2.4 that was discussed in Section 2.2.1.2 in Chapter 2, because the shaft friction coefficient (effective stress ratio) is depend on the earth pressure coefficient and it is likely to change with it. Generally, the trenching process reduces the earth pressure coefficient as presented in

Figure 3-20 in Chapter 3 (range between 0.7 and 0.9). In addition, it is not clear how far from the trench is the effect of such a reduction.

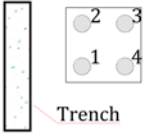
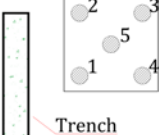
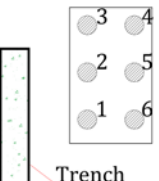
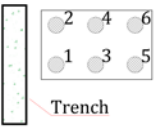
This parametric study presented the shaft friction of the piles at several condition before and after trenching. The amount of change of shaft friction values provides an indication to the change of the shaft friction coefficient. In many cases, the shaft friction presented in this chapter showed a decrease along the pile at some parts and an increase at another parts.

The percentage of reduction in shaft friction is calculated here as the absolute value of the amount of change caused by trenching related to the original shaft friction. This percentage gives an indication of the amount of reduction in the shaft friction coefficient which is presented as the reduction factor  $k_r$ . The shaft friction coefficient due to trenching ( $k_t$ ) can then be calculated as the reduction factor ( $k_r$ ) multiplied by the original shaft friction coefficient ( $k$ ). The following table shows the percentage of the shaft friction after trenching related to its value before trenching (loading case) and the reduction factor ( $k_r$ ) in different cases.

Table 5-5: Shaft friction coefficient reduction factor due to trenching ( $k_r$ )

Parameter				Percentage from the original shaft friction	Reduction factor ( $k_r$ )
Trench dimension	Panel depth (H) (WL =2.0m) (x = 3.5m)	20 m		89.8 %	0.9
		30 m		89.7 %	0.9
		40 m		89.6 %	0.9
		50 m		89.7 %	0.9
	Panel length (L) (WL =2.0m) (x = 2.0m)	Single	3 m	93.0 %	0.9
			6 m	80.3 %	0.8
	Pile within group G1-9 PII-MG1	Multiple	3 m	88.7 %	0.85
			6 m	74.6 %	0.75
	Thickness (T= 0.6m), (L=6m)			94.0 %	0.9
	Pile group location (x) (WL = 2.0m) (L=6.0m)	2.0 m			80.3 %
3.5 m			89.7 %	0.9	
5.5 m			93.1 %	0.9	
7.5 m			95.2 %	0.95	
Soil properties (WL = 2.0m) (L=6.0m)	1			86.5 %	0.85
	2			89.7 %	0.9
	3			91.8 %	0.9
	4			88.8 %	0.9
	5			91.1 %	0.9

Parameter		Percentage from the original shaft friction		Reduction factor ( $k_r$ )		
Slurry level (SL) (WL = 2.0m) (L=6.0m) (x = 2.0m)	0.5 m		80.3 %		0.9	
	1 m		77.8 %		0.75	
	1.5 m		71.3 %		0.7	
	2 m		71.0 %		0.7	
Groundwater level (WL)	Single panel (WL = 2.0m) (L=6.0m) (x = 3.5m)	1.0 m	70.2 %		0.7	
		2.0 m	89.7 %		0.9	
		3.0 m	89.6 %		0.9	
		4.0 m	91.3 %		0.9	
		5.0 m	91.7 %		0.9	
	Multiple panels near piled raft foundation (Pile 1-7)	1.0 m	78.9 %		0.75	
		2.0 m	80.0 %		0.8	
		3.0 m	90.0 %		0.9	
		4.0 m	92.7 %		0.9	
		5.0 m	94.2 %		0.9	
Slurry reduction at some levels (SP) (WL = 2.0m) (L=6.0m)	Distance from trench (x)		<b>x = 2.0 m</b>	<b>x = 3.5 m</b>	<b>x = 2.0 m</b>	<b>x = 3.5 m</b>
	9.0 to 10.0 m		48.5 %	84.0 %	0.5	0.85
	10.0 to 11.0 m		46.5 %	81.0 %	0.45	0.8
	11.5 to 12.5 m		48.3 %	79.0 %	0.5	0.8
	13.0 to 14.0 m		57.7 %	77.0 %	0.55	0.75
	14.5 to 15.5 m		72.7 %	77.5 %	0.7	0.75
Pile length (hp) (WL = 2.0m) (L=6.0m) (x = 3.5m)	12 m		89.7 %		0.9	
	14 m		88.25 %		0.9	
	16 m		85.45 %		0.85	
	18 m		81.0 %		0.8	
	20 m		80.6 %		0.8	
	25 m		73.4 %		0.7	
	30 m		52.7 %		0.5	
Pile diameter (D) (WL = 2.0m) (L=6.0m) (x = 3.5m)	0.2 m		100 %		1.0	
	0.4 m		96.8 %		1.0	
	0.6 m		93.3 %		0.95	
	1.0 m		89.2 %		0.90	
	1.2 m		89.1 %		0.90	
Panels construction stages* effect on pile 11-1 within the raft	Panel 1		69.8 %		0.7	
	Panel 2		71.5 %		0.7	
	Panel 3		80.75 %		0.8	
	Panel 4		80.35 %		0.8	

Parameter		Percentage from the original shaft friction		Reduction factor ( $k_r$ )		
(model group MG1) (WL = 2.0m) (L=6.0m)	Panel 5	77.8 %		0.75		
	Panel 6	95.6 %		0.95		
	Panel 7	>100 %**		1.0		
	Panel 8	>100 %**		1.0		
	Panel 9	>100 %**		1.0		
Pile position within a group (WL = 2.0m) (L=6.0m) (x = 3.5m)	4-piles (MG1) 	Pile 1	89.7 %		0.9	
		Pile 2	96 %		0.95	
		Pile 3	103.3 %		1.0	
		Pile 4	101 %		1.0	
	5-Piles (MG2) 	Pile 1	94.0 %		0.95	
		Pile 2	99 %		1.0	
		Pile 3	101 %		1.0	
		Pile 4	102 %		1.0	
		Pile 5	93.0 %		0.9	
	6-Piles (MG3) 	Pile 1	49.2 %			
		Pile 2	86.0 %		0.85	
		Pile 3	97.0 %		0.95	
		Pile 4	87.7 %		0.85	
		Pile 5	95.0 %		0.95	
		Pile 6	100 %		1.0	
	6-Piles (MG4) 	Pile 1	85.0%		0.85	
		Pile 2	99.7%		1.0	
		Pile 3	95.0%		0.95	
		Pile 4	94.0%		0.95	
		Pile 5	>100 %*		1.0	
Pile 6		100 %		1.0		
Pile position within raft foundation (panel 1)	Panels	<b>Panel 1</b>	<b>Panel 9</b>	<b>Panel 1</b>	<b>Panel 9</b>	
	Pile 11-1	81.6 %	>100 %**	0.8	1.0	
	Pile 11-3	57.0 %	-ve***	0.55	-ve***	
	Pile 11-5	74.5 %	67 %	0.75	0.65	
	Pile 11-7	91.0 %	76 %	0.9	0.76	
	Pile 11-9	82.0 %	80 %	0.8	0.8	
	Pile 11-11	75.0 %	74 %	0.75	0.75	
	Pile 11-15	>100 %*	>100 %*	1.0	1.0	

\* These piles have a higher value of loading due to the rearrangement of load due to trenching

\*\* The concreting process of the panels near the pile could cause the increase of the shaft friction

\*\*\* The negative sign indicated that this pile is under negative skin friction.

The reduction factor presented in the table was calculated for some combinations. Accordingly, it is necessary to make some corrections for the reduction factor. These corrections were made for the most effective parameters such as panel length (L) and pile location from the trench (x).



The reduction factor  $k_r$  at panel length ( $L = 6.0$  m) is considered to be 1.125 times higher than that at panel length ( $L = 3.0$  m), while the normalized reduction factor related to pile group at distance ( $x = 3.5$  m) can be corrected using the correction factor ( $k_{cr}$ ) which can be calculated from the following Equation 5.1 or Figure 5-64.

$$K_{cr} = 0.1243\ln(x) + 0.8184 \quad 5.1$$

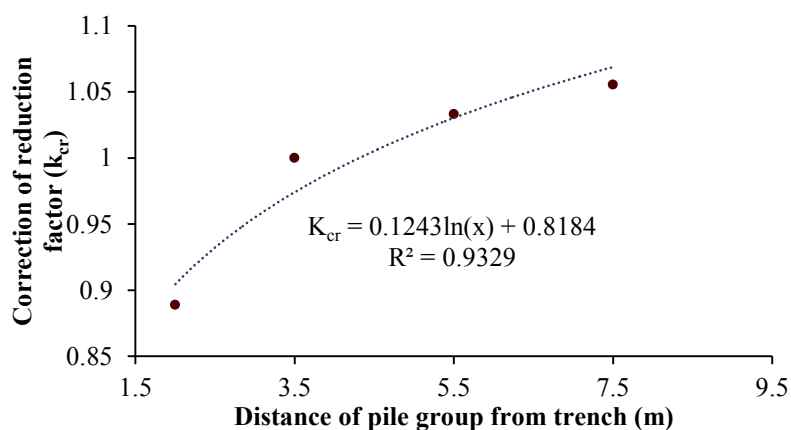


Figure 5-64: Correction of reduction factor related to distance from the trench

## 5.6 SUMMARY

In this chapter a wide range of parameters were studied through several combinations to cover different cases that could happen in the real field work situations. The numerical modeling was made in view of the numerical verification that was discussed in the previous chapter. The studied parameters were divided into three main categories such as the surrounding medium, the trench and the deep foundation. The surrounding medium is considered to be the soil and groundwater table. The soil was sand that was modeled with five different friction angles and stiffness, also five different levels of ground water were used in the study. The trench was modeled with different dimensions, while the guide wall dimension was chosen to be constant. The slurry level inside the trench was varying between four different values. The slurry pressure was reduced at seven different depths to simulate the situation of a weak or squeezed soil located at some depth along the trench depth. The foundation was modeled as an isolated pile group (Part I), connected pile group (Part II) and pile raft foundation (Part III), while each part was divided into several model groups according to the pile formation within the foundation. The different parameters were studied using 13 parameter combination for Part I and four parameter combinations for parts II and III with a total number of 21 parameter combinations. The total number of model runs were 299 runs from all the combinations.

The results of the parametric study were presented for all the parameter combinations in this chapter and in Appendix B through figures and tables. The outputs were presented as the deflection, bending moment and shaft friction of the pile. However, it was not necessary that

the effect of trenching was the same on each of these outputs and not all the parameters showed the same effect on the general pile behavior. The most effective parameters on pile deflection and bending moment were the panel length, slurry level and the reduction of the slurry pressure at some locations, while, the effect of the groundwater level on deflection and bending moment was obvious only between the shallower levels. The piles with a larger diameter tend to deflect lower than piles with smaller one, while their bending moment was relatively higher. The deeper the pile tip the smaller it deflects because the lower part acts as a fixation. There was a noticeable difference in pile deflection and bending moment within some piles in the same group. The group formation has also an effect. The construction stages effect on pile deflection and bending moment was varying according to its location within the foundation. The density of piles within the group is an influencing factor on pile behavior.

The pile shaft friction was effected relatively different by trenching than its deflection and bending moment because it generated due to the relative movement between the soil and the pile. The shaft friction showed a general trend of reduction due to trenching; however, it could increase in some cases due to the rearrangement of loads on piles. The coefficient of shaft friction was calculated using a reduction factor that was calculated from the parametric study. The highest reduction factor was found when the slurry pressure was reduced near the pile tip. As a general conclusion, the pile general behavior was greatly affected by the unusual situation such as the low slurry level or presence of weak soil layer that could cause a reduction on the slurry pressure. The length of panel played also a rule in such effect. It is recommended to use panels with a small length and to control the slurry level inside the trench in order to avoid any big movement of nearby piles. A good soil investigation is required which should take into consideration the existence of any lenses of weak soil which could cause a reduction in slurry pressure during trenching process.

## CHAPTER 6: ANALYTICAL APPROACH

### 6.1 INTRODUCTION

The previous chapter has shown the effect of the trenching process on piled foundation, but it did not show the effect of the existing pile on the stability of the nearby trench. Accordingly, this chapter concerns creating an analytical approach based on the wedge method in order to understand such an effect. The load transfer mechanism from the pile to the trench can be obtained through the wedge analysis or by the results from the previous parametric study. In order to understand such a mechanism, the analytical approach was made for two situations. The first situation is simple and simulates a single pile near a single panel. The second situation simulates trenching a single panel near a group of piles with different formations. Two and three-dimensional analyses were adopted in the analysis for situation one, while it was more logic to simulate the second situation only with a three-dimensional analysis.

The analytical approach in this chapter was made by assuming a failure surface of the soil wedge attached to the trench. The pile could be totally above the failure surface or intersect with the failure surface. If it is totally above the failure surface, then its load will be totally transferred to the failure wedge. In this case, the pile will reduce the stability of the nearby slurry trench, but if the pile intersects with the failure surface its load will be partially transferred to the failure wedge through its fraction only. An additional resistance to the wedge movement could be generated due to such an intersection. In this case, the pile could cause an increase to the stability of the trench rather than a decrease.

A comparative study is made using this analytical approach to understand the effect of different parameters and analysis procedures on the factor of safety. The analytical approach was checked using the  $\phi/c$  reduction mechanism implemented in FLAC 3D.

### 6.2 TRENCHING NEAR A SINGLE PILE (SITUATION I)

Trenching of a single panel near a single pile is not a common situation in the real field projects. However, it was assumed in order to simplify the complex problem. Two cases were assumed in the analytical approach. The first is assuming the pile is totally above the failure surface, while the second assumed the pile is intersecting the failure surface. Both cases are analyzed in two and three dimensions.

#### 6.2.1 CASE 1: PILE ABOVE THE FAILURE SURFACE

The pile is assumed to be located on the centerline of the panel and subjected to a vertical load  $F_{tot}$ . The pile length is  $h_p$  with diameter  $D$ , while its centerline is assumed to be at a distance  $x$

from the trench. The trench has a depth of  $H$  and its length is  $L$ . The failure surface is assumed inclined with an angle  $\theta$  from the horizontal. The suggested two- and three- dimensional analytical approaches were based on understanding the literature. The following subsection shows both approaches.

### 6.2.1.1 Two-dimensional approach of Case 1

The wedge of failure of the trench is presented by a slip surface inclined by an angle  $\theta$  from the horizontal as shown in Figure 6-1. The trench depth is  $H$  and the groundwater and slurry levels are at distances of  $H_w$  and  $H_s$  from the trench bottom. The pile is located inside the wedge of failure and subjected to a vertical load  $F_{tot}$ . This load is transferred to the wedge as a shear force  $f_s$  and end bearing force  $f_b$ , the bearing force is transferred with an angle of  $60^\circ$  ( $\approx 2$  vertical : 1 horizontal) according to Tomlinson and Woodward (2008). If the load on the pile is equal to its capacity, then these forces will be equal to the shear bearing capacity of the pile. The weight of the wedge ( $W$ ) is considered as an acting vertical force while the slurry pressure  $p_s$  is considered to be a resisting force. The shear force acting along the base of the sliding surface is ( $S$ ), while the reaction normal to the sliding surface is  $N$ . If the pile is too close to the trench ( $x < 1.5D$ ) the bearing pressure of the pile will be effecting horizontally on the trench wall as shown in Figure 6-1 (b).

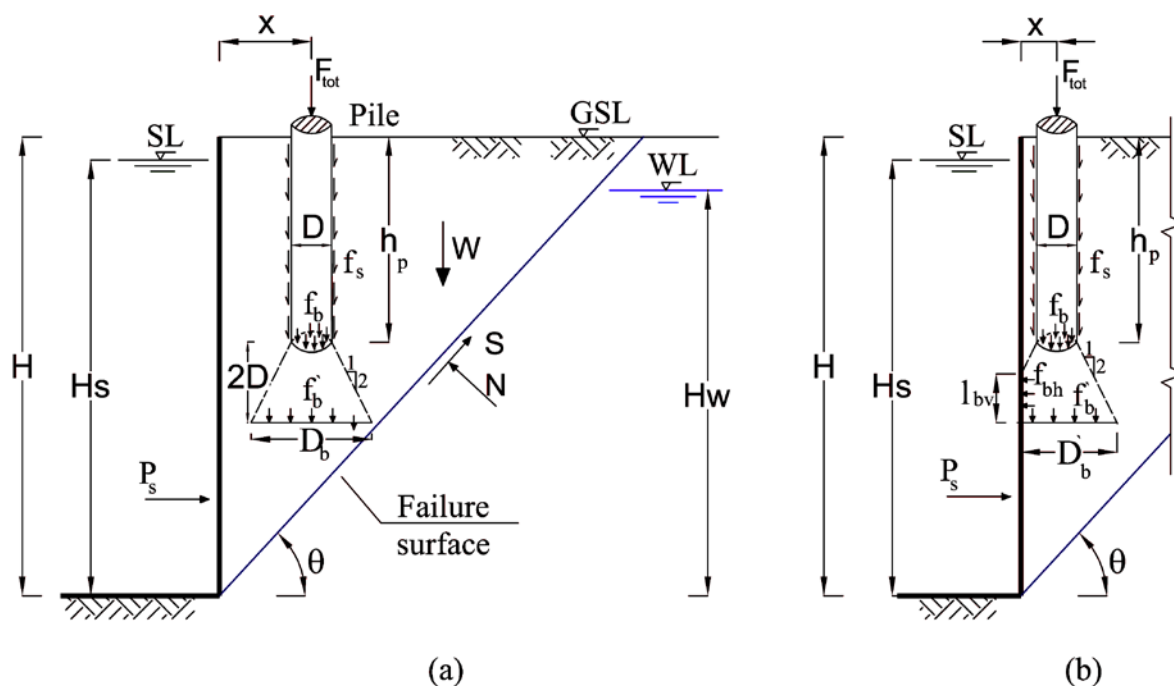


Figure 6-1: Pile above the failure surface (two-dimensional approach)

The wedge is subjected to vertical and horizontal forces that should be under equilibrium. If the pile is at distance  $x \geq 1.5D$  the vertical and horizontal equilibrium can be achieved through Equations 6.1 and 6.2, respectively.

$$S + (P_s) \cos \theta = (W + F_s + F_b) \sin \theta \quad 6.1$$

$$N = (W + F_s + F_b) \cos \theta + (P_s - F_{bh}) \sin \theta \quad 6.2$$

The vertical and horizontal equilibrium could be achieved in case of  $X < 1.5D$  through Equations 6.3 and 6.4, respectively.

$$S + (P_s - F_{bh}) \cos \theta = (W + F_s + F_b) \sin \theta \quad 6.3$$

$$N = (W + F_s + F_b) \cos \theta + (P_s - F_{bh}) \sin \theta \quad 6.4$$

Since the bearing load of the pile is assumed to be transferred on the soil with a slope of 1(horizontal): 2(vertical), so it is assumed to spread over an area with a diameter calculated from the following equation:

$$D_b = 3D \quad \text{and} \quad f_b = f_b D^2 / D_b^2 \quad 6.5$$

If the  $x$  value was less than  $1.5 D$  the bearing load will be distributed vertically over a non-full circular area with a distance from the wall calculated from Equation 6.6., while it is assumed to spread on the trench wall with a vertical distance calculated from Equation 6.7.

$$D_b = 1.5D + x \quad 6.6$$

$$l_{bv} = 2(1.5D - x) \quad 6.7$$

The applied forces from the pile can then be calculated from the following equations:

$$F_s = f_s \pi D \quad 6.8$$

$$F_b = \frac{f_b \pi D^2}{4} \quad 6.9$$

$$F_b = f_b \left[ \frac{\pi D_b^2 \sin^{-1} \left( \frac{2x}{D_b} \right) + 180}{720} + \frac{x D_b \cos \left( \sin^{-1} \left( \frac{2x}{D_b} \right) \right)}{2} \right] \quad 6.10$$

$$F_{bh} = f_b \left[ \frac{\pi D_b^2}{4} - \left( \frac{\pi D_b^2 \sin^{-1} \left( \frac{2x}{D_b} \right) + 180}{720} + \frac{x D_b \cos \left( \sin^{-1} \left( \frac{2x}{D_b} \right) \right)}{2} \right) \right] \quad 6.11$$

The weight of the triangle wedge ( $W$ ), slurry pressure ( $P_s$ ) and water pressures ( $U$ ) are presented in the following Equations 6.12, 6.13 and 6.14, respectively.

$$W = \frac{\gamma H^2}{2 \tan \theta} \quad 6.12$$

$$P_s = \frac{\gamma_s H_s^2}{2} \quad 6.13$$

$$U = \frac{\gamma_w H_w^2}{2} \quad 6.14$$

where:

$\gamma$  is the soil density

$\gamma_s$  is the slurry density

$\gamma_w$  is the slurry density

The shear force (S) is a function of the active normal force and friction angle ( $\phi'$ ) with respect to the shear failure factor of safety F.

$$S = \frac{N' \tan \phi'}{F} = \frac{\left(N - \frac{U}{\sin \theta}\right) \tan \phi'}{F} \quad 6.15$$

By substitution in Equations 6.1 and 6.2 for the case of  $x \geq 1.5D$  then

$$F = \frac{\left[(W + F_s + F_b) \cos \theta + P_s \sin \theta - \frac{U}{\sin \theta}\right] \tan \phi'}{(W + F_s + F_b) \sin \theta - P_s \cos \theta} \quad 6.16$$

This equation can be written by replacing W, Ps and U with the values in Equations 6.12, 6.13 and 6.14.

$$F_s = \frac{\left[\gamma H^2 \cos^2 \theta + \gamma_s H_s^2 \sin^2 \theta - \gamma_w H_w^2\right] \tan \phi'}{(\gamma H^2 \cos \theta + 2(F_s + F_b) \sin \theta - \gamma_s H_s^2 \cos \theta) \sin \theta} \quad 6.17$$

Similarly, the slurry density can be calculated for the pile at a distance of  $x < 1.5D$  as follows:

$$F_s = \frac{\left[\gamma H^2 \cos^2 \theta + (\gamma_s H_s^2 - 2F_{bh}) \sin^2 \theta - \gamma_w H_w^2\right] \tan \phi' \csc \theta}{\gamma H^2 \cos \theta + 2(F_s + F_b) \sin \theta - (\gamma_s H_s^2 - 2F_{bh}) \cos \theta} \quad 6.18$$

The factor of safety is considered to be lower in the case of  $x < 1.5D$  because the  $F_{bh}$  was added. However, the value of  $F_b'$  is relatively lower than the value of  $F_b$ . Indeed, the effect of  $F_{bh}$  could be only local and its effect on the global stability is considered to be a conservative assumption.

### 6.2.1.2 Three-dimensional approach of Case 1

This method takes into consideration the length of the panel (L), while the slip surface was assumed to be straight line and inclined with an angle  $\theta$  from the horizontal. A surcharge load (q) was assumed to be applied on the surface. The soil is considered to be cohesion-less soil with an effective friction angle  $\phi'$ , bulk density  $\gamma$  and saturated density  $\gamma_{sat}$ . The soil wedge in the three dimensions is assumed to be resisted by side shear forces (Ss) as shown in Figure 6-2. The failure surface is subjected to tangential and normal forces. The tangential forces as well as the normal forces should be in equilibrium as shown in Equations 6.19 and 6.20, respectively, in case of pile is at a distance  $x \geq 1.5D$ .

$$S + 2Ss + P_s \cos \theta = (W + Q + F_s + F_b) \sin \theta \quad 6.19$$

$$N = (W + Q + F_s + F_b) \cos \theta + P_s \sin \theta \quad 6.20$$

If the pile is at a distance  $x < 1.5D$ , Equation 6.21 shows the equilibrium of the tangential forces while Equation 6.22 shows the equilibrium of the normal forces.

$$S + 2Ss + (P_s - F_{bh}) \cos \theta = (W + Q + F_s + F_b) \sin \theta \quad 6.21$$

$$N = (W + Q + F_s + F_b) \cos \theta + (P_s - F_{bh}) \sin \theta \quad 6.22$$

The forces from the pile are calculated as Equations 6.8 through 6.11, while the other forces are to be calculated based on the following equations:

$$W = \frac{[\gamma(H^2 - H_w^2) + \gamma_{sat}H_w^2]L}{2 \tan \theta} \quad 6.23$$

$$Q = \frac{HqL}{\tan \theta} \quad 6.24$$

$$P_s = \frac{\gamma_s H s^2 L}{2} \quad 6.25$$

$$U = \frac{\gamma_w H_w^2 L}{2} \quad 6.26$$

By Substitution with the values of S that was presented in Equations 6.15, 6.19 and 6.20 the factor of safety in case of  $x > 1.5D$  and  $x < 1.5D$  can be found from Equation 6.27 and 6.28.

$$FS = \frac{[(W + Q + F_s + F_b) \cos \theta + P_s \sin \theta - U \csc \theta] \tan \phi'}{(W + Q + F_s + F_b) \sin \theta - P_s \cos \theta - 2Ss} \quad 6.27$$

$$FS = \frac{[(W + Q + F_s + F'_b) \cos \theta + (P_s - F_{bh}) \sin \theta - U \csc \theta] \tan \phi'}{(W + Q + F_s + F'_b) \sin \theta - (P_s - F_{bh}) \cos \theta - 2Ss} \quad 6.28$$

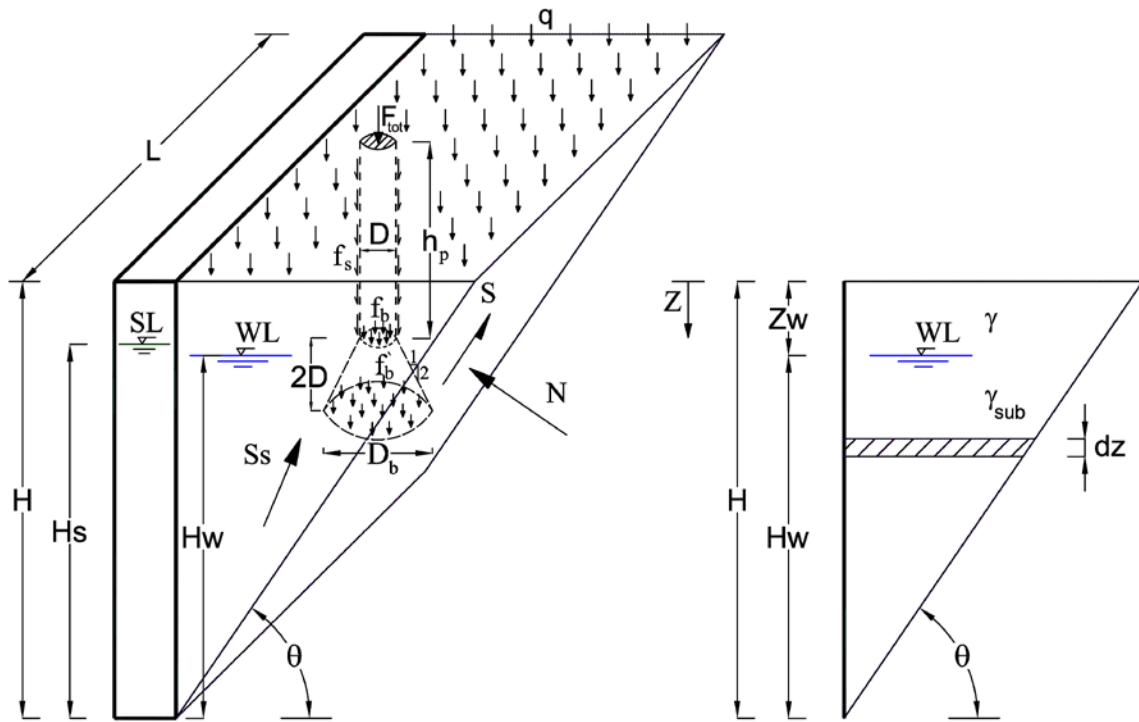


Figure 6-2: Pile above the failure surface (three-dimensional approach)

The side resistance  $Ss$  is also a function of the factor of safety and horizontal stress. It can be calculated by partial integration a slice, which is located in the side panel as shown in Figure 6-2. The following Equation 6.29 presents the shear resistance due to the side panel.

$$Ss = \frac{1}{FS \tan \theta} \left[ \int_0^{Z_w} \sigma_{h1}' \tan \phi' (H - Z) dz + \int_{Z_w}^H \sigma_{h2}' \tan \phi' (H - Z) dz \right] \quad 6.29$$

where

$Z$  is the variable depth from the surface

$Z_w$  is the water depth from the surface

dz is a slice at a certain depth

The horizontal earth pressure is calculated above and below the water level from the following equations:

$$\sigma_{h1} = K(q_r + \gamma Z_w) \quad 6.30$$

$$\sigma_{h2} = K(q_r + \gamma_{sub}Z + \gamma_w Z_w) \quad 6.31$$

where

K is the coefficient of earth pressure and its value can be used as discussed in section 3.5.1 in Chapter 3.

$q_r$  is the surcharge transfer to the side panels and it could be equal to or less than the value of the surface surcharge.

$\gamma_{sub}$  is the submerged soil density ( $= \gamma - \gamma_w$ )

$$S_s = \frac{k \tan \phi'}{F \tan \theta} \left[ \begin{array}{l} \left( \gamma - \frac{\gamma_{sub}}{3} \right) H_w^3 + \left( \gamma - \frac{\gamma_w}{2} \right) H^2 H_w + \frac{q_r H^2}{2} + \frac{\gamma_w H^3}{2} \\ - \left( 2\gamma + \frac{\gamma_{sub}}{2} \right) H H_w^2 \end{array} \right] \quad 6.32$$

The factor of safety in case of  $x > 1.5D$  can be rewritten as

$$FS = \frac{\tan \phi'}{\tan \theta} \left[ \frac{\Omega_1 \gamma + \Lambda_1 \gamma_{sat} - \Psi_1 \gamma_w + \zeta_1 \gamma_s + 2Hq + \Phi_1 q_r + \Gamma_1}{(H^2 - H_w^2) \gamma + H_w^2 \gamma_{sat} + 2Hq - H_s^2 \gamma_s + \Gamma_1} \right] \quad 6.33$$

Or in case of  $x < 1.5D$  it can be rewritten as

$$FS = \frac{\tan \phi'}{\tan \theta} \left[ \frac{\Omega_1 \gamma + \Lambda_1 \gamma_{sat} - \Psi_1 \gamma_w + \zeta_1 \gamma_s + 2Hq + \Phi_1 q_r + \Gamma_2 - \frac{2F_{bh}}{L} \tan^2 \theta}{(H^2 - H_w^2) \gamma + H_w^2 \gamma_{sat} + 2Hq - H_s^2 \gamma_s + \Gamma_2 + \frac{2F_{bh}}{L}} \right] \quad 6.34$$

where

$$\Omega_1 = H^2 - H_w^2 + \frac{2K}{3L \cos \theta} (H^3 - H_w^3) \quad 6.35$$

$$\Lambda_1 = H_w^2 + \frac{2K}{3L \cos \theta} H_w^3 \quad 6.36$$

$$\Psi_1 = H_w^2 \sec^2 \theta + \frac{2K}{3L \cos \theta} H_w^3 \quad 6.37$$

$$\zeta_1 = H_s^2 \tan^2 \theta \quad 6.38$$

$$\Phi_1 = \frac{2kH^2}{L \cos \theta} \quad 6.39$$

$$\Gamma_1 = \frac{2(F_s + F_b) \tan \theta}{L} \quad 6.40$$

$$\Gamma_2 = \frac{2(F_s + F'_b) \tan \theta}{L} \quad 6.41$$



The factor of safety from the three-dimensional analysis provides higher values of factor of safety than that calculated from the two dimensional and it gives the same results as Fox (2004) if the values of pile forces were set to zero. The existence of the pile above the failure surface reduces the factor of safety. However, if the panel length was infinite in the three dimensional analysis the effect of the pile on the trench is neglected. The location of the pile within the trench was not considered in the analysis.

### 6.2.2 CASE 2: PILE INTERSECTS THE FAILURE SURFACE

The pile could intersect with the slip surface if it is located at a short distance from the trench or its tip is deep. It is considered to intersect the slip surface if the pile with depth  $h_p$  is located at distance

$$x > \frac{H - h_p}{\tan \theta} \tag{6.42}$$

In this case, the pile end bearing is expected to be applied below the slip surface and hence it will not be a driving force, but only part of the pile friction will be added to the driving force. Additionally, the intersection of the pile structure with the slip surface creates a force that likely acts as a resistance for the failure wedge. The following subsections describe this case using two and three dimensional approaches.

#### 6.2.2.1 Two-dimensional approach of Case 2

In this case, the two-dimension analysis is the same as the first case but the pile bearing pressure is not acting and the friction force is partially acting. In addition, the difference in displacement between the soil and the pile during trenching creates resisting forces ( $F_{pr}$ ) at the intersection between the pile and the slip surface as shown in Figure 6-3.

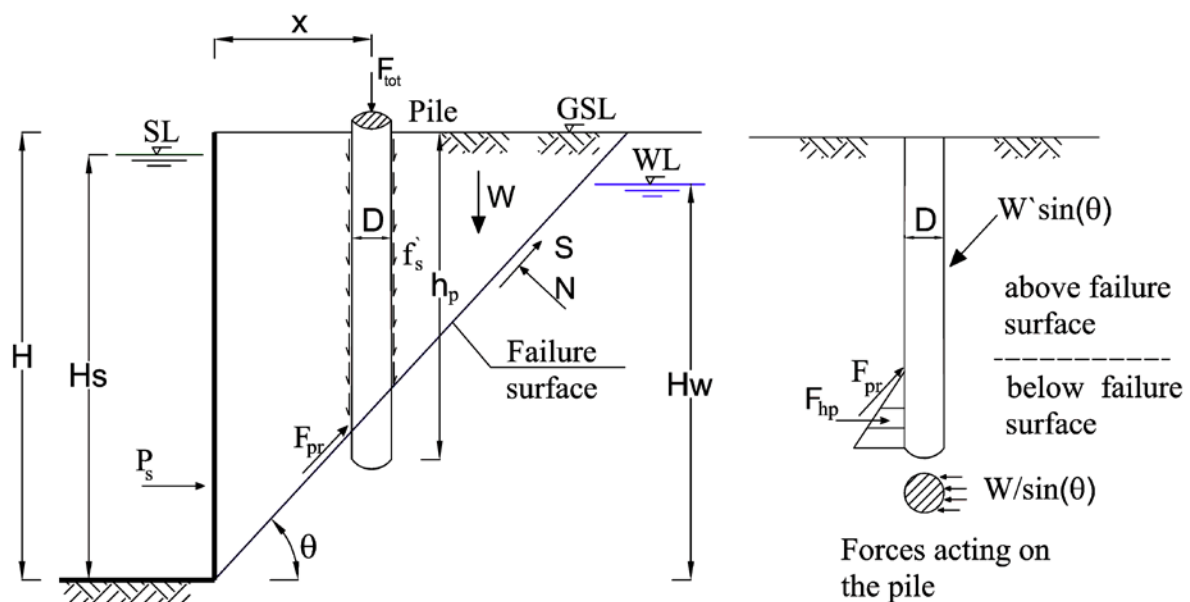


Figure 6-3: Pile intersects the failure surface (two-dimensional approach)

Above the failure surface an active force is assumed to be applied to the pile, while below the failure surface a passive earth pressure force ( $F_{hp}$ ) is created. The force of the pile that resists the failure wedge is assumed to be equal to the passive force if the active force is higher than the passive force, because the passive force is fully mobilized. The active force and passive pressure forces are calculated from Equations 6.43 and 6.44, respectively.

$$W = \frac{\gamma \pi D}{4} \left( \frac{H^2}{\tan \theta} - 2Hx + x^2 \tan \theta \right) \quad 6.43$$

$$F_{hp} = \frac{\gamma \pi D}{2} k_p (hp + x \tan \theta - H) \quad 6.44$$

In this case, where ( $W \sin \theta > F_{hp} \cos \theta$ ) the pile resisting force  $F_{pr}$  can be calculated from the following equation:

$$F_{pr} = F_{hp} \cos \theta \quad 6.45$$

The passive force is not fully mobilized for the piles which are far from the trench because they move from top higher than its bottom as presented in the parametric study. Accordingly, the pile resistance force to the moving wedge ( $F_{pr}$ ) is equal to the active force as follows:

$$F_{pr} = W \sin \theta \quad 6.46$$

The force transfer from the shaft to the wedge can be calculated from the following equation:

$$F_s = \frac{(H - x \tan \theta)}{h_p} F_s \quad 6.47$$

The factor of safety can then be calculated from Equation 6.48.

$$F_s = \frac{[\gamma H^2 \cos^2 \theta + \gamma_s H_s^2 \sin^2 \theta - \gamma_w H_w^2 + 2F_s \sin \theta \cos \theta] \tan \phi}{(\gamma H^2 \cos \theta + 2F_s \sin \theta - \gamma_s H_s^2 \cos \theta - 2F_{pr}) \sin \theta} \quad 6.48$$

### 6.2.2.2 Three-dimensional approach of Case 2

The three-dimensional effect of the pile intersection is similar to that previously discussed in the two-dimensional. The weight of the wedge in the active zone acting on the pile ( $W$ ) is shown in Figure 6-4 and it can be calculated from Equation 4.43 if  $H - H_w \geq H - x \tan \theta$ , but if it is smaller it can be calculated from Equation 4.49. The surcharge load that acts on the pile, was ignored.

$$W = \frac{\pi D \tan \theta}{4} [\gamma (H^2 - H_w^2) + \gamma_{sat} (H^2 - 2Hx \tan \theta + x^2 \tan^2 \theta)] \quad 6.49$$

The value of  $F_{pr}$  can be calculated as previously mentioned, while the new value of  $W$  should be taken into consideration. The factor of safety in this case is similar to Case 1 except for adding the value of the pile resisting force as shown in the following equation.

$$FS = \frac{\tan \phi'}{\tan \theta} \left[ \frac{\Omega_1 \gamma + \Lambda_1 \gamma_{sat} - \Psi_1 \gamma_w + \zeta_1 \gamma_s + 2Hq + \Phi_1 q_r + \Gamma_3}{(H^2 - H_w^2) \gamma + H_w^2 \gamma_{sat} + 2Hq - H_s^2 \gamma_s + \Gamma_3 - \frac{2F_{br}}{\cos \theta}} \right] \quad 6.50$$

The other factors were previously mentioned while the pile load effect is calculated from the following equation:

$$\Gamma_3 = \frac{2F_s \tan \theta}{L} \quad 6.51$$

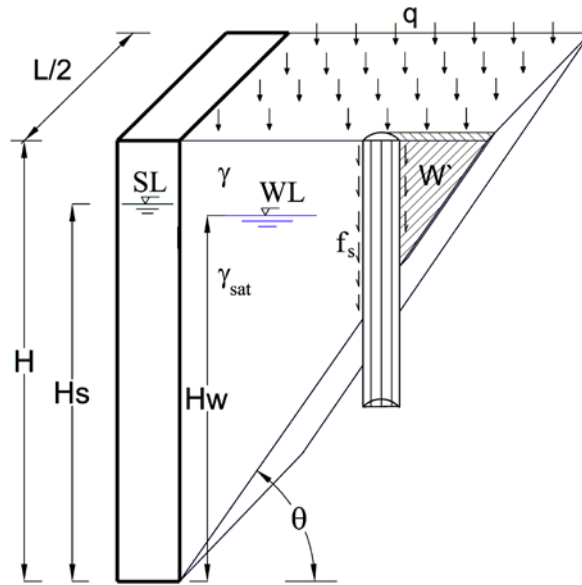


Figure 6-4: Pile intersects the failure surface (three-dimensional approach)

### 6.3 TRENCHING NEAR GROUP(S) OF PILES (SITUATION II)

The existing group(s) of piles near a trench may cause simultaneity, the both cases that were discussed in the previous section. The load of the pile near the trench could be fully added to the wedge of failure while the other piles far from the trench will be partially added or even act as a resistance for the wedge of failure. The pile near the trench could be in three locations as shown in Figure 6-5, two locations are presenting the first case (pile above failure surface) while the other locations presents the second case (pile below failure surface). If the pile is at a distance  $x > H/\tan \theta$  it will not have any effect on the trench stability. The trench stability could then be found for several piles from Equation 6.52.

$$FS = \frac{\tan \phi'}{\tan \theta} \left[ \frac{\Omega_1 \gamma + \Lambda_1 \gamma_{sat} - \Psi_1 \gamma_w + \zeta_1 \gamma_s + 2Hq + \Phi_1 q_r + n_c \left( \Gamma_2 - \frac{2F_{bh}}{L} \tan^2 \theta \right) + n_m \Gamma_1 + n_i \Gamma_3}{(H^2 - H_w^2) \gamma + H_w^2 \gamma_{sat} + 2Hq - H_s^2 \gamma_s + n_c \left( \Gamma_2 + \frac{2F_{bh}}{L} \right) + n_m \Gamma_1 + n_i \left( \Gamma_3 - \frac{2F_{br}}{\cos \theta} \right)} \right] \quad 6.52$$

where

$n_c$  is the number of piles that are very close to the trench and located at  $x < 1.5D$

$n_m$  is the number of piles that are located above the failure surface and at a distance  $x \geq 1.5D$  and  $n_i$  is the number of piles at certain distance  $x$  and intersect with the slip surface.

The above equation could be used to check the trench panel stability near a group of piles. However, the shaft friction value of the pile is subjected to be change depending on the pile location from the trench as mentioned before in Chapter 5. The amount of decrease in shaft friction according to the pile location was previously presented in Table 5-5.

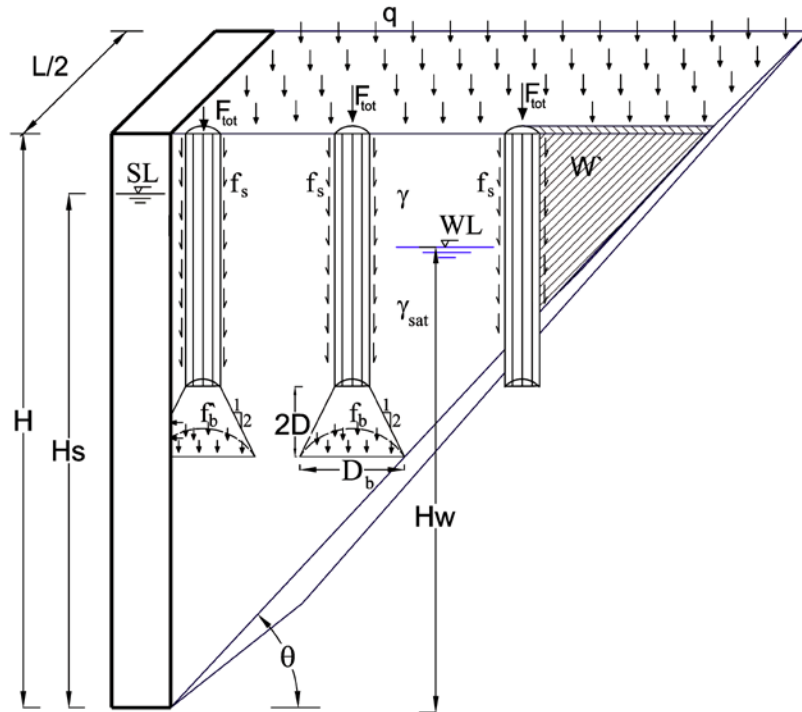


Figure 6-5: Several piles intersect the failure surface (three-dimensional approach)

## 6.4 COMPARATIVE STUDY

This study compared between the factor of safety according to Fox (2004) in case of no piles and the present approach with piles at different locations and numbers. The factor of safety calculated from the present approach is the same as that calculated by Fox (2004) in case of no piles. The following sections show the different parameters used in the comparative study calculated using the two- and three-dimensional analytical approaches. In all cases, the pile forces  $f_s$  and  $f_b$  are assumed to be equal to the pile shear resistance  $\tau_s$  and end bearing resistance  $q_b$ , respectively. These values are calculated based on Equations 2.2 and 2.4 presented in Chapter 2 and they were divided by a factor of safety based on the Egyptian code of Practice 202/4(2001).

### 6.4.1 COMPARISON REGARDING TWO-DIMENSIONAL ANALYSIS APPROACH

The comparison in two dimensions was made for different friction angles, slurry densities and water levels. The following Figures 6-6, 6-7 and 6-8 show the different effect of each parameter in case of no pile and existing pile with different locations. The trench depth was

fixed to be 30 m, while its thickness and length were not considered in the two-dimensional analysis. The failure plane inclination angle ( $\theta$ ) was fixed to be  $45 + \phi/2$ . The pile length and diameter were 12 m and 0.8 m, respectively. The soil density equal to  $18 \text{ kN/m}^3$  and the slurry level was 0.5 m below ground surface.

The values of factor of safety presented did not necessarily show the minimum factor of safety value because the failure surface angle is not always to equal  $45 + \phi/2$ . However, these values are not expected to be far from the minimum factor of safety values, also the trend of factor of safety change is not greatly affected by the surface inclination. The friction angle, slurry density and water levels have an effect on the stability of the slurry trench. The pile existence within the slip surface reduces the factor of safety values. However, it did not show a noticeable difference when it located very close to the trench because the generated horizontal force ( $F_{bh}$ ) is relatively small.

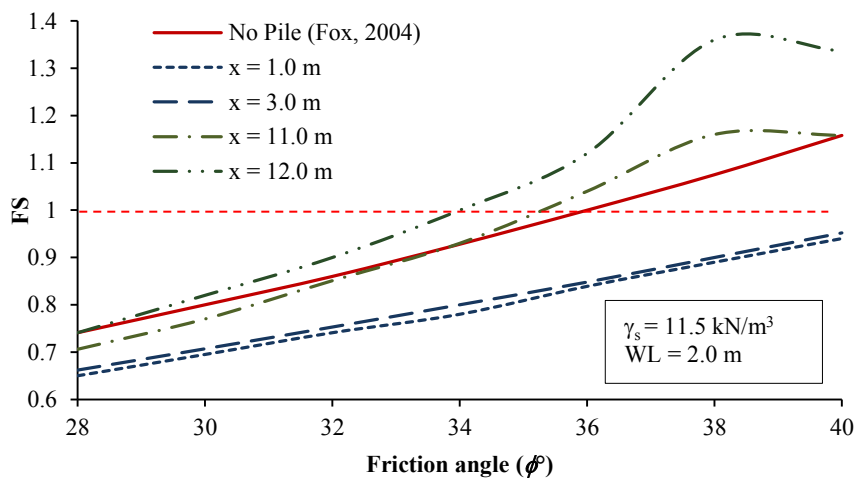


Figure 6-6: Effect of different friction angles on factor of safety (two-dimensional approach)

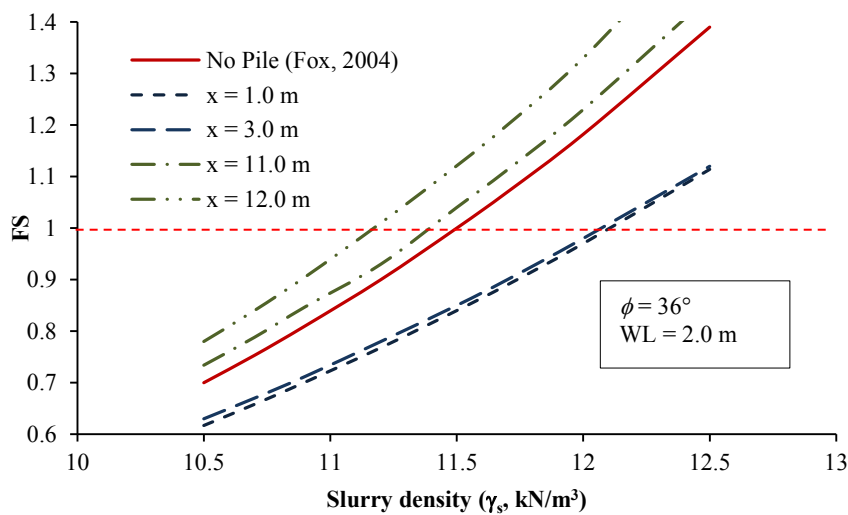


Figure 6-7: Effect of different slurry densities on factor of safety (two-dimensional approach)

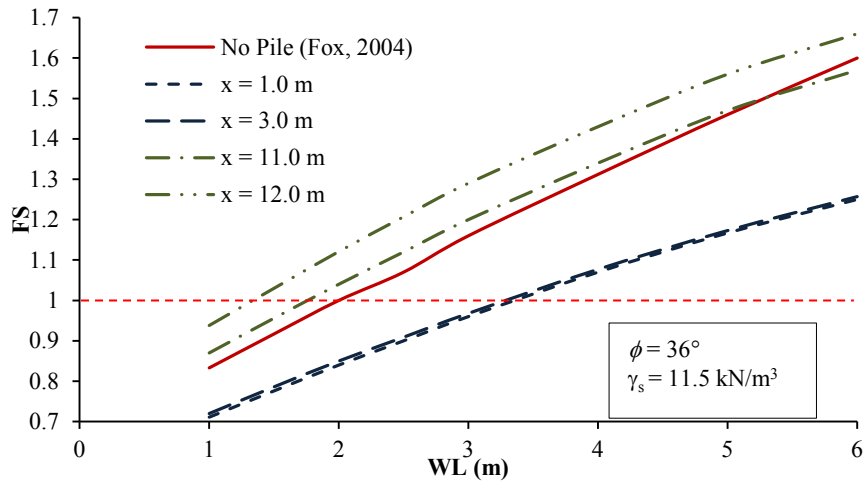


Figure 6-8: Effect of different water levels on factor of safety (two-dimensional approach)

The pile intersection with the slip surfaces increases the factor of safety but according to the position of intersection and amount of retained soil by the pile. The following Figure 6-9 shows the change in the factor of safety values at different locations of the pile near the trench.

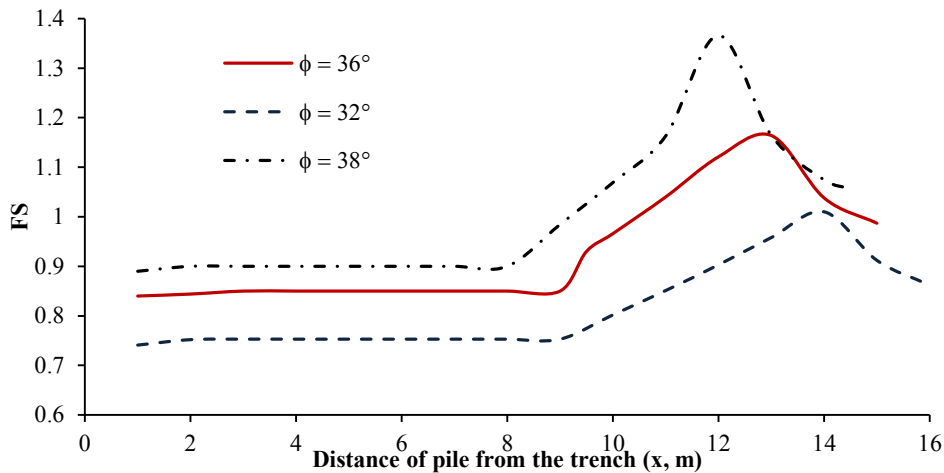


Figure 6-9: Effect of pile location on factor of safety (two-dimensional approach)

#### 6.4.2 COMPARISON REGARDING THREE-DIMENSIONAL ANALYSIS APPROACH

In all cases, the three-dimension analysis provides a higher factor of safety than the two-dimension analysis. The following Figure 6-10 shows a comparison between the three and two-dimensional analysis approaches. The comparison was made for the pile at different locations from the trench. The panel length was chosen to be 6 m. All the other effective parameters are the same.

The three-dimension analysis shows a higher factor of safety than the two-dimension analysis, because it takes into consideration the effect of side friction and panel length. Such a difference was discussed and presented by Fox (2004 and 2006). However, if the panel length was chosen to be more than 6 m the results could be different. Accordingly, the effect of panel length on the factor of safety was separately studied and presented in Figure 6-11.

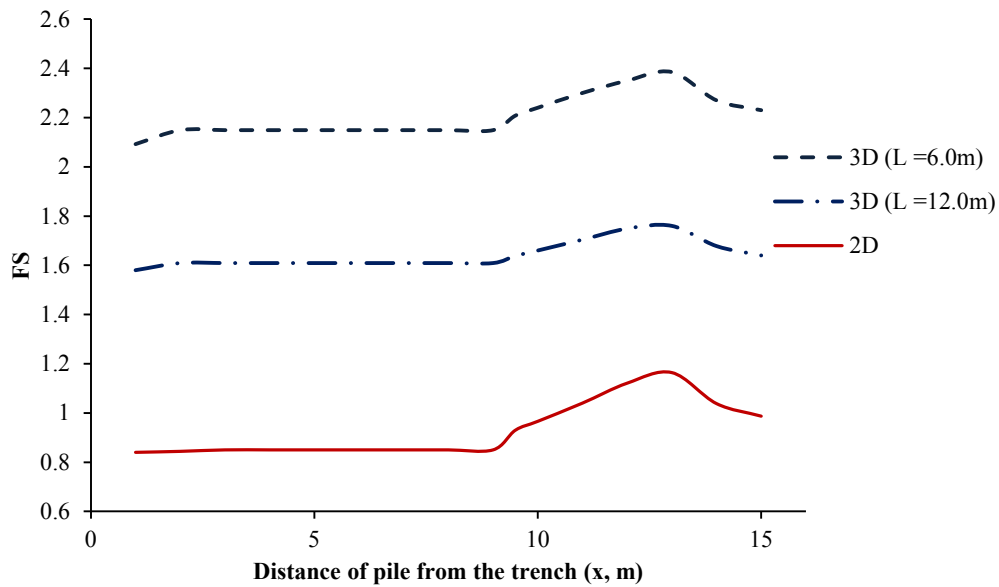


Figure 6-10: Difference between two and three dimensional analytical approaches

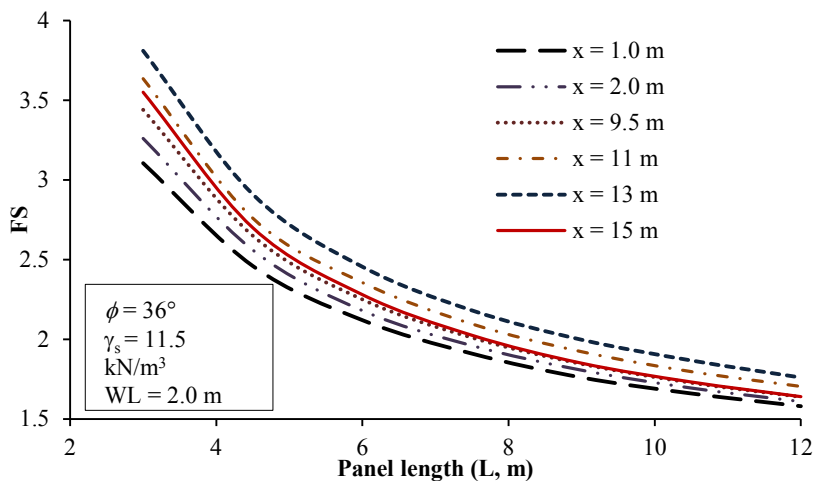


Figure 6-11: Effect of panel length at different pile locations on safety factor

The effect of different inclination angles on the factor of safety at different pile distances from the trench ( $x$ ) is presented in Figure 6-12. The inclination angle values were chosen around the value of  $45 + \phi/2$  and the friction angle in this case is equal to  $36^\circ$ .

The inclination angle of failure surface ( $\theta$ ) that provides the lowest factor of safety could be considered to be  $50 + \phi/2$  according to the results presented in the figure. However, the rest of the work will depend on the value of  $45 + \phi/2$ .

The different slurry level effects on the factor of safety for the three values of panel lengths are presented in Figure 6-13. The friction angle considered constant and equal to  $36^\circ$ , while the pile was chosen to be fully inside the failure wedge. The effect of the slurry level on the factor of safety is linear. The low level of slurry could cause the trench to be unsafe, especially if the trench panel has a greater length.

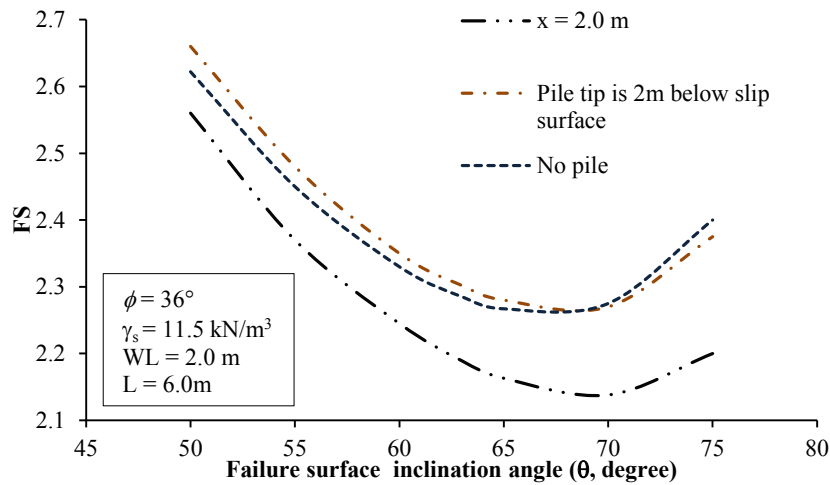


Figure 6-12: Effect of failure surface inclination angle on safety factor

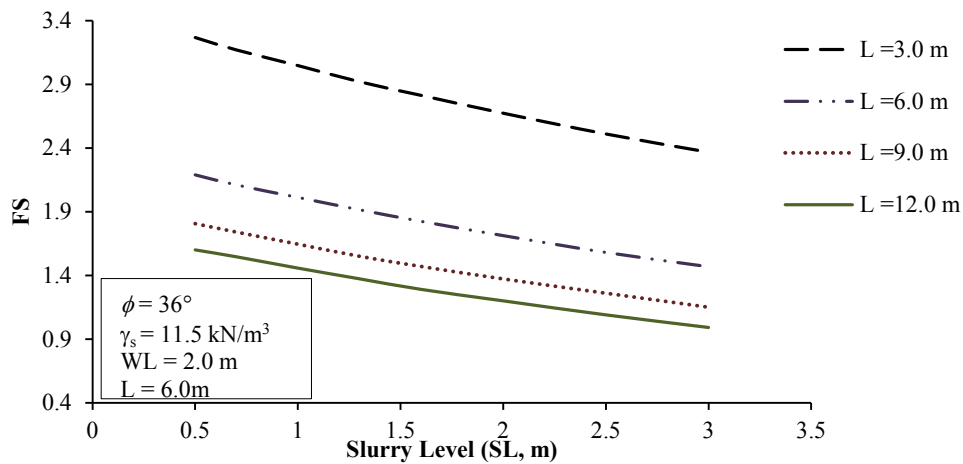


Figure 6-13: Effect of slurry level on safety factor

### 6.4.3 COMPARISON REGARDING THE EFFECT OF SEVERAL PILES

The effect of several piles on the trench factor of safety was presented in Equation 6.52. The comparison was made for different panel lengths, while friction angle was  $36^\circ$ , the water level was 2.0 m and slurry level was 0.5 m below ground surface. Different piles locations were chosen in the comparison including the case of no piles. The following Figure 6-14 describes the cases.

As shown in the sketched figure, the first case considered two piles that are fully inside the failure wedge and do not cause horizontal forces. The second considered four piles fully inside the failure wedge, while two of them are close to the trench and creating force ( $F_{bh}$ ). The third case added another two piles that intersect with the failure surface and penetrate 4m below it. The fourth and last case considered two piles fully inside the failure wedge and four piles intersect the failure surface, while two of them penetrate 4 m below the failure surface and the other two penetrate 8 m below the failure surface. Figure 6-15 shows the comparison between the different cases for different panel lengths.



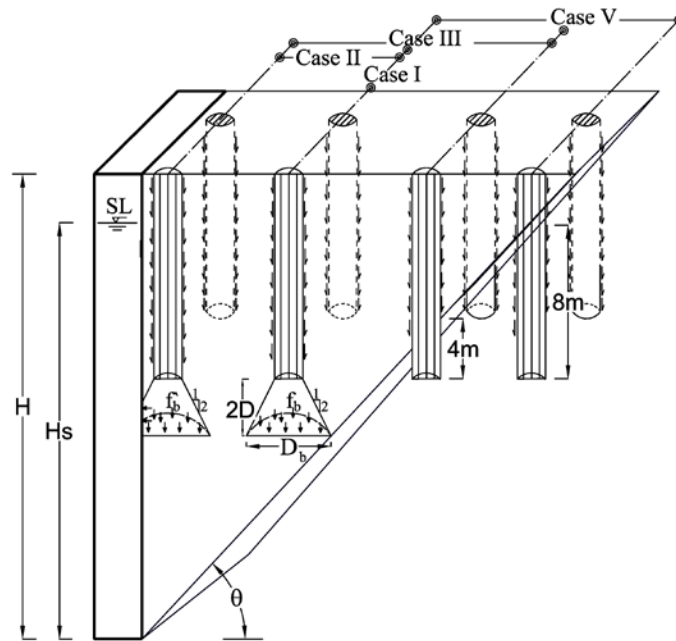


Figure 6-14: The cases used for comparison

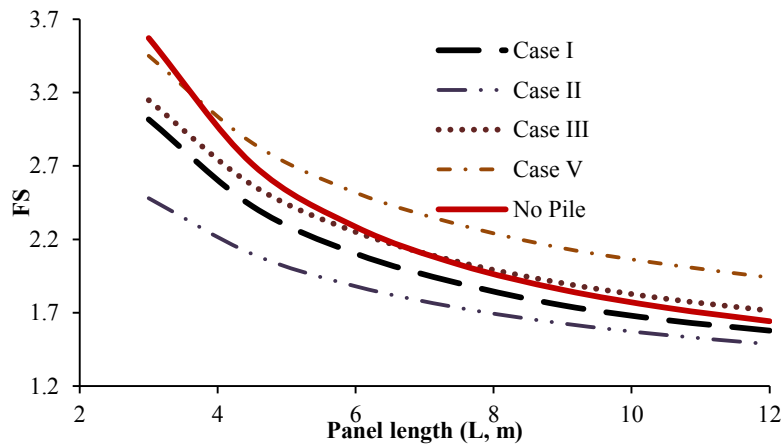


Figure 6-15: Comparison between the different cases

The previous curve showed that the factor of safety from Case I and Case II was lower than the factor of safety in case of no pile, while in Case III the factor of safety was higher because the intersection of two piles with the failure surface balanced with the other two piles that are located above the failure surface. The factor of safety in Case V was the highest because more number of piles intersect the failure surface.

## 6.5 COMPARISON BETWEEN FACTOR OF SAFETY FROM THE PROPOSED APPROACH AND NUMERICAL ANALYSIS

This section uses the numerical analysis to find out the factor of safety and compare it with that from the proposed analytical approach. The method that used to calculate the safety factor in FLAC 3D and the numerical modeling are presented in the following two sections. The factor of safety results calculated from the numerical analysis were compared to that from the proposed approach and presented in the last section.

### 6.5.1 FACTOR OF SAFETY CALCULATION IN FLAC 3D

The safety factor in FLAC 3D is determined based upon the strength reduction method (parameter reduction technique). This method can be applied to different underground structures including the slurry trench and is described in detail by (Itasca (2011)). In this method, The factor of safety is calculated by reducing the shear strength of the material to bring the soil around the trench (failure wedge) to the limit equilibrium state. The safety factor is calculated for the cohesion-less soils by using a series of simulations with different trial values of safety factor to reduce the friction angle until failure occurs. The following Equation 6.53 presents this technique.

$$\phi^{trial} = \arctan\left(\frac{1}{F^{trial}} \tan \phi\right) \quad 6.53$$

The safety factor in FLAC 3D is calculated by finding initially the stable and unstable states, and then the difference between these states could be reduced to a specified tolerance. A separated run with different strength reduction factors determines the stability and instability. Each run determines the continuity of the plastic flow or the equilibrium.

### 6.5.2 NUMERICAL MODELING FOR FACTOR OF SAFETY CALCULATION

The Mohr column model was used for modeling the soil while the trench and the pile were modeled as described before in Chapter 4. The problem was modeled and half of it is shown in the typical mesh model in Figure 6-16a, while the typical shape of failure is shown in Figure 6-16b. The trench was chosen to be 30 m depth and the pile diameter was 0.8 m.

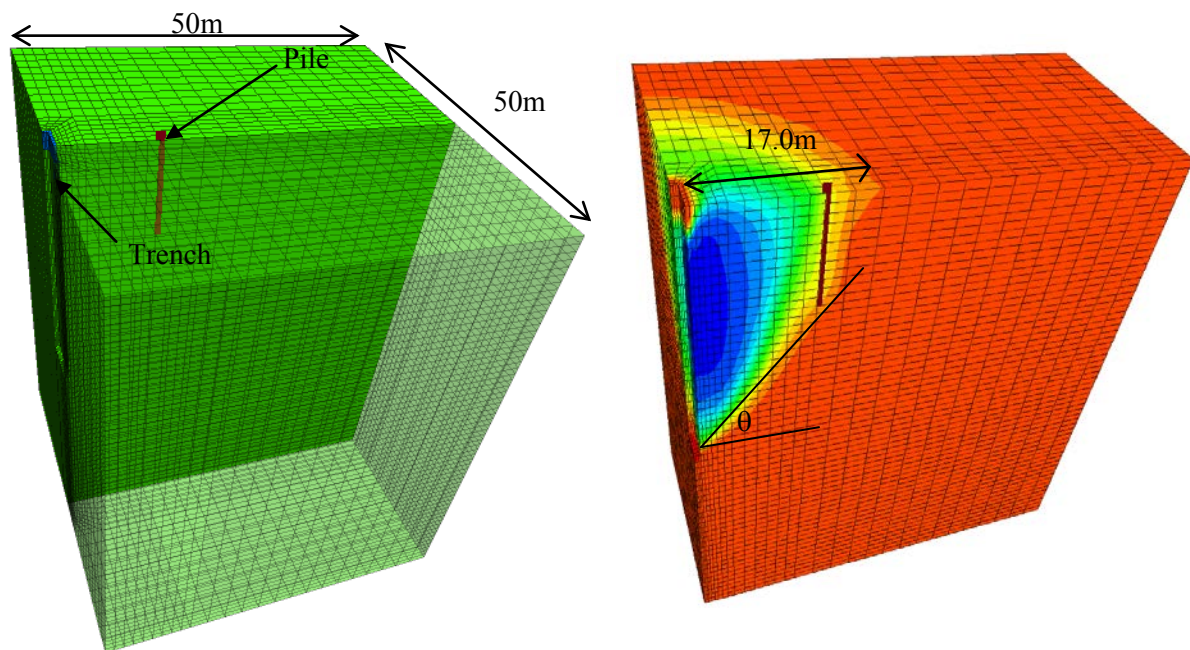


Figure 6-16: Typical numerical modeling mesh for factor of safety calculation

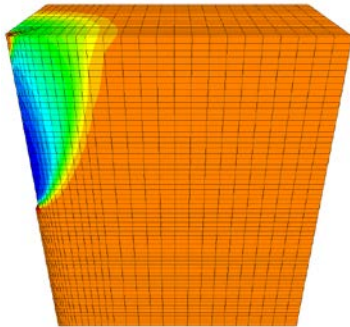
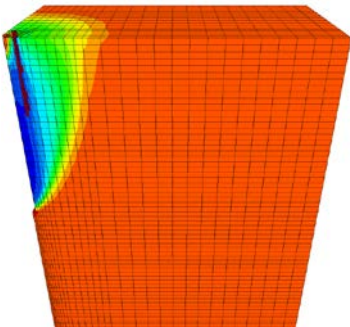
### 6.5.3 Factor of safety values and comparison

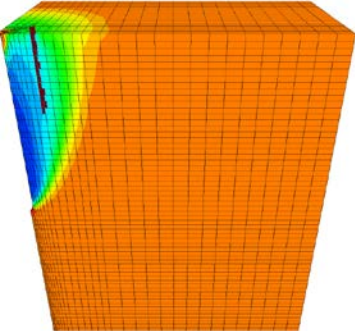
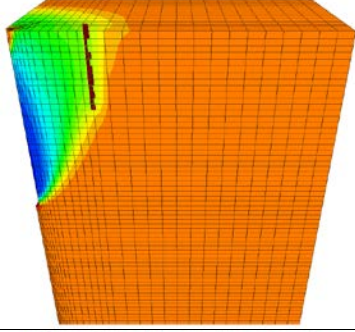
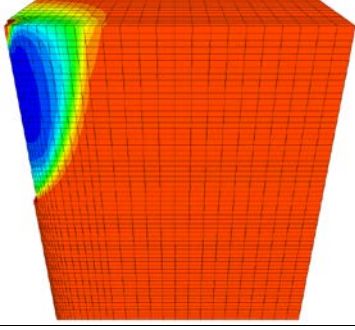
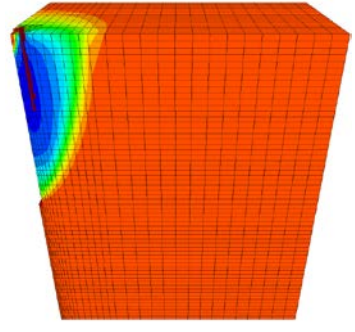
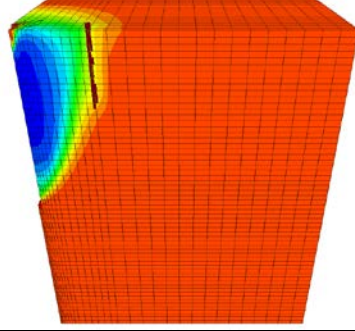
Different cases including different pile locations were simulated with FLAC 3D. Table 6.1 presents the shape of failure and the results of the factor of safety from the numerical analysis before and after correction. The values of the proposed simple analytical approach are also presented.

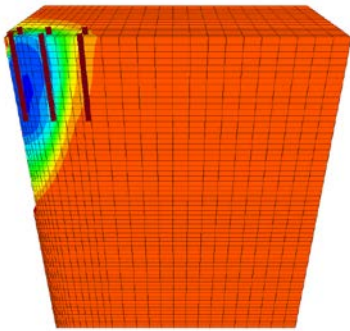
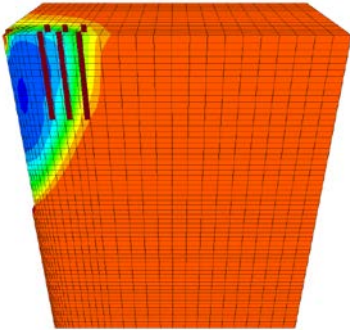
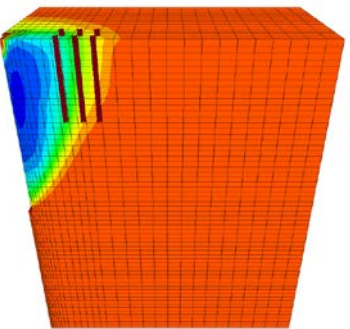
The factor of safety from the numerical analysis was corrected by dividing it with a factor of 1.30 because the strength reduction method is more oriented to the slope stability problem, and in the slurry trenching problems it provides a higher safety factor. In addition, this method did not take into consideration the reduction in tensile strength which may have an effect. The assumed shape of failure from the top was rectangular while in the numerical analysis it was half shape. The correction factor value was chosen as the average ratio between the numerical and analytical approach for the case of no pile. The ratio between the corrected numerical analysis factor of safety values and the proposed simple analytical approach was not exceeding 1.11 with an average different value of 1.01.

The effect of pile on the shape of failure in the numerical analysis was obvious on the shape of failure presented in Table 6.1. The slip surface from the numerical approach is inclined by an angle of approximately  $60^\circ$  ( $42 + \phi/2$ ) but after it intersects the pile the angle of inclination slightly changed.

Table 6-1: Different studied cases for trench stability

Case number	Description			Shape of failure	Values of FS		
	Panel	Pile	x (m)		Numerical analysis		Proposed approach
					Results	Corrected	
1	3 m	No pile			3.75	2.89	3.19 (Fox, 2004)
2		Single pile	2.5		3.63	2.79	2.93

Case number	Description			Shape of failure	Values of FS		
	Panel	Pile	x (m)		Numerical analysis		Proposed approach
					Results	Corrected	
3			5.0		3.66	2.81	2.93
4			12.0		3.73	2.87	3.33
5	6 m	No pile			2.89	2.2	2.0 (Fox, 2004)
6	6 m	Single pile	2.5		2.8	2.15	1.93
8			12.0		2.88	2.2	2.12

Case number	Description			Shape of failure	Values of FS		
	Panel	Pile	x (m)		Numerical analysis		Proposed approach
					Results	Corrected	
9	6 piles		2.3, 6.5 and 11.8		2.52	1.93	1.85
10			6.5, 9.1 and 11.8		2.65	2.2	1.89
11			9.0, 11.8 and 14.0		2.76	2.3	2.08

## 6.6 SUMMARY

This chapter provided a simple analytical approach to show the effect of a single pile or several piles on the stability of the slurry trench. The approach provided equations in two and three dimensions to solve the factor of safety in case of different pile locations from the trench.

A comparative study was made in order to understand the different parameters effect on the trench stability. The pile that is located totally inside the failure zone causes a decrease in the factor of safety, while the pile that intersects the slip surface could increase the factor of safety. The piles row which contains piles intersects the failure surface and others that are totally inside the failure wedge could cause the factor of safety to be almost equal to that from the case of no piles. This fact could explain the reason behind the stable trench near the piled foundations in the previously discussed case studies.

The last part of the chapter provided a comparison between the numerical analysis and the proposed analytical approach regarding factor of safety values. The correct values of safety factor from the numerical approach were in a good contrast with those obtained from the

proposed approach. The shape of failure from the numerical analysis was almost identical to that assumed in the numerical analysis but in the top it takes a half circle rather the assumed rectangular shape. The proposed analytical approach provided equations that are useful to solve the stability problem of the trench that trenched near a piled foundation.

This method is limited to the cohesion less soil and the local stability of the trench. It also considered the slurry pressure is fully acting on the trench wall. It did not take into consideration the increase of trench stability due to the penetration of the bentonite slurry into the soil through the filter cake.

## CHAPTER 7: CONCLUSIONS AND RECOMMENDATIONS

The existing deep foundations inside the city were normally designed to carry a certain amount of loads under specified conditions. These piles could be subjected to a passive load due to the different construction activities inside the cities. Slurry trenching causes a passive load but a very limited research was made about such a source of passive load on existing piles. This research has focused on the effect of the trenching process on ground surface and the nearby piled foundation. In addition, it studied the effect of the existing piles on the trench panels stability. The following sections discuss the conclusion and recommendation from this research.

### 7.1 SOIL DEFORMATION DUE TO TRENCHING

In this research, the values of settlement and horizontal movement associated with the trenching process were discussed based on the data from the literature. These values vary from project to another based on several factors such as groundwater level, slurry level, soil profile and panels dimension. The construction stages of the panels also affect the ground deformation. During the trenching process of a panel, the ground is deformed to a maximum but after concreting the deformation reduces. However, the deformation could be affected by constructing other nearby panels. Generally, the trenching effect on the ground deformation decreases with distance far from the trench.

The data of the settlement were plotted from different construction sites. These data were divided into three main bounds and each bound was defined by a curve. The upper bound defines the values related to very low values of settlement due to short panels and good soil conditions. The middle bound related to the larger panel length and relatively poor ground conditions. The lower bound showed high settlement values that could have happened due to a problem during trenching such as weak soil layer at some levels.

The values of the soil horizontal displacement were collected from different articles. The maximum values were located at different depths according to soil condition and groundwater level. Two bounds were chosen for dividing the data. The upper bound was used to define the low values which related to the small panel length, high slurry level and good soil conditions, while some of these values were found far from the trench. The lower bound was the limit of values under the normal conditions. The values that were higher than those of the lower bound were due to lowering the slurry level. The negative values of horizontal displacement were found due to the high values of slurry level.

## 7.2 EFFECT OF TRENCHING ON THE EARTH PRESSURE COEFFICIENT

The slurry trenching process affects the horizontal earth pressure of the soil and the earth pressure coefficient. Several researchers monitored the change in horizontal earth pressure during trenching. The available data from six different articles showed that the coefficient of earth pressure reduced due to trenching with a percentage varying between 10% and 30%.

## 7.3 NUMERICAL MODELING OF THE TRENCHING PROCESS NEAR PILED FOUNDATION

The numerical simulation of the trenching process in general and near piled foundation in specific was done using FLAC 3D for several cases. The simulations were made for one field panel test and two different projects and one laboratory test with different sets.

The horizontal displacement shape and value from the numerical analysis were in a good agreement with those from the field tests but the settlement values did not show such an agreement. However, the settlement values and shapes predicted from the numerical analysis were quite close to those from the two case histories and laboratory works.

The results of pile deflection, bending moment and shaft friction from the laboratory were not in a good contrast with those from the numerical analysis. The results from the laboratory were affected by the pile eccentric loading.

Generally, it is not possible to find a perfect match between the numerical analysis results and those from field or laboratory. The output data from the field or laboratory are subjected to several conditions and they did not have a constant trend, while the results from the numerical analysis depend on mathematical equations, which provide a systematical trend. Accordingly, the verification was made for field test, two case histories and one laboratory test to achieve a wide comparison between numerical analysis and the field or laboratory results. Generally, the comparison showed that the numerical analysis is a reliable tool that can be used for simulating such a problem with acceptable accuracy.

## 7.4 PARAMETRIC STUDY

The effect of trenching process on the ground surface and hence nearby piled foundation is affected by several parameters. The verified numerical analysis method and software were used to study the effect of some of these parameters on pile deflection, bending moment and shaft friction. The studied parameters included trench dimension, groundwater level, soil strength parameters, slurry level, pile group location, slurry pressure reduction at some levels, pile length and pile diameter. In addition, the effect of multiple panels on connected pile groups and piled raft foundation was studied as well. The effect of each parameter combined with



some other parameters was presented through 21 parameter combinations. The effect of the different parameters on the pile deflection bending moment and shaft friction is presented in the following sections.

#### 7.4.1 DEFLECTION OF THE PILE

The soil deformation due to trenching causes the pile to deflect towards the trench. The shape and value of this deflection vary according to several variables. The soil horizontal movement due to trenching and the pile position within the pile group are the main factors that control the pile deflection shape. The piles within the group and nearest to the trench tend to move with the soil. In this way, its maximum deflection could be found within the middle or lower third of them, while the maximum deflection of the rear piles within the group is normally found at the top. The rear piles are normally affected by the drag force from the front piles more than the soil deformation itself. However, the deflection values of the piles are affected by their stiffness, length, location from the trench and position within the group as well as the soil deformation. The deformation of the soil is affected by the trench dimension, groundwater level, soil properties, slurry level and continuity of the slurry pressure.

The panel length has a greater effect on the pile deflection than the other two dimensions. The slurry level and groundwater level have a great effect on the pile deflection as well. In general, the reduction of the slurry pressure at some levels causes an increase in pile deflection. The greatest increase was found when the slurry pressure reduced near the pile tip. The larger the pile diameter the lower its deflection. The deflection shape of the pile is affected by its length and the deflection values for the longer piles are lower than for the shorter ones, because the fixation depth is longer.

During staged construction of multiple panels, the deflection values and shape of the piles are subjected to change. The amount of change is depending on the pile location from the initial panel and within the piled foundation. The deflection of the pile nearest to the initial panel decreases with advancing on trenching the other panels.

Generally, the amount of deflection is considered to be low for the normal cases but it is very high and could be critical in case of a very low slurry pressure, high groundwater table or decrease of slurry pressure.

#### 7.4.2 BENDING MOMENT OF THE PILE

The trenching process causes a passive load on the pile. This passive load is a lateral load that causes a bending moment on the pile. The bending moment value and shape are affected by the relative movement between the pile and the soil. The maximum bending moment value is found at the pile top and it decreases gradually until it reaches a minimum value at its tip. For

this reason, the pile within the group considered fixed from its top and it moves with the soil at its tip.

The different values of trench depth and thickness cause a very low change in the bending moment values, while the change in panel length greatly affects the binding moment values. The pile bending moment values were slightly affected by the pile position within the group but they were greatly affected by its location from the trench. The change in pile length did not show a great effect on the bending moment, while the change in diameter causes a great effect. The slurry level and the reduction of the slurry pressure affects the bending moment values. The greatest effect was due to the slurry pressure reduction near the pile tip. The values and signs of the bending moment of a pile within a piled foundation changed during different stages of panels construction. This change was greater in case of piled raft foundation and it was less in case of connected pile group, because the connection between the piles in case of piled raft foundation is higher.

#### 7.4.3 PILE SHAFT FRICTION

During the trenching process, the shaft friction of the pile is affected by the change in the soil effective horizontal stress. The relative vertical movement between the pile and the soil affect the shaft friction. The piles within the pile group tend to balance the load carried by the pile cap. Accordingly, the shaft friction reduces from the origin value for the piles closest to the trench while it could increase for the other piles. However, it was not greatly affected by the location of the pile from the trench. The different in trench depth and thickness did not show a great effect on the shaft friction as well as the difference values of slurry levels and soil properties. The different values of groundwater levels, panel length and pile diameter are corresponding to a big difference of shaft friction values. The reduction of slurry pressure at some locations causes a great decrease in pile shaft friction.

#### 7.5 EFFECT OF PILE ON TRENCH STABILITY

The stability of the trench is affected by the existence of the piled foundation. A wedge of failure was assumed and analyzed in two and three dimensions in order to predict the factor of safety equations for slurry trench near piled foundation. If the pile is located in the failure wedge its vertical force will be totally transferred to the wedge as an active force. In addition, a horizontal force from the pile end bearing is assumed to be applied on the trench wall if the pile is located at a distance less than  $1.5D$  from the trench. A horizontal passive force is assumed to be created if the pile intersects the failure surface.

A comparative study was made to understand the effect of the different locations of the pile or pile row on safety factor. The pile located inside the failure wedge reduces the safety factor, but

if the pile is located at very close distance from the trench ( $<1.5D$ ) its horizontal force that created on the trench wall has very low effect. The pile that intersects the failure surface will not necessarily increase the factor of safety and it depends on the horizontal passive force. The pile group effect on the slurry trench stability is depend on the number of piles located inside the failure wedge and the other intersects the failure surface.

The factor of safety was calculated using numerical analysis. The numerical analysis provides a slightly higher safety factor than the proposed analytical solution.

## 7.6 RECOMMENDATION FOR FURTHER WORK

This research focused on studying the trenching process on nearby piled foundation. As recommended by Choy (2004), this research took into consideration the effect of the groundwater table. It also considered the trenching effect on the pile group, the connected pile groups and the piled raft foundation. However, this research did not study the problem in cohesive and layered soils.

The following is recommended for future research

- Includes the soil cohesion and considers the layered soils in the parametric study.
- Model the pile using solid or shell element.
- Use the silo shaped failure wedge in the analytical approach instead of the planer failure wedge.
- Verify the analytical approach and main results from the parametric study using laboratory experiments.
- Study the effect of deep excavation and trenching process together on the nearby piled foundations.

## REFERENCES

- Aas, G. (1976): Stability of slurry trench excavation in soft clay. In *Norwegian Geotechnical institute Oslo* 111.
- Abdel Rahman (2007): Construction Risk Management of Deep Braced Excavations in Cairo. In *Australian Journal of Basic and Applied Sciences* 1 (4), pp. 506–518.
- Abdel-Rahman, A. H.; El-Sayed, S. M. (2002b): Building Subsidence Associated with Cut-and-Cover Excavations in Alluvial Soils. In *Faculty of Engineering Scientific Bulletin, Ain Shams University* 37 (4), pp. 55–71.
- Abdel-Rahman, A. H.; El-Sayed, S. M. (2002a): Settlement Trough Associated with Diaphragm Wall Construction in Greater Cairo. In *the Journal of the Egyptian Geotechnical Society*.
- Abdel-Rahman, A. H.; El-Sayed, S. M. (2009): Foundation subsidence due to trenching of diaphragm walls and deep braced excavations in alluvium soils. In Proceedings of the 17th international geotechnical engineering conference. Alexandria, Egypt (3), pp. 1935–1938.
- American Petroleum Institute (2002): Recommended practice for planning, designing, and constructing fixed offshore platforms - Working stress design. 21<sup>st</sup> ed. Washington, DC: American Petroleum Institute.
- Bauer, Jörg (2016): Seitendruck auf Pfahlgründungen in bindigen Böden infolge quer zur Pfahlachse wirkender Bodenverschiebungen. PhD dissertation. Kassel University.
- Byrne, P. M., S. S. Park and M. Beaty. (2003): Seismic Liquefaction: Centrifuge and Numerical Modeling. in FLAC and Numerical Modeling in Geomechanics. In *Proceedings of the 3rd International FLAC Symposium, Sudbury, Ontario, Canada*, pp. 321–331.
- Carter, J. P.; Booker, J. R.; Yeung, S. K. (1986): Cavity expansion in cohesive frictional soils. In *Géotechnique* 36 (3), pp. 349–358.
- Chen, J.; Lei, H.; Wang, J. (2014): Numerical analysis of the installation effect of diaphragm walls in saturated soft clay. In *Acta Geotechnica* 9, pp. 981–991.
- Chen, L. T.; Poulos, H. G. (1996): Piles Subjected to Lateral Soil Movements. In *Journal of Geotechnical and Geoenvironmental Engineering* 123 (9), pp. 802–811.
- Chin, F. K. (1970): Estimation of the Ultimate Load of Piles from Tests Not Carried to Failure. In Proceedings of the Second Southeast Asian Conference on Soil Engineering. Singapore, 11-15 June, pp. 81–92.
- Choy, C. K. (2004): Installation effects of diaphragm walls on adjacent piled foundations. PhD Dissertation. University of Cambridge, UK.

- Choy, C. K., Standing, J. R. and Mair, R. J. (2007): Stability of a loaded pile adjacent to a slurry-supported trench. In *Géotechnique* 57 (10), pp. 807–819.
- Clough, G. W. and O'Rourke, T. D. (1990): Induced Movements of Insitu Walls. In *Design and Performance of Earth Retaining Structures, ASCE Geotechnical Special Publications 25*, pp. 439–470.
- Cole, K. W. (1980): The South abutment of Kessock Bridge. Scotland. In. Proceeding of IABSE Conference. Vienna.
- Comodromos, E. M.; Papadopoulou, M. C.; Konstantinidis, G. K. (2013): Effects from diaphragm wall installation to surrounding soil and adjacent buildings. In *Computers and Geotechnics* 53, pp. 106–121.
- Cowland, J. W.; Thorley, C. B.B. (1985): Ground and building settlement associated with adjacent slurry trench excavation. In. Proceedings of the Third International Conference on Ground Movements and Structures. Cardiff, England, pp. 723–738.
- Davies, R.V. and Henkel, D. (1982): Geotechnical problems associated with the construction of Charter Station, Hong Kong. In *The Arup Journal* 17 (1), pp. 4–10.
- De Moor, E. K. (1994): An analysis of bored pile/diaphragm wall installation effects. In *Géotechnique* 44 (2), pp. 341–347.
- DiBiagio, E.; Myrvoll, F. (1972): Full Scale Field Tests of a Slurry Trench Excavation in Soft Clay. In *Norwegian Geotechnical institute Oslo* 91, pp. 39–49.
- Egyptian code of Practice 202/4, 2001: Egyptian code of soil mechanics and foundation design.
- Ellis, E. A.; Durrani, I. K.; Reddish, D. J. (2010): Numerical modelling of discrete pile rows for slope stability and generic guidance for design. In *Géotechnique* 60 (3), pp. 185–195.
- Elson, W. K. (1968): An Experimental Investigation of the Stability of Slurry Trenches. In *Géotechnique* 18, pp. 37–49.
- Farmer, I. W. and Attewell, P. B. (1973): Ground movements caused by a bentonite-supported excavation in London Clay. In *Géotechnique* 23 (4), pp. 577–581.
- Filz, G.; Adams, T.; Davidson, R. (2004): Stability of Long Trenches in Sand Supported by Bentonite-Water Slurry. In *Journal of Geotechnical and Geoenvironmental Engineering* 130 (9), pp. 915–921.
- Finno, R. J.; Lawrence, S. A.; Allawh, N. F.; Harahap, I. S. (1991): Analysis of Performance of Pile Groups Adjacent to Deep Excavation. In *Journal of Geotechnical and Geoenvironmental Engineering* 117 (6), pp. 934–955.
- Fleming, K.; Weltman, A.; Randolph, M.; Elson, K. (2009): Piling engineering. 3rd ed. London, New York: Taylor & Francis.

- Fleming, W. G.K. (1992): A new method for single pile settlement prediction and analysis. In *Géotechnique* 42 (3), pp. 411–425.
- Fox, P. J. (2004a): Analytical Solution for Stability of Slurry Trench. In *Journal of Geotechnical and Geoenvironmental Engineering* 130 (7), pp. 749–758.
- Fox, P. J. (2004b): Analytical solutions for stability of slurry trench. In *Journal of Geotechnical and Geoenvironmental Engineering ASCE* 130 (7), pp. 749–758.
- Fox, P. J. (2006): Discussion of 'Stability of Long Trenches in Sand Supported by Bentonite-Water Slurry' by George M. Filz, Tiffany Adams, and Richard R. Davidson. In *Journal of Geotechnical and Geoenvironmental Engineering* 132 (5), p. 666.
- Frydman, S.; Burd, H. (1997): Numerical Studies of Bearing-Capacity Factor  $N_{\gamma}$ . In *Journal of Geotechnical and Geoenvironmental Engineering* 123 (20), pp. 20–29.
- Georgiadis, K.; Georgiadis, M. (2012): Development of p-y curves for undrained response of piles near slopes. In *Computers and Geotechnics* 40, pp. 53–61.
- Ghee, H. (2010): The behaviour of axially loaded piles subjected to lateral soil movements. PhD dissertation. Griffith University, Australia.
- Goh, A. T.C.; Teh, C. I.; Wong, K. S. (1997): Analysis of Piles Subjected to Embankment Induced Lateral Soil Movement. In *Journal of Geotechnical and Geoenvironmental Engineering* 123 (9), pp. 792–801.
- Goh, A. T.C.; Wong, K. S.; Teh, C. I.; Wen, D. (2003): Pile Response Adjacent to Braced Excavation. In *Journal of Geotechnical and Geoenvironmental Engineering* 129 (4), pp. 383–386.
- Gourvenec, S. M.; Powrie, W. (1999): Three-dimensional finite-element analysis of diaphragm wall installation. In *Géotechnique* 49 (6), pp. 801–823.
- Grandas-Tavera, C. E.; Triantafyllidis, T. (2012): Simulation of a corner slurry trench failure in clay. In *Computers and Geotechnics* 45, pp. 107–117.
- Gunn, M. J.; Clayton, C. R.I. (1992): Installation effects and their importance in earth retaining structures. In *Géotechnique* 42 (1), pp. 137–141.
- Gunn, M. J.; Satkunanathan, A.; Clayton, C. R.I. (1993): Finite element modeling of installation effects. In *Retaining Structures*, Edt. C.R.I. Clayton, Thomas Telford. London, pp. 46–55.
- Hajnal, I.; Márton, J.; Regele, Z. (1984): Construction of diaphragm walls. Budapest: Akadémiai Kiadó.
- Hamza, M.M., Atta, A. and Roussin, A. (1999): Ground Movements Due to the Construction of Cut-and-Cover Structures and Slurry Shield Tunnel of the Cairo Metro. In *Tunnelling and Underground Space Technology* 14 (3), pp. 281–289.

- Han, C.; Chen, J.; Wang, J.; Xia, X. (2013): 2D and 3D stability analysis of slurry trench in frictional/cohesive soil. In *Journal of Zhejiang University-SCIENCE A (Applied Physics & Engineering)* 14 (2), pp. 94–100.
- Han, C.; Wang, J.; Xia, X.; Chen, J. (2015): Limit Analysis for Local and Overall Stability of a Slurry Trench in Cohesive Soil. In *international Journal of Geomechanics* 15 (5). DOI: 10.1061/(ASCE)GM.1943-5622.0000268,
- Hansen, J. B. (1961): The ultimate resistance of rigid piles against transversal forces. In *Danish Geotechnical Institute, Bulletin No. 12, Copenhagen*, pp. 5–9.
- Hirari, H. (2016): Analysis of piles subjected to lateral soil movements using three dimensional displacement approach. In *International Journal for Numerical and Analytical Methods in Geomechanics* 40, pp. 235–268.
- Hutchinson, M. T.; Daw, G. P.; Shotton, P. G.; James, A. N. (1974): The properties of bentonite slurries used in diaphragm walling and their control. In *Proceedings of Conference on Diaphragm Walls and Anchorages*, ICE. London, pp. 33–39.
- Itasca (2011): *FLAC 2D (Fast Lagrangian analysis of continua) version 7.0 user's manual*, Itasca Consulting Group, Minneapolis, MN, USA.
- Itasca (2013): *FLAC 3D (Fast Lagrangian analysis of continua in three dimensions) version 5.1 user's manual*, Itasca Consulting Group, Minneapolis, MN, USA.
- Ito, T.; Matsui, T. (1975): Methods to estimate lateral force acting on stabilizing piles. In *Soils and Foundations* 15 (4), pp. 43–59.
- Jeong, S.; Kim, B.; Won, J.; Lee, J. (2003): Uncoupled analysis of stabilizing piles in weathered slopes. In *Computers and Geotechnics* 30, pp. 671–682.
- Kantartzi, C. (1993): *Ground movements during diaphragm wall installation in clays*. PhD dissertation. Queen Mary and Westfield College, University of London.
- Karlsrud, K. (1983): Performance and design of slurry walls in soft clay. In *Norwegian Geotechnical institute Oslo* 149, pp. 1–9.
- Katagiri, M.; Saitoh, K.; Masuda, T.; Aizawa, F.; Ugai, K. (1997): Shape effect on deformation behaviour and stability of slurry trench walls constructed in sandy ground. In *Proceedings of the International Symposium on Deformation and Progressive Failure in Geomechanics*. Nagoya, Japan, pp. 665–670.
- Katzenbach, R.; Weidle, A.; Vogler, M. (2012): Bau der Nord-Süd Stadtbahn in Köln - Wechselwirkungen zwischen Baugrund und Bauverfahren. In *32. Baugrundtagung*. Mainz, Germany, pp. 143–149.
- Kishida, H.; Uesugi, M. (1987): Tests of interface between sand and steel in the simple shear apparatus. In *Géotechnique* 37 (1), pp. 45–52.

- Korff, Mandy (2013): Response of piled buildings to the construction of deep excavations. PhD Dissertation. University of Cambridge, UK. Available online at <http://www.dspace.cam.ac.uk/handle/1810/244715>.
- Kulhawy, F. H. (1984): Limiting tip and side resistance: fact or fallacy? In R.J. Meyer San Francisco (Ed.). In Proceedings of symposium on Analysis and Design of Pile Foundations. New York. American Society of Civil Engineers., pp. 80–98.
- L'Amante, D.; Flora, A.; Russo, G.; Viggiani, C. (2012): Displacements induced by the installation of diaphragm panels. In *Acta Geotechnica* 7, pp. 203–218.
- Lehane, B. M.; Jardine, R. J.; Bond, A. J.; Frank, R. (1993): Mechanisms of shaft friction in sand from instrumented pile tests. In *Journal of Geotechnical and Geoenvironmental Engineering* 119 (1), pp. 19–35.
- Lei, G. H.; Ng, C. W.W.; Rigby, D. B. (2001): Stress and Displacement around an elastic artificial rectangular hole. In *Journal of Engineering Mechanics, ASCE*, 127 (9), pp. 880–890.
- Lei, G. H.; Sun, H. S.; Ng, C. W.W. (2014): An approximate analytical solution for calculating ground surface settlements due to diaphragm walling. In *Computers and Geotechnics* 61, pp. 108–115.
- Leung, C. F.; Chow, Y. K.; Shen, R. F. (2000): Behavior of Pile Subject to Excavation-Induced Soil Movement. In *Journal of Geotechnical and Geoenvironmental Engineering* 126 (11), pp. 947–954.
- Leung, C. F.; Lim, J. K.; Shen, R. F.; Chow, Y. K. (2003): Behavior of Pile Groups Subjected to excavation-Induced soil Movement. In *Journal of Geotechnical and Geoenvironmental Engineering* 129 (1), pp. 58–65.
- Leung, C. F.; Ong, D. E.L.; Chow, Y. K. (2006): Pile Behavior Due to Excavation-Induced Soil Movement in Clay. II: Collapsed Wall. In *Journal of Geotechnical and Geoenvironmental Engineering* 132 (1), pp. 45–53.
- Li, Y.; Pan, Q.; Cleall, P. J.; Chen, Y.; Ke, H. (2013): Stability Analysis of Slurry Trenches in Similar Layered Soils. In *Journal of Geotechnical and Geoenvironmental Engineering* 139 (12), pp. 2104–2109.
- Lings, M. L.; Nash, D. F.T.; Ng, C. W.W. (1993a): Reliability of earth pressure measurements adjacent to a multi-propped diaphragm wall. In *Retaining Structures*, Edt. C.R.I.Clyton, Thomas Telford. London, pp. 258-269; discussion 301-304 and 312-313.
- Lings, M. L.; Nash, D.F. T.; Ng, C. W.W. (1993b): Reliability of earth pressure measurements adjacent to a multi-propped diaphragm wall. In *Retaining Structures*, Edt. C.R.I.Clyton, Thomas Telford. London, pp. 258-269; discussion 301-304 and 312-313.



- Liyanapathirana, D. S.; Nishanthan, R. (2016): Influence of deep excavation induced ground movements on adjacent piles. In *Tunnelling and Underground Space Technology* 52, pp. 168–181.
- Loganathan, N.; Poulos, H. G.; Stewart, D. P. (2000): Centrifuge model testing of tunnelling-induced ground and pile deformations. In *Géotechnique* 50 (3), pp. 283–294.
- Matlock, H.; Reese, L. C. (1960): Generalized solutions for laterally loaded piles. In *Journal of Soil Mechanics and Foundation Division, ASCE* 86, pp. 63–91.
- Meyerhof, G. G. (1976): Bearing capacity and settlement of pile foundations. In *Proceedings of American Society of Civil Engineers* 102 (GT3), pp. 197–228.
- Meyerowitz, Joel (2006): *Aftermath*. New York: Phaidon Press.
- Mohamed, A. A. (2014): Prediction of soil deformation due to diaphragm wall installation. In *Proceeding 9th Freiburger – St. Petersburger Kolloquium für Junge Wissenschaftler (BHT)*. TU Bergakademie Freiberg, Germany.
- Mohamed, A. A.; Klapperich, H. (2015): Effect of slurry trenching on load distribution and movement of adjacent piles. In *Topical issues of subsoil usage: volume of science work part 2*, National Mineral Resources University, St. Petersburg, Russia.
- Moormann, C.; Sieler, U.; Kahlen, G.; Schwarze, J. (2014): Herstellung der 34 m tiefen Besichtigungsbaugrube am Waidmarkt in Köln - Spezialtiefbau unter besonderen Anforderungen. In *Heft 64. Vorträge zum 10. Hans Lorenz Symposium*. Berlin, Germany, pp. 139–163.
- Morgenstern, N., and Amir-Tahmassebi, I. (1965): The stability of a slurry trench in cohesionless soils. In *Géotechnique* 15 (4), pp. 387–395.
- Nash, J. K.T.L.; Jones, G. K. (1963): The Support of Trenches Using Fluid Mud. In *Proceedings symposium Grouts and Drilling Muds in Engineering Practice*. Butterworths, London, pp. 177–180.
- Ng, C. W.W. (1998): Observed Performance of Multipropped Excavation in Stiff Clay. In *Journal of Geotechnical and Geoenvironmental Engineering* 124 (9), pp. 889–905.
- Ng, C. W.W.; Lei, G. H. (2003): An explicit analytical solution for calculating horizontal stress changes and displacements around an excavated diaphragm wall panel. In *Canadian Geotechnical Journal* 40, pp. 780–792. DOI: 10.1139/T03-027.
- Ng, C. W.W.; Lings, M. L.; Simpson, B.; Nash, D. F.T. (1995): An approximate analysis of the three-dimensional effects of diaphragm wall installation. In *Géotechnique* 45 (3), pp. 497–507.
- Ng, C. W.W.; Yan, R. W.M. (1998): Stress transfer and deformation around a diaphragm wall. In *Journal of Geotechnical and Geoenvironmental Engineering* 124 (7), pp. 638–648.

- Ng, C. W. W., Rigby, D., Lei, G. H., and Ng, S. W. L. (1999): Observed performance of a short diaphragm wall panel. In *Géotechnique* 49 (5), pp. 681–694.
- Ong, D.; Leung, C.; Chow, Y. (2009): Behavior of Pile Groups Subject to Excavation-Induced Soil Movement in Very Soft Clay. In *Journal of Geotechnical and Geoenvironmental Engineering* 135 (10), pp. 1462–1474.
- Ong, D. E.L.; Leung, C. E.; Chow, Y. K. (2006): Pile Behavior due to Excavation-Induced Soil Movement in Clay. I: Stable Wall. In *Journal of Geotechnical and Geoenvironmental Engineering* 132 (1), pp. 36–44.
- Ou, C. Y.; Yang, L. L. (2011): Observed Performance of Diaphragm Wall Construction. In *Geotechnical Engineering Journal of the SEAGS & AGSSAE* 42 (3), pp. 41–49.
- Pan, J. L.; Goh, A. T.C.; Wong, K. S.; Teh, C. I. (2002): Ultimate Soil Pressure for Piles Subjected to Lateral Soil Movement. In *Journal of Geotechnical and Geoenvironmental Engineering* 128 (6), pp. 530–534.
- Piaskowski, A.; Kowalewski, Z. (1965): Application of thixotropic clay suspensions for stability of vertical sides of deep trenches without strutting. In Proceedings of the 6th International Conference on Soil Mechanics and Foundation Engineering. Montreal: University of Toronto, pp. 526–529.
- Poh, T. Y.; Goh, A. T.C.; Wong, I. H. (2001): Ground Movements Associated with Wall Construction: Case Histories. In *Journal of Geotechnical and Geoenvironmental Engineering* 127 (12), pp. 1061–1069.
- Poh, T. and Wong, I. (1998): Effects of Construction of Diaphragm Wall Panels on Adjacent Ground: Field Trial. In *Journal of Geotechnical and Geoenvironmental Engineering* 19 (2), pp. 285–300.
- Poulos, H. G. (1976): Behaviour of laterally loaded piles near a cut or slope. In *Australian Geomechanics Journal* G5 (1), pp. 6–12.
- Poulos, H. G. (1995): Design of reinforced piles to increase slope stability. In *Canadian Geotechnical Journal* 32 (5), pp. 808–818.
- Poulos, H. G.; Chen, L. T. (1996): Pile response due to unsupported excavation-induced lateral soil movement. In *Canadian Geotechnical Journal* 33 (4), pp. 670–677.
- Poulos, H. G.; Chen, L. T. (1997): Pile response due to excavation-induced lateral soil movement. In *Journal of Geotechnical and Geoenvironmental Engineering* 123 (2), pp. 94–99.
- Poulos, Harry George; Davis, Edward Hughesdon (1980): Pile foundation analysis and design. New York, Chichester: Wiley (Series in geotechnical engineering).
- Powrie, W.; Kantartzi, C. (1996): Ground deformation due to diaphragm wall installation in clay: Centrifuge model test. In *Géotechnique* 46 (4), pp. 725–739.

- Prater, E. G. (1973): Die Gewölbewirkung der Schlitzwände. In *Der Bauingenieur* 48 (4), pp. 125–131.
- Qin, H.; Guo, W. D. (2013): Group Effects of Piles Due to Lateral Soil Movement. In *International Journal of GEOMATE* 4 (1), pp. 450–455.
- Randolph, M. F. (1981): The response of flexible piles to lateral loading. In *Géotechnique* 31 (2), pp. 247–259.
- Randolph, M. F. (2003): Science and empiricism in pile foundation design. In *Géotechnique* 53 (3), pp. 847–875.
- Randolph, M. F.; Dolwin, J.; Beck, R. (1994): Design of Driven Piles in Sand. In *Géotechnique* 44 (3), pp. 427–488.
- Reese, L. C.; Cox, W. R.; Koop, F. D. (1974): Analysis of laterally loaded piles in sand. In vol. 2. 6th Annual Offshore Technology Conference. Houston, OTC 2080, pp. 473–485.
- Reese, Lymon C.; van Impe, W. F. (2001): Single piles and pile groups under lateral loading. Rotterdam: Balkema.
- Reuter, Oltmann (2001a): Berlin. Der Spreebogen 1994-2001: Die bauliche Entwicklung in Luftbildern: Lehrter Bahnhof, Regierungsbauten, Pariser Platz. Berlin: Luftbildverlag.
- Reuter, Oltmann (2001b): Berlin. Potsdamer Platz 1994 - 2001: Die bauliche Entwicklung in Luftbildern: Gleisdreieck, Potsdamer Platz, Tiergartentunnel B96. Wolfschlugen: Luftbildverl. [u. a.] (Berlin).
- Rotisciani, G. M.; Miliziano, S.; Sacconi, S. (2016): Design, construction, and monitoring of a building with deep basements in Rome. In *Canadian Geotechnical Journal* 53 (2), pp. 210–224.
- Rowe, R. K.; Poulos, H. G. (1979): A method for predicting the effect of piles on slope behaviour. In. Third International Conference on Numerical Methods in Geomechanics. Aachen, 2-6 April, pp. 1073–1085.
- Schwarze, J.; Steiger, H.; Wild, J. (2016): Aussteifung einer ca. 25 m tiefen und unter Wasser auszuhebenden Baugrube im innerstädtischen Bereich. In Vorträge zum 23. Darmstädter Geotechnik-Kolloquium. Darmstadt, Germany, pp. 127–130.
- Shi, J.; Liu, G.; Huang, P.; Ng., C. W.W. (2015): Interaction between a large-scale triangular excavation and adjacent structures in Shanghai soft clay. In *Tunnelling and Underground Space Technology* 50, pp. 282–295.
- Sieler, U.; Pabst, R.; Moormann, C.; Neweling, G. (2012): Der Einsturz des Stadtarchivs in Köln: Bauliche Maßnahmen zur Bergung der Archivalien und zur Erkundung der Schadensursache. In 32. Baugrundtagung. Mainz, Germany, pp. 135–141.

- Sieler, U.; Schwarze, J.; Moorman, C.; Neweling, G. (2015): Aktueller Stand der Maßnahmen zur Erkundung der Schadensursache nach dem Einsturz des Stadtarchivs in Köln: Komplexe Randbedingungen und bautechnische Herausforderungen bei der 34 m tiefen Besichtigungsbaugrube. In *Forschung + Praxis* 46. Proceedings of STUVA Conference: The International Forum for Tunnels and Infrastructures. Dortmund, Germany, pp. 190–195.
- Springman, S. M.; Ng, C. W. W.; Ellis, E. A. (1995): Centrifuge and analytical studies of full height bridge abutment on piled foundation subjected to lateral loading. Crowthorne, Berkshire: Civil Engineering Resource Centre, Transport Research Laboratory (Project report / Transport Research Laboratory, 98).
- Stewart, D. P.; Jewell, R. J.; Randolph, M. F. (1994): Design of piled bridge abutments on soft clay for loading from lateral soil movements. In *Géotechnique* 44 (2), pp. 277–296.
- Stround, M. A. and Sweeney, D.J. (1977): A review of diaphragm wall. Discussion Appendix. In *Institution of Civil Engineers*.
- Symons, I. F. and Carder, D. R. (1993): Stress changes in stiff clay caused by the installation of embedded retaining walls. In *Proceedings of the Conference on Retaining Structures*. Robinson College, Cambridge, United Kingdom, pp. 227–236.
- Tamano, T.; Fukui, S.; Suzuki, H.; Ueshita, K. (1996): Stability of Slurry Trenches Excavated in Soft Clay. In *Soils and Foundations* 36 (2), pp. 101–110.
- Tamano, T., Fukui, S., Suzuki, H. and Ueshita, K. (1996): Stability of Slurry Trench Excavation in Soft Clay. In *Japanese society of soil mechanics and foundation engineering, Tokyo* 36 (2), pp. 101–110.
- Tedd, P.; Chard, B. M.; Charles, J. A.; Symons, I. F. (1984): Behaviour of a propped embedded retaining wall in stiff clay at Bell Common Tunnel. In *Géotechnique* 34 (4), pp. 513–532.
- Terzaghi, Karl (1943): *Theoretical soil mechanics*. New York, London: J. Wiley and Sons inc.; Chapman and Hall limited.
- Thorley, C. B.B.; Forth, R. A. (2002): Settlement due to Diaphragm Wall Construction in Reclaimed Land in Hong Kong. In *Journal of Geotechnical and Geoenvironmental Engineering* 128 (6), pp. 473–478.
- Timoshenko, S. P.; Goodier, J. N. (1951): *Theory of elasticity*. New York: McGraw-Hill.
- Tomlinson, M. J.; Woodward, John (2008): *Pile design and construction practice*. 5th ed. London, New York: Taylor & Francis.
- Tsai, J.; Chang, J. (1996): Three-dimensional stability analysis for slurry-filled trench wall in cohesionless soil. In *Canadian Geotechnical Journal* 33 (5), pp. 798–808.
- Tsai, J.; Jou, L.; Hsieh, H. (2000): A full-scale stability experiment on a diaphragm wall trench. In *Canadian Geotechnical Journal* 37 (2), pp. 379–392.

- Tsai, J. and Chang, J. (1996): Three-dimensional stability analysis for slurry-filled trench wall in cohesionless soil. In *Canadian Geotechnical Journal* 33 (5), pp. 798–808.
- Tsai, J.-S., Jou, L.-D., and Hsieh, H.-S. (2000): A full-scale stability experiment on a diaphragm wall trench. In *Canadian Geotechnical Journal* 37 (2), pp. 379–392.
- Tse, C. M.; Nicholson, D. P. (1993): Design, construction and monitoring of the basement diaphragm wall at Minster Court, London. In *Retaining Structures*, Edt. C.R.I.Clyton, Thomas Telford. London, pp. 323–332.
- Tse, C.M. and Nicholson, D.P. (1993): Design, construction and monitoring of the basement diaphragm wall at Minster Court, London. In *Proceedings of the conference on Retaining structures*. Robinson College, Cambridge, United Kingdom, pp. 323–332.
- Vermeer, P. A.; Borst, R. de (1984): Non-associated plasticity for soils, concrete and rock. [Delft]: [Heron] (Heron, vol. 29, no. 3).
- Vesić, A. S. (1969): Experiments with instrumented pile groups in sand. Durham, N.C.: Duke University, School of Engineering (Duke University. School of Engineering. Soil mechanics series, no. 14).
- Vesić, Aleksandar Sedmak (1977): Design of pile foundations. Washington: Transportation Research Board National Research Council (Synthesis of highway practice, 42).
- Walz, B.; Prager, J. (1978): Der Nachweis der äusseren Standsicherheit suspensionsgestützter Erdwände nach der elementscheiben-theorie. In *Veröffentlichungen des Grundbauinstituts der Technischen Universität Berlin* Heft 4.
- Weiss, Fritz; Winter, Knut (1985): Erläuterungen zu den Schlitzwandnormen DIN 4126, DIN 4127, DIN18313. 1. Aufl. Wiesbaden, Berlin, Berlin, Köln: Bauverlag; Beuth (Beuth-Kommentare, Bd. 1).
- Wit, de J. C. W. M. & Lengkeek, H. J. (2002): Full scale test on environmental impact diaphragm wall trench installation in Amsterdam – the final results. In *Proceedings of the 3rd International Symposium on Geotechnical Aspects of Underground Construction in Soft Ground*. Toulouse, France.
- Wit, de J. C. W. M., Roelands, J. C. S. and de Kant, M. (2000): Full scale test on environmental impact of diaphragm wall trench excavation. In *Geotechnical Aspects of Underground Construction in Soft Ground*. Balkema, pp. 723–730.
- Xanthakos, Petros P. (1994): Slurry walls as structural systems. 2nd ed. New York [etc.]: McGraw-Hill.
- Xu, K. J.; Poulos, H. G. (2001): 3D elastic analysis of vertical piles subjected to passive loadings. In *Computers and Geotechnics* 28, pp. 349–375.

- Yu, H. S.; Houlsby, G. T. (1991): Finite cavity expansion in dilatant soils. Loading analysis. In *Géotechnique* 41 (2), pp. 173–183.
- Zhang, C. R.; Zheng, J.; Pu, H.; Zhang, L. (2011): Analysis of excavation-induced responses of loaded pile foundations considering unloading effect. In *Tunnelling and Underground Space Technology* 26, pp. 320–335.
- Zhang, F.; Gao, Y. F.; Leshchinsky, D.; Zhu, D. S.; Lei, G. H. (2016): Three-dimensional stability of slurry-supported trenches: End effects. In *Computers and Geotechnics* 74, pp. 174–187.



## APPENDIX A: TYPICAL CODE USED FOR MODELING WITH FLAC3D

```
;-----  
; soil and geometry layers  
;-----  
new project  
set fish autocreate off  
title 'Tested panel'  
def setup  
global fri_fill = 30.  
global fri_ssilt = 15.  
global fri_coral = 40.  
global fri_medsand = 30  
global fri_densand = 40.  
global fri_granite = 40  
local eoed_fill = 38.4e6 ; 59.411e6  
local eur_fill = 115e6 ; 178.25e6  
local eoed_ssilt = 12.4e6  
local eur_ssilt = 37e6  
local eoed_coral = 128e6  
local eur_coral = 380e6  
local eoed_medsand = 27.7e6  
local eur_medsand = 83.2e6  
local eoed_densand = 10.5e6  
local eur_densand = 31.75e6  
local eoed_granite = 32.7e6  
local eur_granite = 98e6  
local _nu = 0.2  
global m_fill = 0.9  
global m_ssilt = 0.9  
global m_coral = 0.9  
global m_medsand = 0.9  
global m_densand = 0.9  
global m_granite = 0.9  
global _beta = 1.0  
global _rf = 0.9  
global _pa = 100e3  
global _k0 = 0.5 ; this value was just used for tryal  
global _pmax = 1e7  
global mul_fill = 5 ; eur_fill/(3.*(1.-2.*_nu)*eoed_fill)-1  
global mul_ssilt = 5 ; eur_marine/(3.*(1.-2.*_nu)*eoed_marine)-1  
global mul_coral = 5  
global mul_medsand = 5 ; eur_allu1/(3.*(1.-2.*_nu)*eoed_allu1)-1  
global mul_densand = 5 ; eur_allu2/(3.*(1.-2.*_nu)*eoed_allu2)-1  
global mul_granite = 5 ; eur_allu2/(3.*(1.-2.*_nu)*eoed_allu2)-1  
global gr_fill = eur_fill/(2.*(1.+_nu))  
global gr_ssilt = eur_ssilt/(2.*(1.+_nu))  
global gr_coral = eur_coral/(2.*(1.+_nu))  
global gr_medsand = eur_medsand/(2.*(1.+_nu))  
global gr_densand = eur_densand/(2.*(1.+_nu))
```



```

global gr_granite = eur_granite/(2.*(1.+_nu))
global _coek = 2.*(1.+_nu)/(3.*(1.-2.*_nu))
global _al = 3.*sqrt(0.5*(1.-_k0)/(1.+2.*_k0))
global ki_fill = eoed_fill
global ki_ssilt = eoed_ssilt
global ki_coral = eoed_coral
global ki_medsand = eoed_medsand
global ki_densand = eoed_densand
global ki_granite = eoed_granite
global m_fill = min(m_fill,0.9)
global m_ssilt = min(m_ssilt,0.9)
global m_coral = min(m_coral,0.9)
global m_medsand = min(m_medsand,0.9)
global m_densand = min(m_densand,0.9)
global m_granite = min(m_densand,0.9)
global _num = 200
global _nt = 1
global _gr = gr_densand
global _fri = fri_densand
global _em = m_densand
global _mul = mul_densand
global _ki=ki_densand
end
@setup
gen zone radtunnel ...
p0 (0,0,0) p1 (2,0,0) p2 (0,0,-50) p3 (0,5,0) ...
size 4 50 10 6 ...
rat 1. 1.025 1.0 1.2 ... ;1.0114
dim 0.6 3.1 fill
gen zone brick p0 (2.0, 0, 0) P1 (20.0, 0, 0) P2 ( 2.0, 0, -50) P3 (2.0, 5.0 ,0) ...
size 18 50 10 ...
rat 1. 1.025 1. ;1.0114
gen zone brick P0 (0, 5.0, 0) P1 (2, 5, 0) P2 ( 0, 5.0, -50) P3 (0, 20 ,0) ...
size 4 50 15 ...
rat 1. 1.025 1. ;1.0114
gen zone brick p0 (2, 5, 0) P1 ( 20, 5, 0) P2 (2, 5, -50) P3 (2.0 , 20 , 0)...
size 18 50 15 ...
rat 1. 1.025 1. ; 1.0114
gen zone reflect dip 270 dd 90
gen zone reflect dip 90 dd 00 origin (7.5 0 0) ;range y 6.2 15
model mech strainsoft
group zone fill range z 0 -3 ;x 0.8 20 y 0 30
prop density=1750.0 bulk=5.56E6 shear=4.17E6 friction= @fri_fill &
dilation=0.0 coh = 500 range group fill
group zone ssilt range z -3 -5
prop density=1800.0 bulk=5.56E6 shear= 4.17E6 friction= @fri_ssilt &
dilation=0.0 coh = 25000 range group ssilt
group zone Coral range z -5 -6
prop density=1850.0 bulk=5.56E7 shear= 4.17E7 friction= @fri_coral &
dilation=10.0 coh = 5000 range group Coral
group zone medsand range z -6 -15
prop density=1850.0 bulk= 2.78E7 shear= 2.08E7 friction= @fri_medsand &

```

```

dilation=0 range group medsand
group zone densand range z -15 -36
prop density=2000.0 bulk= 4.05E7 shear=3.7E7 friction= @fri_densand &
dilation=6.0 range group densand
group zone granite range z -36 -50
prop density=2200.0 bulk=4.76E7 shear=4.35E7 friction= @fri_granite &
dilation=10.0 range group granite
def fric_table
local _Gi = _beta*( _gr/_pa)
local ii
global _num
loop ii (1,_num+1)
local _phic = ( _fri/float(_num))*float(ii-1)
local sval = sin(_phic*degrad)
local _coe = sin( _fri*degrad)/_rf
local xval = ( _coe/(1.-sval/_coe)-_coe)/_Gi
ytable(_nt,ii) = _phic ; draw the table
xtable(_nt,ii) = xval
end_loop
ytable(_nt,_num+2) = _phic
xtable(_nt,_num+2) = 0.2
end
set @_nt=1 @_num=200 @_gr=@gr_fill @_beta=@_beta @_fri=@fri_fill
@fric_table
prop ftable 1 range z 0 -3 ;x 0 20 y 0 30
set @_nt=2 @_num=200 @_gr=@gr_ssilt @_beta=@_beta @_fri=@fri_ssilt
@fric_table
prop ftable 2 range z -3 -5 ;x 0 20 y 0 30
set @_nt=3 @_num=200 @_gr=@gr_coral @_beta=@_beta @_fri=@fri_coral
@fric_table
prop ftable 3 range z -5 -6 ;x 0 20 y 0 30
set @_nt=4 @_num=200 @_gr=@gr_medsand @_beta=@_beta @_fri=@fri_medsand
@fric_table
prop ftable 4 range z -6 -15
set @_nt=5 @_num=200 @_gr=@gr_densand @_beta=@_beta @_fri=@fri_densand
@fric_table
prop ftable 5 range z -15 -36
set @_nt=6 @_num=200 @_gr=@gr_granite @_beta=@_beta @_fri=@fri_granite
@fric_table
prop ftable 6 range z -36 -50
fix x y z range z -50.1 -49.9
fix x range x 19.9 20.1
fix x range x -19.9 -20.1
fix y range y 19.9 20.1
fix y range y -19.9 -20.1
set gravity 0,0,-10.0
into consideration in the add Sxx
ini szz 0.0 grad 0 0 17500.0 range z -3 0
ini szz 1500.0 grad 0 0 18000.0 range z -5 -3
ini szz -4000.0 grad 0 0 18500.0 range z -15 -5
ini szz -26500.0 grad 0 0 20000.0 range z -36 -15
ini szz -198500.0 grad 0 0 22000.0 range z -50 -36

```

```

ini sxx 0.0 grad 0 0 4375.0 range z -3 0
ini sxx 375.0 grad 0 0 4500.0 range z -5 -3
ini sxx -1000.0 grad 0 0 4625.0 range z -15 -5
ini sxx -4676.5 grad 0 0 3529.4 range z -36 -15
ini sxx -35029.4 grad 0 0 3882.4 range z -50 -36
ini sxx add 22500.0 grad 0 0 7500.0 range z -5 -3
ini sxx add 15000.0 grad 0 0 7500.0 range z -15 -5
ini sxx add 82352.9 grad 0 0 8235.3 range z -36 -15
ini sxx add 172941.2 grad 0 0 8235.3 range z -50 -36
ini syy 0.0 grad 0 0 4375.0 range z -3 0
ini syy 375.0 grad 0 0 4500.0 range z -5 -3
ini syy -1000.0 grad 0 0 4625.0 range z -15 -5
ini syy -4676.5 grad 0 0 3529.4 range z -36 -15
ini syy -35029.4 grad 0 0 3882.4 range z -50 -36
ini syy add 22500.0 grad 0 0 7500.0 range z -5 -3
ini syy add 15000.0 grad 0 0 7500.0 range z -15 -5
ini syy add 82352.9 grad 0 0 8235.3 range z -36 -15
ini syy add 172941.2 grad 0 0 8235.3 range z -50 -36
water density 1000
water table origin 0 0 -2.13 normal 0 0 -1
hist add unbala
solve
save ini
;-----
; Trenching of the first panel
;-----
ini xdisp 0 ydisp 0 zdisp 0
ini xvel 0 yvel 0 zvel 0
;Guide wall
group zone guidewall range x 0.6 1.649 y -4.13 4.13 z 0 -2.13
model mech elastic range group guidewall
prop density= 1900.0 bulk=118.6E8 shear=108.6E8 range group guidewall ; bulk 11.86GPa
shear 10.86GPa according to the conc E = 25GPa
group zone guidewall range x -0.6 -1.649 y -4.13 4.13 z 0 -2.13
model mech elastic range group guidewall
prop density= 1900.0 bulk=118.6E8 shear=108.6E8 range group guidewall ; bulk 11.86GPa
shear 10.86GPa according to the conc E = 25GPa
group zone guidewall range x -0.6 0.6 y 3.1 3.52 z 0 -2.13
model mech elastic range group guidewall
prop density= 1900.0 bulk=118.6E8 shear=108.6E8 range group guidewall ; bulk 11.86GPa
shear 10.86GPa according to the conc E = 25GPa
group zone guidewall range x -0.6 0.6 y 0.31 0.0 z 0 -2.13
model mech elastic range group guidewall
prop density= 1900.0 bulk=118.6E8 shear=108.6E8 range group guidewall ; bulk 11.86GPa
shear 10.86GPa according to the conc E = 25GPa
solve
;excavate the panel in 5 m stage
ini xdisp 0 ydisp 0 zdisp 0
ini xvel 0 yvel 0 zvel 0
model mech null range x -0.3 0.3 y 7.875 14 z 0 -5.0
apply nstress 0 grad 0 0 11e3 range x 0.29 0.31 y 7.875 14 z -0.5 -5.0
apply nstress 0 grad 0 0 11e3 range x -0.29 -0.31 y 7.875 14 z -0.5 -5.0

```

```

apply nstress 0 grad 0 0 11e3 range x -0.3 0.3 y 7.7 8.0 z -0.5 -5.0
apply nstress 0 grad 0 0 11e3 range x -0.3 0.3 y 13.9 14.1 z -0.5 -5.0
apply nstress -4.95e4 range x -0.3 0.3 y 7.875 14 z -4.9 -5.1
solve rat 1e-6
model mech null range x -0.6 0.6 y 0.31 3.1 z 0 -9.94
apply nstress 5.457e3 grad 0 0 10.7e3 range x 0.59 0.61 y 0.31 3.1 z -0.51 -9.94
apply nstress 5.457e3 grad 0 0 10.7e3 range x -0.59 -0.61 y 0.31 3.1 z -0.51 -9.94
apply nstress 5.457e3 grad 0 0 10.7e3 range x -0.6 0.6 y 0.3 0.32 z -0.51 -9.94
apply nstress 5.457e3 grad 0 0 10.7e3 range x -0.6 0.6 y 3.0 3.1 z -0.51 -9.94
apply nstress -10.6e4 range x -0.6 0.6 y 0.31 3.1 z -9.8 -10.1 ; -9.63e4
solve ;rat 9e-6
model mech null range x -0.6 0.6 y 0.31 3.1 z 0 -15.68
apply nstress 5.457e3 grad 0 0 10.7e3 range x 0.59 0.61 y 0.31 3.1 z -0.51 -15.68
apply nstress 5.457e3 grad 0 0 10.7e3 range x -0.59 -0.61 y 0.31 3.1 z -0.51 -15.68
apply nstress 5.457e3 grad 0 0 10.7e3 range x -0.6 0.6 y 0.3 0.32 z -0.51 -15.68
apply nstress 5.457e3 grad 0 0 10.7e3 range x -0.6 0.6 y 3.0 3.1 z -0.51 -15.68
apply nstress -16.32e4 range x -0.6 0.6 y 0.31 3.1 z -15.5 -15.8 ; -14.98e4
solve
model mech null range x -0.6 0.6 y 0.31 3.1 z 0 -20.444
apply nstress 5.457e3 grad 0 0 10.7e3 range x 0.59 0.61 y 0.31 3.1 z -0.51 -20.444
apply nstress 5.457e3 grad 0 0 10.7e3 range x -0.59 -0.61 y 0.31 3.1 z -0.51 -20.444
apply nstress 5.457e3 grad 0 0 10.7e3 range x -0.6 0.6 y 0.3 0.32 z -0.51 -20.444
apply nstress 5.457e3 grad 0 0 10.7e3 range x -0.6 0.6 y 3.0 3.1 z -0.51 -20.444
apply nstress -21.4e4 range x -0.6 0.6 y 0.31 3.1 z -20.4 -20.5 ; -20.3e4
solve
model mech null range x -0.6 0.6 y 0.31 3.1 z 0 -25.8
apply nstress 5.457e3 grad 0 0 10.7e3 range x 0.59 0.61 y 0.31 3.1 z -0.51 -25.8
apply nstress 5.457e3 grad 0 0 10.7e3 range x -0.59 -0.61 y 0.31 3.1 z -0.51 -25.8
apply nstress 5.457e3 grad 0 0 10.7e3 range x -0.6 0.6 y 0.3 0.32 z -0.51 -25.8
apply nstress 5.457e3 grad 0 0 10.7e3 range x -0.6 0.6 y 3.0 3.1 z -0.51 -25.8
apply nstress -26.75e4 range x -0.6 0.6 y 0.31 3.1 z -25.7 -25.9 ; -25.68e4
solve
model mech null range x -0.6 0.6 y 0.31 3.1 z 0 -30.63
apply nstress 5.457e3 grad 0 0 10.7e3 range x 0.59 0.61 y 0.31 3.1 z -0.51 -30.63
apply nstress 5.457e3 grad 0 0 10.7e3 range x -0.59 -0.61 y 0.31 3.1 z -0.51 -30.63
apply nstress 5.457e3 grad 0 0 10.7e3 range x -0.6 0.6 y 0.3 0.32 z -0.51 -30.63
apply nstress 5.457e3 grad 0 0 10.7e3 range x -0.6 0.6 y 3.0 3.1 z -0.51 -30.63
apply nstress -32.24e4 range x -0.6 0.6 y 0.31 3.1 z -30.5 -30.7 ; -37.45e4
solve
model mech null range x -0.6 0.6 y 0.31 3.1 z 0 -35.948
apply nstress 5.457e3 grad 0 0 10.7e3 range x 0.59 0.61 y 0.31 3.1 z -0.51 -35.948
apply nstress 5.457e3 grad 0 0 10.7e3 range x -0.59 -0.61 y 0.31 3.1 z -0.51 -35.948
apply nstress 5.457e3 grad 0 0 10.7e3 range x -0.6 0.6 y 0.3 0.32 z -0.51 -35.948
apply nstress 5.457e3 grad 0 0 10.7e3 range x -0.6 0.6 y 3.0 3.1 z -0.51 -35.948
apply nstress -37.985e4 range x -0.6 0.6 y 0.31 3.1 z -35.8 -36.1 ; -37.45e4
solve
save Bite1
;-----
; settlement and horizontal displacement
;-----
def sett
loop foreach local _g gp_list

```

```

if gp_xpos(_g) > 0 then
if gp_ypos(_g) < 2.1 then ; trench 0.1 Bite 1&2 2.1
if gp_ypos(_g) > 1.9 then ; trench -0.1 Bite 1&2 1.9
if gp_zpos(_g) > -0.1 then
local _x = gp_zdisp(_g)
local _y = gp_xpos(_g)
endif
endif
endif
endif
; horizontal displacement
if gp_xpos(_g) > 2.9 then ; I2 ---1.6 I5 ---- 2.9 I3 ---- 5.9
if gp_xpos(_g) < 3.1 then ; I2 ---1.7 I5 ---- 3.1 I3 ---- 6.1
if gp_ypos(_g) < 0.1 then
if gp_ypos(_g) > -0.1 then
if gp_zpos(_g) < 0.0 then
local _xx = gp_xdisp(_g)
local _yy = gp_zpos(_g)
endif
endif
endif
endif
endif
endif
table (7, _y) = _x
table (8, _yy) = _xx
endloop
end
@sett

```

## APPENDIX B: PARAMETRIC STUDY FIGURES

This appendix contains some of the parametric study Figures and it divided into the main three parts.

### B.1 RESULTS OF PART I MODEL GROUPS

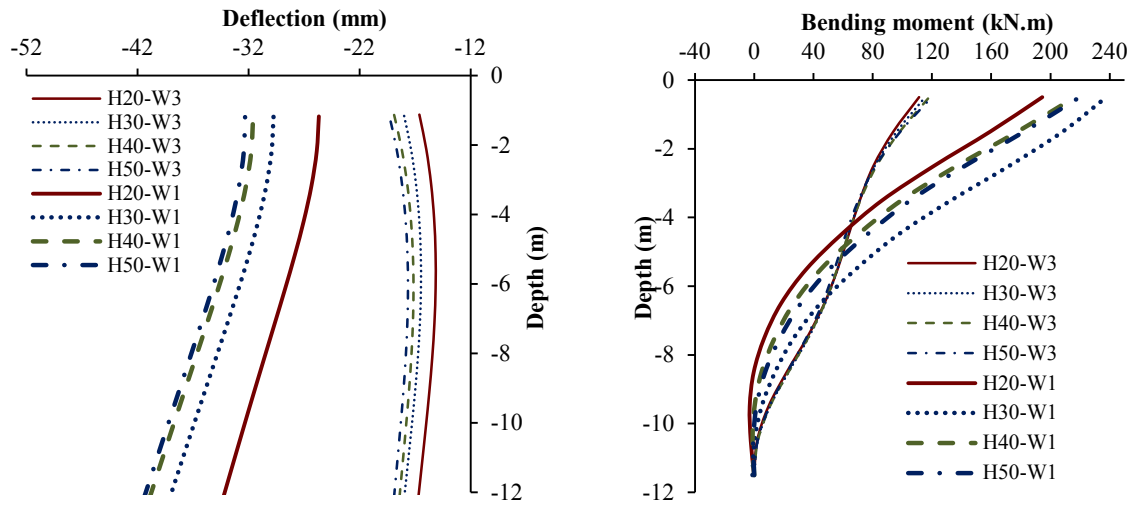


Figure B-1: Pile deflection and bending moment for parameter combination (PI-MG1-C1) for pile offset distance (x) = 3.5 m

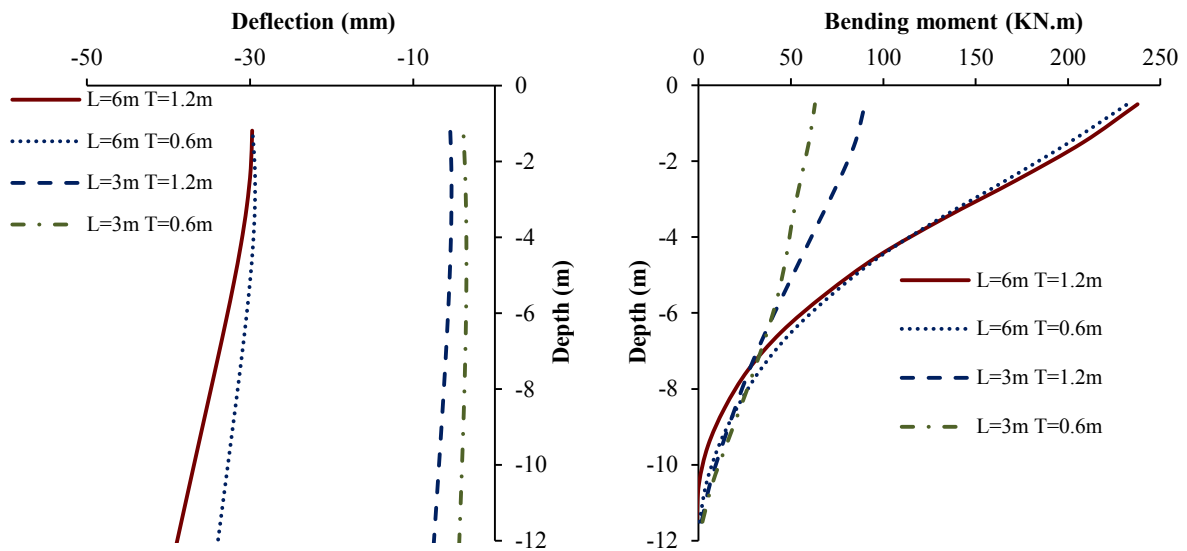
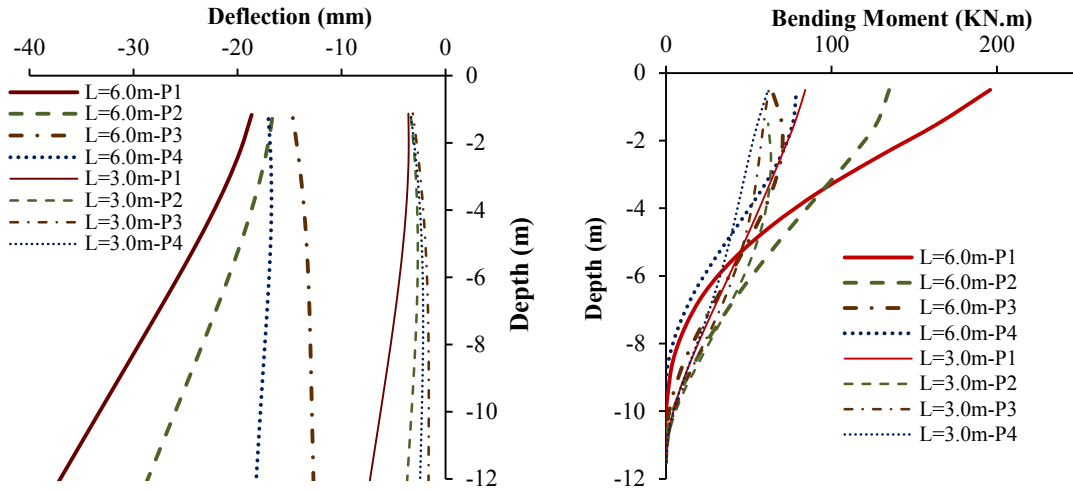
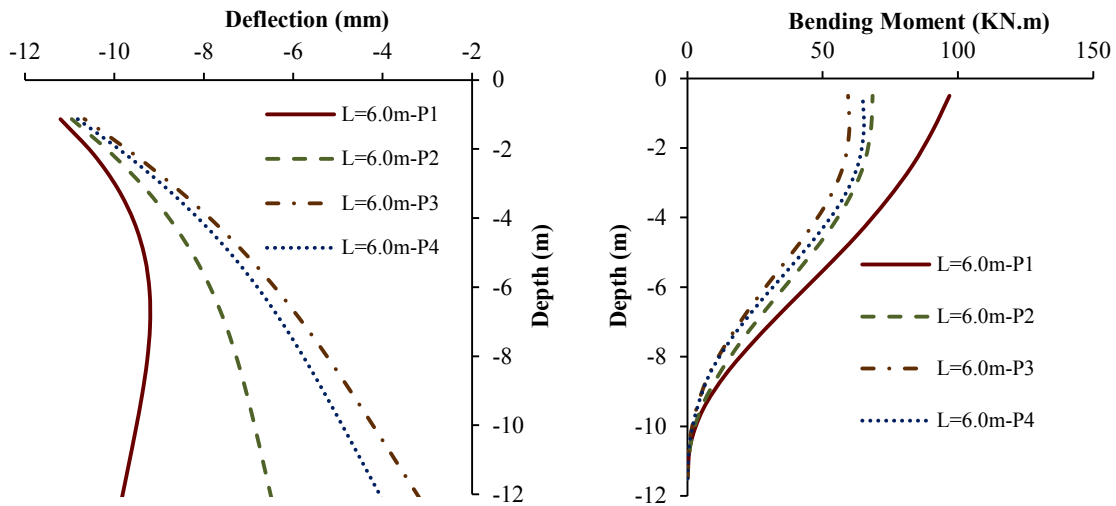


Figure B-2: Pile deflection and bending moment for parameter combination (PI-MG1-C2) for pile offset distance (x) = 3.5 m

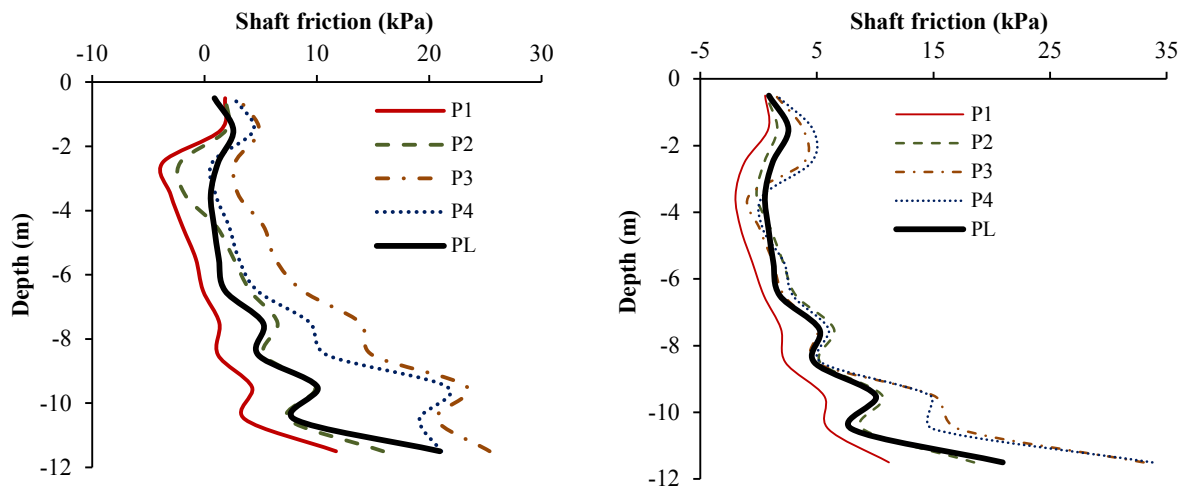


(a)  $x = 2.0$  m



(b)  $x = 5.5$  m

Figure B-3: Piles deflection and bending moment for parameter combination (PI-MG1-C3)



(a)  $x = 2.0$  m

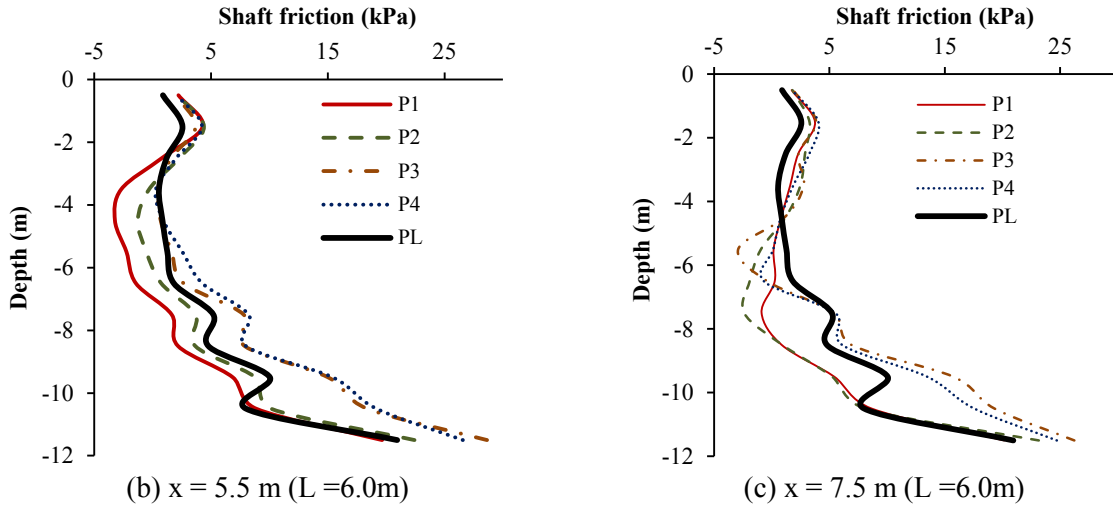


Figure B-4: Piles shaft friction for parameter combination (PI-MG1-C3)

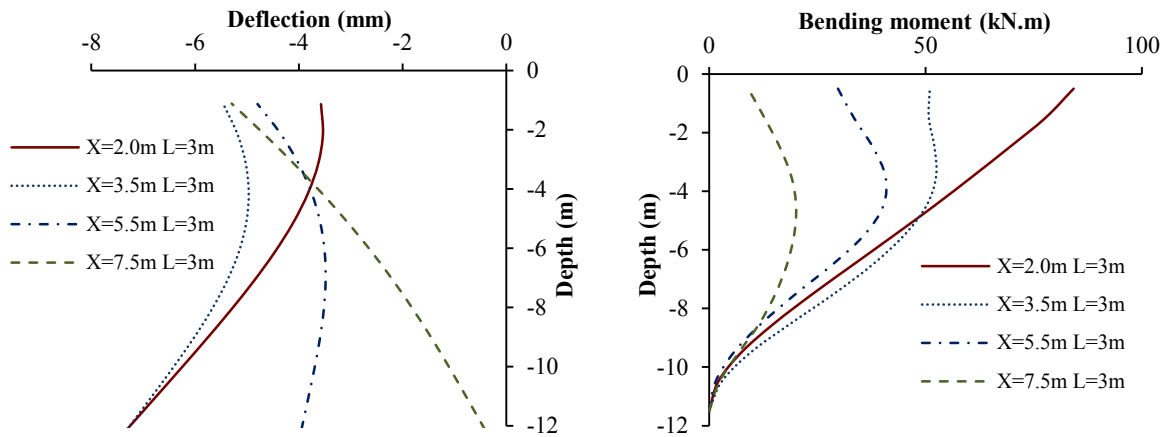


Figure B-5: Pile deflection and bending moment for parameter combination (PI-MG1-C3) for panel length ( $L = 3.0\text{m}$ )

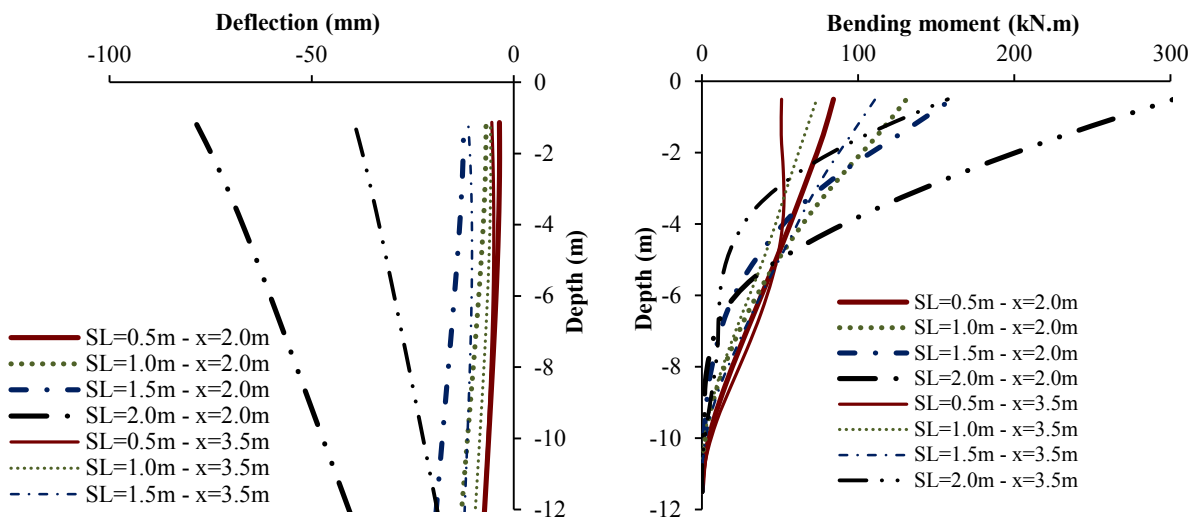


Figure B-6: Pile deflection and bending moment for parameter combination (PI-MG1-C5) for panel length ( $L = 3.0\text{m}$ )



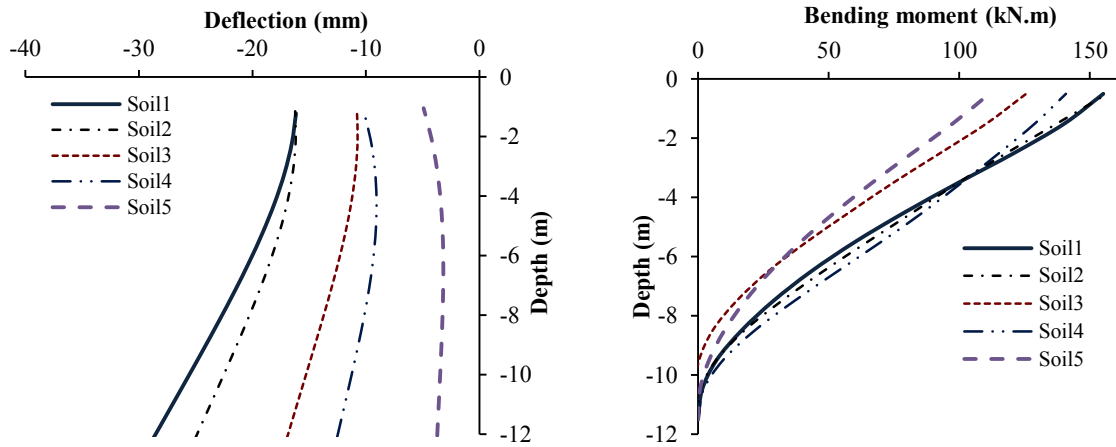


Figure B-7: Pile deflection and bending moment for parameter combination (PI-MG1-C6) for slurry level of 0.5m

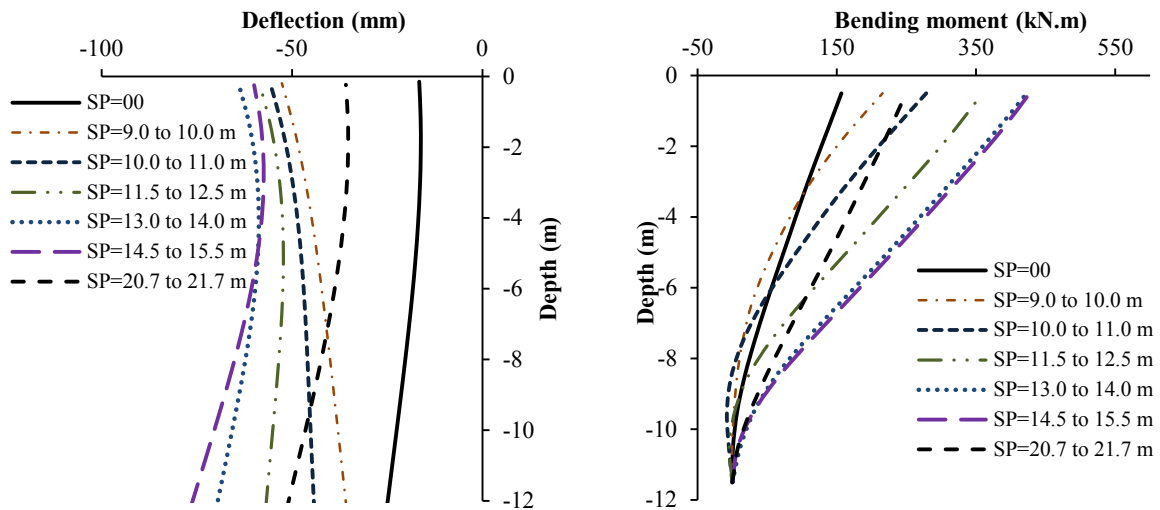


Figure B-8: Pile deflection and bending moment for parameter combination (PI-MG1-C7) for pile offset distance ( $x$ ) = 3.5 m

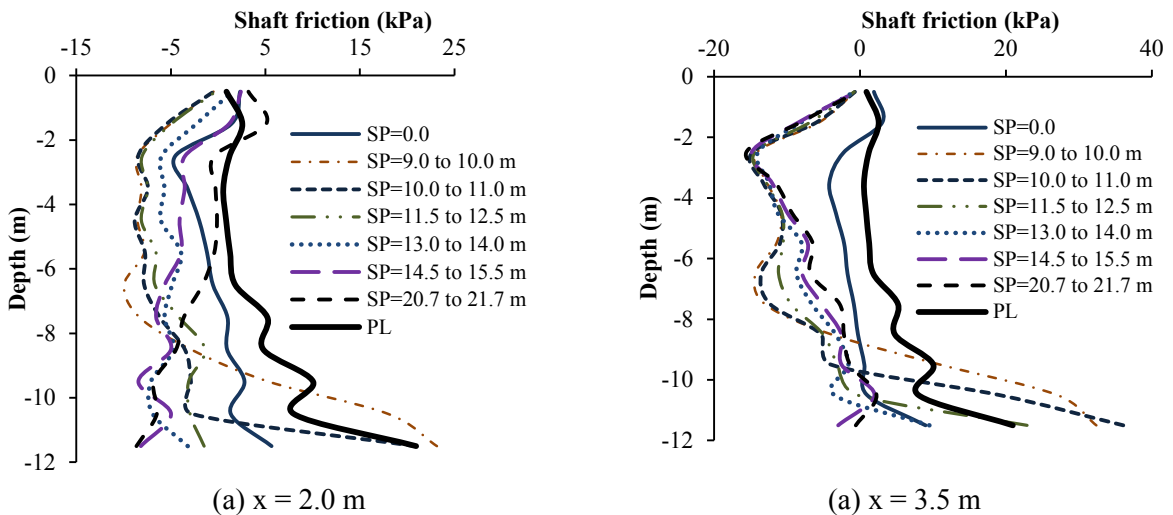


Figure B-9: Pile shaft friction at different slurry pressure reduction levels for parameter combination (PI-MG1-C7) at SL = 0.5 m

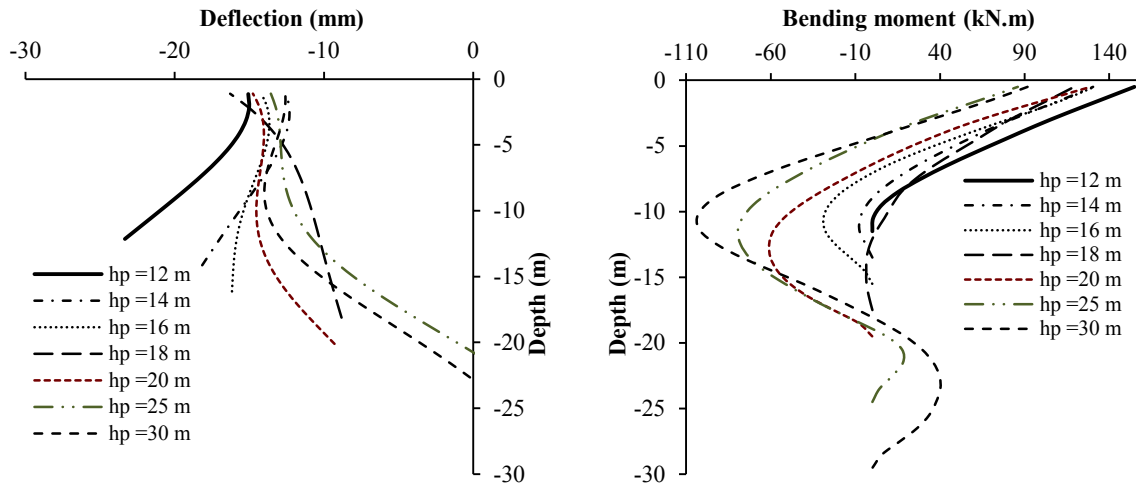


Figure B-10: Pile deflection and bending moment for at different values of pile impeded length for parameter combination (PI-MG1-C8) at trench depth 20m

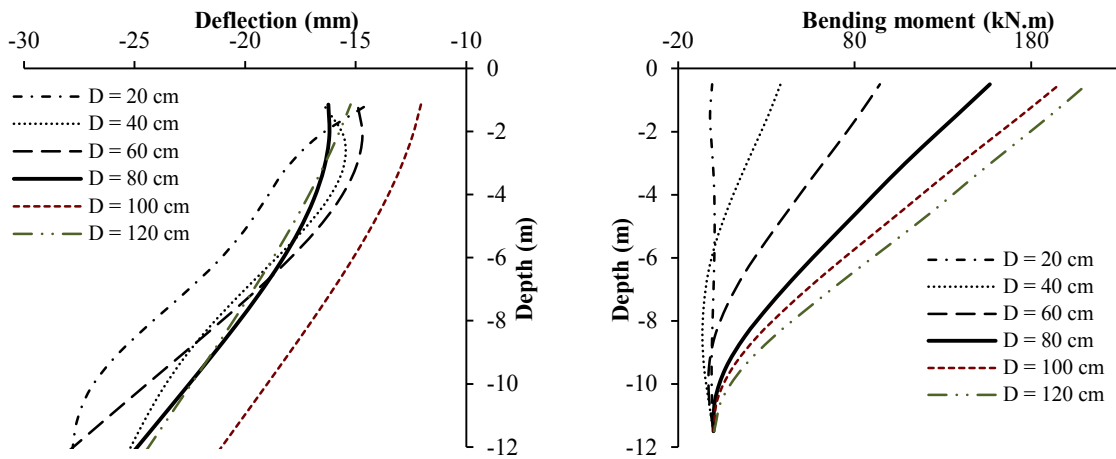


Figure B-11: Pile deflection and bending moment for at different values of piles diameter (PI-MG1-C8) at trench depth 20m

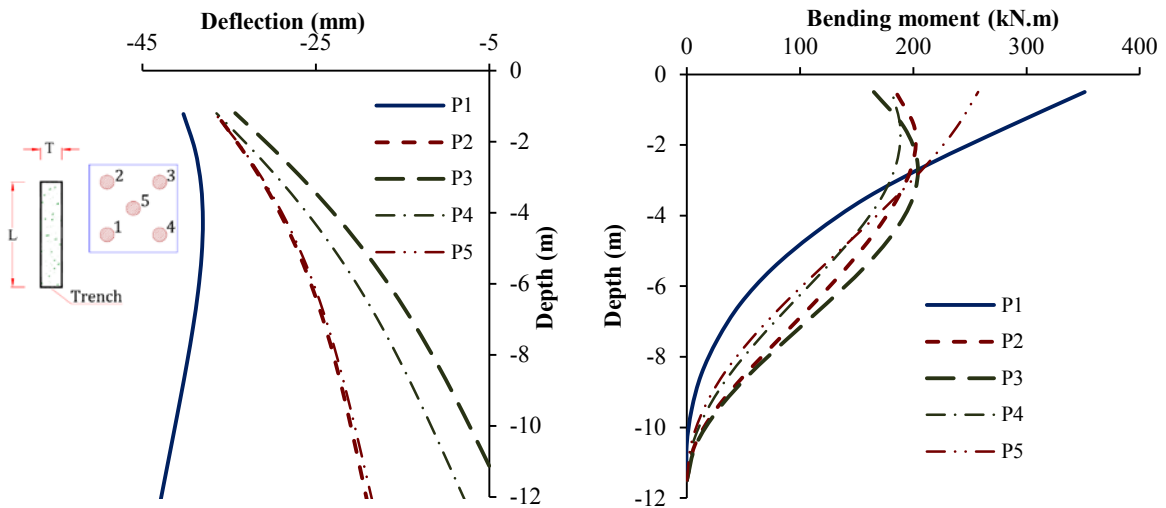


Figure B-12: Pile deflection and bending moment at different values of pile impeded length for parameter combination (PI-MG2-C1) at slurry level (SL = 1.5 m)

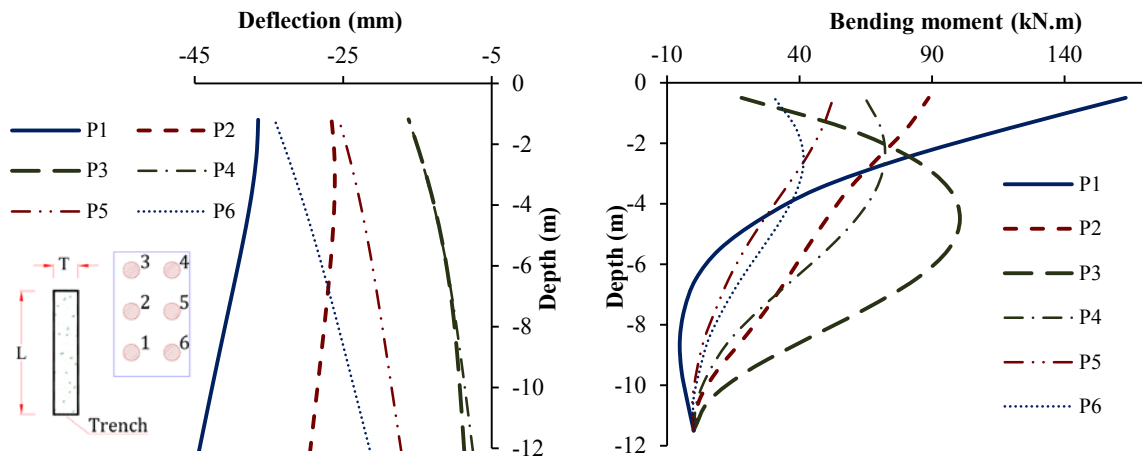


Figure B-13: Pile deflection and bending moment for different piles within the model group (PI-MG3-C1) at slurry level (SL = 1.5 m)

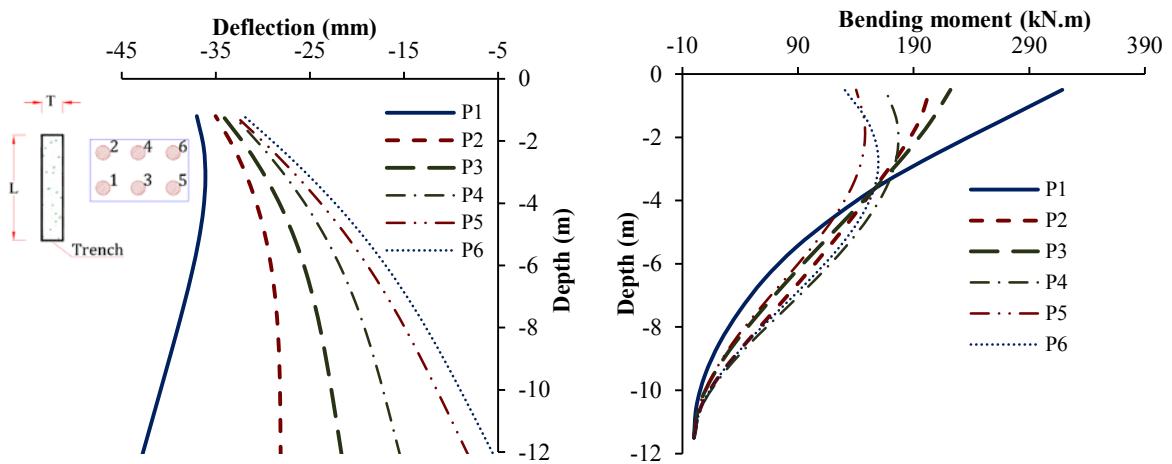


Figure B-14: Pile deflection and bending moment for different piles within the model group (PI-MG4-C1) at slurry level (SL = 1.5 m)

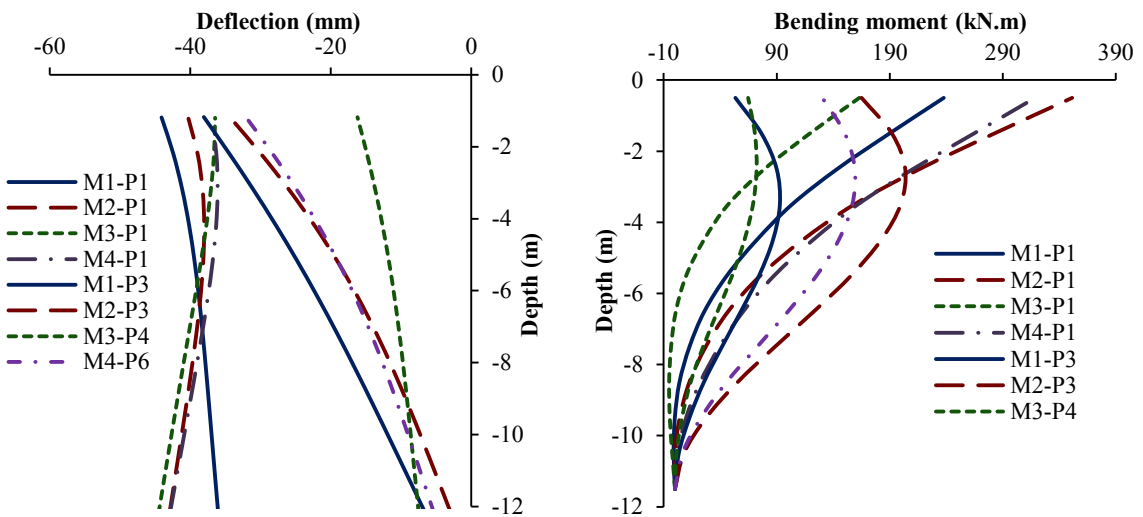
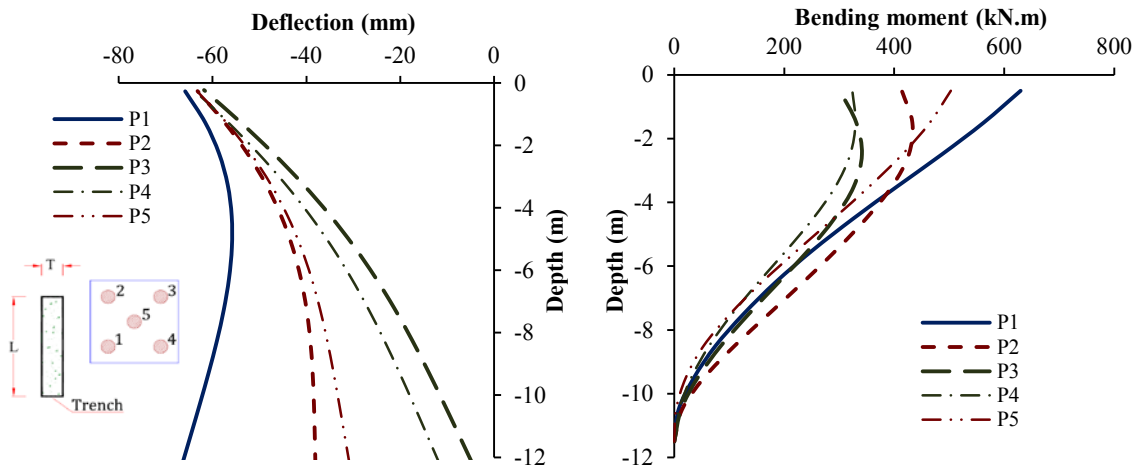
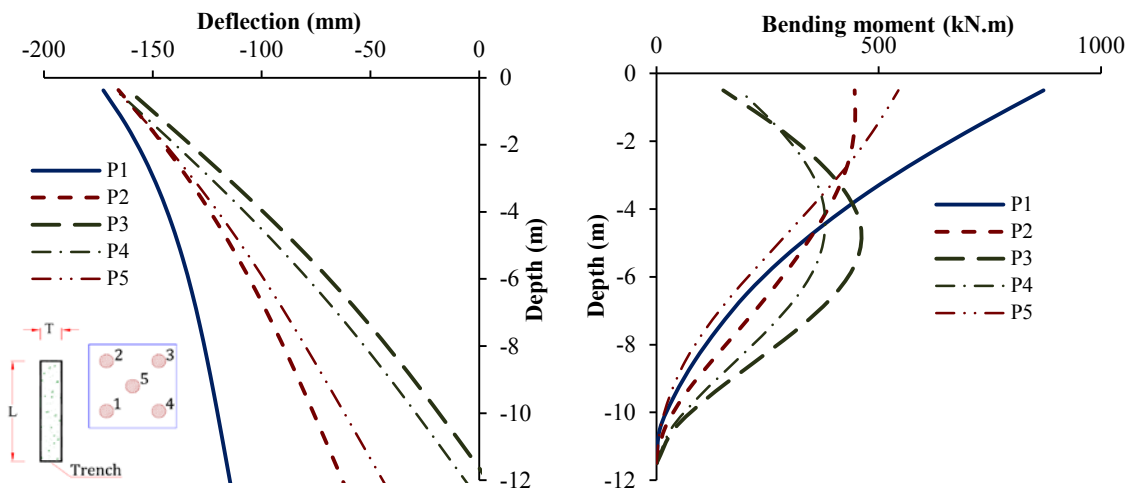


Figure B-15: Pile deflection and bending moment for different pile formations at slurry level (SL = 1.50m)

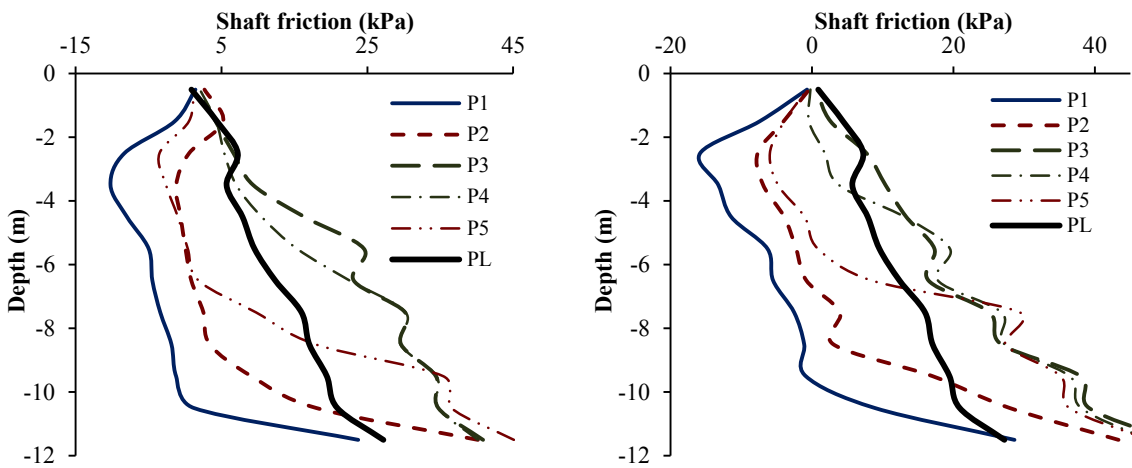


(a) slurry level (SL = 0.5 m)



(b) slurry level (SL = 1.0 m)

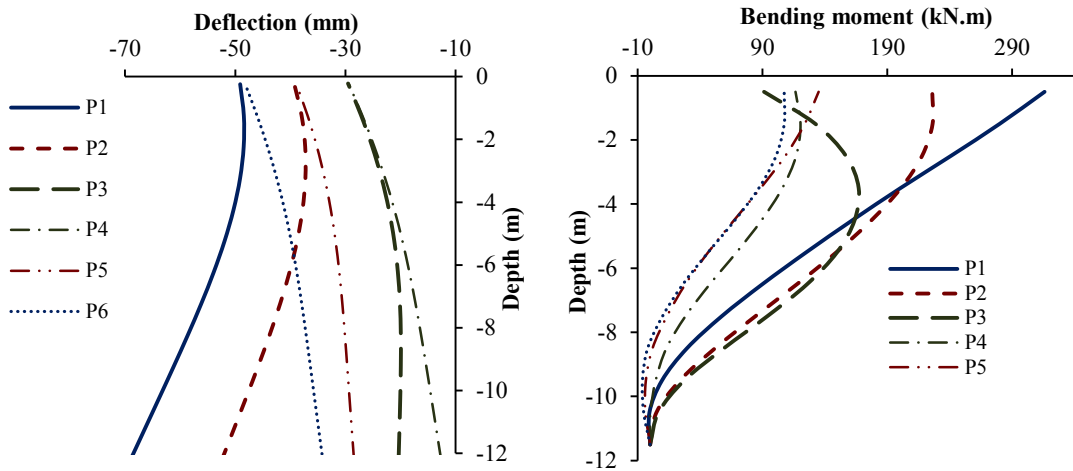
Figure B-16: Pile deflection and bending moment of piles within model group (MG2) at slurry reduction position (SP = 13.0 to 14.0 m)



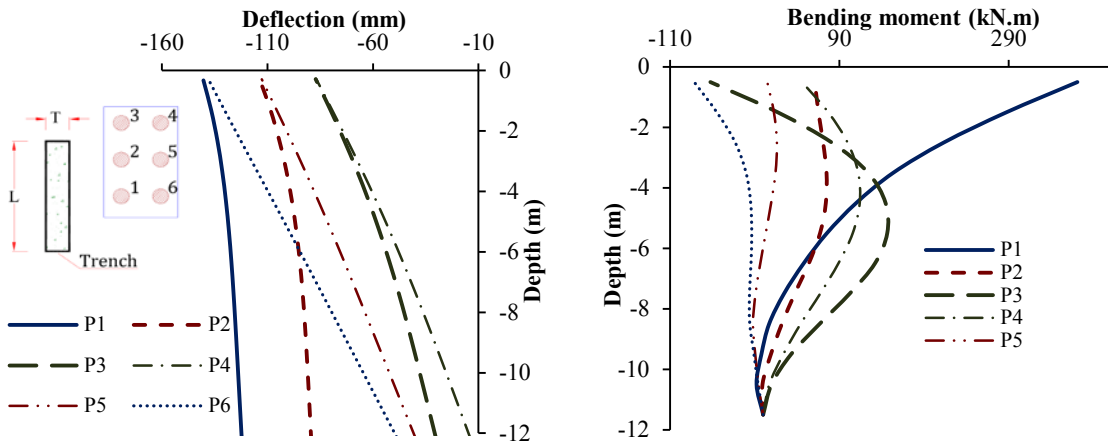
(a) Slurry level (SL = 0.5 m)

(b) Slurry level (SL = 1.5 m)

Figure B-17: Pile shaft friction at different values of piles within model group (MG2) at slurry reduction position (SP = 13.0 to 14.0 m) and slurry level

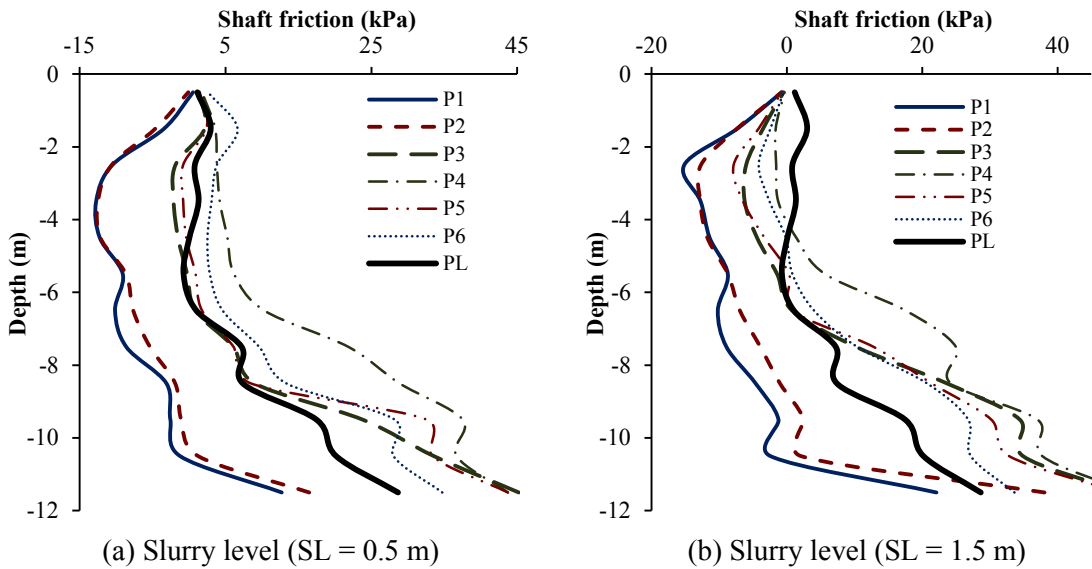


(a) slurry level (SL = 0.5 m)



(b) slurry level (SL = 1.0 m)

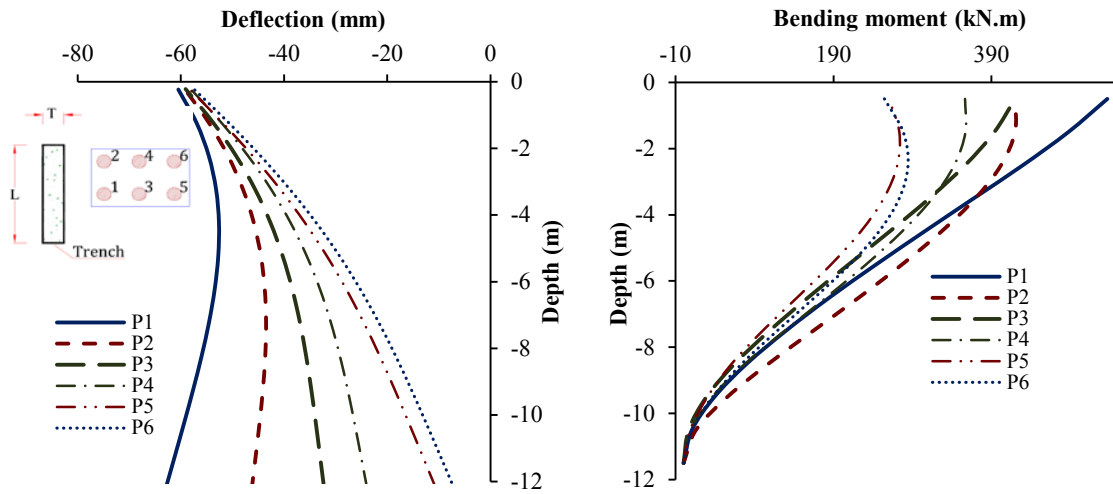
Figure B-18: Pile deflection and bending moment of piles within model group (MG3) at slurry reduction position (SP = 13.0 to 14.0 m) and slurry level (SL = 1.0m)



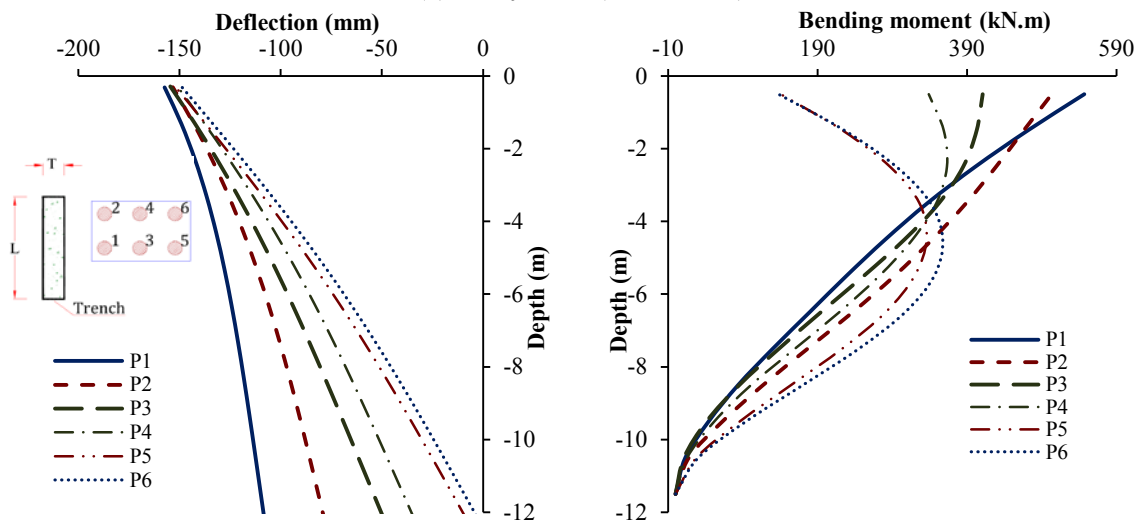
(a) Slurry level (SL = 0.5 m)

(b) Slurry level (SL = 1.5 m)

Figure B-19: Pile shaft friction at different values of piles within model group (MG3) at slurry reduction position (SP = 13.0 to 14.0 m)

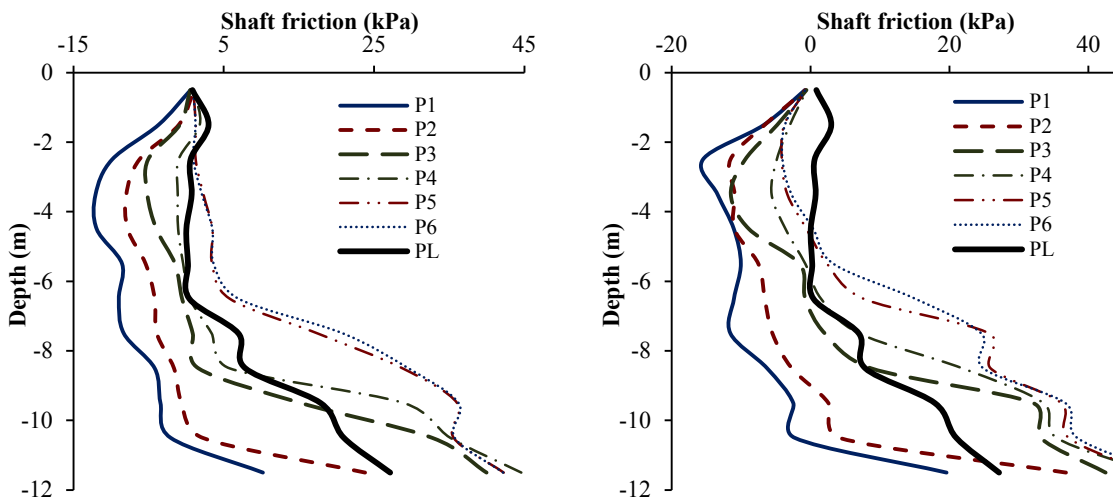


(a) slurry level (SL = 0.5 m)



(b) slurry level (SL = 1.0 m)

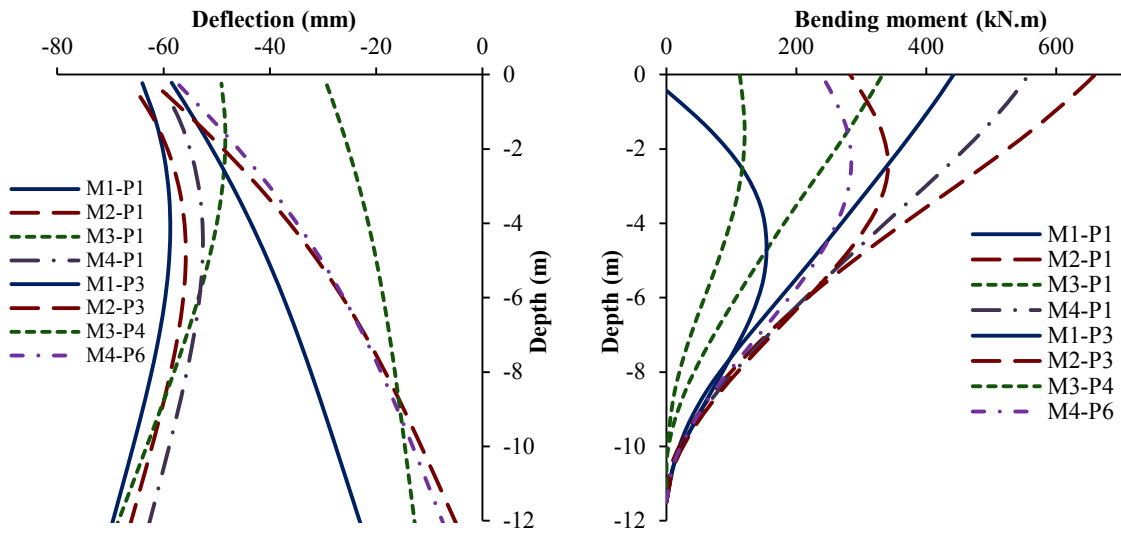
Figure B-20: Pile deflection and bending moment of piles within model group (MG4) at slurry reduction position (SP = 13.0 to 14.0 m)



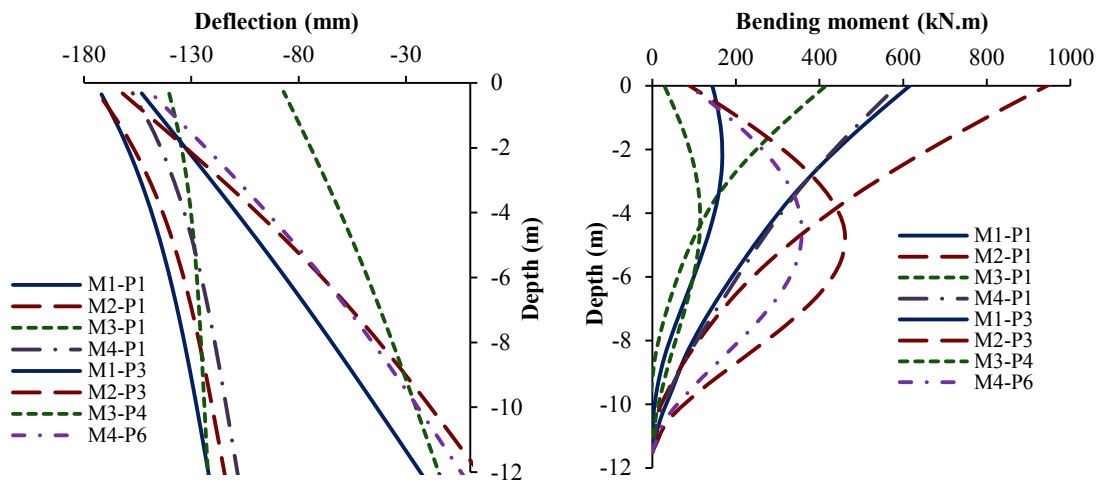
(a) Slurry level (SL = 0.5 m)

(b) Slurry level (SL = 1.5 m)

Figure B-21: Pile shaft friction at different values of piles within model group (MG4) at slurry reduction position (SP = 13.0 to 14.0 m)

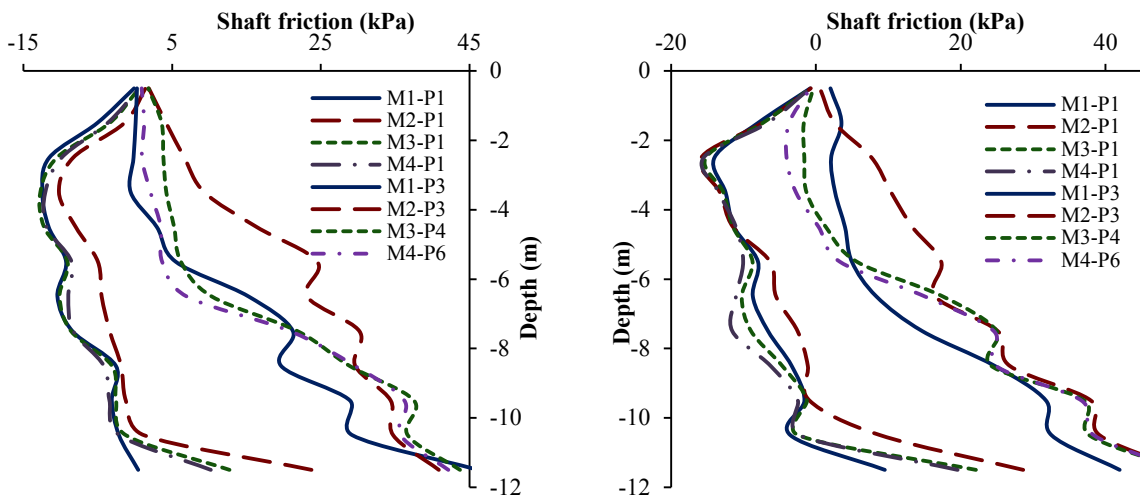


(a) slurry level (SL = 0.5 m)



(b) slurry level (SL = 1.0 m)

Figure B-22: Pile deflection and bending moment at different formations and slurry reduction position (SP = 13.0 to 14.0 m)



(a) Slurry level (SL = 0.5 m)

(b) Slurry level (SL = 1.5 m)

Figure B-23: Pile shaft friction at different formations and slurry reduction position (SP = 13.0 to 14.0 m)

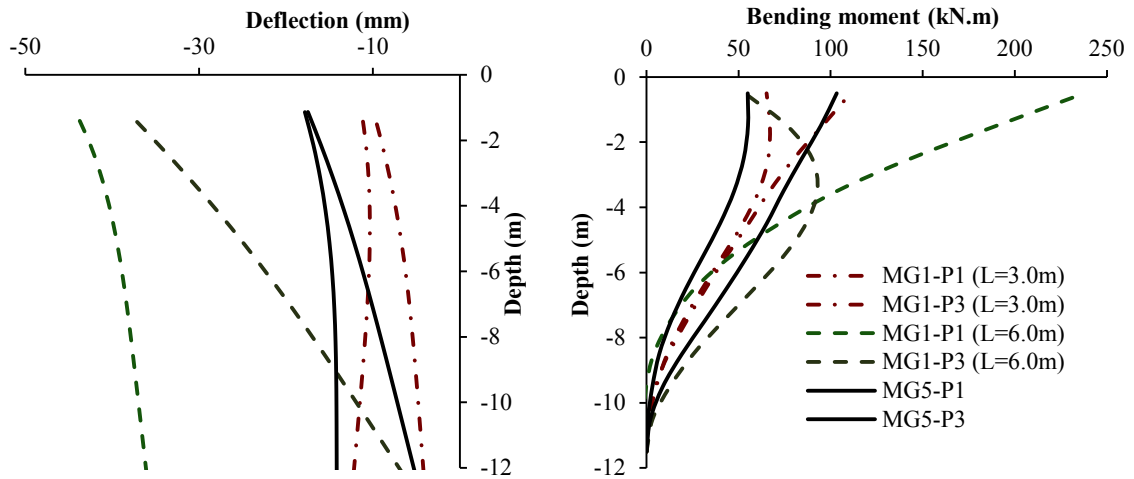


Figure B-24: Pile deflection and bending moment near double panel or single panel with different lengths (SL = 1.5)

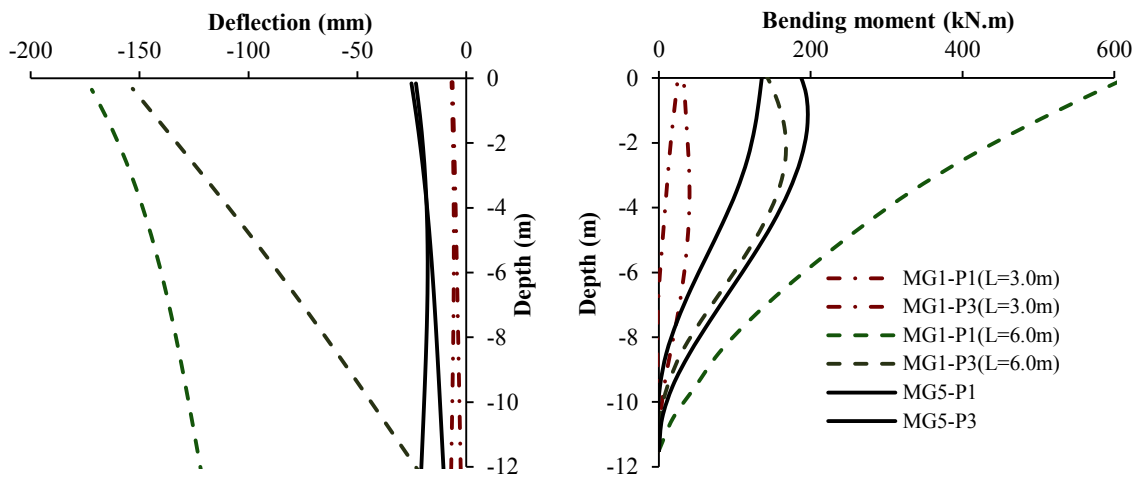
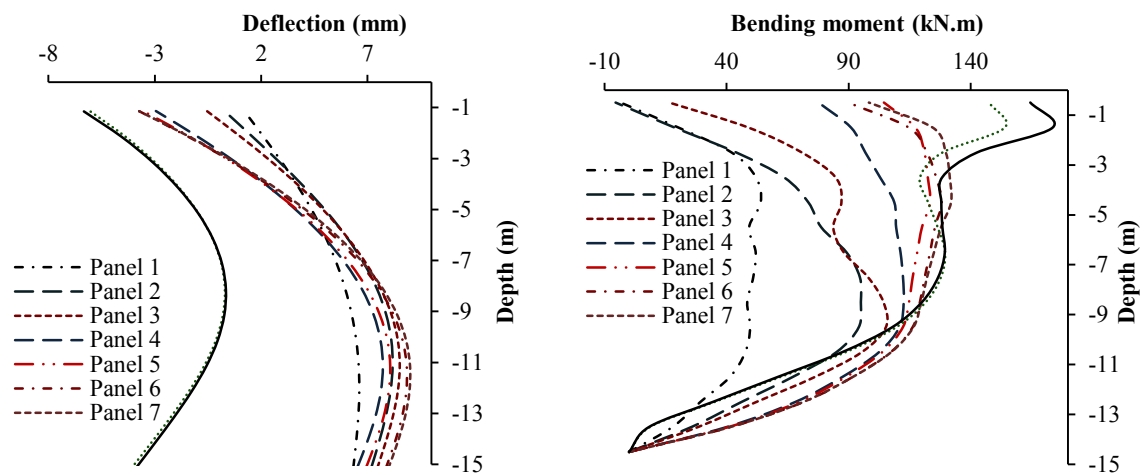


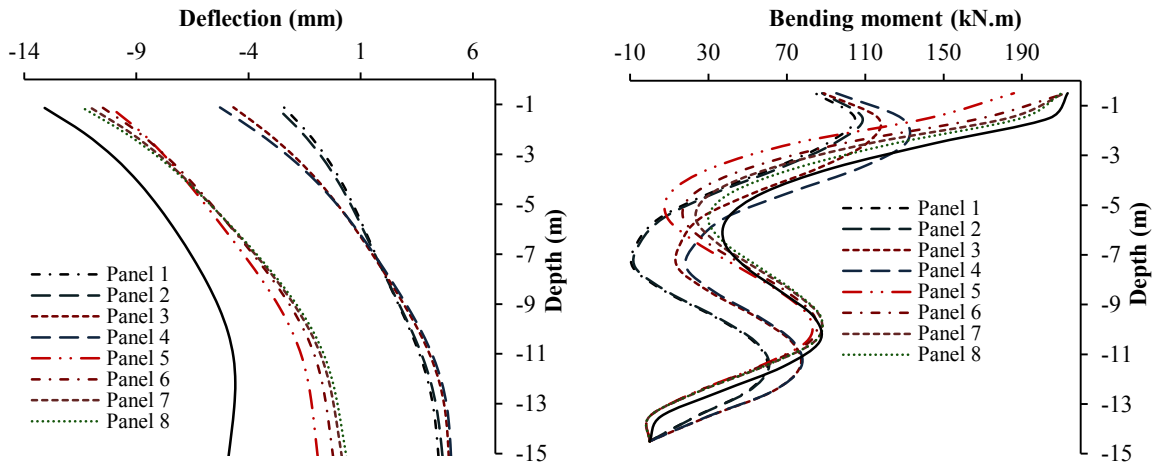
Figure B-25: Pile deflection and bending moment near double panel or single panel with different lengths (SP= 13.0 to 14.0m) and (SL = 1.0)

## B.2 RESULTS OF PART II MODEL GROUPS

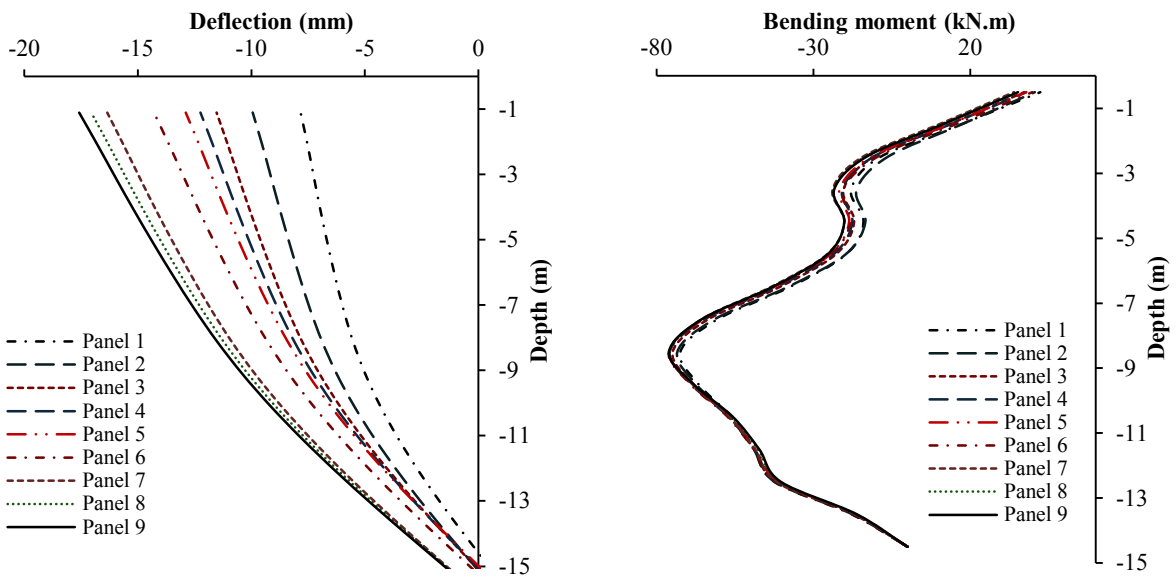


(a) Pile group G1-1





(b) Pile group G1-9



(c) Pile group G6-5

Figure B-26: Pile deflection and bending moment for first pile in different pile groups

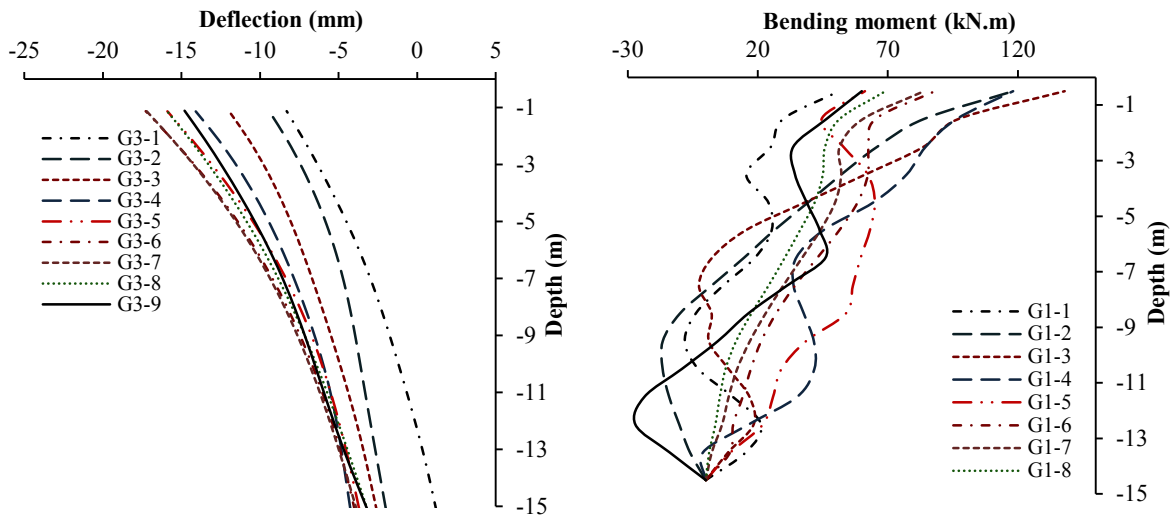


Figure B-27: Pile deflection and bending moment for Row<sub>L3</sub>

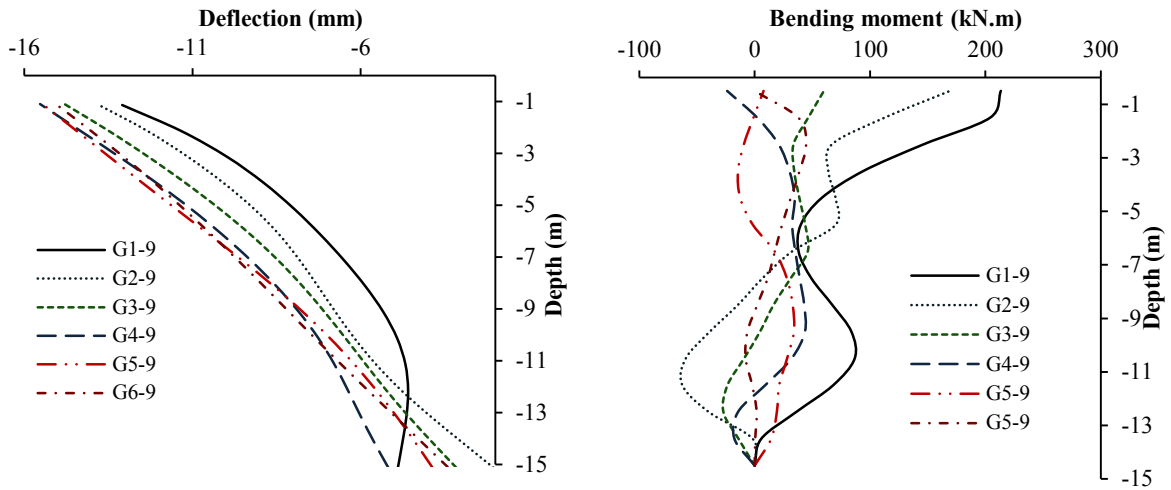


Figure B-28: Pile deflection and bending moment for Row<sub>p9</sub>

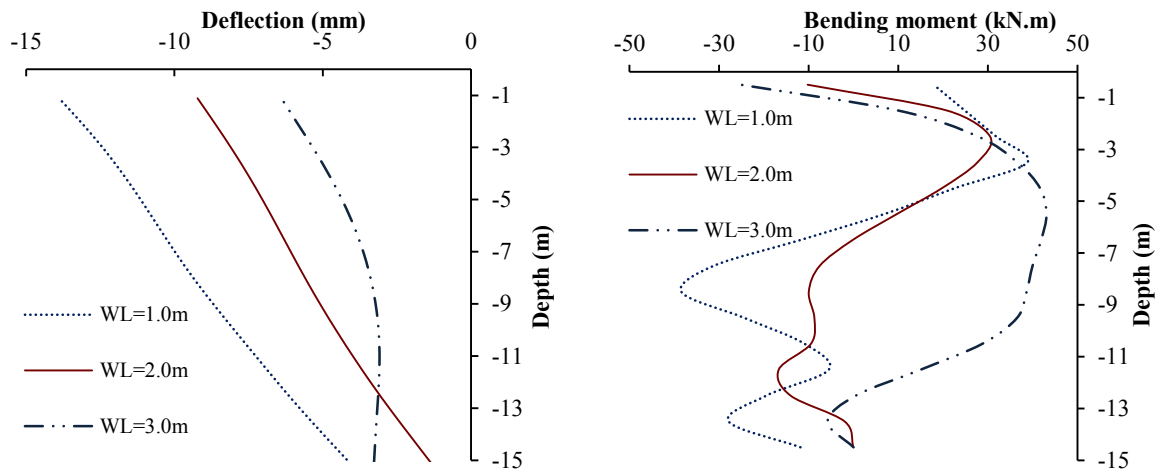


Figure B-29: Pile deflection and bending moment for different groundwater levels for G<sub>6-1</sub>

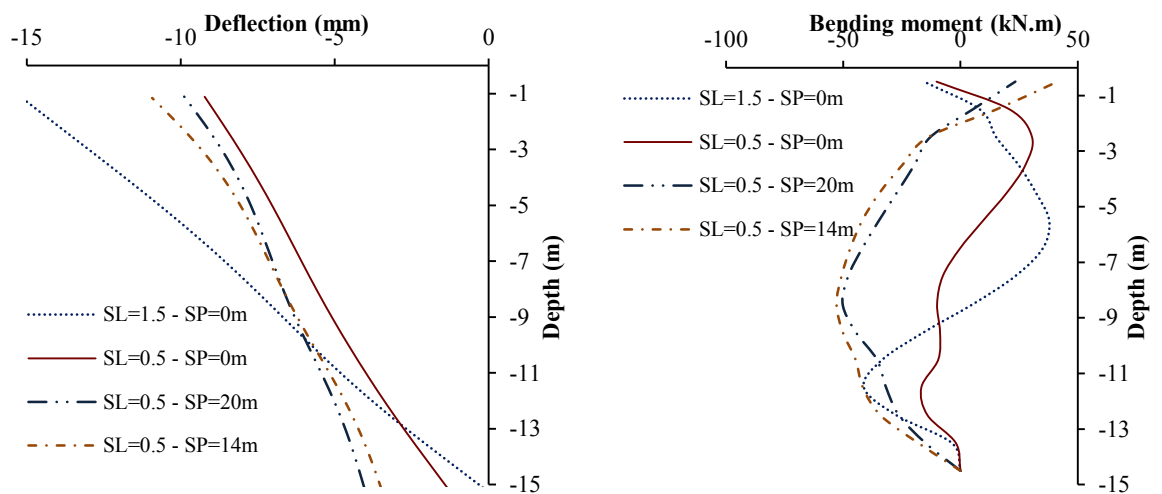


Figure B-30: Pile deflection and bending moment at different slurry pressure reduction positions and slurry levels G<sub>6-1</sub>

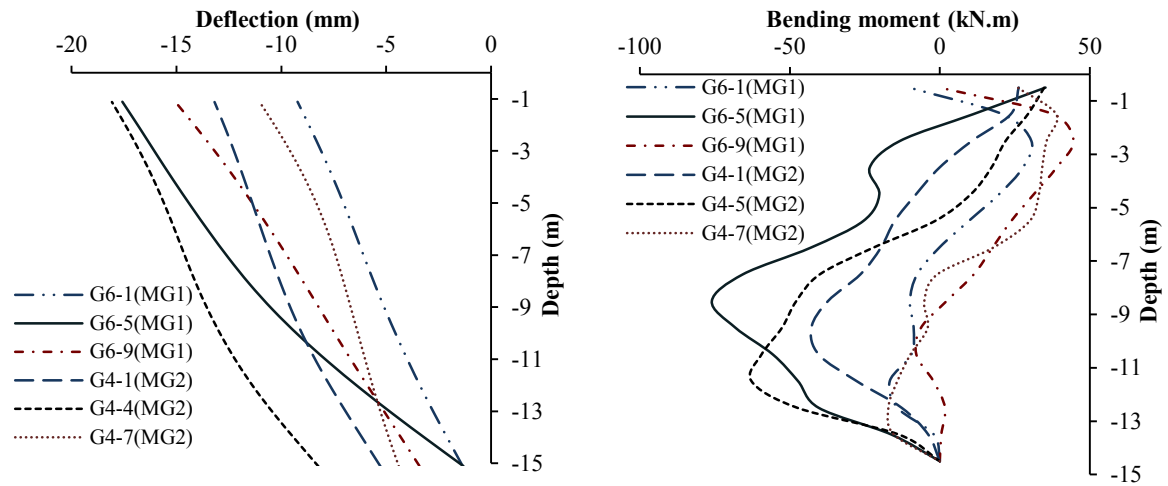


Figure B-31: Pile deflection and bending moment for different pile group models formation at Row<sub>L4</sub>

### B.3 RESULTS OF PART III MODEL GROUPS

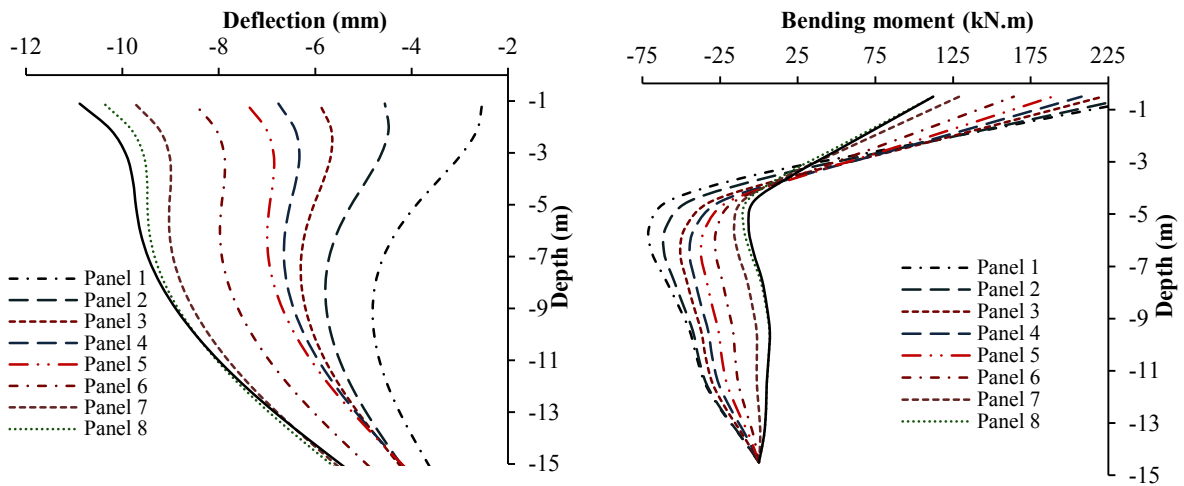


Figure B-32: Pile deflection and bending moment at different panels construction stages for pile P15-11

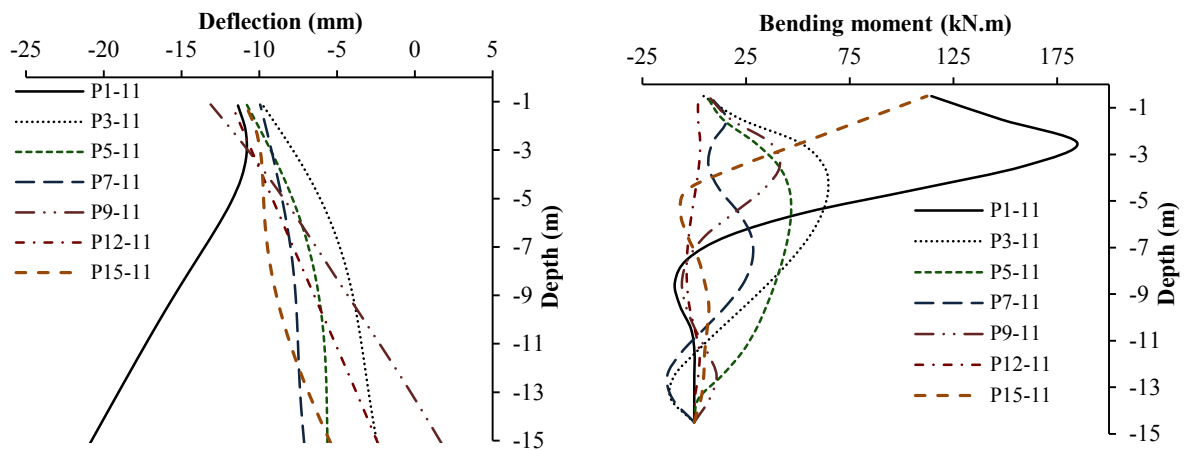


Figure B-33: Pile deflection and bending moment for different piles within the middle row perpendicular to the trench (Row<sub>P11</sub>)

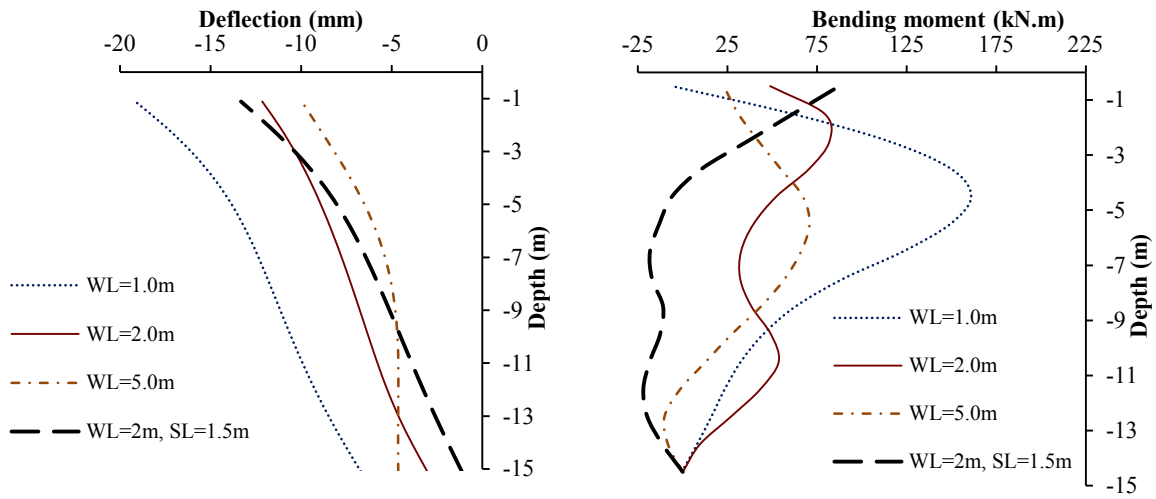


Figure B-34: Pile deflection and bending moment for different groundwater levels for pile P<sub>15-21</sub>

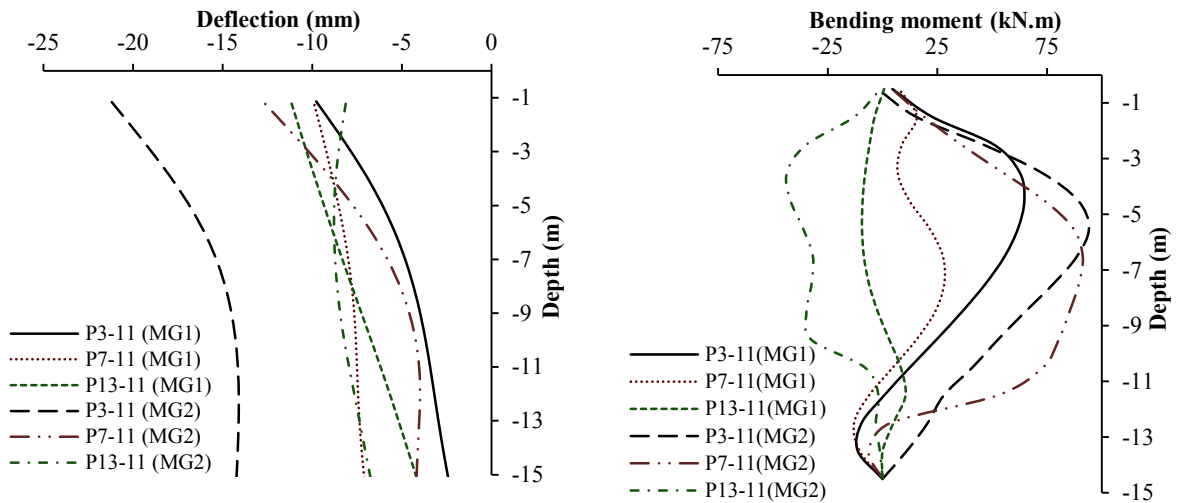


Figure B-35: Pile deflection and bending moment for different model groups and piles in the middle row perpendicular to the trench (Row<sub>p11</sub>)

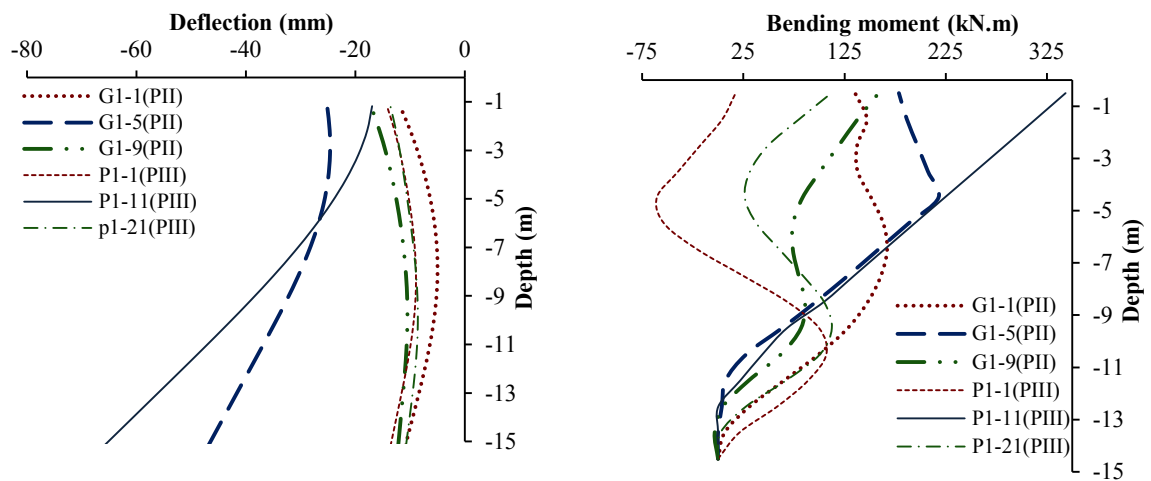


Figure B-36: Pile deflection and bending moment for some piles in Part II compared to corresponding piles in Part III at slurry level (SL = 1.5 m)

## **Declaration**

I hereby declare that I completed this work without any improper help from a third party and without using any aids other than those cited. All ideas derived directly or indirectly from other sources are identified as such. In the selection and use of materials and in the writing of the manuscript I received support from the following persons:

-----  
-----  
-----

Persons other than those above did not contribute to the writing of this thesis. I did not seek the help of a professional doctorate-consultant. Only those persons identified as having done so received any financial payment from me for any work done for me.

This thesis has not previously been published in the same or a similar form in Germany or abroad.

Date:

signature: